DISS. ETH NO. 18390

ENGINEERING CELL BEHAVIOR: ADDING DIMENSIONALITY TO THE CELL SENSORY TOOLBOX

A dissertation submitted to

ETH ZURICH

for the degree of

Doctor of Sciences

presented by

MIRJAM OCHSNER

Dipl. Werkstoff-Ing. ETH

born on February 10, 1978

citizen of Einsiedeln (SZ)

accepted on the recommendation of

Prof. Dr. Marcus Textor, examiner

Prof. Dr. Viola Vogel, co-examiner

Prof. Dr. Matthias Lutolf, external co-examiner

Prof. Dr. Michael Smith, external co-examiner

2009

Nothing shocks me. I'm a scientist.

DR. INDIANA JONES

Acknowledgements

This work would not have been possible without the input, advice, and encouragement of many people. I would hereby like to take the opportunity to thank them properly.

First, I would like to thank my Professor, Marcus Textor. Marcus, I am happy for the opportunity to do my PhD thesis in your lab. I appreciate the way you supported me during my thesis giving inputs and guidance while leaving me lots of freedom to choose how I wanted to do my work and what I wanted to follow. I further appreciated the possibility to attend several international scientific conferences, gaining valuable experience.

Another huge "thank you" I want to say to Michael Smith. Michael, without you, this thesis would have been impossible. I was very glad for your biological input and the encouraging words when experiments did not work out as we expected or when I was doubting all the things I am working on. Furthermore, I was happy to have you in my committee.

Viola Vogel was another important person involved in my PhD thesis. Viola, I want to thank you for the input for additional experiments, the feedback on my papers and thesis as well as being part of my committee.

Matthias Lütolf was a co-referee of my thesis. Matthias, I want to thank you for being part of my committee.

Michelle Grandin was my supervisor at the beginning of my thesis. Michelle, I want to thank you for introducing me into my PhD life and the support I got from your side. It helps a lot to get a nice start and have a person that I could ask everything. Furthermore, I really appreciated that you proof read my thesis even though you were already back in Canada and expecting your second child.

Another person involved in proof reading my thesis was Mirren Charnley. Even though I thank her together with the other people working on microwells, I think, she

earns a special "thank you" for proof reading my thesis and always being there when I did not see how it should be possible to write everything up.

Marc Dusseiller was the PhD student that started the microwell project. Marc, I want to thank you for the introduction into the topic and into the practical work and for the many hours you spent with me in the clean room, replicating microwells or sitting in front of the microscope.

Fernanda Rossetti introduced me to the work with vesicles and bilayers. Fernanda, I would like to thank you for the introduction. The work with the bilayers is now an important part of this thesis and would not have been possible without your introduction.

Another important person for the lipid part of my thesis was Erik Reimhult. Even though he was not officially involved in my project he was always helpful and willing to discuss some QCM-D curves, FRAP images and answer some stupid vesicle question.

The microwell people earn another huge "thank you". The first year I was the only PhD student on the project and I really appreciated it when some more people were working on the same subject. I want to thank Fabian, Maria and Mirren for the useful discussions (as well as for the occasional swearing) about cells in wells and all the other more or less science related topics.

A PhD student does not all the time stand in the lab and do crazy experiments, they spend also a reasonable amount of time inside the office. During my PhD I was mainly sharing my office with Thomas Blättler, Martina Baumann, Katrin Barth and Maria Håkanson. I want to thank all of you for being such brilliant office mates. I always enjoyed talking with you about our projects and life, complaining about some stupid proteins, bacteria or peptides and drinking a coffee or two. During the time of writing my thesis, Jia and Tolga replaced the other people in the lab, during this stressful time I did not really had the chance to know you two better, but i wish you all the best for your PhD thesis.

Another special "thank you" goes to Esther Stähli and Josephine Baer who made the bureaucratic life a lot easier.

I enjoyed my time at LSST, and that is not only because of my PhD project, a great deal is due to the people at LSST. I really enjoyed spending time with you outside of science; laughing in the coffee room, partying, climbing in the mountains, relaxing in the spa, skiing and so on. Thank you all for a great time!

Abstract

Tissue function is the summation of cell responses and therefore closely coupled to the stimuli the cell experiences in its microenvironment. In addition to substrate rigidity, matrix composition, and cell shape, dimensionality is now considered an important physical property of the cell's microenvironment which directs cell behavior. Studies have shown differences in cell behavior when cells are cultured in a three-dimensional (3-D) matrix, in comparison to cells cultured on flat surfaces. Therefore, next to the physical and chemical microenvironment, the structural environment of a cell plays a crucial role in its shape and function.

Microwell fabrication

The merger of microfabrication and cell biology has led to a variety of new tools to investigate the behavior of cells when cultured *in vitro*. However, available tools for the study of cell behavior in two-dimensional (2-D) versus 3-D environments are difficult to compare. Current 3-D models, such as gels or fibrous networks, provide no 3-D shape control of individual cells and are often difficult to combine with high-resolution microscopy imaging, such as confocal laser scanning microscope (CLSM). M. Dusseiller, M. Smith, V. Vogel, and M. Textor at ETH Zurich have developed a set of tools which combines 2-D chemical patterning with topographical microstructuring, thus presenting to the cells a structurally and biochemically defined, reductionist microenvironment. The technique combines master fabrication in silicon and replication techniques which allows us to create polydimethylsiloxane (PDMS) chips that display defined microwells of various shapes with dimensions in the order of single cells. By making use of different cross-linking densities of the PDMS substrate, tailoring of the mechanical properties of the material surrounding a cell becomes possible.

In addition to geometry, we were also able to control the chemistry of the micro-environment such that the surface inside the wells presented specific chemical functionality, *e.g.* adhesion proteins, while the plateau surface between the wells is passivated against non-specific protein adsorption and cell adhesion. The passivation is critical to ensure cells adhere only within the microwells and thereby within a controlled microenvironment. Therefore, Dusseiller *et al.* have developed a method for the wet-printing of a protein resistant graft-co-polymer, poly(L-lysine)-*g*-poly(ethylene glycol) (PLL-*g*-PEG) using an inverted microcontact printing approach. In view of the promising potential of this culture technique, the work of this thesis has been to further optimize and develop more advanced chemical modification tools of the microwells as well as to answer a number of fundamental question as to how cells respond to variations of microenvironmental parameters, individually and in concert.

Presentation of a mobile E-cadherin coating inside microwells

As many proteins of interest in cell studies are membrane proteins, wherein mobility may play an important role, a new methodology to coat the inside of the wells with supported phospholipid bilayers (SPB) functionalized with human E-cadherin was developed in this thesis. Characterization of mobility revealed that SPBs were mobile on an oxidized PDMS surface and that the edges of the microwells did not limit the lateral diffusion of the lipids. The selection of a phospholipid with a liquid-gel transition temperature, T_M, of 35 °C meant the mobility within the microwell could be manipulated through adjusting the temperature of the environment within a small temperature range. The combination of the microwell structure with the mobile and immobile SPB provides a new tool for the study of membrane protein clustering and actin organization in well controlled 3-D environments. First preliminary experiments with Chinese hamster ovary (CHO) cells demonstrated that cells were able to adhere inside E-cadherin-functionalized SPB microwells, and furthermore, that mobility influenced actin organization of the cell in 2-D and therefore impacted cell behavior in general.

Microwells with heterogeneous display of proteins

In vivo, adhesion molecules often have tightly controlled spatial patterns, for example in epithelial cells which have cell-cell contacts laterally and basement membrane underneath the cell. Therefore, in addition to a homogeneous coating inside the microwells, we developed a technique to coat the wall and bottom with different proteins. To this end, a line-of-sight deposition of titanium (Ti) allowed for the creation of a TiO_2 (bottom)/SiO_2 (wall)

contrast inside the microwell. The passivation of the plateau by inverted microcontact printing and the subsequent vesicle exposure led to vesicle rupture and SPB formation on the SiO_2 wall surface. The protein-resistant properties of the PLL-g-PEG on the plateau and the SPB on the SiO_2 side walls allowed for selective fibronectin (Fn) coating on the TiO_2-coated bottom of the microwell. The functionalization of the SPB with cell-cell adhesion molecules provides a microenvironment for the cell which possibly mimics more closely the environment present *in vivo*. Therefore, this culture substrate is potentially suited to the investigation of cell responses, such as cell polarity, division, differentiation and stem cell fate.

Dimensionality and its impact on apoptosis, viability, actin fibril assembly and mechanosensation

Cells cultured inside 3-D microwells showed altered cell responses to environmental stimuli compared to cells on a 2-D surface. We asked whether cell size and shape within 3-D environments could control cell viability. Endothelial cells constrained within microwells were viable up to 7 days. Furthermore, cells in very small microwells (spreading area between 100 and 200 μm^2) were viable, while cells on 2-D patterns with the same projected adhesive area underwent apoptosis. Dimensionality seems to enable the cell to overcome spreading limitation induced apoptosis.

Next, we studied the assembly of the cytoskeleton, since an intact actin cytoskeleton is necessary for cells to migrate, apply contractile forces to their surroundings, and divide. Fibroblast cells constrained within microwells assembled a robust actin network which was in stark contrast to the limited actin filament assembly found within cells on 2-D patterns with equivalent projected spreading areas. Moreover, the cytoskeleton exhibited 3-D arrangement in microwells and was not only limited to the cell-substrate interface as on 2-D surfaces. The ECM is a dynamic structure; it also undergoes changes and is constantly rebuilt and rearranged by the cell itself. Since extracellular Fn matrix fiber formation requires cell contractility, we next asked whether fibroblast cells in microwells rearranged surface adsorbed Fn into fibers in situations where actin filament assembly was observed. Cell containment on 2-D patterned surfaces progressively limited Fn rearrangement with decreasing size. In contrast, cells which adequately filled microwells rarely rearranged Fn from the microwell surfaces. The formation of an actin skeleton and the hindrance of Fn matrix rearrangement made it difficult to draw any definitve conclusions about cell contractility inside the microwells, but it suggested that actin filament assembly is driven

by other cues and might help to explain some other differences seen in cells in 3-D gels versus on 2-D substrates.

Since the mechanosensing abilities of a cell are coupled to the actin skeleton, we investigated actin filament assembly in both hard and soft microwells. Interestingly, cells in soft microwells with limited spreading and substrate stiffnesses of approximately 20 kPa did not assemble a detectable actin cytoskeleton, which was in contrast with cells on flat, homogeneous 2-D substrates where actin filament assembly was observed. Therefore, we have to conclude that it is not mechanosensation alone, but also dimensionality that influences the cell's ability to probe its environment and to respond to the stiffness of its surrounding.

Finally, we investigated the dependence of the metabolism of cells on spreading area and dimensionality. Increasing the spreading area of the cell led to increased metabolic activity on both 2-D patterns and inside 3-D microwells. Furthermore, our results indicate that the metabolic activity of the cell was greater in a 3-D environment, indicating that metabolic activity was also affected by dimensionality.

Conclusion

These observations demonstrate that single-cell microwell substrates are a valuable addition to the toolbox of engineered cell culture platforms and can produce micro-environments for the study of cell behavior in reductionist 3-D environments. The possibility to control the spreading area of the cell, the stiffness of the substrate, and the coating inside the wells made it possible to evaluate the impact of varying a single parameter and furthermore, the interplay between different parameters. Additionally, the microwell thin PDMS film substrates are compatible with conventional culturing assays, live imaging and high-resolution microscopy often used in cell biology. The microwell substrate is a useful platform to study biophysical fundamentals. However, it needs to be taken into consideration that such an engineered platform is never able to simulate exactly the environment of a cell *in vivo* as these substrates are constrained by the reduced and simplified presentations of biochemical ligands and the absence of real cell-cell contacts. Furthermore, the imitation of very soft tissue is limited since the transference of the microwell structure into very soft materials is difficult. Nevertheless, the microwell substrate is a suitable platform to address biological questions, such as the influence of dimensionality on cell division or stem cell differentiation. Furthermore the microwell platform provides a microarray format for high-thoughput cell-based assays in drug or toxicity screening.

Zusammenfassung

Die Funktionsfähigkeit von lebendem Gewebe ist ein Zusammenspiel von Zellfunktionen und deshalb an die Stimuli gekuppelt, welche die Zelle in ihrer Umgebung erfährt. Neben Substratsteifigkeit, Matrixzusammensetzung und Zellform zählt die Dimensionalität zu den wichtigen physikalischen Eigenschaften der Mikroumgebung der Zelle, die das Zellverhalten steuert. Studien haben gezeigt, dass sich Zellen in dreidimensionalen (3-D) Systemen anders verhalten als auf flachen Substraten. Deshalb spielt neben dem physikalischen und chemischen Mikroumfeld das strukturelle Umfeld für die Zellform und -funktion eine kritische Rolle.

Fabrikation der Mikrostrukturen

Die Verschmelzung von Mikrofabrikation und Zellbiologie führte zu einer Vielzahl neuer Methoden, mit denen sich das Verhalten von Zellen *in vitro* studieren liess. Jedoch sind die vorhandenen Techniken, welche das Zellverhalten im zweidimensionalen (2-D) Umfeld zum Verhalten in 3-D Umgebungen gegenüberstellt, schwierig zu vergleichen. Geläufige 3-D Modelle, wie z.B. Gele oder faserförmige Netzwerke, ermöglichen keine Kontrolle über die Form einzelner Zellen und sind schwierig mit hochauflösender Mikroskopie zu kombinieren. M. Dusseiller, M. Smith, V. Vogel und M. Textor von der ETH Zürich haben eine Technik entwickelt, die 2-D, chemische Muster mit topographischer Mikrostrukturierung kombiniert und die Möglichkeit eröffnet, den Zellen eine strukturelle und biochemisch definierte, jedoch vereinfachte Mikroumgebung reduzierter Komplexität zu präsentieren. Die Methode kombiniert Mikrostrukturierung in Silizium mit einer Replikationstechnik, welche es ermöglicht, ein Polydimethylsiloxan (PDMS) Substrat herzustellen, das Mikrostrukturen in der Grössenordnung einer Zelle enthält. Ausserdem kann man die mechanischen Eigenschaften des PDMS Substrats steuern, indem man dessen Quervernetzungsdichte variiert.

Zusätzlich zur Geometrie konnte auch die Chemie der Mikroumgebung kontrolliert werden: Die Oberfläche innerhalb der Mikrostrukturen präsentierte eine spezifische chemische Funktionalität, wie z.B. Adhäsionsproteine, während das Plateau zwischen den Strukturen gegen unspezifische Proteinadsorption passiviert ist. Die Passivierung ist ein kritischer Schritt, der gewährleisten soll, dass die Zellen nur innerhalb der Strukturen adherieren, in denen eine kontrollierte Mikroumgebung präsentiert wird. Deshalb hat Dusseiller *et al.* eine Stempelmethode entwickelt, die ein graft-co-polymer, poly(L-lysine)-*g*-poly(ethylene glycol) (PLL-*g*-PEG), mit einem hydrierten Stempel auf das Plateau aufträgt. Wegen des viel versprechenden Potentials dieser neuen Zellkulturplatform wurde in dieser Arbeit die chemische Modifikation in den Mikrostrukturen weiterentwickelt und erste detaillierte Zellstudien ausgeführt.

Präsentation einer beweglichen E-cadherin Schicht innerhalb der Mikrostrukturen

Da viele für Zellstudien interessante Proteine Membranproteine sind, bei denen die Beweglichkeit der Liganden eine wichtige Rolle spielt, wurde eine neue Methodologie entwickelt, die im Inneren der Mikrostrukturen eine Doppellipidschicht aufträgt, die mit E-Cadherin funktionalisiert wird. Die Charakterisierung der Mobilität hat gezeigt, dass die Doppellipidschicht auf oxidiertem PDMS beweglich war und die Kante der Mikrostrukturen die laterale Beweglichkeit der Lipide nicht einschränkte. Durch die Wahl eines Phospholipids mit einer Transitionstemperatur von 35 °C konnten wir die Beweglichkeit innerhalb der Mikrostruktur durch die Temperatur steuern.

Die Kombination der Mikrostruktur mit der beweglichen Doppellipidschicht hat eine neue Technik hervorgebracht, mit der sich das Anhäufen von Membranproteinen und die Aktinorganisation in einer gut kontrollierten, 3-D Umgebung studieren lässt. Erste Experimente mit Zellen (Chinese Hamster Ovary Zellen) haben gezeigt, dass sich die Zellen innerhalb der Mikrostrukturen, die mit einer Cadherin-funktionalisierten Doppellipidschicht beschichtet waren, anhaften konnten. Des weitern hat die Mobilität die Aktinorganisation der Zelle in 2-D beeinflusst und somit auch das Verhalten der Zelle im Allgemeinen.

Mikrostrukturen mit heterogener Proteinanordnung

Adhäsionsmoleküle *in vivo* haben oft kontrollierte räumliche Anordnung, wie z. B. in Epithelzellen, welche Zell-Zell-Kontakte lateral und Kontakte zur Basalmembran unterhalb der Zelle aufweisen. Deshalb haben wir neben dem homogenen Beschichten der Mikrostrukturen eine Technik entwickelt, die es ermöglicht, die Wände und den Boden der

Mikrostrukturen mit verschiedenen Proteinen zu beschichten. Mit Hilfe einer senkrechten ("line-of-sight") Abscheidung von Titan (Ti) wurde ein TiO_2 (Boden)/SiO_2 (Wand) Kontrast kreiert. Die Passivation des Plateaus und die anschliessende Exposition mit einer Vesikellösung hat zur Bildung einer Doppellipidschicht auf dem SiO_2 geführt. Die proteinresistenten Eigenschaften von PLL-*g*-PEG auf dem Plateau und der Doppellipidschicht auf den SiO_2 Wänden ermöglichte die selektive Adsorption von Fibronektin auf dem Boden der Mikrostruktur. Die Funktionalisierung der Doppellipidschicht mit Zell-Zelladhäsionsmolekülen hat den Zellen eine Mikroumgebung geschaffen, welche die *in vivo* Umgebung besser imitieren dürfte. Deshalb ist diese Platform potenziell geeignet um Zellverhalten, wie z.B. Polarität, Zellteilung, sowie Differenzierung von Stammzellen besser zu untersuchen.

Dimensionalität und ihr Einfluss auf Apoptosis, Lebensfähigkeit, Aktinfaserbildung und Mechanosensation

Je nachdem ob die Zellen in 3-D Mikrostrukturen oder auf 2-D Oberflächen gezüchtet wurden, haben Stimuli aus der Umgebung unterschiedliches Zellverhalten provoziert. Deshalb wurde untersucht, ob die Zellgrösse und -form innerhalb 3-D Mikrostrukturen die Lebensfähigkeit von Zellen beeinflussen kann. Endothelzellen, die in einer Mikrostruktur gezüchtet wurden, haben 7 Tage lang überlebt. Sogar in kleinen Strukturen (Ausbreitungs-fläche ("spreading area") $< 200 \ \mu m^2$) haben die Zellen überlebt, während die Zellen auf 2-D Mustern mit derselben Ausbreitungsfläche gestorben sind. Dimensionalität scheint folglich die im 2-D-Fall als Folge mangelndem Ausbreitungsgrad induzierte Apoptose zu überwinden.

Da ein intaktes Zytoskelett eine wichtige Voraussetzung für Zellmigration, Zellteilung und Zellkontraktilität ist, haben wir die Bildung des Zytoskeletts in den Mikrostrukturen untersucht. Es konnte beobachtet werden, dass Zellen innerhalb der 3-D Strukturen ein Aktinskelett aufbauen konnten, während Zellen auf 2-D Mustern mit der gleichen projezierten Fläche hingegen nur limitierte Aktinbildung aufwiesen. Das Zytoskelett hatte eine 3-D Anordnung und war nicht nur auf die Zell-Substrat Grenzfläche limitiert. Die extrazelluläre Matrix ist eine dynamische Struktur, die konstant von den Zellen neu gebildet und angeordnet wird. Da Zellkontraktilität eine Voraussetzung für Fibronektin Matrixfasernbildung ist, wurde untersucht, ob der Aufbau eines Aktinskeletts ein Hinweis darauf ist, dass Fibroblasten in Mikrostrukturen mit adsorbiertem Fibronektin Fasern bilden können. Zellen, bei denen mit Hilfe von 2-D Mustern die Ausbreitungsfläche kontrolliert wurde, haben mit kleiner werdender Fläche weniger Fibronektin reorganisiert. Zellen in den

Mikrostrukturen haben im Gegensatz dazu selten Fibronektin innerhalb der Mikrostrukturen reorganisiert und Fasern gebildet. Der Widerspruch zwischen dem Aufbau eines Zytoskeletts und der Verhinderung von Fibronektin Reorganisation hat es schwierig gemacht, definitiven Schlussfolgerungen über Zellkontraktilität in den Mikrostrukturen zu ziehen. Er hat jedoch darauf hingewiesen, dass Aktinfaserbildung wahrscheinlich durch andere Faktoren beeinflusst ist und zudem helfen könnte, andere Unterschiede zwischen dem Zellverhalten in 3-D Gelen und auf 2-D Substraten zu erklären.

Die Fähigkeit einer Zelle zur Mechanosensation sind ans Aktinskelett gekuppelt. Darum wurde die Aktinorganisation in weichen und harten Mikrostrukturen untersucht. Interessanterweise habe Zellen in weichen Mikrostrukturen (Substratsteiffigkeit von etwa 20 kPa) mit limitierter Ausbreitungsfläche keine feststellbaren Aktinfasern ausgebildet; ganz im Gegensatz zu Zellen auf flachen, homogenen Oberflächen. Deshalb liegt der Schluss nahe, dass nicht Mechanosensation alleine, sondern ebenso Dimensionalität, die Fähigkeit der Zelle ihre Umgebung abzutasten und auf deren Steifigkeit zu reagieren, beeinflusst.

Schlussendlich wurde untersucht, wie der Metabolismus einer Zelle von deren Ausbreitungsfläche und Dimensionalität abhängt. Mit grösserer Ausbreitungsfläche einer Zelle nahm deren Aktivität sowohl auf 2-D Mustern als auch in 3-D Mikrostrukturen zu. Ausserdem wurde beobachtet, dass die metabolische Aktivität in einer 3-D Umgebung grösser ist als in 2-D.

Schlussfolgerungen

Diese Beobachtungen haben gezeigt, dass die für Einzelzellen konzipierten Mikrostrukturen eine wertvolle Ergänzung zu den schon vorhandenen Zellkultursubstraten und nützlich sind, um das Verhalten einer Einzelzelle in einer vereinfachten 3-D Umgebung zu studieren. Die Möglichkeit, die Ausbreitungsfläche der Zelle, die Steifigkeit des Substrates und die Beschichtung innerhalb der Mikrostrukturen zu steuern, hat es ermöglicht, den Einfluss einzelner Parameter auf das Zellverhalten und deren Zusammenspiel zu untersuchen. Die Mikrostrukturen sind ausserdem mit konventionellen Untersuchungsmethoden kompatibel, d.h. erlauben die Beobachtung lebender Zellen mit hochauflösender Mikroskopie. Das mikrostrukturierte Substrat ist dabei geeignet, biophysikalische Grundfragen zu erörtern. Nichtsdestotrotz muss bedacht werden, dass eine künstlich konzipierte Platform nie die genaue *in vivo* Umgebung einer Zellen imitieren kann. Die Aussagekraft solcher Substrate wird immer mehr oder weniger eingeschränkt sein durch die reduzierte und vereinfachte Präsentation biochemischer Liganden und der Abwesenheit richtiger Zell-Zell-Kontakte. Ausserdem ist die Imitation von sehr weichem Gewebe schwierig zu gestalten,

da die Replikation der Mikrostruktur in sehr weiches Material nur beschränkt möglich ist. Trotzdem ist das mikrostrukturierte Substrat geeignet, biologische Fragestellungen zu untersuchen, wie z.B. in Bezug auf die Frage, inwieweit die Dimensionalität die Zellteilung und Stammzellendifferenzierung beeinflusst. Ferner sind zukünftige Anwendungen solcher Zell-basierter Technolgien im Gebiet der Medikamenten-Entwicklung und der Toxizitätsprüfung denkbar.

Contents

2-D	two-dimensional
3-D	three-dimensional
AFM	atomic force microscope/microscopy
APS	ammonium persulfate
ARP	actin related protein
ATP	adenosine-5'-triphosphate
bAB	biotinylated antibody (biotin goat anti-human IgG Fcg)
bDOPE	1,2-Dioleoyl-sn-Glycero-3-Phosphoethanolamine-N-(Cap Biotinyl)
CHO	chinese hamster ovary cell
CLSM	confocal laser scanning microscope
CAM	cell-adhesion molecule
DDPO$_4$	dodecyl phosphate, diacid state
DOPC	1,2-Dioleoyl-sn-Glycero-3-Phosphocholine
E-cad/Fc	human E-cadherin/Fc chimera
ECM	extracellular matrix
EDTA	ethylenediaminetetraacetic acid
FCS	foetal calf serum
FM	fluorescence microscope/microscopy
Fn	fibronectin
Fn 488 / Fn 633	fibronectin labeled with alexa fluor488 / fluor 633 dyes
FRAP	fluorescence recovery after photobleaching
GAG	glycoaminoclycan
GTP	guanosine 5-triphosphate
HeLa	immortal human cervical cancer cell line
HEPES	4(2-hydroxyethyl)piperazine-1-ethanesulfonic acid

HEPES buffer	10 mM HEPES, 150 mM NaCl, adjusted to pH 7.4
HFF	human foreskin fibroblast (primary cells)
HUVEC	human umbilical vein endothelial cell (primary cells)
IHC	immunohistochemistry
M phase	mitotic phase
MAPL	molecular assembly patterning by lift-off
mDIA1	diaphanous-related formin
MPPC	1-myristoyl-2-palmitoyl-*sn*-glycero-3-phosphocholine
MSC	mesenchymal stem cell
MTOC	microtubule-organizing center
NBD-PC	1-Oleoyl-2-[12-[(7-nitro-2-1,3-benzoxadiazol-4-yl)amino]dodecanoyl]-*sn*-Glycero-3-Phosphocholine
NMP	N-Methyl-2-pyrrolidone
NTA	nitrilotriacetic acid
PAAm	polyacrylamide
PBS	phosphate buffered saline
PDMS	polydimethylsiloxane
PEG	poly(ethylene glycol)
PLL-*g*-PEG	poly(L-lysine)-*graft*-poly(ethylene glycol)
PLL-*g*-PEG-biotin	biotinylated PLL-*g*-PEG
PLL-*g*-PEG-rhod	PLL-*g*-PEG labeled with rhodamine
PC	phospho choline
PE	phospho ethanolamine
poly-HEMA	poly (2-hydroxyethyl methacrylate)
POPC	1-palmitoyl-2-oleoyl-*sn*-glycero-3-phosphocholine lipid
PS	phosphoserine
QCM-D	quartz crystal microbalance with dissipation monitoring
RGD	arginine-glycine-aspartic acid
R_{MS}	root-mean-square roughness
R_{SK}	asymmetric roughness, skewness
SA	streptavidin
SA 488	streptavidin labeled with alexa fluor488 dye
SAM	self-assembled monolayer
SiO_2	silicon oxide
SEM	scanning electron microscope/microscopy

SMAP	selective molecular-assembly patterning
SPB	supported phospholipid bilayers
SPR	surface plasmon resonance
TCPS	tissue culture polystyrene
TEMED	N, N, N, N-tetramethyl ethylenediamine
TiO_2	titanium oxide
T_M	liquid-gel transition temperature
TMRE	tetramethylrhodamine, ethyl ester, perchlorate
XPS	X-ray photoelectron spectroscopy

Introduction

This chapter starts with a short overview of eucaryotic cells, with a particular focus on the cytoskeleton and the cell membrane. The behavior of cells in culture as well as a variety of cell culturing platforms, such as 3-D model systems and microwells, are discussed next. Finally, an overview of how the microenvironment of a cell might influence cell behavior is presented, focusing on biophysical parameters, such as cell shape, substrate rigidity, and dimensionality. The conclusion provides a brief, critical overview of the previously discussed cell culturing approaches. Furthermore it focuses on the presentation of our microwell platform while examining the different aspects and advantages compared to traditional cell culturing methods. The motivation of studying cells in a reductionist microwell platform are considered here, while the individual biological questions are introduced in the following chapters.

1.1 The cell

Cells are the structural and functional building blocks for every living organism (fig 1.1) and are the smallest living unit of any organism. A human, for example, has about 10^{14} cells; with typical cell sizes of $10 - 100$ μm and a mass of 1 ng [1]. In this chapter, some general characteristics of a cell, which are relevant for this thesis, are described with emphasis on the cytoskeleton and the cell membrane.
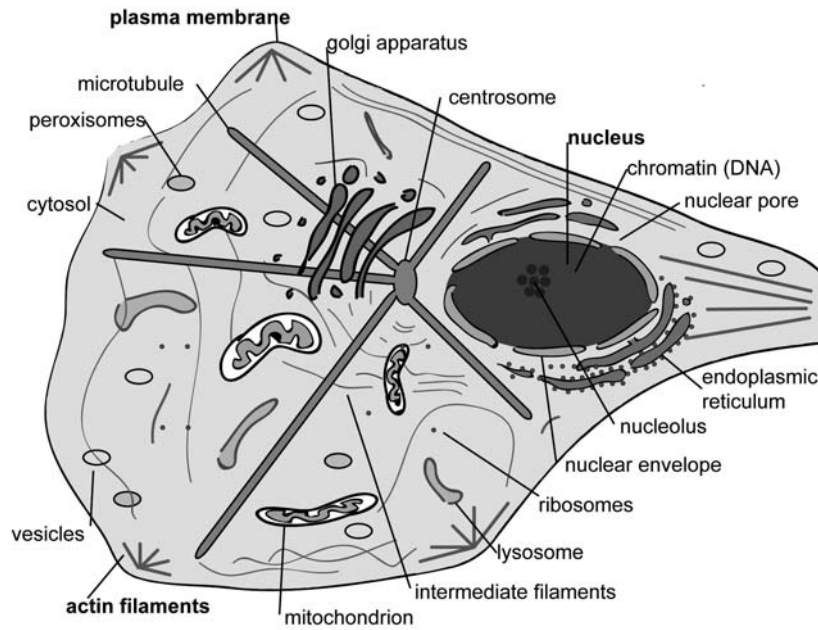
Figure 1.1: *Schematic of an eucaryotic cell.* This schematic presents an eucaryotic cell and its intracellular features. The components described in this chapter as well as the cell nucleus are printed in bold (adapted from [1]).

1.1.1 The cytoskeleton

The cytoskeleton is a system of protein filaments in the cytoplasm of eucaryotic cells. It is responsible for cell shape and for the cell's capacity for directed movements. The cytoskeletal structures consist of small subunits which are only a few nanometers in size. Because the subunits are so small, they can quickly diffuse through the cytoplasm, rendering the cytoskeleton a flexible construct, therefore allowing for fast structural reorganization, disassembly, and reassembly of subunits.

Its most abundant structures are microtubules, intermediate filaments and actin filaments. Microtubules are crucial in the development and maintenance of cell shape, in the transport of vesicles and mitochondria through the cell, positioning of organelles inside the cytoplasm, as well as in cell division and mitosis. The main role of intermediate filaments is in the maintenance of cell-shape by bearing tension and tolerating stretching and bending. The cytoskeletal aspect investigated in this thesis is actin fiber formation (chapter 7), thus a brief overview of the role of actin, and motor proteins are presented in the following paragraphs.

Actin

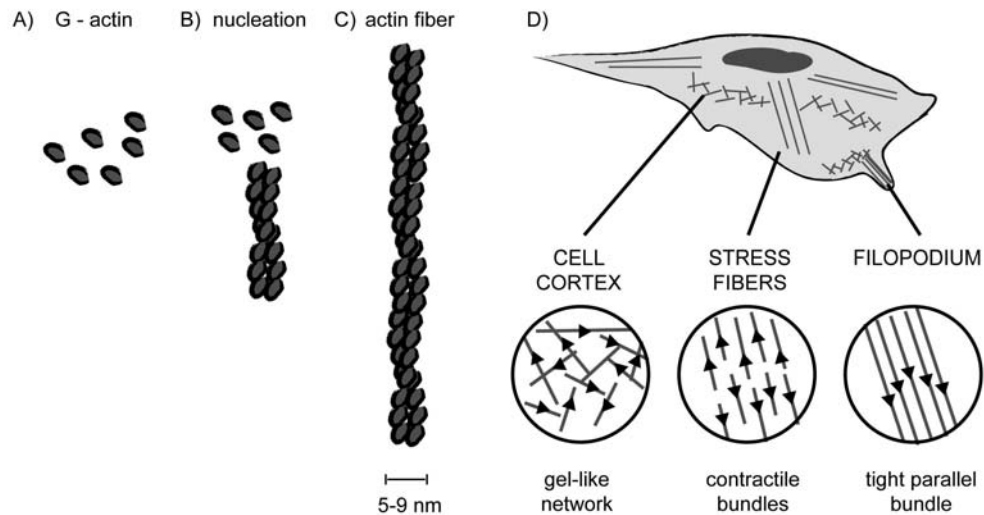***Figure 1.2:*** *Schematic of actin organization.* A) The globular actin molecules are the building blocks of the actin skeleton. B) Single actin molecules nucleate into C) an actin fiber. The actin inside a cell can be organize as gel-like networks, contractile bundles, and tight aligned bundles.

The actin skeleton consists of the protein actin, which has a globular shape. The nucleation of the actin skeleton occurs primarily at the plasma membrane. The actin filaments underlying the plasma membrane determine the shape and movement of the cell. The nucleation is often regulated by external stimuli, such as substrate stiffness or dimensionality, which allows the cell to respond to its environment. Nucleation is catalyzed by a protein complex including two actin related proteins (ARP), each of which is about 45% identical to actin [1]. The ARP complex nucleates actin filaments from the minus to the plus end building a treelike web (fig 1.2 A-D). In most nonmuscular vertebra cells, 50% of the actin is in filaments and 50% in soluble form. Actin filaments can become cross-linked by two different types of proteins, the bundling proteins or the gel-forming proteins. Bundling proteins cross-link actin filaments into aligned bundles; conversely gel-forming proteins hold filaments together in a non-aligned way resulting in a loose network (fig 1.2 D). Two abundant bundling proteins are α-actinin and fimbrin. α-actinin contains two actin filaments that are further apart and it is responsible for the relatively loose cross-linking of actin filaments in contractile bundles. It is also involved in

forming focal complexes and anchoring the stress fiber ends at the plasma membrane. The density of the actin fibers determines if certain proteins, such as myosin (discussed below), can enter the structure and interact with the actin bundles. The looser packing caused by α-actinin allows myosin to enter the structure, interact with the actin filaments, and make stress fibers contractile [1]. Conversely, fimbrin holds two chains closely together with a single peptide chain. It is enriched in aligned actin bundle filaments in filopodia at the leading edge of cells. The very close packing of actin filaments caused by fibrim excludes myosin and thus filopodia are not contractile.

Recent studies have defined regulatory mechanisms that control stress fiber formation. Members of the Rho family of small GTPases, especially RhoA, may be involved in the signalling that controls stress fiber formation [2, 3]. In support, injection of RhoA into subconfluent fibroblast cells has been shown to cause the cells to form extensive stress fibers [4].

The identification of downstream effectors of RhoA, in particular the ROCK protein kinases, lead to an early breakthrough in the understanding of the regulation of stress fibers (fig 1.3). The ROCK protein kinase is a key player in the complex signaling network that controls stress fiber assembly. ROCK is activated by RhoA binding and causes prominent stress fiber formation [5, 6]. ROCK phosphorylates different targets in the pathway leading to actin fiber formation via increased myosin light chain phosphorylation (MLP-PP) and therefore, to increased actomyosin contractility [7].
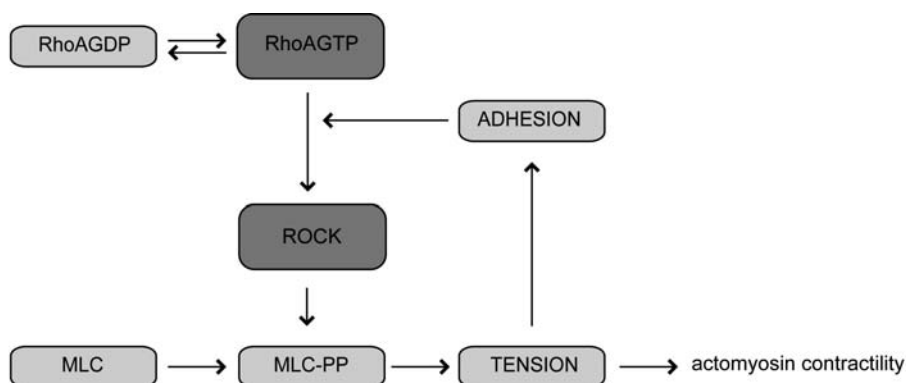

Figure 1.3: *Signaling pathways controlling actin bundling.* Part of the signaling pathway that is influenced in actin bundling is illustrated here. RhoA activation triggers mDia1 expression which provides the actin nucleation activity. RhoA also activates ROCK which initiates different pathways leading to actinmyosin contractility (adapted from [8]).

Motor proteins - Myosin

Motor proteins are a class of molecular motors inside a cell which are able to move along a filament. Motor proteins differ in the type of filament they bind to, the direction in which they move and the cargo they carry. Some are responsible for the transport of membrane-enclosed organelles, such as mitochondria, golgi stack, or secretory vesicles, others are involved in ciliary beating, and cell division. An exemplification is the motor protein myosin, which moves along the actin filament, and is involved in the generation of muscle contraction and contractile forces. Motor proteins, associating with the cytoskeleton, bind to a polarized cytoskeletal filament using energy derived from adenosine-5'-triphosphate (ATP) (fig 1.4).

Myosins are actin-based motor proteins which form bipolar filaments and are presumed to contract the actin skeleton. Myosin II is the "conventional" form of myosin, consisting of two isoforms, muscle and nonmuscle myosin II. The subunits myosin IIA and IIB are found in stress fibers and are important in generating forces within cells. They are normally constructed of a motor, neck and tail domain. The motor domain interacts with the actin and uses ATP hydrolysis to generate force and walk along the actin filament. The neck domain transfers force generated by the motor domain and has binding sites for light chains, which often have regulatory functions. The tail domain is responsible for the anchoring of cargo molecules and positioning of the motor domain so that it can interact with the actin.
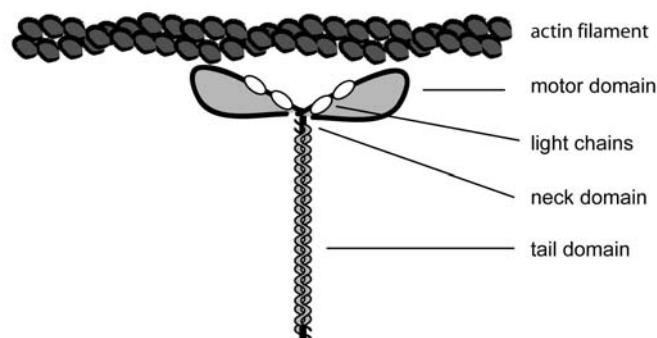

Figure 1.4: *Schematic of a myosin II interacting with an actin filament.* The myosin moves with its motor group along actin tracks. The subunits nonmuscle myosin IIA and IIB are found in stress fibers and are important in generating forces within cells.

1.1.2 The cell membrane

To present a biomimetic system, we also work with artificial cell membranes. A biological membrane defines the inside and the outside of a cell, furthermore it surrounds organelles inside a cell. The observation that cells change their size depending on the osmotic pressure led to the discovery, in 1877, of semipermeable cell membranes [9]. In 1895, the oily or lipid like structure of cell membranes was first described [10]. The first statements describing the electrical membrane potential date back to 1910 (qualitatively) and 1917 (quantitatively) [11]. From these first steps it took until 1972 for the famous fluid mosaic model to be proposed [12, 13]. The fluid mosaic model explains the plasma membrane as a lipid bilayer doped with proteins which are embedded to varying degrees, randomly distributed and have free lateral and rotational mobility. Except for some redefining, such as the more active role of lipids in the membrane, the model is still valid today. The plasma membrane acts as a semipermeable barrier preventing the free diffusion of molecules, water, and ions across the membrane. Specific proteins embedded in the membrane perform several distinctive functions and work as pumps, channels, enzymes and receptors maintaining chemical and electro-physical gradients required for cell survival (fig 1.5). The cell membrane is composed primarily of lipids, but depending on the cell type, the mass percentage ratio of lipids to proteins can vary between 25 and 75% [1].
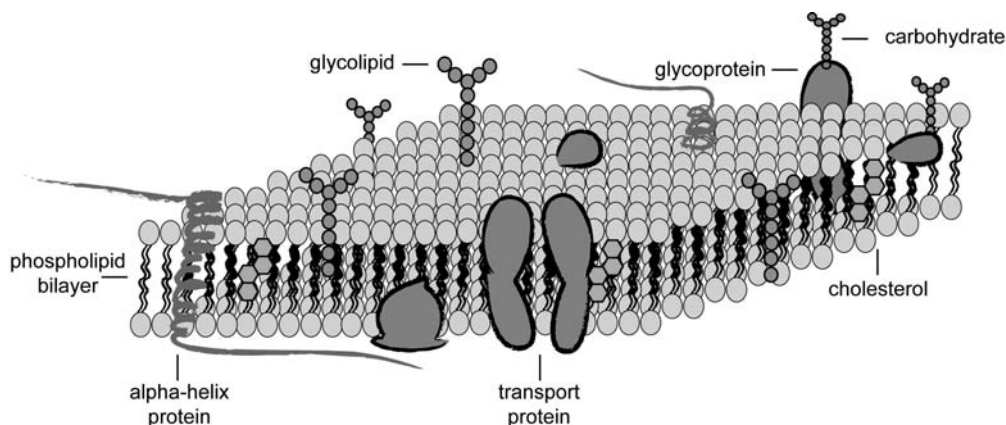

Figure 1.5: *Fluid mosaic model of a cell membrane.* The cell membrane consist of a phospholipid bilayer. It is doped with proteins which are embedded, randomly distributed and have free lateral and rotational mobility.

1.1.3   Lipids and membranes

Phospholipids and lipid assemblies

Phospholipids are the main constituents of biological membranes. Their chemical structure has a common motif: two fatty acid tails and a polar head group (fig 1.6 A). The fatty acid tails are usually composed of a variable number of double bonds ranging from 0 to 3. The number of carbon atoms in the most common lipids is 16 or 18. The polar head group is formed by a phosphate group [1]. In phosphoglycerides, acyl chains are linked to the polar group via glycerol. Because of the presence of hydrophobic tails and polar hydrophilic head groups, these molecules are amphiphiles.

The driving force for the assembly of a cell membrane in an aqueous environment is the hydrophobic effect. Amphiphilic molecules try to shield their hydrophobic parts by arranging themselves into aggregates. The observed lipid assembly is largely dependent on the geometric shape of the monomer (fig 1.6 B). In aqueous solution, large hydrophilic heads compared to the hydrophobic tails result in micelle packing. Cylindrical molecules rearrange themselves into a bilayer structure as in the cell membrane. Cone shaped molecules organize themselves into inverted micelles [14].

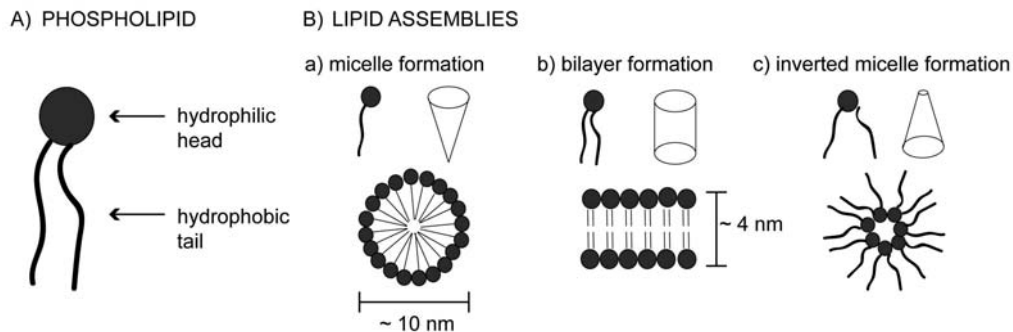**Figure 1.6:** *Phospholipids and lipid assembly.* A) A phospholipid consists of a hydrophilic head and a hydrophobic tail. B) The geometry of the lipid in aqueous solution defines the shape of the assembly. a) A large hydrophilic head and a smaller tail results in micelles. b) Cylindrical shaped molecules form a planar bilayer structure. c) A small head group and larger tail results in an inverted micelle structure (adapted from [14].

Supported phospholipid bilayers

SPBs are interesting model systems for cell membranes [15, 16] and a novel system for cell culture substrates [17–21]. Supported phospholipid bilayers (SPB) can be formed on a solid support by vesicle rupture (fig 1.7 A). An SPB consists of two leaflets where the hydrophilic head groups are exposed on both sides of the membrane and the hydrophobic tails are hidden within the membrane. They have a planar structure and are approximately 5 nm thick and separated from the substrate by a $1 - 1.5$ nm thick layer of water [22]. Several factors seem to play an important role for vesicle adsorption and bilayer formation, for example charge, hydrophilicity and roughness of the substrate [23], as well as charge of the vesicle [24] and lipid phase, which is dependent on temperature [25], are all known to play a role. Furthermore, osmotic pressure [26], vesicle size [26] and concentration [27] might influence the vesicle surface interaction. Once an SPB is formed, it normally does not tolerate exposure to air. However, polymerized SPBs [28], poly(ethylene glycol) (PEG) [29], cholesterol [30] and streptavidin (SA) functionalization [31] have been shown to increase the stability of the SPB structure in air.

Individual lipids within an SPB have lateral mobility (fig 1.7 B) and the diffusion coefficient depends on the size of the hydrophobic tail, where a larger lipid anchor results in slower diffusion [32]. The diffusion coefficient also depends on the temperature of the surrounding of the SPB. The liquid-gel transition temperature (T_m) divides the lamellar liquid phase above T_m (fig 1.7 B) from the lamellar gel phase below T_m (fig 1.7 C). In the more ordered state of the gel phase, the lipids are more closly packed and their hydrophobic chains stretched. This results in the suppression of diffusion. The lateral diffusion can be followed and quantified by the fluorescence recovery after photobleaching technique (FRAP) (see section 3.7.3).

Besides lateral mobility, individual lipids can also move between the leaflets, this process is called flip-flop. However this movement is relatively slow (fig 1.7 D) [33]. The flip-flop rate is increased at T_m due to defects at the boundaries between the liquid crystalline and gel crystalline phase [34]. The slow flip-flop rate is important for biological membranes as an asymmetric distribution of lipids is crucial for the functionality. Lipid head groups can specifically act as docking sites for proteins on one side of the membrane, and some extracellular signals act through membrane receptor proteins to stimulate intracellular signaling molecules [35].

SPBs made with PC lipids have been reported to be resistant against protein adsorption [36] and cell adhesion [37–39]. This characteristic is not fully understood yet, but

the large number of water molecules that associate with the PC head group and as well as the lateral fluidity of the SPB creating a water-like interface are assumed to play a critical role [40].
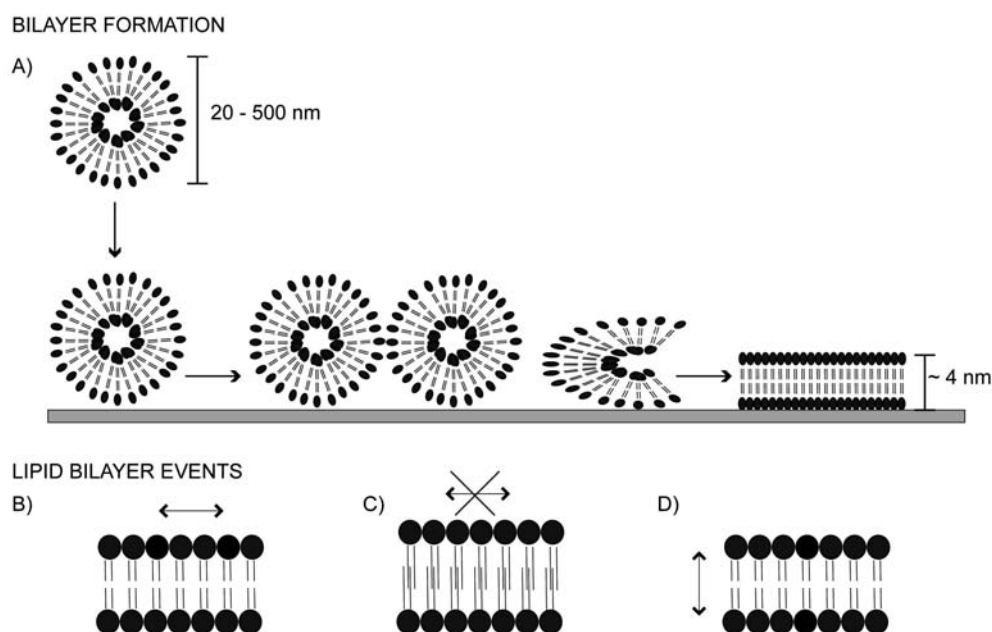
Figure 1.7: *SPB formation on a planar substrate.* A) Vesicles adsorb on a surface and at a certain density rupture and fuse into a planar SPB. Individual lipids in an SPB have lateral mobility and they exist in two different phases, B) the mobile lamellar liquid phase above T_M and the C) immobile lamellar gel phase below T_M. D) Additionally, they can also flip-flop, move between the different leaflets.

Interactions of vesicle with different surfaces

Depending on the surface, the possible interactions of liposomes with a surface result in bilayer formation, monolayer formation, or vesicle adsorption. In this study, quartz crystal microbalance with dissipation monitoring (QCM-D) (see section 3.7.1) was used to study the bilayer formation. The QCM-D response for the possible interactions are described in detail by Keller *et al.* [23]. Briefly, on oxidized gold, for example, vesicles adsorb as intact vesicles and do not rupture (fig 1.8 A). On very hydrophobic surfaces, such as pure gold, a monolayer formation is observed, the typical frequency decrease is 13 Hz (fig 1.8 B). On glass, SiO_2 or mica, vesicles build an SPB on the surface (fig 1.8 C). The resonance frequency decreases when vesicles adsorb onto the surface until it reaches a minimum. When vesicles start to rupture, they release their water content. The frequency decreases

to -26 Hz, the characteristic frequency change of an SPB formation. Meanwhile, the dissipation increases when the vesicles start to attach to the surface which correlates with the rigidity of the adsorbate. After rupturing, the dissipation goes back to its initial value because an SPB is a very thin and rigid layer.
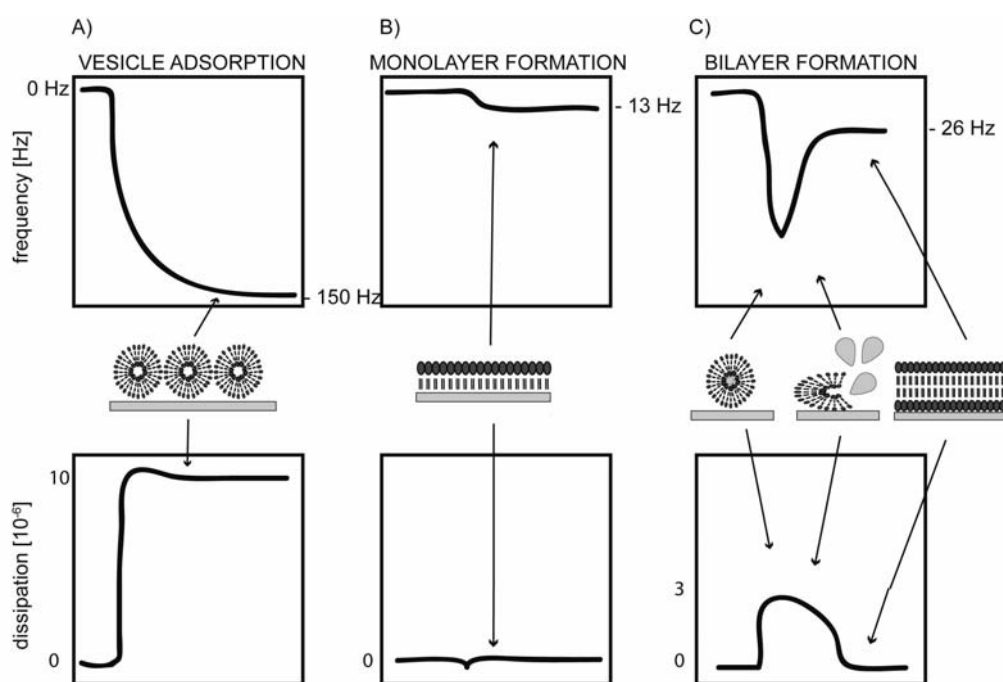
Figure 1.8: *Schematic QCM-D response of the interaction of vesicles with different surfaces.* The interaction of vesicles with a surface can result in A) vesicle adsorption as on gold, B) monolayer formation as observed on very hydrophobic surfaces, and C) SPB formation as described for glass, mica, and SiO_2. The top row shows the typical frequency changes for the three different cases, the bottom row the dissipation change after the vesicles had interacted with the surface (adapted from [23]).

SPB formation and PDMS

Polydimethylsiloxane (PDMS) is a material frequently used in biomedical research, for microfluidic chips and cell culture platforms. Therefore, the ability to form SPB on PDMS is briefly discussed in this paragraph. PDMS is a hydrophobic elastomer, the surface of which can be converted into hydrophilic SiO_x by oxygen plasma treatment. Oxidized PDMS has been shown to be suitable for SPB formation and the SPB can even be transferred to a glass substrate by microcontact printing [41]. Furthermore, depending on the oxygen plasma treatment time, the lipid interaction with PDMS can be tuned. Unmodified PDMS favors the formation of fluid lipid monolayers; with increasing plasma oxidation, PDMS rejects lipid adhesion, adsorbs intact vesicles, and finally favors SPB formation [42].

SPBs in cell studies

SPBs are a novel system for cell culture substrates [17–21]. Non-cell adhesive SPBs [43] can be functionalized with other molecules, such as carbohydrates, amino acids and proteins. Coupling is typically done to the headgroup functionalized lipid anchor. Possible functionalization strategies include: i) biotinylated lipids that can be linked to a biotinylated protein via streptavidin [44, 45]; ii) nitrilotriacetic acid (NTA) functionalized head groups that can be modified by chelating of nickel ions, followed by conjugation of proteins exposing sequential histidines [46]; iii) maleimide functionalized head groups that can couple to proteins with available free thiols [17, 47]; iv) N-hydroxysuccinimide (NHS) functionalized head groups that can covalently bind to amines common in many proteins [48].

Early studies used the phospholipids primarily to investigate the cell response to a certain system. For example, the question of cell-cell interactions in the adaptive immune system was investigated. The main purpose of the SPB was to mimic a specific cell type and the SPBs were modified such that they exposed a Fc fragment [16, 49]. Immunospecific cells settled on this SPB and the cell response was studied [50, 51]. Mossmann *et al.* found a correlation between the geometrical distribution of receptors and activation which could explain noise suppression in immunological amplification [52].

Later studies involved non-antigen mediated cell adhesion and focused on the aspect of mobility in cell-extracellular matrix (ECM) interactions. Therefore, SPBs have been functionalized with ECM peptide sequences [17, 21, 53]. Cells can rearrange the ligands resulting in clustering of cell receptors, strengthened cell attachment [18, 49, 53–56] and facilitated cell spreading [16, 44]. The presentation of the ligand is crucial to cell response and important factors are ligand conformation [57, 58], orientation [59], availability [60] and density [17, 21, 59–61].

1.2   Cells and their microenvironment

Scientists have long been interested in identifying the signals which dictate the shape and structure of cells, tissues, and whole organisms. Every cell is embedded into a microenvironment which consists of other cells and ECM. This matrix consists of a variety of fibrous proteins, such as fibronectin (Fn), collagen, elastin, and laminin. The other main component is polysaccharide chains called glycosaminoglycans (GAGs) which normally covalently link to proteins. These macromolecules are secreted locally and assembled into

an organized meshwork by the cell itself. The cell's microenvironment can be divided into geometrical, mechanical, and chemical components. The geometry is determined by the cell shape, the mechanics by the rigidity of the microenvironment and the chemistry by the extracellular molecules with which the cell interacts. These properties of the local cell microenvironment regulate cell behavior in concert with autocrine and paracrine soluble or matrix bound signaling molecules [62]. *In vivo*, these properties are defined by the ECM and adjacent cells.

Further understanding and insight into biology is often driven by advances in technology. Both curiosity and a desire for efficiency have advanced our ability to manipulate materials with great precision on the micrometer and, more recently, on the nanometer scale. Therefore, progress in technology is also a crucial step toward studying and manipulating the cell and its microenvironment. The following paragraph briefly describes the technical progress in observing the cellular world.

The discovery of light microscopy during the 17th century opened a new era for biology. This instrument permitted the discovery of a previously unknown cellular world. With the development of fluorescence microscopy, it was possible to detect specific proteins and other molecules in cells and tissues, giving more precise information on how a cell responds to certain stimuli. In the 20th century the appearance of microelectronics provided the tools to overcome the observer status and to start manipulating objects (some of them living) at the micron scale. The Nobel-prize winning inventions of electron microscopy in 1931 and scanning tunneling microscopy in 1981 allowed us to look into the 'nano-world'. The images provided by these new technologies, particularly in biology, made us quickly realize that we needed new tools to access the individual building blocks of living organisms (*e.g.* proteins, DNA, and supramolecular complexes). A controlled microenvironment for cells might help to improve the understanding of how the microenvironment influences cellular response. Finally we are getting closer to understanding the miracles of the complicated processes of life [63].

1.2.1   Cells in culture

Given appropriate surroundings, most animal cells can live, multiply and express differentiated proteins in culture. The advantage is that cultured cells can be monitored continuously or analyzed biochemically. The effects of adding or removing certain molecules, growth factors, or signaling molecules can be explored. From the beginning of cell cul-

ture in the early 20th century until the present day, there has been a great deal of progress in controlling the cell environment and tuning its properties. This section gives a short overview on cells in culture, including cell culture inside microwells.

Cells on surfaces

The surface itself is seen as increasingly important for materials employed in biomedical technology [64–66]. Surface properties, such as topography and surface chemistry, have a strong impact on cell behavior. As early as 1914 Harrison *et al.* showed that cells respond to solid structures such as spider webs or vinyl music records [67].

Anchorage dependent cells need the attachment to a solid substrate to survive. They have a number of different adhesion receptors, such as integrins, which can interact with the chemistry presented on a surface [68–71]. Their interaction with the surrounding is very complex since they can bind to various matrix proteins, such as Fn, laminin, and collagen. The linkage between the cell and the ECM takes the form of large, dynamic protein complexes, called focal adhesions [72]. Integrins, vinculin, paxilin, and many other proteins are involved in focal adhesions, rendering it an extremely complicated structure [73]. After binding to ECM ligands, the cell initiates an initial clustering of integrins which is associated with the formation of focal adhesions. With time, the focal adhesions progressively mature into adhesion complexes which provide an ever stronger linkage between the ECM and the cytoskeleton. In motile cells, focal adhesions are being constantly assembled and disassembled as the cell establishes new contacts at the leading edge, and breaks old contacts at the trailing edge of the cell.

Focal adhesions function not only as the mechanical linkages that anchor the intracellular cytoskeleton to bound integrins and the ECM, but also as biochemical signals for many regulatory pathways [74–77]. They have been heavily studied during the last decades and are known to have a crucial impact in cell development, mechanotransduction, the organization of the actin skeleton, and thereby on cell behavior in general [71, 78, 79]. Integrins are involved both in the inside-out and the outside-in signaling and serve therefore as a communication unit across the plasma membrane [68].

3-D substrates for cell culturing

Cells live in a complex 3-D environment, therefore there is a need for 3-D tissue models *in vitro* as they are closer to the *in vivo* situation of a cell. Animal models can capture important aspects of human responses and bear many similarities to humans. However, they fail to capture important aspects, for example many pathogens (*e.g.* Hepatitis C) are species specific. Another issue is the ethical considerations. Therefore, it would be helpful to have a model system that successfully mimics the cellular response in humans, so that the need for animal models can be reduced.
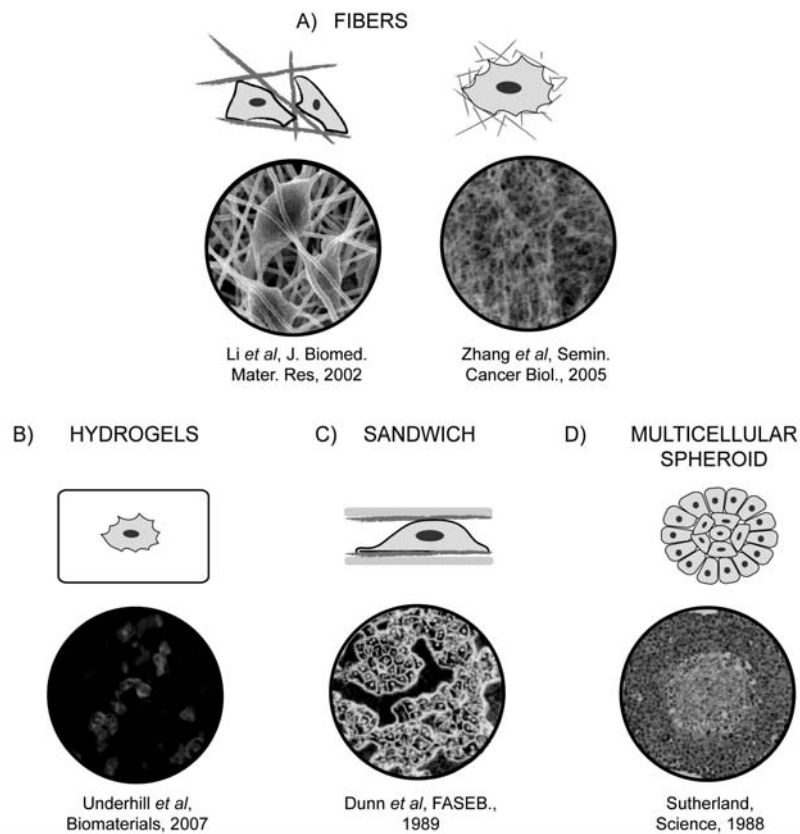
Figure 1.9: *3-D cell culture models.* A) Artificial 3-D models can consist of fibers of different length scales and different materials, such as biodegradable electro-spun fibers made of poly(D,L)-lactide-*co*-glycolide [80] or peptide nanofibers [82]. B) Gels, like hydrogels are a popular 3-D model system. They can be used to maintain the phenotype of hepatocytes by encapsulation of the cells in a PEG-hydrogel [91]. C) Sandwich cultures allow for long term culturing of hepatocytes [86]. D) In multicellular spheroids, the cell itself provides the 3-D environment for the other cells and this model system shows an intermediate complexity between a real tissue and cells on a Petri dish [89].

The commonly used 3-D matrices can be divided into 4 classes: (i) Fibers (fig 1.9 A) [80, 81]; (ii) peptide scaffolds (fig 1.9 A) [82]; (iii) microfabricated substrates, such as microchannels [83]; (iv) and gels including hydrogels (fig 1.9 B) [84], Matrigels [85], collagens [86], cell-derived gels [87], or gel sandwich culture [86, 88] (fig 1.9 C). Another approach to provide a 3-D environment is the multicellular spheroid system where the cells provide the 3-D environment for the other cells [89] (fig 1.9 D). This model has high potential in high-throughput drug screening especially for cancer therapy [90]. Animal-derived matrices, *e.g.* matrigel, collagen gels, have been used widely. They present to the cell an *in vivo* like situation, but they often contain residual growth factors and undefined or non-quantified impurities. Furthermore, they might trigger a different cell response from experiment to experiment due to batch to batch variations. Additionally, animals are still needed to provide the matrices. Therefore, it is also of great interest to work with synthetic 3-D matrices.

Even though cells in 3-D models capture the dimensional aspects of the cell environment, they also have certain limitations. Within 3-D systems, concentration gradients might exist [92]. Since the cell behaves differently depending on the chemical microenvironment, this might result in different behavior of cells in the middle from cells on the surface. Furthermore, it can trigger chemotaxis, meaning cells start to migrate through the system depending on the chemical gradient that a cell experiences [92]. More specific limitations and comparisons between the different systems relevant for this thesis are discussed in the conclusion of this chapter.

Microwells as cell culture platforms

This section gives a short overview of the use of microwells by other groups. The primary differences between our microwell approach and those described in the literature, namely the confinement of single cells and as an alternative 3-D cell culture platform, are discussed in the conclusion section of this chapter.

Microwells in biology have the advantage of reduced volume requirements, and provide a defined localization. The wells confine the migrating area of highly motile cells and facilitate time lapse imaging [99]. Early studies in microwells investigated the transport and activity of enzymes [100] and cell population control [101]. Furthermore, the curiosity to understand how the cell response depends on environmental stimuli and the awareness of the heterogeneity within a cell population, increased the interest to analyze a huge number of single cells [102]. This allows for the determination of the distribution of cell responses to an external stimuli, instead of an average over the whole cell
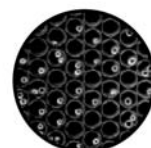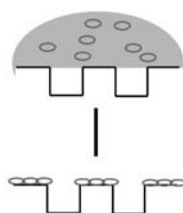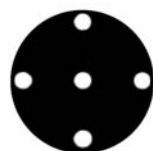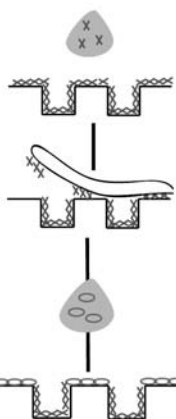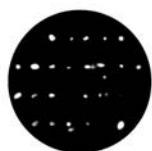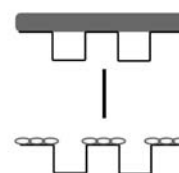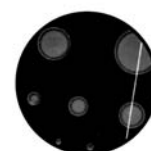
Figure 1.10: *Microwells as cell culture platforms.* A) Microwells can be used as cell culture platforms without any specific surface modification. U-shaped wells in PDMS allow for hydrodynamic trapping of single cells with special geometry that catch only one single cell [93]. Microwells made in photo resist offer the potential for a parallel, quantitative analysis of single cells [94]. Trapping of single cells in large arrays of microwells in PDMS was optimized to capture as many single cells as possible [95]. B) Microwells with a cell-adhesive coating inside the microwell and a passivated plateau are presented here. a) Trapping of air bubbles inside the microwells allows for coating of the plateau with a passivating protein while in a second step a cell-adhesive protein can be adsorbed inside the microwell [96]. b) In a first step the microwell platform is completely covered with a cell-adhesive protein. In a second step the protein on the plateau is subtracted and the subsequent incubation with a protein solution that is resistant to protein adsorption renders the plateau non-cell-adhesive [97]. c) First the plateau is passivated against protein adsorption via a inverted microcontact printing method and in a second step, the cell-adhesive protein can adhere inside the microwell [98].

population. Furthermore, inside microwells all the cells interact with exactly the same microenvironment which can be controlled and is well defined [93, 103].

Microwells have been used for both adherent and non-adherent cells [104]. They have been produced in a variety of different materials using microfabrication techniques without any specific surface chemistry (fig 1.10 A). They can be etched in silicon [105] or photo resist [94], transferred into agarose [101, 106], PEG-hydrogels [107–109], or PDMS [93, 95, 110, 111]. These microwells enabled the fabrication of arrays of bacteria [105], characterization and sorting of individual leukocytes [108], studying stem cell fates [94, 109–111], and the analysis of the effect of cell-cell contact on proliferation behavior [106].

The interest to present the cell a specific ligand only inside the microwell, led to different techniques of specific protein deposition inside microwells (fig 1.10 B). Ostuni *et al.* trapped air bubbles inside the microwells and subsequently passivated the top with BSA and coated the wells with Fn (fig 1.10 B,a) [96]. Lovchik *et al.* introduced substractive patterning where they simply removed the protein coating on the plateau and backfillled it with BSA (fig 1.10 B,b) [97]. The inverted microcontact printing technique was developed by Dusseiller *et al.* [98] and is the main technique used in this thesis (for more details see section 3.5.1).

1.2.2 Biologically relevant patterns

Non-fouling surfaces

The vast majority of biological interactions are based on highly selective and specific interactions. Uncontrolled, non-specific interactions are usually the cause of device failure in a biological environment as the cell is unable to recognize and respond to it in a specific manner. For example, the rejection of an implant due to immune reactions or the false response of biosensors are often caused by the non-specific adsorption of proteins.

Providing a substrate, which the cell can interact with through specific interactions, requires the ability to define areas of specific interactions in a non-interacting background. Biology evolved to utilize a combination of lipids, sugars, and proteins (i.e. cellular membranes) as the mobile and highly hydrated surface at which most bioprocesses take specifically place. Several groups have managed to mimic this strategy using lipid based micro- and nanopatterns. In biotechnology, approaches utilizing non-ionic and hydrophilic materials, such as polyacrylamide (PAAm) [112] or poly(ethylene glycol) (PEG) [113], has

been shown to be more stable and compatible with the processing steps of current technology methods. Various techniques exist to attach PEG to surfaces, *e.g.* end-grafting methods [114, 115], block copolymers, such as pluronics [116, 117], self-assembled monolayers (SAM) [118, 119], interpenetrating networks [120] and the spontaneous adsorption of polyelectrolyte grafted PEG [121]. In our lab the passivation is achieved with a graft-copolymer that consists of a poly(L-lysine) (PLL) backbone presenting PEG side chains (PLL-*g*-PEG). In solution the positively charged backbone adsorbs spontaneously onto negatively charged surfaces and effectively blocks the adsorption of proteins or cells [122, 123]. After eliminating the non-specific interactions with a surface, different micro- and nanopatterning methods can be used to introduce selected biofunctionalities onto well defined spots on the substrate, in an otherwise 'silent' background. Proteins, DNA, sugars, or short peptide sequences are commonly introduced onto surfaces to elicit specific cellular responses or to capture specific ligands from a complex biological sample.

Molecular assembly patterning by lift-off

An example of such a patterning technique is the 'molecular assembly patterning by lift-off' (MAPL) technique, developed by Falconnet *et al.* [124]. MAPL allows for the fabrication of patterns in the micrometer range by photolithography [124]. X-ray interference lithography or nanoimprint lithography allowed patterning using this technique to be expanded into the nanometer range [125]. In the first step a pattern was transferred into a resist onto a negatively charged surface, such as niobium oxide (Nb_2O_5), silicon oxide (SiO_2) or titanium oxide (TiO_2) (fig 1.11 A). Afterwards, functionalized PLL-*g*-PEG was adsorbed from solution. The resist was removed with an organic solvent without removing the functionalized PLL-*g*-PEG from the surface. To render the background protein-resistant unfunctionalized PLL-*g*-PEG was subsequently adsorbed. A similar principle was used to prepare 2-D patterned samples with Fn islands in a PLL-*g*-PEG background (details see section 3.3.2) (fig 1.11 B).

Selective molecular assembly patterning

Michel *et al.* developed the 'selective molecular assembly patterning' (SMAP) as a patterning technique that takes advantage of the chemical contrast between SiO_2 and TiO_2 [126]. Alkane phosphates form ordered self-assembled monolayers (SAM) from aqueous solutions on the TiO_2, but not on the SiO_2. Exposing a SiO_2-TiO_2 surface to a SAM solution therefore transformed the TiO_2 structures into hydrophobic, strongly protein interactive regions. A polycationic PEG-grafted polymer solution was then exposed to the

sample. The negatively charged SiO_2 regions allowed for adsorption of the polymer and rendered them protein resistant. The subsequent protein exposure led to protein adsorption on the SAM coated region and thereby a protein-PLL-*g*-PEG pattern was created. The basic feasibility of SMAP had been successfully demonstrated on TiO_2/SiO_2 2-D micropatterned surfaces produced by photolithography [126, 127]. The same principle was used to coat the bottom of a microwell differently from the walls (see chapter 5).
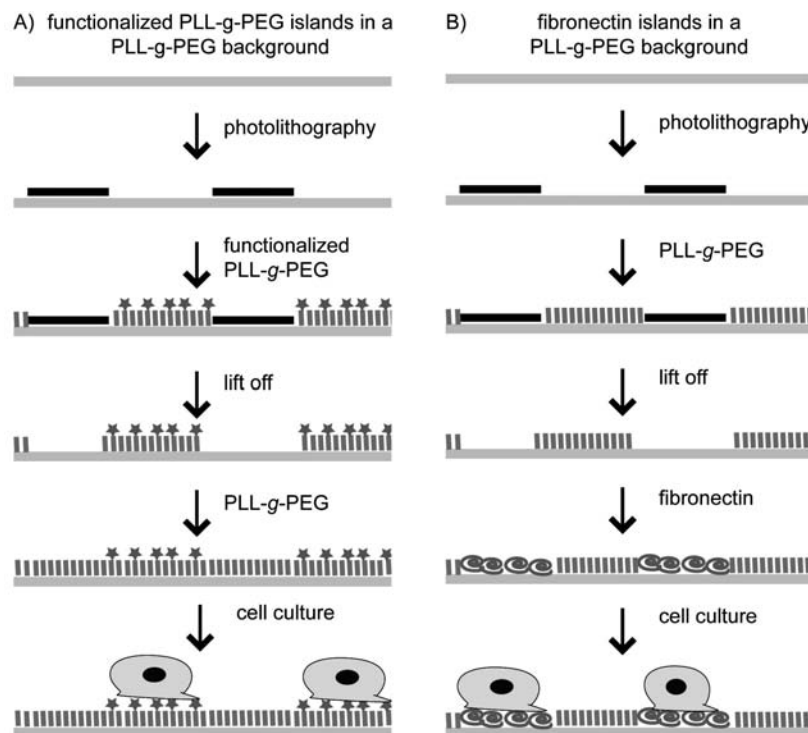
Figure 1.11: *MAPL process for 2-D patterns using two methodologies.* A) After transferring the pattern into a photo resist, functionalized PLL-*g*-PEG was adsorbed onto the sample. The photo resist was removed and the blank areas are backfilled PLL-*g*-PEG [124]. B) After transferring the pattern into photo resist, PLL-*g*-PEG was adsorbed onto the sample. The photo resist was removed and the blank areas were backfilled with Fn. The resulting Fn-PLL-*g*-PEG pattern allowed for cell attachment on the Fn islands and while the PLL-*g*-PEG areas were resistant to cell adhesion.

1.2.3 Influence of geometrical, mechanical and dimensional properties of the microenvironment on cell behavior

Much of our understanding of the role of the microenvironment in regulating cell physiology has been revealed using reductionist cell culture systems with tunable substrate stiffness, ligand density, topography, or shape in two or three dimensions. Controlling and regulating biological processes with engineered cell culture platforms or scaffolds might prove useful for tissue engineering applications where a specific cell phenotype must be stimulated or maintained. The knowledge of the influence of the microenvironment on cell behavior might also permit the maintenance of a specific phenotype, for instance hepatocytes [86], or be important for *in vitro* cytotoxicity [128] and drug screening applications [129, 130].

Defining cell shape - Cells on patterned surfaces
The demonstration of anchorage independence in malignant or transformed cells initiated broad efforts to determine the relationship between cell adhesion and shape on cell function. Transformed cells have been shown to loose their shape-responsiveness controls which may give some indication about tumor progression [131]. Early efforts demonstrated that virus-transformed cells grew into colonies in agar suspension in the absence of physical support [132, 133]. In addition, adhesion to glass fibers of increasing length was used to demonstrate that not only adhesion to a solid support but cell extension beyond a minimum distance was critically important for progression through the cell cycle [134]. Cell spreading was also investigated by modulating the adhesivity of tissue culture polystyrene (TCPS) with poly-(2-hydroxyethyl methacrylate)(poly-HEMA), and a clear correlation between proliferation and spreading of individual cells on planar surfaces was confirmed [135]. Early efforts tried to determine how cell adhesion and shape impact cell function. But the relationship was complicated and research was limited by the rudimentary tools available, which, for instance, were incapable of differentiating between the effects of ligand density from the extent of cell spreading.
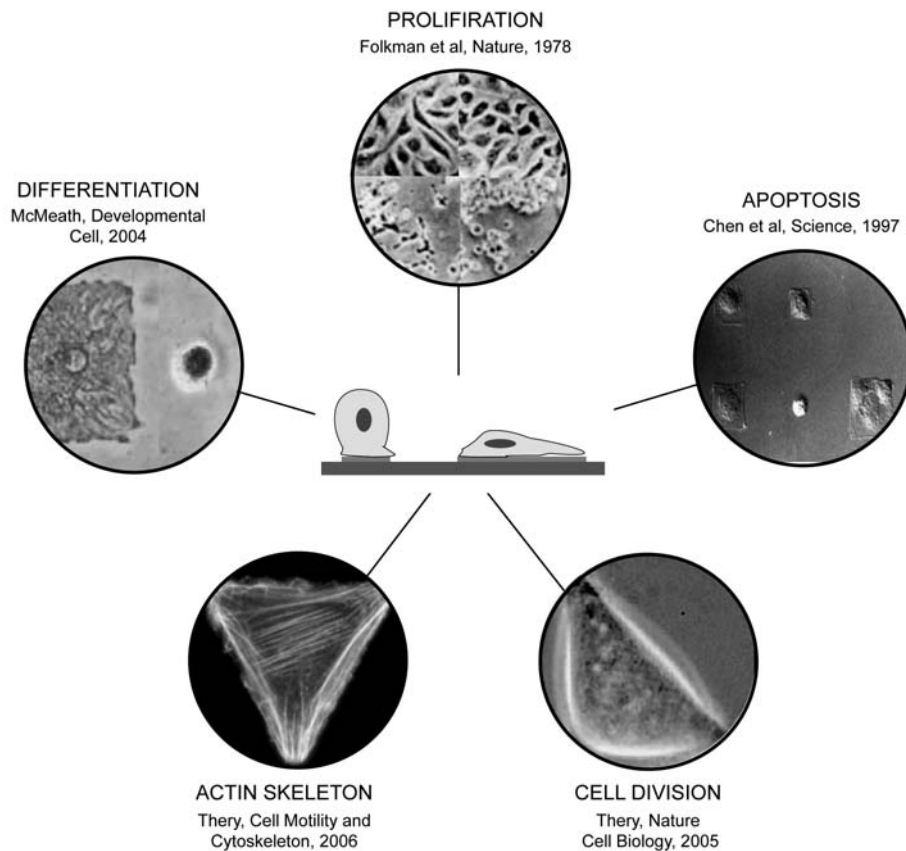
Figure 1.12: *Influence of cell shape on cell behavior.* The images are explained clockwise. *Proliferation*: The more a cell is allowed to spread, the greater is the observed DNA synthesis and cell growth [135]. *Apoptosis*: Cells on a small spreading area undergo apoptosis, in contrast cells on bigger spreading areas survived [136]. *Cell division*: The cell shape guides the orientation of the cell division axis, and therefore the future position of the daughter cells [137]. *Actin skeleton*: Cells distribute stress fibers in response to the geometry of the adhesive environment [138]. *Differentiation*: Cell shape regulates commitment of human mesenchymal stem cells (hMSCs). hMSCs on small patterns differentiate into adipocyte cells on bigger patterns into osteoblast [139].

The technology platform of microfabrication, developed primarily for and by the semiconductor industry, has since become a useful tool in the emerging field of biotechnology for generating patterns on surfaces in the micrometer range. By generating cell-adhesive patterns on a surface one can tailor well-defined model surfaces for biological studies [140, 141]. Generally, cell adhesive patterns consist of a protein pattern in a protein resistant background, such that cells can only adhere to the protein areas [142–144]. As described above, a crucial point to produce an effective pattern is the passivation of the background. In the fields of biology and implantology, the development of patterned substrates became important because it allowed for the decoupling of the properties of a microenvironment in reductionist systems. These advancements were a major break-

through since they allowed the independent decoupling of cell spreading from the quantity of bound matrix ligands. Using chemical 2-D micron-sized patterns, a number of seminal studies have shown that these properties regulate a seemingly endless variety of observable cell responses (fig 1.12) and contribute to a number of biomaterial-related research fields ranging from biosensors and tissue engineering to fundamental cell-surface interactions [140, 142, 145–148]. 2-D patterns have proved very useful for the controlled study of apoptosis [136], cell spreading, migration, proliferation, mechanics and communication [149–154]. Control over spatial arrangement of the cell adhesive patterns influences stress fiber formation [138] and enables one to steer, *e.g.* the mitotic spindle during cell division [137] or the placement of neuron cells [155] which can be used in sensors [156, 157]. Furthermore, even stem cell differentiation could be tuned depending on the cell shape and its interplay with cytoskeletal tension [139].

More recently, other tools have become available which can be used to vary the nanometer spacing of individual adhesive molecules [158, 159]. Therefore, investigating or manipulating features in the range of single protein/receptor molecules [160, 161], such as controlled binding of integrins or the investigation of integrin clustering [162], is now possible. These tools also contributed to our understanding of cell behavior by demonstrating that there is a maximal ECM ligand separation, above which integrin clustering-mediated stimulation of cell spreading and adhesion is hindered [163].

An interesting example of how cell shape steers cell fate is presented by Chen, Ingber *et al.* [136]. Cell spreading was restricted by progressively decreasing the size of ECM coated adhesive islands (fig 1.13 A). The shape of bovine adrenal capillary endothelial cells, or spreading area, was found to govern whether individual cells grew or died. Cells on squares with a side length of 10 μm showed increased apoptosis rate while cells on 20 μm squares survived. Cell spreading was also varied while maintaining the total cell-matrix contact area constant (fig 1.13 B). Cells, which could spread over many small islands, but with the same total amount of ECM attachment sites per cell (many circles 3 μm in diameter separated by 6 μm), showed similar survival rates to cells on a homogenously coated substrate. Cells on one single cell-ECM contact site of the same total area (circle 20 μm in diameter and separated by 40 μm) showed decreased cell survival and growth. Therefore, Chen, Ingber *et al.* concluded the spreading area and not the area of ECM contact was the critical factor that directed cell survival and the local geometry might represent a fundamental mechanism which is responsible for cell survival and death.
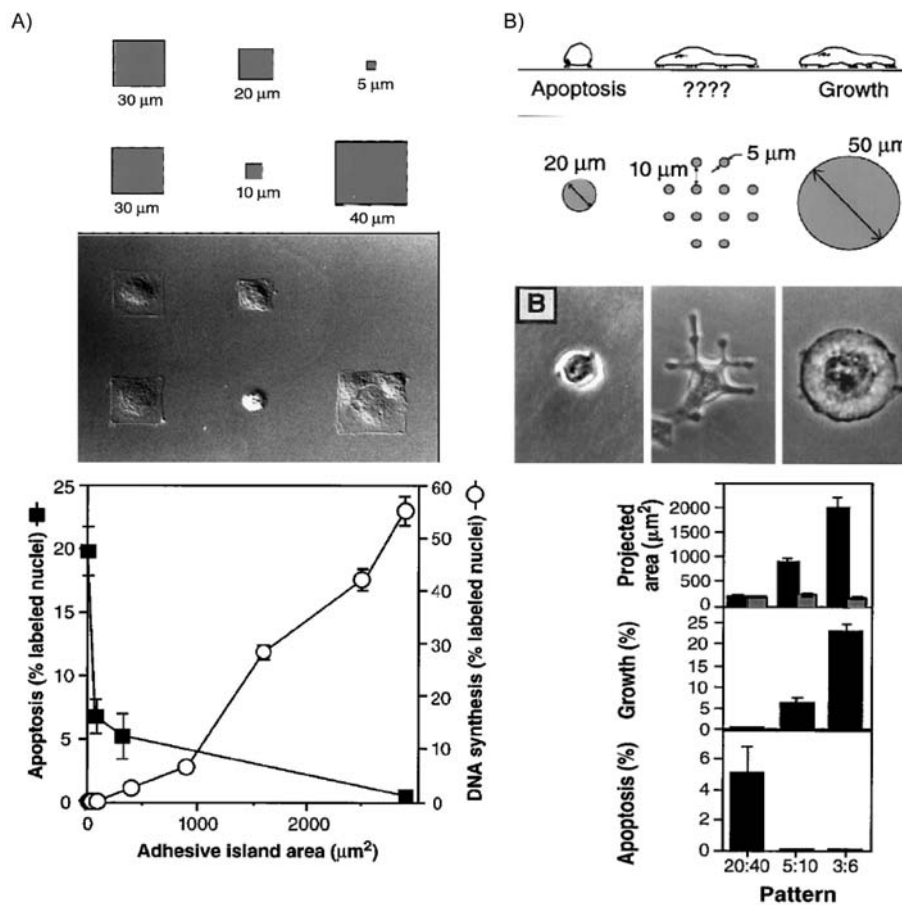
Figure 1.13: *Influence of cell shape on cell life and death.* A) The effect of spreading area on apoptosis is presented here. Schematic pattern design with different sized squares and Nomarski view of the effective shape of bovine adrenal capillary endothelial cells are shown in the first figure. The apoptotic and DNA synthesis index are plotted as a function of pattern size and show that cells on pattern < 1000 μm^2 had reduced DNA synthesis and higher apoptosis rates. B) Cell spreading functioned as a regulator of cell fate rather than cell-ECM contact. The schematic of pattern to vary cell shape independently from cell-ECM contact shows the different geometry of ligand presentation. The 20 μ-m circle hindered cell spreading while the small circles with narrow distance enhanced cell spreading. Growth and apoptotic index were defined when cells were cultured on the different geometric presentations of ECM (total cell-ECM contact area per cell (grey bar), projected cell area (black bar). Cells with a higher spreading area over many small circles showed lower apoptosis rate compared to cells on the 20 μ-m circles [136].

Rigidity sensation

Normal tissue cells are dependent on anchoring to a substrate for survival. However, tissue can have a wide range of stiffness, with brain in the soft range (about 1 kPa), bone in the hard range (about 100 kPa) and many nuances in between. Therefore, a cell experiences different tissue stiffness *in vivo*. Physical properties of tissue are also altered at a wound healing site and can change during disease progression [164–166].

The production of 2-D substrates, such as PAAm gels or PDMS, with variable elasticity or stiffness are good model surfaces to mimic different tissue stiffness and study the downstream consequences of substrate rigidity. Studies using such materials helped to expand our understanding of cell function by demonstrating that cell function was also dependent on the elasticity of the cell microenvironment (fig 1.14) [167–169]. Similar to results obtained through cell spreading confinement, rigidity sensation of flat substrates was shown to influence cell adhesion [170–173] and actin cytoskeleton organization [174]. Therefore, downstream responses of actin assembly, such as cell morphology [175], migration [176–179], and growth [180], are also strongly influenced by substrate stiffness. Engler *et al*. have shown that substrate stiffness also directs mesenchymal stem cell differentiation [181]. Furthermore, rigidity sensation is cell type specific, and this form of environmental stimulation appears to be dysfunctional in transformed cells [182]. Defects in mechanical signaling may allow for survival of transformed cells which may reach the bloodstream and from there transfer into diverse tissue environments [182].

The initial cellular response to mechanical signals occurs in seconds to minutes. A cell in culture for a number of days can therefore be expected to experience countless stimulus-response cycles. The mechanism behind mechanosensing is complex. Focal adhesions, focal complexes, and thereby integrins and cytoskeleton have been identified to play a key role in the mechanosensing ability of cells [183, 184]. Mechanosensing is understood as a bidirectional relationship. The cell senses the mechanical features of the environment which causes a signaling response. While the cell explores the environment, it will modify the signaling response and create new signals. Over time, these intracellular signals change the expression pattern of a cell and thereby its overall state. The process of mechanosensing consists of an inside-outside-inside feedback loop. At a cellular scale, most cells probe the elasticity of their microenvironment as they anchor through focal adhesions and focal complexes, pull on their environment, and responde through cytoskeletal organization to the resistance that the cell senses. In return, the cell responds to the stiffness of the substrate by adjusting adhesion [185] and its cytoskeleton [174]. Formation of these structures requires tension generated within the cell that is built up by the actinmyosin cytoskeleton and transmitted through cellular structures. These forces from the cell to the substrate are called traction forces and are investigated with model systems, such as wrinkling of silicon sheets [186] or bending of elastomeric pillars [187]. The RhoA/ROCK pathway described in section 1.1.1, is also involved in the mechanosensing processes. Studies with drugs affecting the contractility or proliferation behavior of cells led to new insight into mechanosensing abilities of the cell, *e.g*. in stem cell differ-
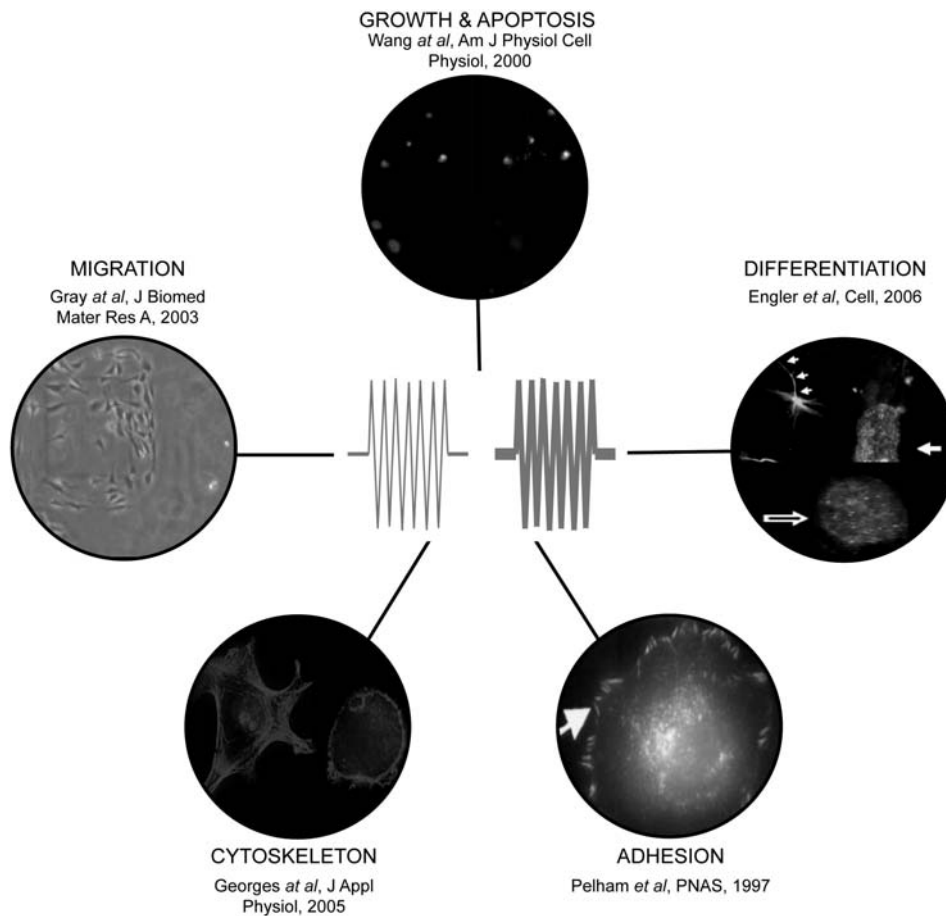
Figure 1.14: *Influence of substrate stiffness on cell behavior.* The images are explained clockwise. *Growth and apoptosis*: Non-transformed cells on flexible substrates showed a decrease in the rate of DNA synthesis and an increase in the rate of apoptosis, while transformed cells maintained their growth and apoptotic characteristics regardless of substrate flexibility [182]. *Differentiation*: Matrix elasticity directed stem cell lineage specification. On soft matrices, that mimicked brain, cells differentiated neurogenic. On stiffer matrices, that mimicked muscle tissue, cells differentiated myogenic. On comparatively rigid matrices, that mimicked collagenous bone, cells favored osteogenic differentiation [181]. *Adhesion*: Focal adhesions on flexible substrates were irregularly shaped and highly dynamic. Those on firm substrates had a normal morphology and were much more stable [170]. *Cytoskeleton*: F-actin showed no articulated stress fibers in cells on soft gels (right), whereas on stiff gels (left) the stress fibers resembled those observed in a fibroblast cells cultured on tissue culture plastic [169]. *Migration*: Over several days in culture, cells accumulated preferentially on stiffer regions of the substrates by mechanotaxis [177].

entiation, but furthermore showed the importance of substrate stiffness for regenerative medicine and drug delivery [188].

An impressive example that demonstrates the influence of substrate stiffness on cell behavior has been presented by Engler, Discher *et al*. [181]. Mesenchymal stem cells (MSCs) on soft hydrogels (E = 0.1 − 1 kPa) which mimicked brain tissue exhibited a
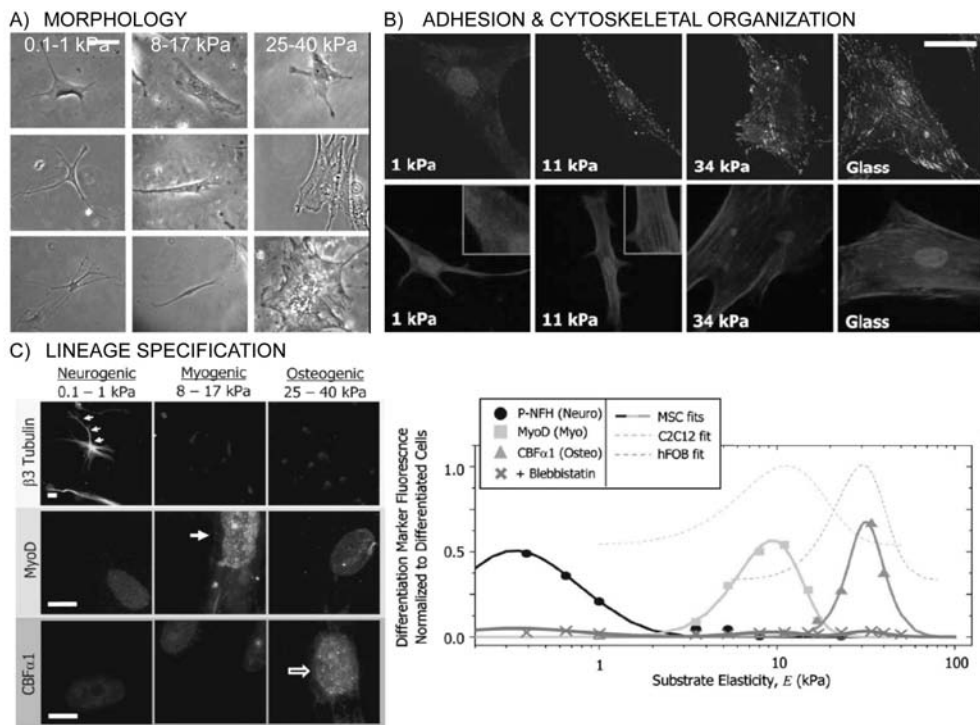
Figure 1.15: *Influence of substrate stiffness on cell morphology and lineage specification.* A) Depending on the substrate stiffness the MSC expressed a branched, spindle or polygonal shape. B) Paxilin-labeled adhesions grew from diffuse staining to punctuate adhesions with increasing stiffness. On the stiffest gels, the adhesions were clearly visible and of a long and thin shape. C) Different differentiation markers of the MSCs were expressed depending on the stiffness of the gel: on soft gels, the neurogenic marker $\beta 3$ tubulin was expressed, on stiffer substrates the myogenic marker MyoD and on the stiffest gel the osteogenic marker CBFα1 was expressed [181].

branched filiapodia-rich morphology, similar to neurons. On stiffer matrices (E = 8 – 17 kPa) MSCs showed a spindle-shaped morphology similar to myoblasts. Even stiffer matrices (E = 25 – 40 kPa) led to cell shapes similar to osteoblasts (fig 1.15 A). Next to cell shape, adhesion and cytoskeletal organization was also influenced by the substrate stiffness. On soft substrates, paxilin-labeled adhesions were difficult to detect and diffuse. They grew to form small punctuated contacts on substrates with intermediate stiffness and on the most rigid substrate, the adhesions were long and thin (fig 1.15 B). A similar trend was observable for actin organization. On soft gels the actin was diffused while it became progressively organized on stiffer substrates. Furthermore the stiffness of the substrate also influenced the lineage specification of MSCs (fig 1.15 C). Culturing MSCs on soft substrates (0.1 – 1 kPa) triggered neurogenic differentiation, stiffer matrices (8 – 17 kPa) caused myogenic differentiation, and on the stiffest matrices (25 – 40 kPa), osteogenic differentiation was favored.

Dimensionality sensation

Most of what is known about cells and their functional regulation has been derived from cell culture studies performed on flat, 2-D culture surfaces, where the effect of cell shape, substrate rigidity or ligand density on cell behavior was investigated. However, virtually every cell *in vivo* possesses a 3-D arrangement of contacts with other cells and/or an ECM. A relatively new consensus has emerged that there are fundamental differences between cells grown on 2-D surfaces versus within 3-D matrices (fig 1.16) [92, 189–191]. Culturing cells in 3-D versus 2-D provides another dimension for external mechanical inputs and cell adhesion.

The additional dimension influences basic cellular processes, such as cell migration [193, 194]. Numerous studies have shown that cell phenotype is heavily dependent upon cell culture in 3-D systems relative to their 2-D counterparts. For example, maintenance of the phenotype of chondrocytes [195] and hepatocytes [86] *in vitro* is heavily dependent upon dimensionality of culture conditions. In addition to cell phenotype, cells grown on 2-D surfaces, versus within 3-D matrices, have altered cell-matrix adhesions [87, 196], which affects integrin ligation, cell contraction and associated intracellular signaling [197, 198]. The gene expression is also drastically altered for cells on 3-D compared to 2-D [192]. The 3-D environment, furthermore, influences the cell response to drugs or toxins. It has been shown that the response of cancer cells to drug candidates seems dependent upon whether cells are grown as 2-D monolayers or in 3-D clumps [85]. Skin cells in 3-D rather than 2-D demonstrated an improved ability to survive exposure to cytotoxic agents [128].

An example of how the spatial arrangement of ECM contacts alters cell behavior is presented by Beningo, Wang *et al*. [88]. Fibroblast cells in 3-D sandwich culture showed changed morphology, they became highly elongated, showing one or several long, thin extensions, but no lamellipodium as observed on 2-D. Furthermore, the actin skeleton was drastically altered in 3-D compared to 2-D (fig 1.17 A). In 3-D actin staining showed fewer prominent stress fibers whereas on 2-D pronounced stress fiber formation was observed. In situations where actin fiber formation occurred, most fibers were found along the lateral borders of the extensions. Cells in 3-D sandwich culture also formed fewer prominent focal adhesions and most adhesions appeared as small dots near protrusive regions at the tip and side of extensions (fig 1.17 B).
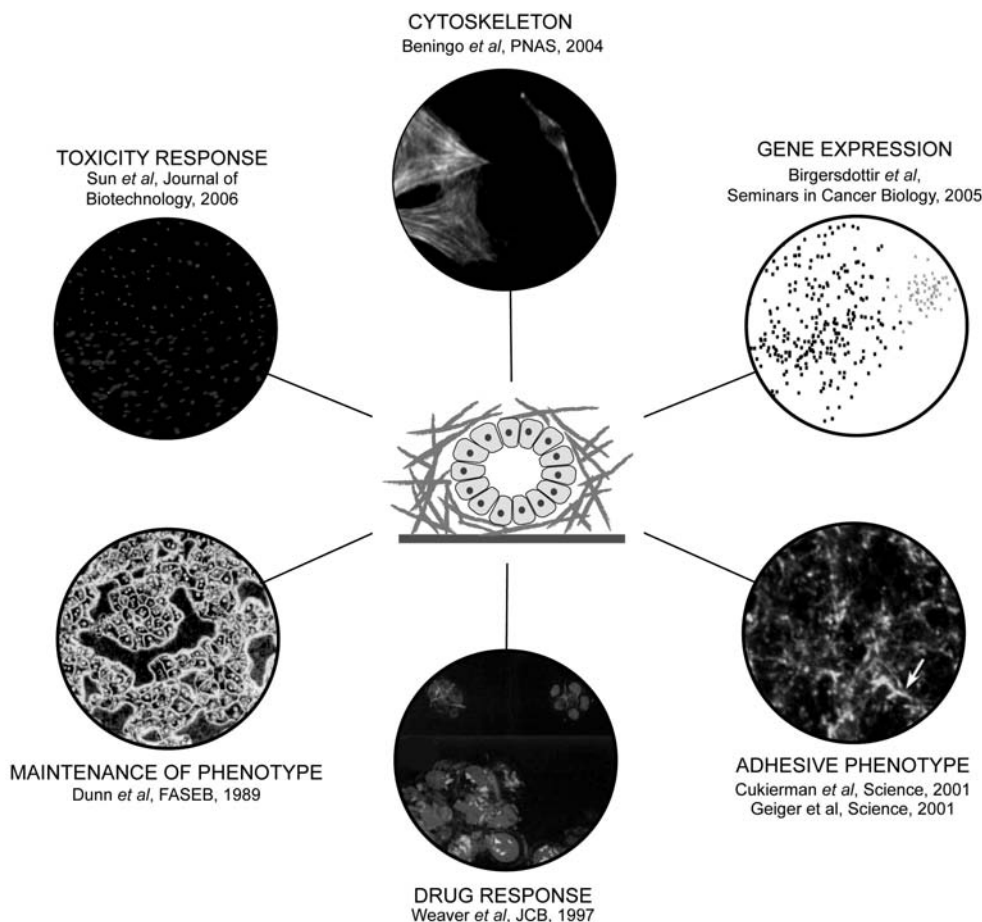
Figure 1.16: *Influence of dimensionality on cell behavior.* The images are explained clockwise. *Cytoskeleton*: Fibroblast cells in 3-D sandwich culture lacked lamellipodia and large actin bundles which was in contrast to the stress fiber formation on 2-D substrates [88]. *Gene expression*: Cells cultured on 2-D surfaces expressed different genes to cells grown in 3-D cultures [192]. *Adhesive phenotype*: 3-D-matrix adhesions differed from focal and fibrillar adhesions characterized on 2-D substrates in structure, localization, and function. Relative to 2-D substrates, 3-D-matrix interactions also displayed enhanced cell biological activities and narrowed integrin usage [73, 87]. *Drug response*: A malignant phenotype was reversed in 3-D culture and *in vivo* by integrin blocking antibodies [85]. *Maintenance of phenotype*: The culture of hepatocytes in a collagen sandwich provided the possibility of maintaining the phenotype and therefore long-term culturing of hepatocytes [86]. *Toxicity response*: Skin cells in 3-D culture had an improved ability to survive exposure to cytotoxic agents in contrast to cells on 2-D substrates [128].

These altered cell responses in a 3-D compared to a 2-D environment show the need for suitable 3-D environments to gain further and more precise knowledge of the cell responses to external stimuli. Unfortunately, only limited attempts have been made to determine the relationship between ligand density, cell shape, substrate elasticity and dimensionality, as yet no tools are available which allow investigation of the interrelationship of these various stimuli in 3-D space.
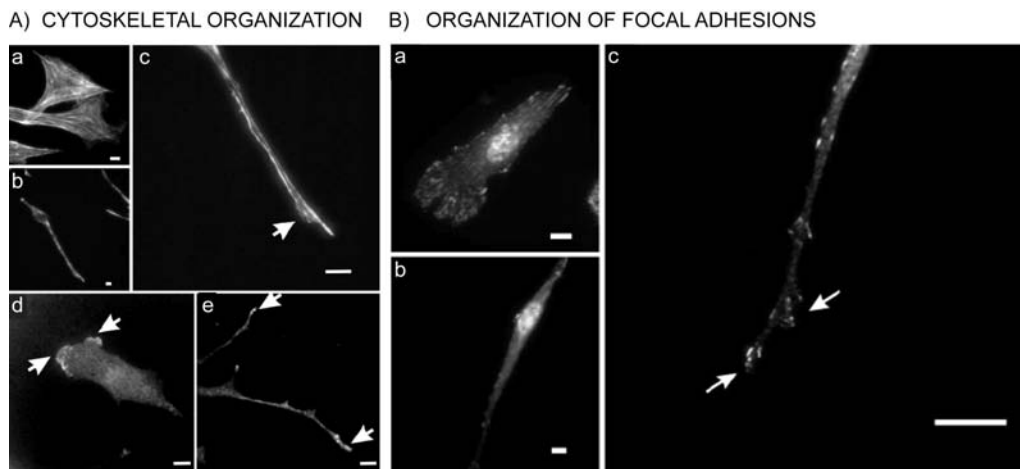
Figure 1.17: *Influence of dimensionality on actin and focal adhesion organization.* A) Organization of actin filaments and ARP 3 in fibroblast cells is shown: a) Phalloidin staining of actin filaments on a 2-D substrates revealed many large actin fibers. b, c) In 3-D sandwich culture the actin was predominantly located at the lateral borders of the extensions. d) On 2-D ARP3 staining showed a band of high concentration at the leading edge while e) on 3-D sandwich ARP3 shows discrete foci at the tips of extension. B) Organization of focal adhesions (paxilin) is presented here: a) On 2-D prominent focal adhesion formation was observed. b) In 3-D only few focal adhesions were formed. c) Higher magnification of focal adhesions in 3-D showed small dot-like adhesions in extensions close to protrusive edges [88].

1.3   Conclusion and open questions

The previous paragraphs discussed the importance of controlling the microenvironment and how the ability to individually vary different parameters in a controlled manner would provide us with the opportunity to learn how a cell reacts to different stimuli. Unfortunately, the differential or synergistic impacts of these properties are less frequently investigated [183]. A predictive understanding of the cellular response to physical cues necessitates the development of tools which permit the independent decoupling of these environmental properties, and their subsequent recombination.

It has been shown how important the control over cell shape is and also how rigidity influences cell behavior. However, the existing approaches for mimicking the 3-D environment of a cell, such as gels or fiber scaffolds, do not allow for the control of cell shape. They often have limited control over stiffness and local mechanical properties, as cells will remodel their surroundings [199]. Therefore, they are not appropriate for a direct comparison to 2-D substrates concerning cell shape and matrix rigidity. In addition, compression of these matrices into 2-D substrates most likely results in substrates with increased stiffness relative to their 3-D counterparts [87]. Finally, these approaches are

difficult to compare in the absence of a widely accepted standard for 3-D culture and an inability to quantify the local rigidity experienced by an individual cell.

However, similar to the limitations which plagued early attempts at understanding spreading effects on cell function, the currently available tools which can be used to delineate the role of dimensionality on cell function are limited. In this project we combined the advantage of 2-D patterning with 3-D cell culturing systems (fig 1.18). M. Dusseiller, M. Smith, V. Vogel and M. Textor at ETH Zurich developed a novel platform with microwells in the size of a single cell and variable substrate elasticity, which can be used to control the 3-D shape of cells [98, 200, 201]. Microwells can be more directly compared to 2-D surfaces, since in both cases cells are in contact with planar surfaces coated with adhesive ligands of defined nature. Other innovative approaches to trap single cells in microwells have been reported [93, 103]. However, these approaches are better suited for the generation of population statistics derived from individual cell measurements than for basic biological investigations since they would have yet to be adapted for 3-D shape control. The size of the microwells in our technique allows for a 3-D shape control since the wells are in the size of a single cell. In addition, only a few of the competing approaches to 3-D cell culture are compatible with high-resolution microscopy. In our approach, however, thanks to a double-replication technique of microfabricated masters into PDMS, it is possible to produce very thin films (on glass cover slips (total thickness < 200 micrometer) containing the microwell structure that are compatible with high-resolution, inverted-stage microscopy.

This thesis builds upon and expands the results obtained by Dusseiller *et al.* [200]. The platform is further developed towards more complex chemistry inside the microwells, namely a mobile E-cadherin coating by means of SPB and a variation in wall and bottom coating. Furthermore, it investigates the interplay between different microenvironmental parameter, such as 3-D shape, substrate stiffness, and ligand specifity, that can be varied independently. Thanks to the ability of independently controlling different environmental properties we hope to improve our understanding of the interrelationship between dimensionality, cell spreading, and stiffness and its influence on cell behavior.
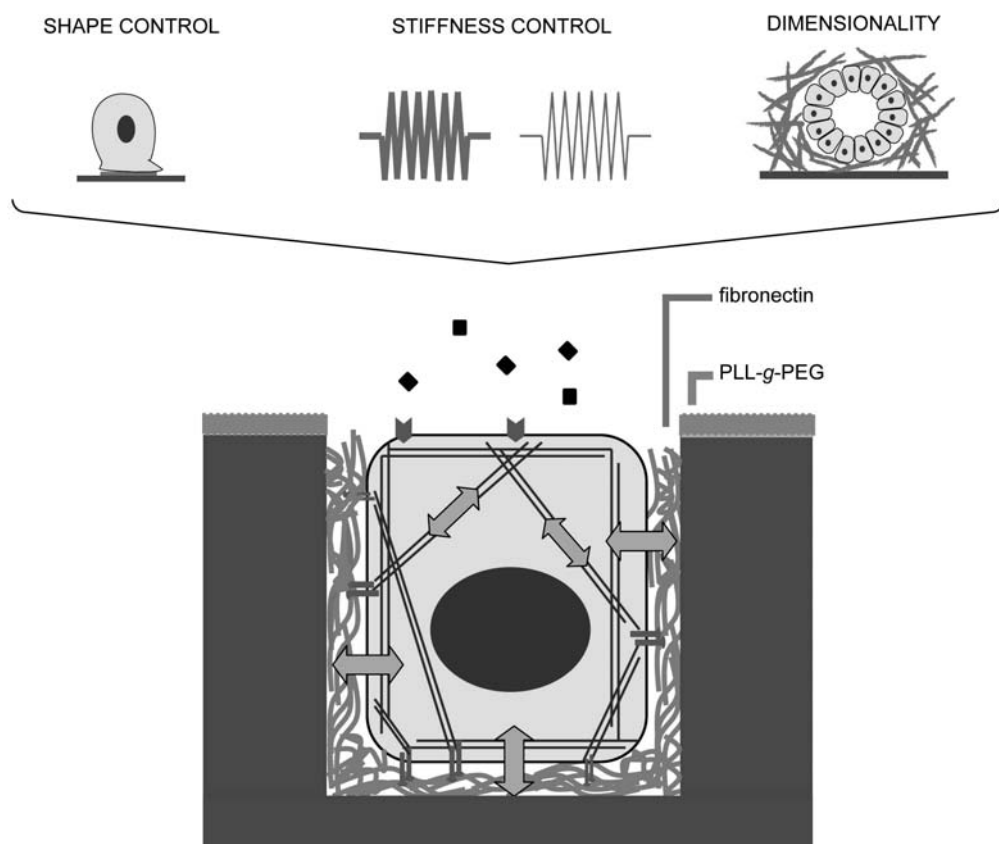
Figure 1.18: *The microwell structure combines control different aspects of cell culture platforms.* It combines the shape control of 2-D patterned substrates, the stiffness control of the surrounding area, and the dimensionality typical for 3-D cell culture dishes. This results in a microwell in the size of a single cell with control over the cell shape and tunable stiffness of the substrate.

Scope of the thesis

A cell *in vivo* experiences many stimuli from the tissue in which it adheres and grows. Neighboring cells, ECM proteins, soluble growth factors, hormones, stiffness of the tissue, and many more factors influence the fate of a single cell. It is this complex interplay of different stimuli and molecules which gives the tissue its final shape and function. Researchers aspire to achieve a greater understanding of the processes of life. Due to the complexity of the *in vivo* environment, simplified reductionist systems *in vitro* are needed to study processes that are crucial for human function and health. To approximate the *in vivo* environment of a real human body from a Petri dish, is difficult and therefore it is also important to combine the knowledge gained from such simplified systems into a bigger context.

The overall objective of this thesis is to establish a novel microwell platform that mimics certain aspects of the cell's microenvironment. This technique was first designed, engineered and tested by M. Dusseiller, M. Smith, V. Vogel and M. Textor [98, 200, 201] at ETH Zurich and is further developed towards a more complex biochemical microenvironment in this thesis, allowing additional cell-biological questions to be addressed. The main advantage of this microwell structure is that it allows for the study of the effect of multiple extracellular stimuli on the cell and further allows the interrelationship between these stimuli to be explored. Many studies have explored how cell shape influences cellular behavior; how substrate stiffness directs cell fate, and how the cell's response is altered in a 3-D environment compared to a Petri dish. The advantage of the microwell platform is that we present to the cell a microwell in the size of a single cell, and inside that well we are able to independently control cell shape, substrate stiffness, and presentation of different biochemical cues in 3-D. To this end, the objective of this thesis is to
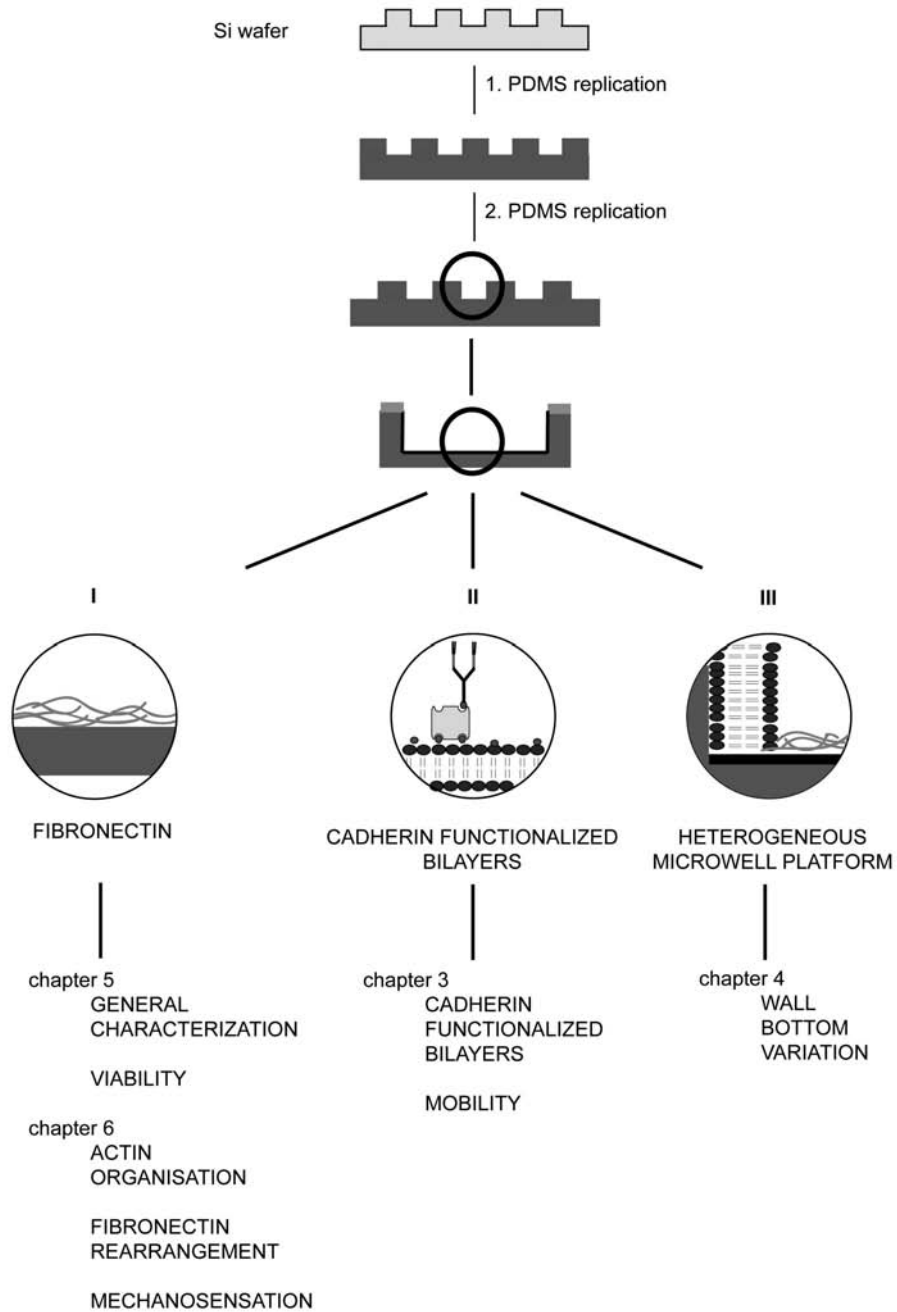
Figure 2.1: *Overview of different microwell platforms used/developed in this thesis and the addressed cell-biological issues.* The microwell structure was produced in a Si wafer and subsequently replicated into PDMS. The inside of the microwell was coated with i) Fn, or ii) with cadherin-functionalized bilayers, or iii) a wall-bottom variation with bilayers on the wall and Fn on the bottom of the well.

study the influence of dimensionality on cell behavior, namely actin fiber assembly and how dimensionality affects cell responses to spreading limitation and mechanosensation (schematically summarized in fig 2.1).

Chapter 3 presents first the replication technique used to transfer a microwell structure from a silicon wafer into PDMS and the subsequent passivation of the plateau area between the microwells and coating of the microwells with fibronectin (Fn) as developed by Dusseiller. Next, the development of the functionalisation of the microwells within this thesis work towards microwells coated with a) a functionalized supported phospholipid bilayer (SPB) and b) a variation in wall and bottom coatings thus creating a biochemical contrast in 3-D is presented. Through this process, individual cells adhere to and interact with a small and well defined microwell of variable geometry. Therefore this platform offers the possibility to control and elucidate the effects of dimensionality in a well defined manner.

Chapter 4 covers the modification of the microwells with a mobile SPB that is functionalized with human E-cadherin (fig 2.1 II). The cell inside the microwell experiences a microenvironment that is expected to be closer to the microenvironment of a cell experiencing cell-cell contacts. The characterization and the presentation of a lateral mobile/immobile bilayer system can be used to present cells with an environment of variable mobility. This allows mobile events to be studied, such as clustering of cell adhesion molecules. The main focus of this chapter was on the engineering and detailed characterization of the mobile E-cadherin coating inside microwells. Preliminary cell studies, though, were performed with the cadherin-functionalized SPB and demonstrated the feasibility of the approach.

Cells are often in a microenvironment composed of a locally heterogeneous arrangement of proteins. Therefore, in a next step addressed in Chapter 5, we engineered a microwell type that should mimic more closely the heterogeneous presentation of both fibronectin and cadherin cues, thus mimicking the environment a cell in a cell sheet. To achieve this, the platform was developed with a contrasting wall-bottom coating ("wall-bottom variation" fig 2.1 III).

In chapter 6, the results of cell survival assays are presented and discussed. These were performed to determine whether cells survive inside microwells for periods of several days to weeks and whether limitation in spreading area can induce apoptosis as has been observed for cells on 2-D patterns. A number of technical issues are also addressed in this chapter: a) The critical well size for optimum control of cell shape in 3-D was

determined using a library of well sizes. b) The technical aspect of compatibility of the microwell substrate with high-resolution microscopy is addressed. c) The ability to perform immunohistochemistry (IHC) with cells in wells is demonstrated; specifically, potential limitations in the ability to visualize intracellular proteins with IHC due to reagent diffusion issues are shown to be absent.

In chapter 7, the cytoskeletal characteristics of single cells either adhering to microfabricated adhesive islands in 2-D or accommodated in microwells (3-D) of controlled size, shape and rigidity were compared. The fundamental question is addressed of whether a 3-D arrangement of cell adhesive contacts stimulates actin cytoskeleton assembly, even under conditions where cell spreading is limited to an extent that did not promote actin cytoskeleton assembly on 2-D surfaces. Furthermore, we investigated whether cell adhesion in 3-D alters the response of cells to substrate stiffness relative to 2-D, and whether cell metabolism is elevated or not in 3-D cultured cells versus cells on 2-D patterns.

The thesis ends with the Conclusion and Outlook chapter which discusses possible future directions in the engineering and application of the microwell platform (chapter 8).

Materials and methods

In this chapter, all materials and methods are listed which were used in this thesis for the general fabrication of the platform and cell culturing. For the sake of convenience, long names are listed with their abbreviations. Additionally, the fabrication process of the standard microwell substrate is presented here. Furthermore, the methods used for characterization are briefly explained. The individual chapters contain additional experimental sections where the specific experiments, concentrations and conditions are described in greater detail.

3.1 Materials

3.1.1 Water

Ultrapure water was used for all buffers and suspensions. A milli-Q system Gradient A 10 (Millipore) equipped with an Elix 3 (three step purification process) and an ultraviolet lamp for photo-oxidation was used. The resistivity and TOC level were in the range of 18.2 MΩcm and < 5 ppb, respectively.

3.1.2 Buffer

Phosphate buffered saline
Phosphate buffered saline (PBS; Fluka Chemie, Switzerland) was diluted in ultrapure

water. The final concentration was 137 mM NaCl, 10 mM Phosphate, 2.7 mM KCl, and a pH of 7.4. The buffer was filtered (0.22 μm filter) prior to use.

HEPES buffer

4(2-hydroxyethyl)piperazine-1-ethanesulfonic acid (HEPES; Fluka Chemie, Switzerland) was prepared at 10 mM concentration with additional 150 mM NaCl and adjusted to pH 7.4 with 6 M NaOH. Prior to use the buffer solution was filtered (0.22 μm filter).

3.1.3   Poly(L-lysine)-*graft*-poly(ethylene glycol)

Poly(L-lysine)-*graft*-poly(ethylene glycol) (PLL-*g*-PEG) was purchased from SuSoS AG (Switzerland). PLL(20)-*g*[3.4]-PEG(2) was the standard polymer used in this study. The numbers in the "()" brackets are the molecular weights of the polymer chains in kDa and the number in the "[]" brackets is the grafting ratio. PLL-*g*-PEG powder was dissolved in HEPES buffer and stored as a stock solution of 1 mg/ml below -18 °C. Prior to use the polymer was dissolved in PBS to a final concentration of 0.1 mg/ml. In this thesis, PLL(20)-*g*[3.4]-PEG(2) is referred as PLL-*g*-PEG. To visualize the PLL-*g*-PEG, PLL-*g*-PEG labeled with rhodamine was used (PLL-*g*-PEG-rhod) (SuSoS AG, Switzerland). Biotinylated PLL-*g*-PEG (PLL-*g*-PEG-biotin, SuSoS AG, Switzerland) was used to functionalized the heterogeneous wall and bottom coating.

3.1.4   Proteins

Fibronectin

Human plasma Fn was isolated from fresh human plasma (Swiss Red Cross) using gelatin-sepharose chromatography based on established methods [202, 203]. Afterwards, Fn was labeled with Alexa 488 or Alexa 633 (Molecular Probes, Switzerland) using established protocols [204]. Fn in amine labeling buffer (PBS with 0.1 M NaHCO$_3$, pH 8.5) was incubated with a 30-fold excess of Alexa 488 or Alexa 633 succinimidyl ester for 1 h. Labeled Fn was separated from free dye using a PD-10 column equilibrated with PBS. The labeling ratio was determined by measuring the absorbance of labeled Fn at 280 and either 496 or 632 nm and using published extinction coefficients for dyes and Fn. Labeled Fn with ∼4 fluorophores per Fn molecule was used in this study. Fn was used in studies for chapters 5, 6, and 7.

Streptavidin

Streptavidin (SA) and Alexa 488 labeled streptavidin (SA 488) were purchased from Invitrogen (Switzerland). The proteins were received in 1 mg powder portions, dissolved in 1 ml HEPES buffer and aliquoted in 20 μg/20 μl portions. The aliquots were stored as a 1 mg/ml stock solution at -18 °C. SA was used in experiments performed for chapter 4.

E-Cadherin

Human E-cadherin/Fc chimera (E-cad/Fc) was received from D. Leckband, University of Illinois, Urbana-Champaign, and engineered by Yuan Hung Chien as described in [205]. E-cad/Fc is used to mimic cell-cell interaction and described in chapter 4.

Bovine serum albumin

Bovine serum albumin (BSA; Fluka Chemie, Switzerland) was diluted in PBS at a concentration of 4 wt%, filtered and stored at -18 °C. To block the surface against unspecific adsorption, the BSA was directly used without further dilution.

3.1.5 Antibodies

Biotinylated antibody

Biotinylated goat anti-human IgG Fcg (bAB; eBioscience) was stored as obtained at -4 °C and used in experiments for chapter 4.

Antibody staining for fibronectin

Sheep anti-human Fn polyclonal antibody (1:200 in PBS; Serotec AHP08) was incubated for 1 h, rinsed thoroughly, and finally incubated with a rhodamine conjugated donkey anti-sheep IgG secondary antibody (1:200 in PBS; Chemicon AP184R) for 1 h. Immunohistochemistry (IHC) for Fn labeling is described in section 6.3.3.

3.1.6 Lipids

All the lipids were purchased from Avanti Polar Lipids (Instruchemie, Netherlands). They were obtained in powder and stored at -18 °C before dilution in chloroform. Full details of vesicle preparation are given in chapter 4. In this studies, lipid mixtures are simply called, *e.g.* 5% bDOPE/DOPC for 5% biotinylated lipids in 95% DOPC.

DOPC

1,2-Dioleoyl-*sn*-Glycero-3-Phosphocholine (DOPC) was diluted to 25 mg/ml and stored at -18 °C before vesicle preparation. These lipids were used in experiments for chapters 4 and 5.

MPPC

1-myristoyl-2-palmitoyl-*sn*-glycero-3-phosphocholine (MPPC) was diluted to 25 mg/ml and stored at -18 °C before vesicle preparation. These lipids were used in experiments for chapter 4.

bDOPE

1,2-Dioleoyl-*sn*-Glycero-3-Phosphoethanolamine-N-(Cap   Biotinyl)   Sodium   salt (bDOPE) was diluted to 25 mg/ml and stored at -18 °C before vesicle preparation. To obtain biotinylated vesicles, between 0.5 and 5% biotinylated vesicles were added to the DOPC or MPPC lipids. These lipids were used in experiments for chapter 4.

NBD-PC

1-Oleoyl-2-[12-[(7-nitro-2-1,3-benzoxadiazol-4-yl)amino]dodecanoyl]-*sn*-Glycero-3-Phosphocholine (NBD-PC) was diluted to 2 mg/ml and stored at -18 °C before vesicle preparation. To obtain fluorescent vesicles, 1% NBD-PC was added to the lipid mixture bevore vesicle preparation. These lipids were used in experiments for chapters 4 and 5.

3.1.7   Vesicle preparation

Lipids with phase transition temperature < room temperature

Pure DOPC, fluorescent (1 wt% NBD-PC and 99 wt% DOPC), and biotinylated vesicles (0.5 – 5 wt% bDOPE and 95 – 99.5 wt% DOPC) were prepared as follows: Lipid solutions were mixed in a clean glass flask. The lipids were dried for at least 30 min under a flow of nitrogen. 1 ml of HEPES buffer was added to hydrate the lipid film forming vesicles. The vesicle suspension was extruded 31 times through a 100 nm polycarbonate membrane (Avestin Inc., Canada) using a Lipofast extruder (Avestin Inc., Canada). The vesicle solution was diluted with HEPES buffer to a final concentration of 0.5 mg/ml and stored in the refrigerator for up to 2 weeks.

Lipids with phase transition temperature > room temperature
The vesicles based on MPPC have a gel-to-liquid-phase transition temperature (T_m) at
35 °C and therefore have to be prepared above this temperature. The lipids were mixed
and dried as described above. To hydrate the lipid film, 40 °C warm HEPES buffer
was used. Instead of extrusion, the vesicles were produced by sonication (Ultrasonik,
Blackstone-Ney) in a water bath set at 40 °C. The cloudy vesicle solution was sonicated
until it turned clear (after about 20 min). Afterwards, the lipids were diluted to 0.5 mg/ml
and stored at 4 °C for up to 2 weeks.

3.2 Substrates

3.2.1 Wafer and glass slide

Silicon wafers (p type, $\langle 100 \rangle$, polished, $\varnothing$ = 100 mm; Si-Mat Silicon Materials, Ger-
many), glass slides (76 mm × 26 mm; Menzel GmbH, Germany) and glass cover slides
(round and squared, $\varnothing$ and $x = 10 - 24$ mm, thickness 0; Menzel GmbH, Germany) served
as substrates.

3.2.2 Polydimethylsiloxane

Polydimethylsiloxane (PDMS) is a cross-linked elastomer with the general chemical
structure $CH_3[Si(CH_3)_2O]_n Si(CH_3)_3$. PDMS is non-toxic, permeable for oxygen, non-
swelling in aqueous solutions and optically clear. This combination of properties makes
PDMS a suitable material for cell culture and microscopy [206, 207]. PDMS was used
for wafer replication or microwell production (see section 3.4). For standard stiffness,
Sylgard®184 (Dow Corning, Germany) was mixed to the ratio of 1:10 (weight ratio,
w/w curing agent to prepolymer) with cross-linker solution and degassed in an exsiccator
until all air bubbles disappeared. For wafer replication, PDMS was poured over the wafer
to a thickness of about 5 mm. The polymer was cured at 80 °C for 4 h. The detailed
fabrication of the microwells is described in section 3.4.

Spin-coating
For measurements of homogeneous flat PDMS with the QCM-D or with the microscope,
it was important to have a very thin and homogeneously flat PDMS layer. Therefore

2 wt% uncross-linked PDMS was dissolved in hexane (Fluka Chemie, Switzerland) and spin-coated for 40 sec at 2000 rpm resulting in a thin film [208, 209]. Afterwards the sample was dried at 80 °C for at least 4 h.

Stiffness variation

PDMS covers a physiologically relevant range of mechanical properties. The stiffness can be controlled by varying the cross-linking density [177, 210]. Curing agent to prepolymer mixtures of 1:10, 1:30, 1:40, 1:50, 1:60, 1:70 and 1:100 ratios were investigated. To create thick films of PDMS, the different mixtures were cast inside a 14 cm TCPS Petri dish and cured for 4 h at 80 °C. The resulting thickness was approximately 1 mm. For the mechanical tests standard dumbbell-shaped specimens were punched out (12 mm gauge length, 2 mm width) and the thickness of each sample was measured. Tensile tests were carried out at room temperature with an Instron tensile tester (model 4411, 1 N load cell, 12 mm/min cross-head speed, corresponding to initial strain rate of 1 min^{-1}). The slope at the start of deformation was used to calculate the Young's modulus (fig 3.1). For each cross-linker concentration, three samples were measured on the day after curing and 16 days later to test if the mechanical properties changed after storage at room temperature. For soft PDMS mixtures from 1:60 or 1:50 ratios of cross-linker to PDMS, a Young's modulus of 3 or 8 kPa was measured and no further cross-linking after 16 days was observed. Variability in the Young's modulus increased in very soft samples (1:60) and may have resulted from cross-linking heterogeneity or insufficient mixing. At lower concentrations of 1:70 or below, the material did not cross-link but remained a highly viscous liquid. These data suggest PDMS is not suitable as a model substrate below 10 kPa.

3.3   2-D patterning techniques

3.3.1   Photolithography for microwell replication

10 μm deep microwells

Photolithography [211] was used to produce masters with microwells for replica molding [160]. Photolithography was carried out in a class 10 clean room. For microwells, silicon wafers (as received) were placed on a hot plate for 5 min at 190 °C for dehydration. SU-8 2010 (negative resist; MicroChem, US) was spin coated for 90 sec with 2000 rpm. To soft bake, the wafer was heated for 2 min at 65 °C, followed by 2 min at 95 °C. The photo
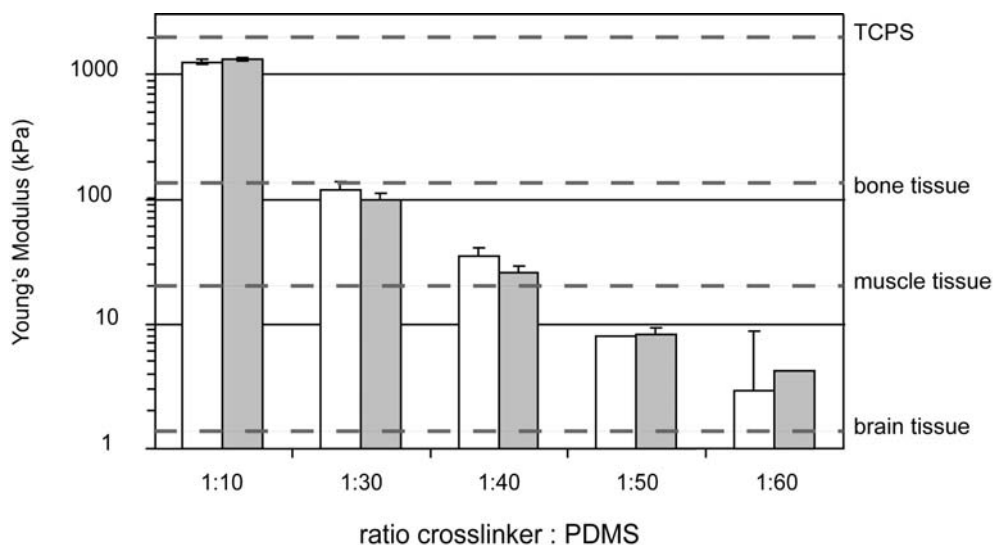
Figure 3.1: *Tunable stiffness of PDMS.* Varying the cross-linking density of PDMS allows one to tailor the mechanical properties of the substrate. The measured Young's modulus ranged between 3 kPa and 1.3 MPa using 1:60 or 1:10 ratios of cross-linker to polymer, respectively.

resist on the sample was then exposed for 15 sec (12 mW/cm^2) to UV light using a mask aligner (Karl Süss MA6, Germany). The exposed regions started to cross-link resulting in a microwell pattern. In the following post-exposure bake, the wafer was placed onto a hot plate at 65 °C and at 95 °C for 2 min each. The photo resist was developed in SU-8 developer (MicroChem, US) for 2 min to remove the non-cross-linked photo resist, rinsed thoroughly with isopropanol and dried with nitrogen. In the final hard baking step the sample was placed onto a hot plate at 65 °C and heated up to 150 °C. The sample was then baked at 150 °C for additional 5 min. These parameters led to a resist thickness of 10 μm.

1- and 5 μm deep microwells

To fabricate shallow wells, the protocol was slightly modified. For 5 μm deep wells, SU-8 2005 (MicroChem, US) was used and spin coated with 2500 rpm for 90 sec. The baking, illumination and development steps were performed the same way as described above. For even more shallow wells, SU-8 2002 (MicroChem, US)) was used and spin-coated for 90 sec at 3000 rpm. The baking and developing steps were reduced to 1 min each and the illumination time was shortened to 10 sec. This led to 1 μm deep microwells on a Si wafer that was used as a master.

3.3.2   Molecular assembly patterning by lift-off

2-D patterned reference sample were produced using the MAPL technique which was developed by Falconnet *et al.* [124] and presented in section 1.2.2 and illustrated in fig 1.11.

The pattern was first transferred from a mask into a photo resist by photolithography. After dehydration of the sample, S1818 (positive resist; Microresist, UK) was spin-coated for 2 min at 4000 rpm and afterward the sample was heated for 2 min at 100 °C. The sample was exposed for 10 sec and developed for 1 min in a water-AZ developer mix (1:1) (Clariant, Switzerland). The exposed photo resist was thereby removed. After rinsing with water, the samples were dried with nitrogen. Afterwards, the prepattern surfaces were modified chemically to transfer the pattern into a biological contrast. In a first step, the sample was exposed to an air plasma for 5 s and afterwards PLL-*g*-PEG (0.1 mg/ml) was adsorbed on the surface for 1 h, adsorbing on the substrate surface itself and on the photo resist. In a second step, the photo resist and therefore the PLL-*g*-PEG on top was removed with N-Methyl-2-pyrrolidone (NMP; Fluka Chemie, Switzerland). To achieve this, the sample was placed in an ultrasonic bath for 2 min, then for additional 2 min in a water-NMP mix (1:1). This resulted in a PLL-*g*-PEG pattern on a glass surface. The PLL-*g*-PEG renders the surface protein-resistant, while on the spots where previously the photo resist was adsorbed, Fn (25 μg/ml, 1 h) can adsorb, resulting in a PLL-*g*-PEG-Fn pattern. The Fn islands allowed for cell attachment while the PLL-*g*-PEG regions were resistant against cell attachment.

3.4   Microwell fabrication

3.4.1   Replica molding

In order to generate arrays of 3-D microwells, a silicon master was first produced using standard photolithography. Through replication into a 1st PDMS master and subsequent replication into the final PDMS sample for cell culture (replication process is illustrated in fig 3.2). To ensure the transfer of the microwell structure from the 1st PDMS stamp into the 2nd, the 1st PDMS master was fluorosilanized. Therefore, the sample was air plasma treated for 30 s and gasphase fluorosilanized (1H,1H,2H,2H-Perfluorooctyltrichlorosilane, ABCR GmbH & Co. KG, Germany) for 1 h. The fluo-
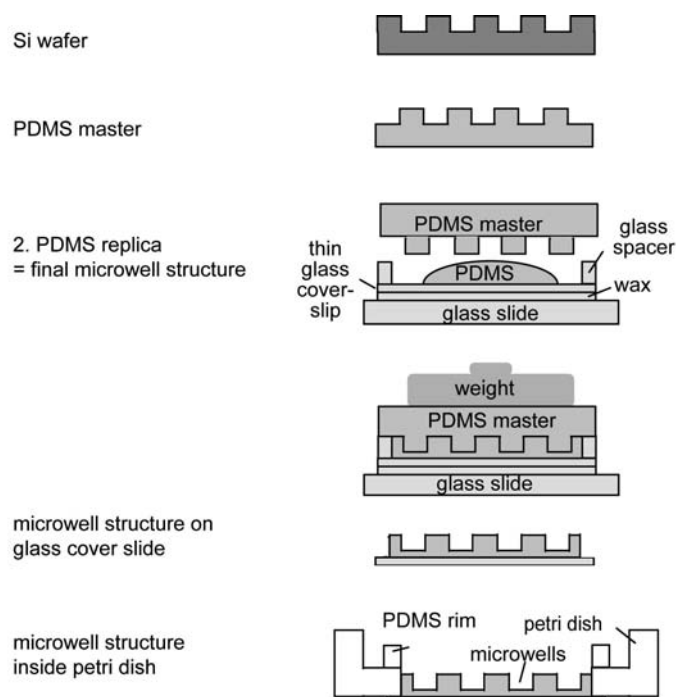
Figure 3.2: *Microwell fabrication.* In order to transfer the microwell pattern from the silicon master into a thin film of PDMS, a thin glass coverslip was glued onto a glass specimen slide between which the PDMS is cast. This sandwich is weighted while the PDMS is cured. The master and glass support are removed leaving behind a thin PDMS film bound to the coverslip which is then glued to the bottom of a Petri dish into which a hole was previously drilled.

rosilanes bound covalently to the PDMS and the 1st PDMS master was used > 10 times without additional fluorosilanization.

In addition, a thin film replication technique was developed to permit high-resolution microscopy of the samples. Therefore, a thin glass coverslip was glued onto a glass specimen slide between which the PDMS was cast. This sandwich was weighted down while the PDMS was cured. The master and glass support were removed leaving behind a thin PDMS film bound to the coverslip. This cover slip was glued to the bottom of a Petri dish into which a hole was previously drilled. In addition to high-resolution microscopy, this set up also allowed for live imaging. The standard Petri dish could be used with almost every microscope.

Although replication into the final PDMS thin film device required multiple steps, the fidelity of the microstructures, as assessed by scanning electron microscope (SEM), was very high. Replication of hard PDMS (1:10) led to microwells with straight walls (fig 3.3 A). Microstructures replicated into the soft mixtures (1:40) showed less accurate retention of shape fidelity due to the low stiffness of the resulting polymer (fig 3.3 B). It
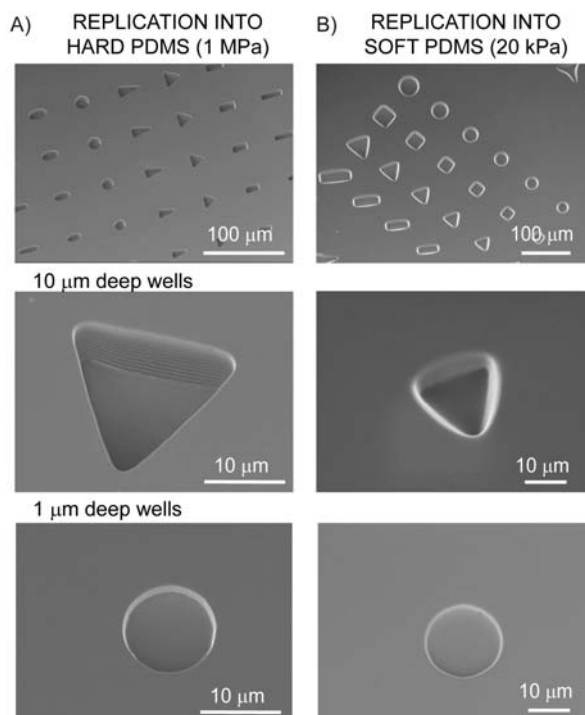
Figure 3.3: *Replication of the microwells into hard and soft PDMS.* A) The microwells could be transferred in a reliable manner into hard (1MPa) PDMS and wells of 10 μm and 1 μm depth could be replicated. B) The transference of the microwell structure into soft (20 kPa) PDMS could also be performed, but the walls of the microwell showed slightly less sharp edges than in the hard PDMS.

was not possible to transfer the microwell structure in a reliable manner into softer PDMS (< 1:50). Normally, for the fabrication of soft microwells the polymer-cross-linker ratio 1:40 was used.

3.5 Surface modification techniques

3.5.1 PLL-*g*-PEG stamping and fibronectin coating

To passivate the top plateau of the PDMS chips and to render it resistant to adsorption of proteins and the adhesion of cells, a hydrogel based inverted microcontact printing method was developed (as illustrated in fig 3.4) by Dusseiller *et al*. [98]. This passivation step of the plateau was the critical step in microwell fabrication. An incomplete passivation of the plateau resulted in cell attachment all over the sample. Since a cell inside the microwell
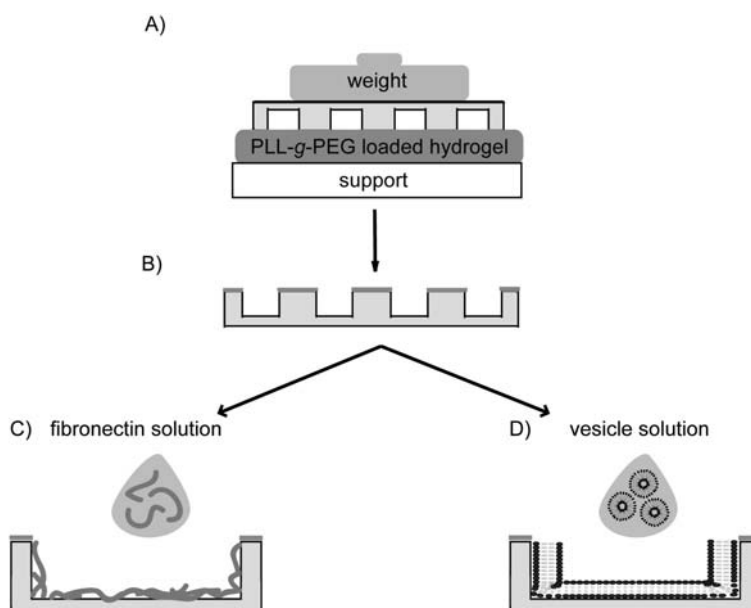
Figure 3.4: *Chemical coating of the microwells.* A) The microwell plateau surface was passivated by inverted micro-contact printing of PLL-*g*-PEG using a PAAm stamp. B) After plateau passivation the sample was either exposed to C) a Fn solution, or D) a vesicle solution. The Fn or vesicles were only able to adsorb inside the microwells and conversely no Fn or vesicles adsorption occurred on the plateau.

needed to be isolated to have a defined shape, cells on the platform might interact with cells in microwells and therefore ruin the controlled shape in 3-D.

While working with a structured substrate, we used a flat stamp for the passivation step. An Acrylamide 4K-Solution (30%) Mix 37.5:1 (AppliChem, Germany) was used to produce the polyacrylamide stamp (PAAm). To obtain a protein-resistant surface, PLL-*g*-PEG (1 mg/20 μm in PBS) was added to 1 ml of PAAm pre-gel solution and the cross-linking reaction was started by the addition of 10 μl of ammonium persulfate (APS; Aldrich, Switzerland; 10% w/v APS in PBS, concentration to PAAm 1:100) and 2 μl of N, N, N, N-tetramethyl ethylenediamine (TEMED; Sigma, Switzerland; concentration to PAAm 1:500). The PAAm hydrogel containing the dissolved PLL-*g*-PEG was then cast and cured between two 1 mm glass slide spacers resulting in a flat stamp. After 1 h the gel was removed from glass spacers, cut into smaller pieces (5x5 mm) and stored in a humid environment.

Before stamping, the microstructured PDMS surface was exposed to air plasma (PDC-32G from Harrick Scientific Corporation, 0.1 mbar, 30 sec) to create negative charges at the substrate surface. This is a prerequisite for the electrostatically driven adsorption of the positively charged backbone of the PLL-*g*-PEG. Subsequently, the flat

hydrogel functionalized with PLL-*g*-PEG was simply placed upside down onto the structured substrate. To enable a sufficient contact between the sample and the stamp, a weight of 5 g was applied during the 15 min stamping procedure (fig 3.4 A). This resulted in a passivation of the background and still enabled protein adsorption inside the microwells. After the passivation of the background (fig 3.4 B), the surface inside the microwells was coated with Fn for the majority of cell culture studies. The sample was exposed to unlabeled or fluorescently labeled Fn at 25 μg/ml in PBS for 1 h. Fn adsorption was limited to the non-passivated PDMS inside the wells due to PLL-*g*-PEG passivation of the top surface (fig 3.4 C). After the coating step, the sample was thoroughly rinsed with PBS. Fn-coated samples were used for studies described in chapters 6 and 7.

3.5.2   PLL-*g*-PEG stamping and bilayer coating

As many proteins of interest in cell studies are transmembrane proteins, where ligand mobility may be an important determinant of cell function, microwells were also coated with SPB. 100 nm diameter DOPC vesicles were produced by extrusion (section 3.1.7) and dispersed into PBS to a concentration of 0.5 mg/ml. The PDMS microstructured surfaces were exposed to air plasma treatment for 30 sec, stamped with PLL-*g*-PEG and then exposed to the vesicle solution at room temperature for 15 min. On the plasma treated PDMS surfaces, vesicles spontaneously adsorbed on the surface and subsequently ruptured to form an SPB inside the microwells. The SPB coating was also limited to microwell surfaces while the plateau remained devoid of vesicles due to the PLL-*g*-PEG stamping (fig 3.4 D). After the coating step the sample was thoroughly rinsed with PBS. The samples were kept in liquid at all times, as SPBs are not stable in air. SPB coated samples were used as described in chapters 4 and 5.

3.6   Cell culture and IHC

3.6.1   Cell lines

HUVEC
Primary human umbilical vein endothelial cells (HUVECs; PromoCell, Germany) were maintained for less than 8 passages in Endothelial Cell Growth Medium plus Supplement (2% fetal calf serum (FCS) ; PromoCell, Germany, 1% Antibiotic-Antimycotic

(pen/strep), Invitrogen, Switzerland). Cells were allowed to adhere within the micro-wells for 30 min, after which the unbound cells on the non-adhesive background were removed by gentle pipetting.

HFF

Human foreskin fibroblasts (HFF) were obtained from ATCC (US) and cultured in fibrob-last growth media with supplement. They were maintained for no more than 10 passages. Fn-coated microwells were seeded with 5×10^4 cells/cm^2. Cells were allowed to adhere within the microwells for 10 min, after which the unbound cells on the non-adhesive background were removed by gentle pipetting.

Myosin knockout cells

The myosin IIA experiments were performed with mouse embryonic fibroblasts with a silenced nonmuscle myosin NMM-IIA (myosin IIB knockdown cells) and were obtained from M. Sheetz Lab, Colombia University, New York. They are cultured in DMEM with high glucose (4.5 g/l), 10% calf serum, and 1% pen/strep.

For the myosin IIB study, fibroblast cells with deleted nonmuscle myosin heavy chain II (myosin IIB knockout cells) were also obtained from M. Sheetz Lab. They are cultured in DMEM with high glucose (4.5 g/l), 10% newborn calf serum, and 1% pen/strep.

CHO cells

Chinese hamster ovary cells expressing GFP-cadherin (CHO cells) were obtained from Deborah Leckband, University of Illinois, Urbana-Champagne. The cells were stably transfected with plasmids encoding the Fc tagged extracellular domain of human E-cadherin as described in [205]. They were cultured in DMEM with 10% serum plus 150 μg/ml G418 (Gibco).

HeLa cells

HeLa cells JW (immortal human cervical cancer line) expressing cherry-tubulin were obtained from the lab of Benny Geiger and Sasha Bershadsky, Weizman Institute of Science, Israel. They were cultured in DMEM (10% FCS, 1% pen/strep).

3.6.2   Cell fixation and staining

Actin and nucleus staining

For actin stress fiber imaging, cells were permeabilized with 0.1% Triton X-100 plus 1.5% formalin in PBS for 10 min and then fixed in 3% formalin in PBS for another 10 min. Samples were next blocked in 4% bovine serum albumin in PBS for 1 h. Samples were rinsed three times with PBS between each stage.

After fixation, samples were incubated with Alexa Fluor 488 Phalloidin for actin staining (1:400 dilution; Molecular Probes, Switzerland) and ethidium homodimer-1 for nucleus staining (1.5 μM; Invitrogen, Switzerland) for 20 min. Samples were rinsed thoroughly prior to imaging. Similar microscopy settings were used for imaging on 2-D and in 3-D, therefore images of actin filament assembly can be compared.

Because actin visualization is a crucial read-out in this thesis, some background about actin fiber staining is provided here. Phalloidin is isolated from the mushroom death cap and belong to the group of toxins known as phallotoxins. It has the property to bind specifically to F-actin subunits and locking them together, therefore preventing its depolymerization [212]. Due to this characteristic phalloidin is a useful tool for investigating the distribution of F-actin in cells by labeling phalloidin with fluorescent analogs. Labeled phalloidin has similar affinity for both large and small filaments, binding in a stoichiometric ratio of roughly one phalloidin molecule per actin subunit [213]. It has been reported that phalloidin is unable to bind to monomeric G-actin, and hence fluorescence is only seen where filaments are present [214]. A saturating concentration of phalloidin allows even for visualization of single actin filaments.

Viability study

The standard protocol is described here; cell type and incubation time are specified in the appropriate chapters (chapters 4 and 6). Viable cells were distinguished from apoptotic cells by the enzymatic conversion of calcein AM to fluorescent calcein and the exclusion of ethidium homodimer-1, which is membrane impermeable but undergoes a 40-fold enhancement of fluorescence upon binding to nucleic acids in dead cells with a compromised membrane [139, 215]. Samples with cells were carefully rinsed with PBS warmed to 37 °C and then simultaneously incubated with 5 μM calcein AM (Invitrogen, Switzerland) and 1.5 μM ethidium homodimer-1 (Invitrogen, Switzerland) in PBS for 20 min. Subsequently they were rinsed with PBS and imaged.

Mitochondrial membrane potential

Tetramethylrhodamine ethyl ester (TMRE; Molecular Probes, Switzerland) was used to stain the mitochondrial membrane potential. The stock solution was 25 μM in 1:1 DMSO/Ethanol and diluted 1:1000 in cell culture media prior to experimentation. The cells were incubated at 37 °C for 30 min, rinsed and imaged. The imaging was performed in an incubator box with controlled temperature and CO_2. The cells were always imaged at 37 °C unless stated otherwise.

3.7   Analytical and imaging techniques

Surface analytical techniques are essential tools to characterize the substrates and materials we were working with. In this thesis analytical techniques, such as Quartz crystal microbalance with dissipation monitoring (QCM-D) and fluorescence recovery after photobleaching (FRAP), were used. Microscopy techniques used for imaging were fluorescence microscopy (FM), confocal laser scanning microscopy (CLSM), and scanning electron microscopy (SEM). These techniques are described here in more detail.

3.7.1   QCM-D

Quartz crystal microbalance with dissipation monitoring (QCM-D) is an *in situ* technique that allows for determination of the adsorbed mass on the surface and the viscoelastic properties of adsorbed molecules, such as polymers, lipids and proteins in liquid [216–218]. A quartz crystal is oscillated at its resonance frequency and frequency changes (mass) as well as changes in the dissipation (rigidity) are measured. A negative frequency shift indicates a mass increase on the surface [219]. The dissipation is the ratio of all energy loss in the system to the total stored energy during one cycle of oscillation change and gives information about the viscoelastic properties of the film. A soft film results in high dissipation and a rigid one in low or no dissipation change.

A QCM-D E4 instrument (Q-Sense AB, Sweden) was used to analyze the bilayer formation on PDMS, test its protein resistance and the functionalization of bilayers with cadherin (chapter 4) and furthermore to investigate the crosstalk between biotinylated SPB and Fn (chapter 5). QCM-D crystals were coated with a thin layer of PDMS as described in section 3.2.2 or purchased already coated with SiO_2.

3.7.2   SEM

Scanning electron microscopes (SEM) images were obtained by scanning a high energy electron beam over the sample and collecting either the back scattered or the secondary electrons. Back scattered electrons give some information about the material contrast, while secondary electrons often provide more distinct topographic information. SEM has the ability to image topographic samples with very high lateral resolution (< 10 nm).

In this work a SEM LEO1530 (Zeiss, Germany) equipped with a field emission electron source was used to characterize the quality of the microwell replication into PDMS (section 3.4). All specimens were coated with a few nanometer thin platinum layer using a sputter coater (SCD 050, BAL-TEC) to prevent charging. The images were taken in-lens (back scattered electrons) as well as using secondary electrons at an acceleration voltage of 2 – 3 kV.

3.7.3   Fluorescence microscopy

Fluorescence is a phenomenon where certain molecules or atoms can absorb light at a certain wavelength and emit it at longer wavelength. The first fluorescence microscopes (FM) were build in the 1910s. The potential of the technique was realized in the 1940s when scientist started to couple fluorochromes to larger molecules like antibodies and the technique found its way into the field of cell biology [1].

Confocal laser scanning microscopy
In a confocal laser scanning microscope (CLSM), a laser beam is focused and scanned over the surface and excites fluorophores. The images are acquired pixel by pixel. A pinhole allows the user to confine the focal plane, leading to much sharper images compared to regular FM. Emitted and scattered light is collected in an objective. Filter sets and beam splitters are used to filter the excitation light allowing only the emitted fluorescent light to pass, which is collected with a CCD (charge-coupled device) camera. Fluorescently labeled proteins and vesicles were visualized using an inverted confocal laser scanning microscope (CLSM, LSM 510, Zeiss), images of the cells were acquired with an Olympus FV1000 confocal microscope with an oil immersion 1.35NA 60× objective.

FRAP

Fluorescence recovery after photobleaching (FRAP) is a simple method to test the lateral mobility of a layer, *e.g.* phospholipids in a supported lipid bilayer which are laterally mobile if they are above their T_M [220–222]. FRAP experiment are normally performed on a bilayer doped with fluorescently labeled lipids. The molecules are bleached with the laser beam in a small, defined area. If the lipids are in a planar lipid bilayer, the bleached molecules are replaced by fluorescent molecules arriving from the non-bleached area and the dark spot disappears over time. By following the bleach spot and its recovery over time, the diffusion coefficient of lipids in the bilayer can be calculated (see fig 3.5). FRAP was performed for mobility studies described in chapter 4.

The FRAP experiment were performed using a Zeiss LSM 510 CLSM equipped with a 25 mW Argon laser (line used: 488 nm) and 1 mW HeNe laser (line used: 633 nm) with the corresponding filter sets.
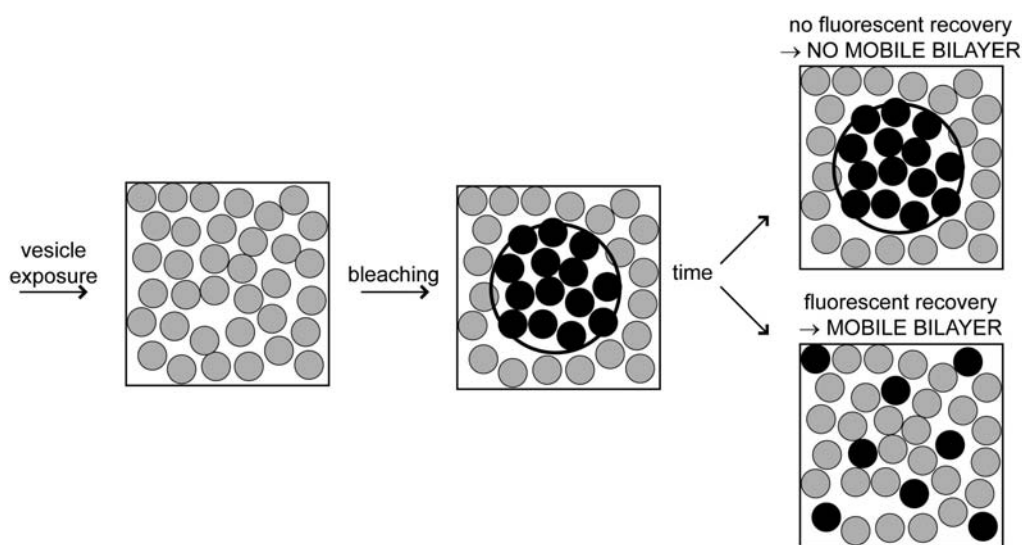
Figure 3.5: *Principle of FRAP.* Initially, the fluorescent molecules are distributed equally in the lipid bilayer and with a focused laser beam a defined area of dyes is bleached. If the fluorescent signal recovers with time, it is an indication of the presence of a mobile bilayer. If the bleached spot stays unchanged, the fluorophores are immobile which might be the case in, for example, vesicle adsorption on the surface.

Mobile and immobile cadherin-functionalized bilayer coatings

Cells in a tissue are, in most cases, in a cellular context and interact with ECM and soluble factors shared with neighboring cells. The microwell platform presented in the previous chapter enables the study of isolated single cells, however, cell-cell contacts have been shown to influence many aspects of normal cell function. It has also been suggested that mobility of these contacts, which is a physiologically relevant mode of presentation, is important for their function. Therefore, the intention of the work presented in this chapter was to mimic cell-cell interactions, in a simplified manner, using a human E-cadherin-functionalized supported phospholipid bilayer (SPB), which is itself a laterally mobile system and can be coated onto the walls of the microwells.

4.1 Background

4.1.1 Cell-cell interaction

Cells in tissues adhere to each other and the ECM through specific surface proteins called cell-adhesion molecules (CAM). CAMs cluster at specific junctions (cell-cell adhesions) or adhere via the binding of adhesion receptors to the ECM (cell-matrix adhesions). The extracellular part of CAMs serves to mediate interactions with other CAMs of the same type (homophilic binding) or to different types of CAMs (heterophilic binding). The intracellular part of CAMs is built of a network of adapter proteins interacting with the cytoplasmic tail of the CAMs. This adapter protein network is in close contact with the cytoskeleton and assures a link between the actin filaments and the CAMs.

Cadherins

Cadherins are a large superfamily of cell-cell adhesion molecules. Several different subtypes of cadherins exist. The most important ones are desmosomal cadherins and classical cadherins. Desmosomal cadherins are found in the adhesive junction of epithelial and muscle cells where they link their intermediate filaments to those of the neighboring cell to help the cell resist shearing forces. Therefore, they usually link their own intermediate filaments to those of the neighboring cell. Classic cadherins consist mainly of epithelial cadherins (E-cadherin) and neural cadherins (N-cadherin). They are usually concentrated in adherent junctions in epithelial and neural cells, where they help to connect the cortical actin cytoskeleton of adjacent cells. The classic cadherins have some universal features, such as homophilicity and Ca^{2+}-dependence binding. The presence of Ca^{2+} is crucial for activation of cadherins since it maintains structural rigidity, protease resistance and adhesive activity in forming cadherin homodimers on the surface. If Ca^{2+} is removed, the extracellular part of the protein loses its defined conformation and is rapidly degraded by proteolytic enzymes. In this project, the main focus was on E-cadherins, because these are known to crucial for cell-cell contacts as discussed below.

Cadherin function is a dynamic process involving cadherin clustering and environmental cues which regulate the cell response. Processes involving cell-cell interactions have been shown to be important for multicellular tissue formation, cell association, and migration. Cadherin regulation is an important mechanism during development. E-cadherin is the first cadherin expressed during embryogenesis; during the eight-cell stage of a mouse embryo, the loosely attached cells become tightly packed together by intercellular junctions [223–225]. It has been shown that the blocking of cadherins with antibodies results in morphological defects and the disruption of tissue structure [226, 227]. Furthermore, the segregation of cells into distinct tissues is accompanied by changes in the complement of cadherins expressed by the cells [228].

In adult tissue, cadherins are crucial to generate stable, tight junctions which form, for example, a strong barrier between the blood stream and the intestine. Furthermore, cadherins are also involved in signaling processes which are important for cell differentiation, movement, and tissue organization [229]. Deregulation in cell-cell adhesion is a characteristic in diseases, such as cancer [230]. It has been shown that a loss of E-cadherin expression or function leads to enhanced cell invasiveness in cell culture. Furthermore E-cadherin deficiencies or mutations correlate with the invasiveness and metastasis of certain human tumors [231, 232].
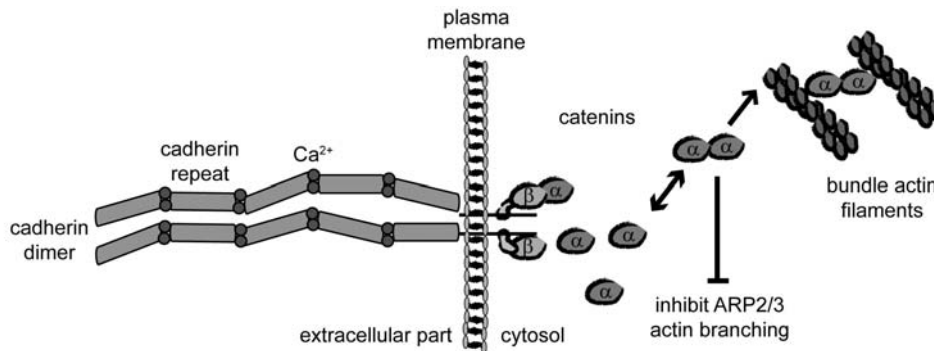
Figure 4.1: *Models of the cadherin-catenin complex and its link to the cytoskeleton.* This schematic illustrates the cadherin architecture and its linkage to the actin cytoskeleton. The extracellular part consists of 5 domains which can interact with a neighboring cell. The intracellular part links the cadherin to the cytoskeleton via catenins (adapted from [235].

Most cadherins are transmembrane proteins that indirectly link the actin cytoskeleton (fig 4.1). The cadherin extracellular part consists of 5 domains, each containing Ca^{2+} binding sites, which are responsible for intercellular interactions. The highly condensed cytoplasmic tail of these cadherins interact with actin via a group of intracellular anchor proteins called catenins. The attachment of the actin cytoskeleton to the cadherin is crucial for the increase of adhesive strength, and for the clustering of cadherins. Cadherins lacking their cytoplasmic domain cannot maintain their interaction sufficiently, leading to disruption of the adhesion bond between cells [233].

Recent studies indicated that the linkage between the cadherins and the cytoskeleton is complex [234, 235]. The α-catenin monomers show an altered binding preference compared to the α-catenin dimer. The monomers preferentially attach to the β-catenin, while the dimer preferentially attaches to actin filaments. Initial contact between cells causes cadherin clustering and therefore a high local concentration of the cadherin bound β-catenin monomers. The binding of α-catenin monomers to the clustered β-catenins creates a high local concentration of α-catenin that can dimerize and preferentially attach to the actin filaments. Meanwhile the α-catenin dimers were also responsible for the suppression of ARP2/3 activity, which results in a cessation of lamellipodia activity and creation of stable cell-cell contacts (fig 4.1 B).

Lateral mobility of cadherins

During processes, such as development of multicellular organisms, tissue regeneration, immunological response and tumor metastasis, the cell-cell contact is dynamic [228]. For example, cell-cell contacts must be transient during morphogenesis to establish new cell

boundaries. Conversely, the maintenance of structural integrity requires strong and stable cell-cell contacts.

Laterally mobile cell adhesion molecules permit the cell to spatially arrange its cell contacts and build clusters which strengthen and stabilize the adhesion site [61, 236, 237]. E-cadherins concentrate at cell-cell contacts and accumulate actin in their perijunctional regions in discrete spots or clusters [238]. Movements of E-cadherin inside the plasma membrane have been shown to be regulated by the cytoplasmic domain via tethering to actin filaments [239]. It has been reported that cadherin adhesion influences actin organization [240], while conversely an intact actin skeleton is necessary for cadherin based cell-cell interaction [237].

4.1.2   Motivation behind mimicking cell-cell interaction

Cell fate is strongly influenced by the properties of the ECM and the interaction of the cell with its surroundings. The interaction of a cell with its environment consists of cell-ECM contacts or cell-cell contacts, where the link is via a mobile transmembrane protein, such as cadherin. The interaction of the cell with the cadherin depends on ligand presentation. Studies investigating cell-cell interaction showed that orientation and dimerization are critical factors for homophilic cadherin interaction [241]. To obtain an orientation of the cadherin closer to the physiological condition of a cell-cell interaction, where cadherins first dimerize and subsequently bind to the neighboring cell, strategies to couple cadherin/Fc chimera via protein A or antibodies have been explored [242, 243].

Mobile presentation of cadherins
In vitro studies with immobilized cell adhesion proteins enables the control of chemistry and density of ligands on the surface [71, 78, 79, 88, 170, 175], but they unfortunately lack lateral mobility, an important feature that steers cell behavior (discussed earlier in this chapter). A seminal study by Yap *et al.* pointed out the fundamental role for lateral clustering and the distribution of cadherin binding sites [236], but was performed on immobilized cadherins. The dynamic aspect of cadherin interactions was captured by Perez *et al.* where they facilitated cell adhesion by patterning Fn islands and presented the cell with cadherin-functionalized SPB between the islands to study cell adhesion. But to our knowledge, there are no previous studies where the lateral clustering of cell adhesion molecules and its implications on cytoskeletal organization on mobile substrates has been investigated.

Our platform is based on an E-cadherin-functionalized SPB-coated on topographically structured PDMS substrates. This permits the study of lateral cadherin clustering on a mobile substrate. Furthermore, due to the choice of the phospholipid, we are able to switch between a mobile and an immobile platform by a minor change in temperature. Thus, we are able to present a mobile and an immobile system with exactly the same chemistry to the cells and to change the mobility during the experiment itself. The arrangement of ligands in 3-D has been shown to stimulate the cell and its responses were altered in comparison to a 2-D surface (as discussed in section1.2.3) [92]. The combination of the E-cadherin-functionalized SPB within a 3-D microwell structure [244] enables a closer mimic to cell-cell contacts *in vitro*. However, it needs to be taken into account that the SPB platform only allows for a coupling of the extracellular part of the cadherin and that the isolation from the intracellular machinery, normally present in the neighboring cell in a tissue, might trigger different behavior compared to a real cell-cell contact situation.

4.2 Experimental section

4.2.1 Cadherin functionalization

Functionalization via biotin-streptavidin

For studies on 2-D surfaces, PDMS was spin-coated onto substrates as described in section 3.2.2. For studies in 3-D, microwells were produced as described in section 3.4 and 3.5.2.

To functionalize the SPB, 0.5 or 5% bDOPE were added to the DOPC before vesicle formation. The surfaces and microwells were exposed to a vesicle solution (100 nm, 0.5 mg/ml in HEPES) for at least 15 min and rinsed with HEPES. For further functionalization, the samples were incubated with SA (50 μg/ml in PBS, 15 min), bAB (10 μg/ml in PBS, 30 min) and E-cad/Fc (10 μg/ml in PBS with 0.2 mM Ca^{2+}, 30 min). They were carefully rinsed with HEPES after every functionalization step.

For cell studies, samples with 5% bDOPE/DOPC bilayers were further functionalized with SA, bAB and E-cad/Fc as described above and the final sample was kept in PBS with 2 mM Ca^{2+} until exposure to the cells.

4.2.2   Characterization techniques

QCM-D

The PDMS spin-coated QCM-D crystals (Q-sense, Sweden) (for spin-coating protocol see section 3.2.2) were treated for 30 sec with air plasma and mounted in the QCM-D flow cells. The SiO_2 coated QCM-D crystals were treated with UV ozone (model 135500, Boekel Industries Inc., US) for 30 min and mounted in the flow cells. The crystals were checked for the resonance frequency of the 3rd and the 5th overtones. The PDMS layer on the crystals was relatively thick and affected the viscoelastic properties. Therefore, the resonance frequencies of the crystals were damped due to internal loss of oscillation energy and higher overtones were not detectable. All the quantitative analysis was performed for the frequency and the dissipation with the 5th overtone. After stabilization of the baseline in HEPES buffer, lipid vesicles were injected. After the adsorption step, the excess molecules were removed by rinsing with HEPES buffer. The further E-cad/Fc functionalization was performed as described above.

Mobility studies inside microwells

For the investigation of lateral mobility across the edge of a microwell, microwell samples were replicated into PDMS as described in section 3.4. In contrast to the standard protocol, the plateau was deliberately not passivated by PLL-*g*-PEG before vesicle exposure. The vesicles could therefore build an SPB on the whole sample, which provided a huge reservoir of lipid, allowing the diffusion of non-bleached lipids from the plateau to the bottom of the well to be observed.

4.2.3   Cell culture

CHO cells expressing GFP-E-cadherin were used for this study. On 2-D substrates, CHO cells were seeded at a density of 10^4 cells/cm^2. For the specific interaction assay with the cadherins, cells were allowed to attach for 2 h and rinsed afterwards. To test cell survival and cytoskeleton formation, cells were cultured for 2 h and subsequently rinsed to remove non-adherent cells. Afterwards they were cultured for an additional 22 h for the cell survival study (section 3.6.2) and 12 h for the bilayer stability study.

Microwells were coated with E-cad/Fc functionalized SPB to test if CHO cells could adhere inside the wells. The cells were seeded inside the microwells (5×10^4 cells/cm^2)

and incubated for 2 h before rinsing and kept for a total of 24 h in cell culture. For actin stress fiber imaging, cells were fixed after 24 h in culture and stained as described in section 3.6.2.

4.3 Results and discussion

4.3.1 Characterization of bilayer functionalization on PDMS

To test if the PDMS microwell platform could be combined with SPB formation and functionalization, SPB formation kinetics, protein resistance, and functionalization with E-cad/Fc was investigated on a flat PDMS surfaces (fig 4.2 A, B illustrates the functionalized SPB inside a microwell). To do so, QCM-D experiments on PDMS spin-coated crystals were performed. QCM-D allowed for the *in situ* monitoring of every step of the E-cad/Fc functionalization via the biotin-SA linkage. Other groups have also successfully shown the modification of a biosensor with PDMS and subsequent SPB or lipid mono-layer coating [56, 245].

Bilayer formation on PDMS
The formation of SPBs composed of DOPC, 0.5% and 5% bDOPE/DOPC on oxidized PDMS was investigated by QCM-D. The vesicle solution was added to the QCM-D crystal and functionalized with E-cad/Fc (schematic of functionalization is illustrated in fig 4.2 C). The QCM-D curves (fig 4.2 C) indicated bilayer formation after vesicle exposure for all three bDOPE concentrations through a residual change in frequency of -26 Hz, the characteristic frequency change for SPB formation.

The different frequency changes in the QCM-D measurement during vesicle adsorption and before rupture are indicative of different kinetics occurring during SPB formation. The kinetics were not further investigated since the final frequency change after vesicle rupture was always -26 Hz. Several different parameters may influence the kinetics, such as surface properties, vesicles size distribution, concentration, volume injected and the speed of injection [246]. Lenz *et al*. have reported that the interaction of vesicles with oxidized PDMS surface can be tuned to yield bilayers, monolayers, or vesicles respectively [42]. In our experiments, the SPB formation on oxidized PDMS was less sensitive to plasma treatment time than has previously been reported and on every oxi-

dized PDMS surface SPB formation occurred. After observing stable SPB formation, the system was further functionalized.

Cadherin functionalization

All the functionalization steps following SPB formation were also monitored by QCM-D (fig 4.2 C). After SPB formation on PDMS, the SPB was exposed to SA; the pure DOPC SPB showed no frequency change as expected. Conversely, 0.5% and 5% bDOPE/DOPC SPB showed a decrease in frequency, indicating SA binding through the biotin groups. The further functionalization steps with injection of bAB and E-cad/Fc resulted in further negative frequency shifts, representing mass uptake.

The decrease in frequency was monitored and the adsorbed mass calculated by Sauerbrey's Equation (fig 4.2 D) [219]. No binding of SA occurred on a 0% bDOPE/DOPC SPB as mentioned above. On a 0.5% bDOPE/DOPC SPB, the average adsorbed mass of SA was 277 ± 55 ng/cm^2. The average adsorbed mass on a 5% bDOPE/DOPC SPB was 463 ± 28 ng/cm^2, which was in good agreement with Höök *et al*. They found an adsorbed mass of 440 ng/cm^2 on SiO$_2$ [247]. The SA density was calculated with the method used by Huang *et al*. [248]. A molar mass of 60 kDa was assumed for SA and the unit cell area of one SA molecule was 24.8 nm^2. Therefore, a close-packed SA monolayer would correspond to 402 ng/cm^2. However, QCM-D measures the mass of the adsorbed molecule and bound water. Therefore, the adsorbed protein mass cannot directly be calculated into a percentage of a close-packed monolayer. Fortunately, the adsorbed mass without bound water has been determined. Reimhult *et al*. used simultaneous QCM-D and surface plasmon resonance (SPR) measurements to demonstrate that SA on a 5% bPE/POPC SPB bound a mass of water equal to 250 ng/cm^2 [249], which corresponds to 56% of the 440 ng/cm^2 total mass. If we apply the same percentage of 56% to our total mass uptake of 463 ng/cm^2, the SA mass is 259 ng/cm^2, which corresponded to a SA layer which was the equivalent of 64% of a closely packed SA monolayer. As a control, the mass of adsorbed SA on SiO$_2$ was also determined and a SA mass of 540 ± 12 ng/cm^2 was calculated. The density of SA on an SPB is discussed later in this section.

The SPB was further functionalized with the bAB and a mass uptake of 267 ± 28 ng/cm^2 for 0.5% bDOPE/DOPC SPB and 424 ± 23 ng/cm^2 for a 5% bDOPE/DOPC SPB was detected. The exposure of the SPB to E-cad/FC resulted in a mass uptake of 33 ± 5 ng/cm^2 for a 0.5% bDOPE/DOPC SPB and 81 ± 5 ng/cm^2 for a 5% bDOPE/DOPC SPB. A monolayer of E-cad/Fc had a mass uptake of 280 ± 52 ng/cm^2 on a oxidized PDMS surface. As a reference experiment the binding of E-cad/Fc via pro-
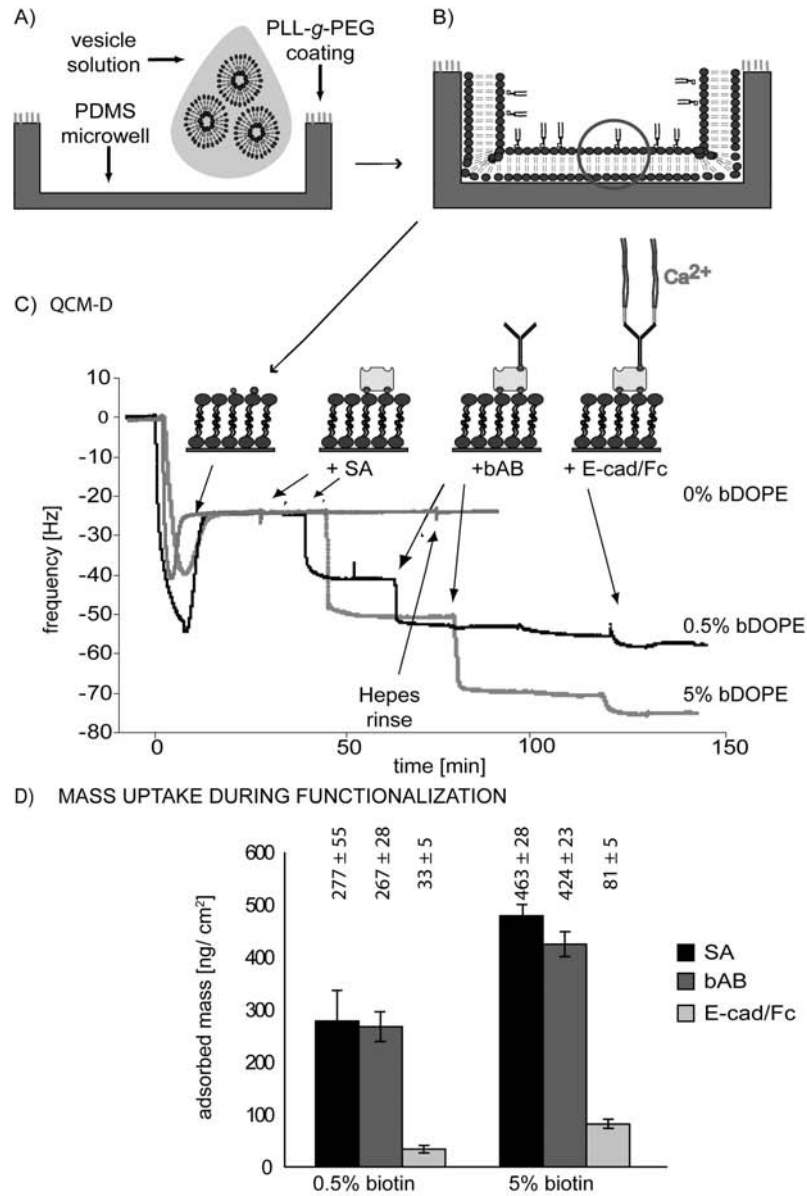
Figure 4.2: *E-cad/Fc functionalization of an SPB.* A) Schematic of a microwell and its exposure to a vesicle solution is shown. B) The vesicles rupture inside the microwell and build a bilayer which can be further functionalized with E-cad/Fc. C) The different functionalization steps of the biotinylated SPB are sketched and monitored by QCM-D. After vesicle injection, the SPB was exposed to SA, bAB and finally to the E-cad/Fc chimera. D) The average calculated mass uptake and standard deviation of SA, bAB and E-cad/Fc for a 0.5% bDOPE/DOPC and a 5% bDOPE/DOPC SPB were calculated.

tein A was performed. The binding via protein A is a method to immobilize cadherin on the surface and should allow for a more ordered arrangement of the E-cad/Fc, similar to the immobilization on a biotinylated SPB. The binding of E-cad/Fc via protein A resulted in a mass uptake of 763 ± 63 ng/cm^2. The mass uptake of E-cad/Fc for a 5% bDOPE/DOPC SPB corresponded to 11% of an E-cad monolayer on protein A, the 0.5% bDOPE/DOPC SPB to 4%.

Protein-resistant SPBs on PDMS

Protein resistance is an important prerequisite for the presentation of E-cad/Fc on the SPB platform and the specific interaction with cells. Because the functionalization with E-cad/Fc involved a SA linkage, the DOPC SPB was exposed to this specific protein and the mass change following SA exposure was monitored. Importantly, no mass change was observed after SA exposure, demonstrating that SA did not adsorb non-specifically on the SPB (fig 4.2 C). Therefore, we concluded a protein-resistant DOPC SPB had been successfully formed on PDMS , which was consistent with previous results on SiO$_2$ [36] and PDMS [250].

PDMS surface alters mobility of streptavidin layer on SPB in comparison to SiO$_2$

An important criterion for the mobile platform was the mobility of the SPB and consequently the SA layer on PDMS. It is known from the literature, that it is possible for SA to crystallize on top of SPBs [251, 252]. A 2-D crystallization or close packing would result in loss of mobility. Therefore, we investigated the mobility of the SA layer. The mobility of a 5% bDOPE/DOPC SPB and the subsequent SA layer was studied by FRAP on PDMS and, as a reference surface, on SiO$_2$.

The control measurements with fluorescently labeled lipids showed a mobile SPB on SiO$_2$ (fig 4.3 A). A diffusion coefficient of 0.28 ± 0.04 μm^2/s with a mobile fraction of $86 \pm 1\%$ was measured. For membranes on glass, Phillips et al. found a value of 4 ± 1.3 μm^2/s for PC on glass, while Rossetti et al. measured a diffusion coefficient of 1.7 ± 0.3 μm^2/s for NBC-PC on SiO$_2$ [250, 253]. However after SA adsorption, the bleached SA layer showed slow and incomplete recovery of its fluorescence even after 400 s (fig 4.3 A).

Interestingly, on PDMS both the lipid and SA were mobile; the SA layer, in particular, did not result in an immobile layer (fig 4.3 B). The diffusion coefficients of the SPB and SA on PDMS were in the same order of magnitude. For oxidized PDMS, a diffusion coefficient for the SPB of 0.1 ± 0.04 μm^2/s with a mobile fraction of $83 \pm 4\%$ was found.
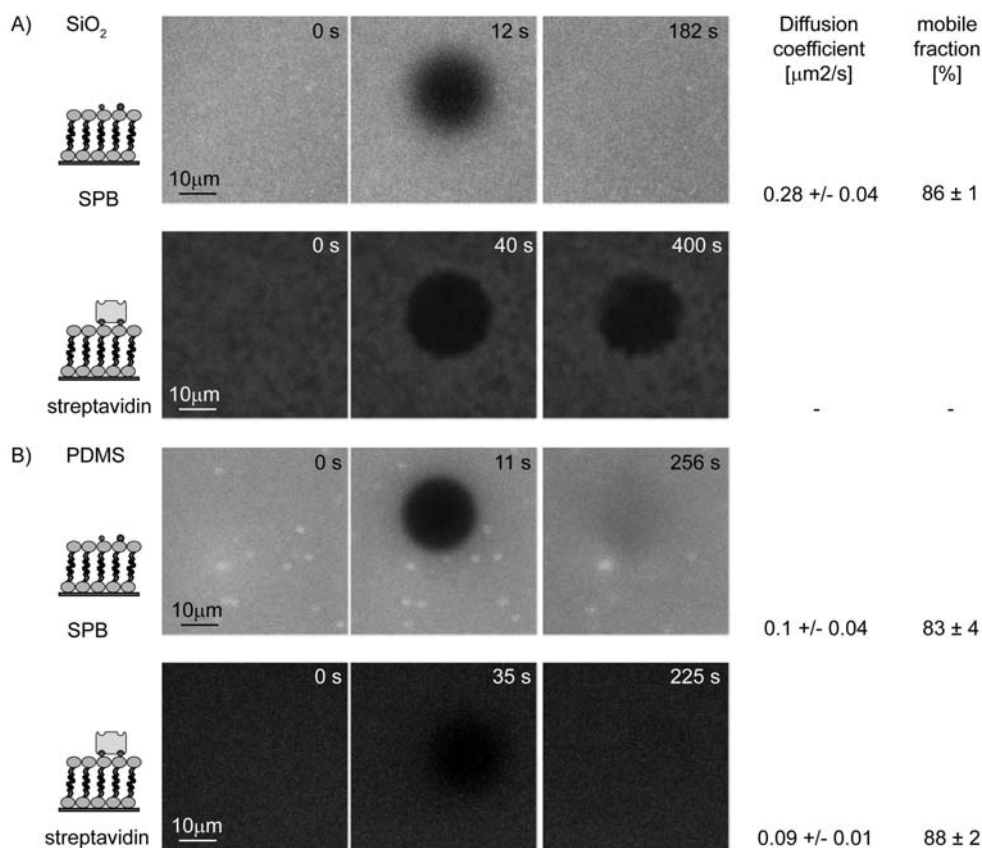
Figure 4.3: *Mobility of SPB and the subsequent layer of SA on SiO$_2$ and PDMS.* A) The mobility of a 5% bDOPE/DOPC SPB on SiO$_2$ was investigated using FRAP and showed lateral mobility. The mobility of the subsequent SA layer was also determined and there was no fluorescent recovery observable, which was indicative of the formation of an immobile layer of SA. B) Furthermore, the mobility of a 5% bDOPE/DOPC SPB on PDMS was investigated by FRAP and showed the presence of laterally mobile lipids. The mobility of the subsequent SA layer was also determined and fluorescent recovery was observed, which was an indication that a mobile layer of SA was formed in this case.

This diffusion coefficient was lower than reported in the literature. Phillips *et al.* reported a diffusion coefficient of 2.2 ± 0.9 μm^2/s for PC on oxidized PDMS [250]. This could be due to differences in SPB used or experimental set up. The diffusion coefficient of SA on PDMS was determined as 0.09 ± 0.01 μm^2/s with a mobile fraction of $88 \pm 2\%$. Since the SA coating is the critical step in determining the mobility in the E-cad/Fc functionalization, it is assumed that the E-cad/Fc coupled via the SA to the SPB was also mobile.

The adsorption of SA on an SPB on PDMS and SiO$_2$ was also monitored by QCM-D. The QCM-D curves after SA injection showed a different response in the frequency and dissipation on PDMS versus SiO$_2$, indicating a different viscoelastic behavior of the SA
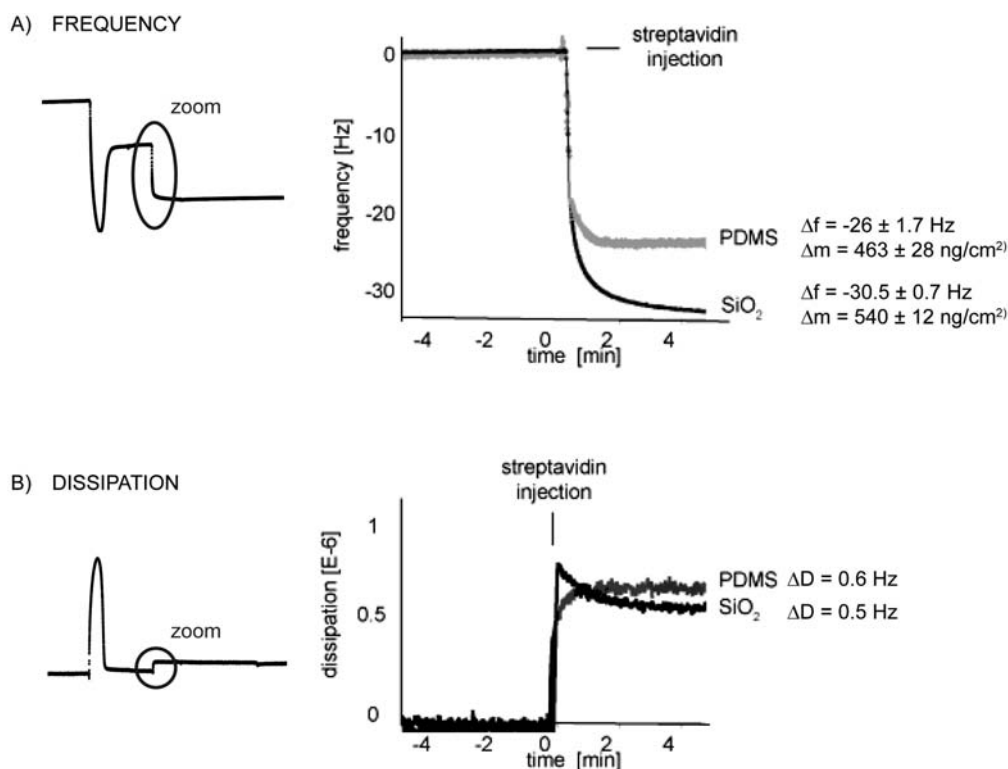
Figure 4.4: *QCM-D curve for SA injection on PDMS and SiO₂.* The small QCM-D curves on the left show the area of zoom in and for clarity there is only one curve shown. A) Frequency change of a QCM-D curves after SA injection showed that more SA adsorbed on SiO₂. B) Dissipation change after SA injection showed that the dissipation of the SA on PDMS remained constant, while the dissipation on SiO₂ decreased. Next to the representative QCM-D curves, average and standard deviation of frequency change and mass uptake (calculated by Sauerbrey's equation) are given.

layer for the two preparations. The frequency changes indicated that there was more SA adsorbing on the SiO₂ (540 ± 12 ng/cm^2) surface versus the PDMS (463 ± 28 ng/cm^2) (fig 4.4 A). On SiO₂, the dissipation curve of 5% bDOPE/DOPC SPB increased and then it decreased slightly (fig 4.4 B). This is indicative of a dissipative non-rigid protein arrangement followed by the formation of a more rigid layer [247]. On PDMS, the dissipation curve increased monotonically and stabilized. This, together with the differences in frequency change, indicated that there was a more dense packing of SA on an SPB on SiO₂ versus PDMS. The shape of the dissipation curves alone cannot be used to determine the 2-D ordering of the SA layer. Other techniques would be needed for the direct measurement of crystallization of SA, such as scattering showing the crystal lattice or imaging techniques, *e.g.* high-resolution AFM [254]. Furthermore, the combination of biosensor techniques, *e.g.* SPR coupled with QCM-D, might also provide useful information about the state of the SA layer. Reimhult *et al.* pointed out the possibility that changes in viscos-

ity with the variation in water content were a possible signal for 2-D SA crystallization [249]. The higher SA layer density and rigidity on SiO_2, indicates the formation of a close packed layer of SA molecules, at least in comparison to the lower density observed on the PDMS.

Table 4.1: Roughness values of PDMS and SiO_2 (measured by Stefan Kaufmann, ETHZ)

Roughness	PDMS master	PDMS wells - ox	PDMS spin coated - ox	SiO_2
R_{max}	3.8	6.8	2.5	4.9
R_{min}	-5.9	-2.0	-4.3	-3.2
R_{ms}	0.9	0.63	1.2	0.73
Skewness	0.06	-0.26	0.42	-0.25
Kurtosis	0.9	0.86	0.27	0.89

The mobility of SA on PDMS might be influenced by parameters, such as surface roughness, interaction between the solid support and the lipids and the diffusivity of the lipids [251]. Therefore, the roughness of the PDMS surface might be critical, decreasing the diffusion coefficient of the lipids and preventing the formation of an ordered surface. The roughness of the PDMS master, the PDMS microwell structure after plasma treatment, spin coated PDMS after plasma treatment and a glass slides coated with SiO_2 was measured by AFM (table 4.1). Different roughness parameters were determined. R_{max} and R_{min} give the highest and lowest spot on the surface but these values are very sensitive to external conditions like dust on the sample or sharpness of the tip and might not be representative of the surface. R_{ms} represents the root-mean-square roughness which was in the same order of magnitude for all surfaces. Skewness is a measure meant to capture the asymmetry of a probability distribution, like the presence of spikes on a flat background compared to small scale roughness. Kurtosis is a comparison of the height distribution with a Gaussian distribution and captures the occurrence of, *e.g.* large infrequent events in the tail of the distribution, such as spikes. Unfortunately, there was no difference in the roughness of the surfaces that could explain why SA becomes immobile on SiO_2 but not on PDMS. The roughness values for spin coated PDMS were slightly different from the values for PDMS on microwells and SiO_2, but since an SPB on spin coated PDMS and in microwells was mobile, which was in contrast with the mobility of the SiO_2 surface, we assume that most likely the different behavior of SA is caused by something other than the surface roughness. A likely explanation is that the difference in mobility is due to different amounts of SA that were adsorbed on the two surfaces, which could be influenced by the underlying substrate despite the same lipid composition being used for both SPBs.

Biotin is slightly hydrophobic and therefore the biotinylated lipid distribution might be asymmetric between the leaflets resulting in a lower concentration towards the SA in solution. PDMS is likely to be less hydrophilic than SiO_2 even after plasma treatment and is also known to experience an increasing contact angle with time after oxidation of the surface. Frank *et al*. demonstrated the concentration required to saturate a biotin-SA bilayer is ~ 2 mol% [255]. 5 wt% bDOPE in our system corresponds to $\sim$3 mol% bDOPE. If the biotinylated lipids are distributed asymmetrically, we could have a system containing less than 2% biotinylated lipids in the upper leaflet and therefore less SA adsorption on the SPB. Fig 4.4 also shows that less SA adsorbed on PDMS (463 ± 28 ng/cm^2) in comparison to on SiO_2 (540 ± 12 ng/cm^2).

In conclusion we can say that the SA layer on an SPB on PDMS was mobile versus the immobile SA layer on SiO_2. Although the diffusion coefficient of SPB and SA was lower on PDMS than reported in the literature, it is still in a physiological relevant range since ligands in a cell membranes show a diffusion coefficient between $0.01 - 0.1$ μm^2/s [61]. The diffusion coefficient of cell membranes is lowered compared to pure SPB because of the interaction of membrane proteins and the cytoskeleton [13].

SPB coating inside microwells and its mobility across the edge
As discussed in section 3.5.2, the PLL-*g*-PEG stamping prevented vesicles from adsorbing on the passivated surface, instead they adsorbed and underwent rupture inside the wells. SPB coating inside the microwells was visualized and the side view demonstrates that the SPB formed both on the side walls and the bottom of the well. There was no vesicle adsorption on the top of the plateau (fig 4.5).

However, to present to the cells a mobile 3-D system that mimics cell-cell interactions, the mobility of the SPB inside microwells and across the edge of the plateau needed to be confirmed. To study the mobility across the edge II (for labeling of edges see fig 4.6 B) of the microwell, the plateau was not passivated with PLL-*g*-PEG and the entire oxidized PDMS surface was exposed to fluorescent vesicles, guaranteeing a huge reservoir of non-bleached lipids. If only the microwell was covered with SPB, the fluorescent signal would not fully recover due to the lack of sufficient fluorescent lipids and not due to hindered mobility (fig 4.6 A).

First, the entire bottom of the well was bleached. With time, the fluorescence signal recovered, indicating that fluorescent lipids from the plateau of the microwell structure moved across the edge I down the wall to the bottom of the microwell (fig 4.5 B). The
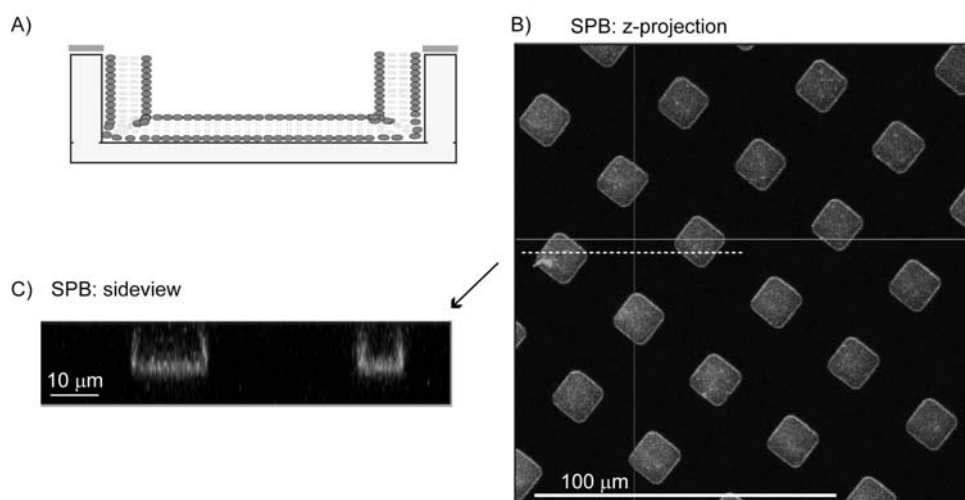
Figure 4.5: *SPB formation inside microwells.* A) A schematic of the SPB inside the microwells and the PLL-*g*-PEG coating on the plateau is shown. B) Z-projection of a confocal image of NBD-PC/DOPC shows specific SPB formation inside microwells. C) The side view shows that there was no vesicle adsorption on the plateau between the microwells.

radius of the edge II of the microwell does not act as diffusion barrier and is probably so large that the SPB does not experience any hinderance of spreading [256]. Brisson *et al.* have shown SPB formation from vesicles on nanoparticles with 100 nm diameter [257]. After replication into PDMS, we can assume that the radius of our edge II is larger than 100 nm. After SA injection, the SA on top of the SPB inside the microwell was bleached. It was confirmed that the SA was mobile on SPB on PDMS and that this mobility was not hindered by the microwell structure (fig 4.5 C).

The calculation of the diffusion coefficient is difficult in a non-radially symmetric 3-D environment. The formula normally used for diffusion coefficient calculation was developed for an initially large reservoir of lipids distributed homogeneously with radial symmetry. As visualized in fig 4.7, the effective neighboring lipid reservoir to the bleached spot inside the microwells is smaller than compared to a flat surface. Therefore, we expect that we would calculate a smaller diffusion coefficient and a non-homogeneous recovery due to geometrical reasons. The diffusion coefficient that was calculated in a triangular well was about two orders of magnitude smaller than coefficients calculated on a flat PDMS surface (fig 4.7). Therefore the coefficient was expected and observed to be lower.
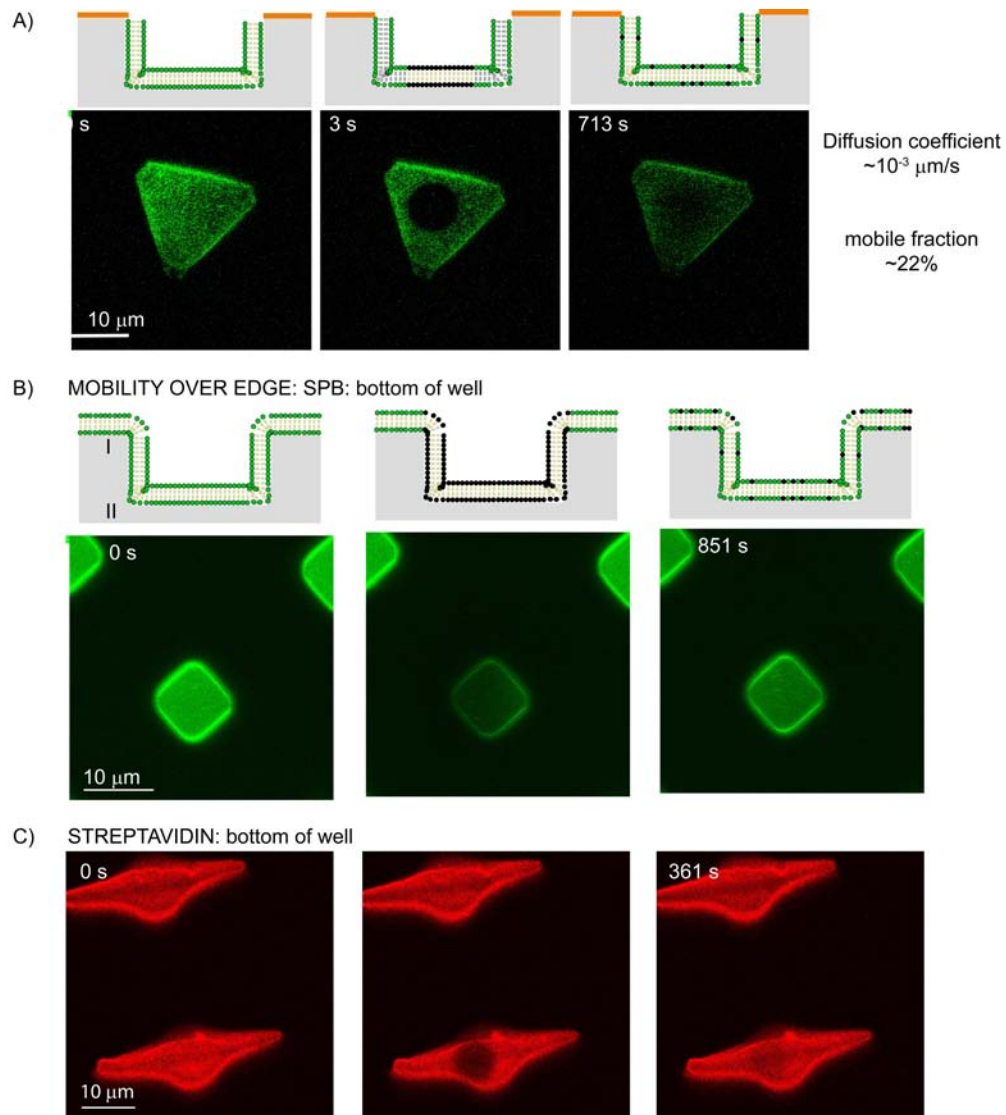
Figure 4.6: *Mobility of the SPB and SA layer inside microwells.* A) The fluorescent SPB was formed only inside the microwell and a FRAP experiment was performed on the bottom of the surface. Due to the limited lipid reservoir, the fluorescent signal could not be restored completely. The calculated diffusion coefficient is lower than on 2-D surfaces (for explanation see text). B) To test the mobility across the edge, the whole bottom of the well was bleached and the fluorescence recovery monitored. C) The SA layer inside microwells was also mobile as shown by the recovery of FRAP.

4.3.2   Immobile and mobile SPB

To study the influence of the mobility of cell adhesion ligands on cell response, a system that presents the same chemical composition in both its mobile and immobile state was developed. Phospholipids allow for the switching from a mobile to an immobile state by temperature change as presented in section 1.1.3. By using lipids with a T_m of 35 °C,

Figure 4.7: *Geometry of the lipid reservoir for FRAP experiments.* A) The FRAP formula is based on the assumption that the lipid reservoir is homogeneously distributed around the bleached spot. B) Inside microwells, the lipid reservoir is smaller due to geometrical reasons.

under normal cell culture condition (37 °C) the cell experiences a mobile ligand presentation, by lowering the temperature cells interact with an immobile platform.

Mobility variation with the same chemical system

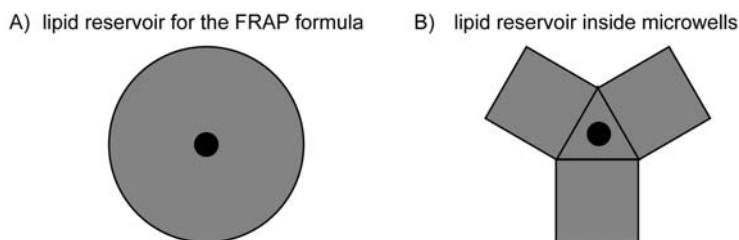The mobility of the SPB was investigated at T = 37 °C and T = 30 °C, using FRAP. These experiments confirmed the mobility of the SPB above T_m at 37 °C (fig 4.8 A). The fluorescence intensity of the bleached spot in the NBD-PC/MPPC SPB fully recovered after 6 min. Below T_m, at 30 °C, the NBD-PC/MPPC SPB was immobile and the fluorescence intensity of the bleached spot did not recover its fluorescent signal after 6 min (fig 4.8 B).

The bright spots visible in the images may be an indication of the presence of larger or multilamellar vesicles which gave a stronger fluorescent signal. In the sample coated with the mobile SPB, the bright spots did not recover with time, as it was observed for the homogeneous fluorescent signal. This also might be indicative of the presence of vesicles since vesicles are not laterally mobile and therefore can not move into the bleached area to aid fluorescent recovery.

In conclusion, the MPPC SPB could be switched between a mobile and an immobile system depending on the temperature. Furthermore, the temperature change was performed in a physiological relevant temperature range, thereby allowing for the culture of cells both below and above the T_m.
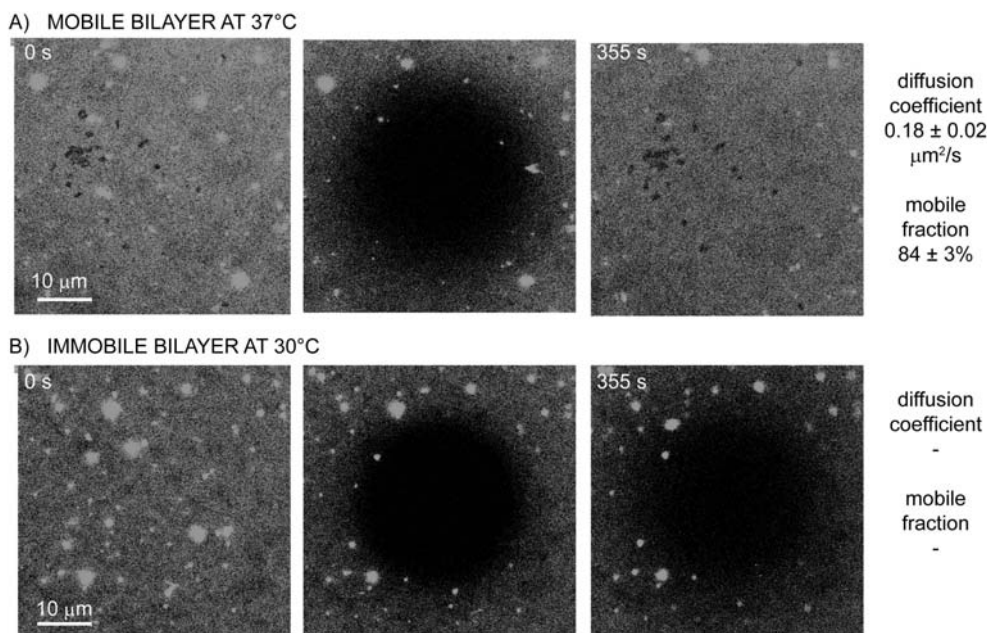
Figure 4.8: *Conversion between mobile and immobile MPPC SPB via temperature change.* A) A mobile MPPC SPB at 37 °C showed fluorescence recovery. B) The same bilayer below T_M at 30 °C did not recover its fluorescence and was therefore immobile.

Mobile and immobile SPB show protein-resistant properties

The protein resistance of the pure MPPC SPB above and below T_m was investigated by QCM-D, since a protein-resistant background is an important prerequisite for specific ligand presentation. It has been shown that vesicles below T_m have slower or do not exhibit SPB formation [25]. Therefore, all our SPBs were assembled above T_m and the temperature adjusted afterwards. After MPPC vesicle injection at 38 °C, the vesicles adsorbed on the PDMS surface and rupture occurred resulting in SPB formation.

To investigate the resistance against protein adsorption of the mobile system, serum injection was performed at 36 °C; for the immobile SPB, the system was first cooled down to 25 °C and after the stabilization of the baseline, serum was injected. Serum exposure to the SPB below and above T_m resulted in no frequency shift indicating protein-resistant SPB (fig 4.9). As a control, a plasma treated PDMS surface was exposed to serum and resulted in a large adsorption of serum (Δf = -50 Hz).

The protein-resistant properties of the MPPC SPB above T_m were similar to the protein-resistant properties described in literature for other SPBs. More interestingly, the MPPC SPB below T_m did not allow for serum adsorption. Due to the higher ordering and closer packing of the frozen SPB, one might expect a lateral shrinking of the SPB and crack formation resulting in reduced protein resistance [14]. The lack of protein

SERUM RESISTANCE

A) MOBILE BILAYER 36°C

B) IMMOBILE BILAYER 25°C
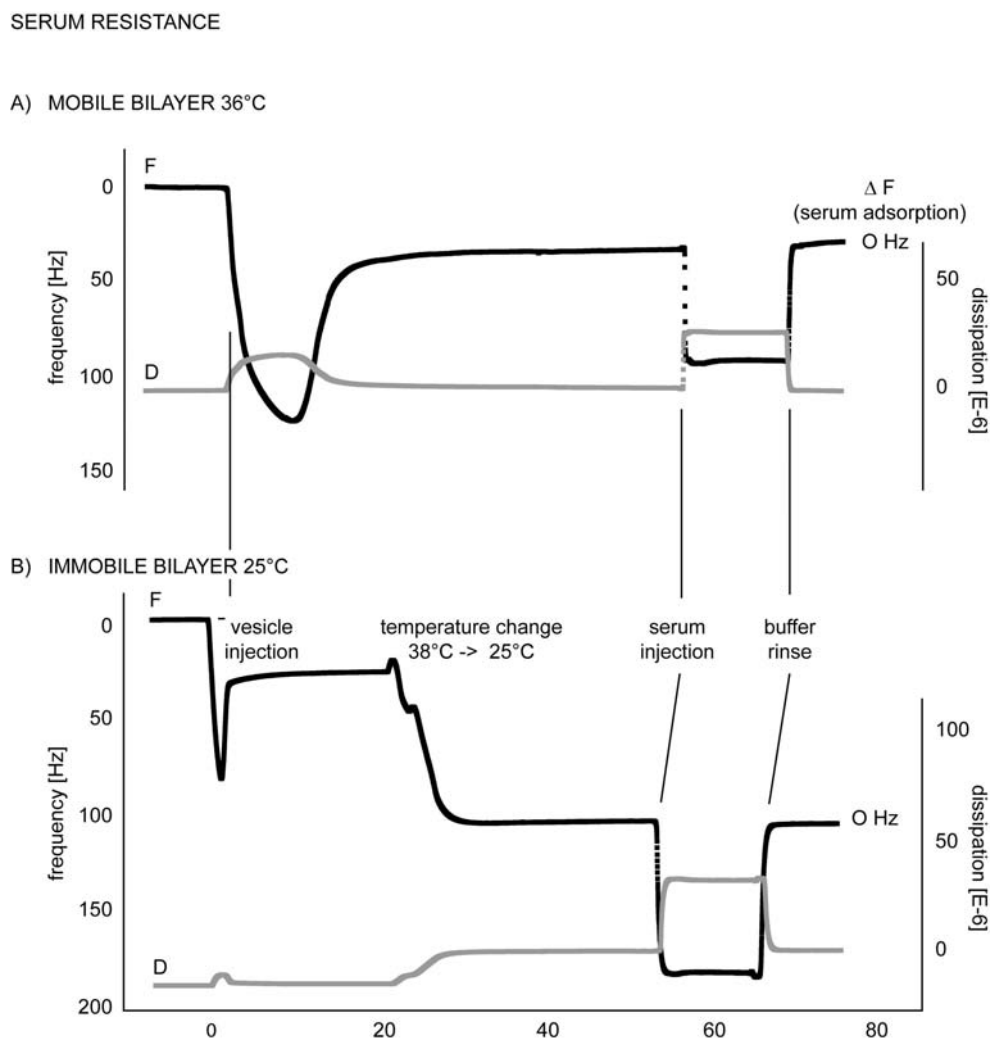
Figure 4.9: *Conversion between mobile and immobile MPPC SPB via temperature change.* The protein resistance of A) a mobile SPB at 36 °C and B) an immobile SPBs at 25 °C was tested with QCM-D and frequency and dissipation monitored. The SPB above and below T_M showed no mass increase after serum exposure.

adsorption indicated that these cracks might be in a small size range, such that the adsorbed proteins were not detected by the QCM-D since they would replace fully trapped water in such cracks. It is, however, more likely that non-specific adsorption was below 2 ng/cm^2, the detection limit of the QCM-D. Furthermore, some single vesicles might still be present after rinsing and act as a lipid reservoir which filled the cracks in the SPB. Further evidence for the protein resistance of the SPB can be obtained from the specific cell interactions with the surface (discussed in the next paragraph).

4.3.3 Cells on the cadherin-functionalized SPB

Specific cell interactions

In section 4.3.1, it was shown that E-cad/Fc can be coupled to a protein-resistant SPB via a biotin-SA linkage. Next, the specific interaction of the E-cad/Fc functionalized SPB with CHO cells was investigated. Therefore, cells were seeded on 2-D, PDMS coated surfaces after every functionalization step and the cell density imaged (fig 4.10). The specific interaction was tested for each of the systems developed, namely SPB of DOPC at 37 °C (fig 4.10 A), mobile MPPC at 37 °C (fig 4.10 B) and immobile MPPC at 29 °C (fig 4.10 C). Fig 4.10 D visualized the increase in cell attachment for the fully functionalized E-cad/Fc SPB. Standard error of the mean was only plotted for the fully functionalized SPB with many cells attached, for the other data points the mark covered the bar representing the standard error of the mean.

On a pure DOPC or MPPC SPB, only one cell was found to adhere to each of the surfaces (fig 4.10) [43]. Culturing cells on surfaces which were coated with 5% bDOPE/DOPC or 5% bDOPE/MPPC SPB functionalized with SA also resulted in limited cell adhesion (1 − 3 cells). After the bAB addition, the cell adhesion was similarly low (1 − 2 cells). Cadherins are known to be only active in the presence of calcium (Ca^{2+}) [236]. Therefore the specific interaction with the surface was investigated in the absence of Ca^{2+} and again very few cells managed to attach to the non-active E-cad/Fc functionalized SPB (1 − 4 cells). On an active E-cad/Fc functionalized SPB in presence of Ca^{2+}, the cells were able to attach to the E-cad/Fc (20 − 35 cells), showing the specificity of the surface and the interaction of the cells with the cadherin functionalized SPB.

The reduction of cell attachment with non-fully functionalized SPB supported the conclusion that the SPB itself and the molecules used for the functionalization steps provided no cell attachment, the cells adhered only to E-cad/Fc. Furthermore, the lack of cell attachment to E-cad/Fc without Ca^{2+} confirmed that cells were only able to adhere specifically to the functionality E-cad/Fc in presence of Ca^{2+}.
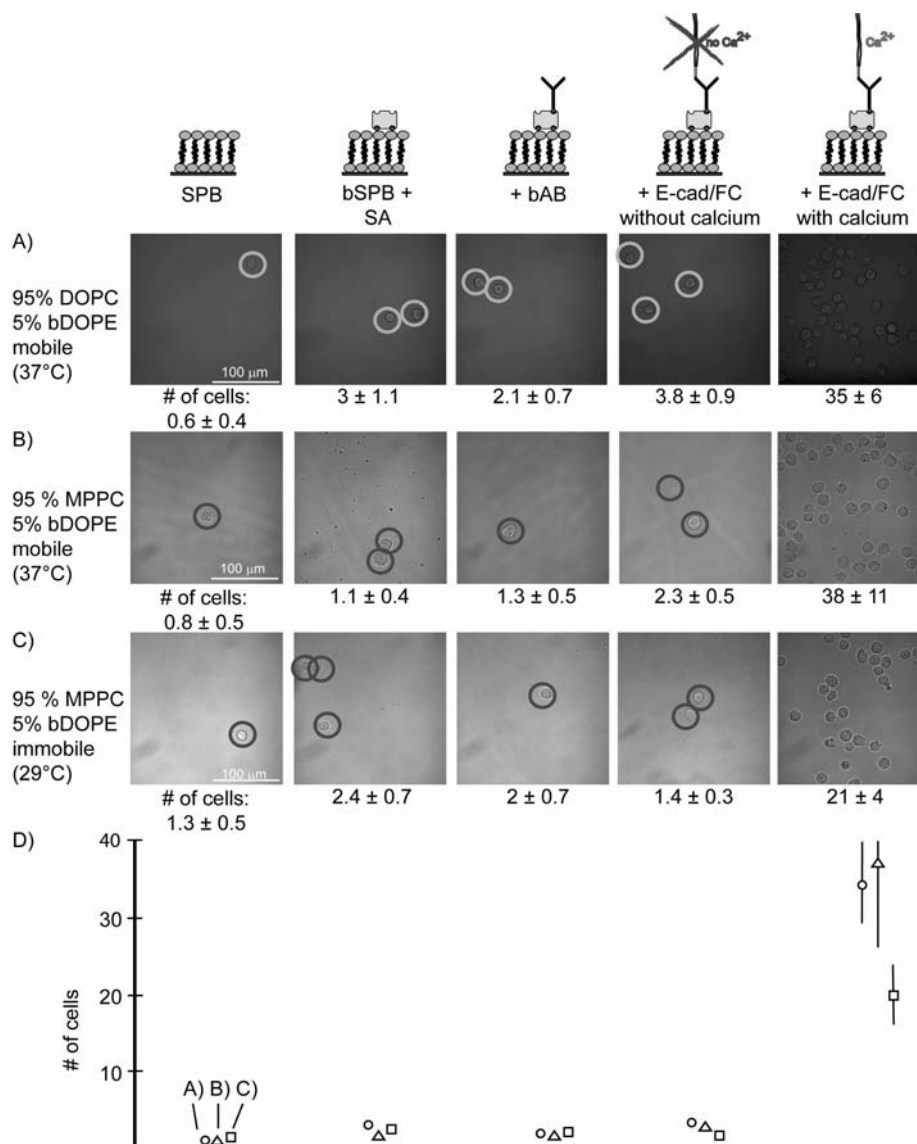
Figure 4.10: *Specific interaction of CHO cells with E-cad/Fc functionalized SPB.* Cells were seeded for 2 h onto A) a 5% bDOPE/DOPC, B) 5% bDOPE/MPPC above T_M, and C) 5% bDOPE/MPPC below T_M after every functionalization step. There was limited cell attachment on a pure SPB, after SA exposure and bAB injection. After E-cad/Fc functionalization the cells were only able to interact with the SPBs in the presence of Ca^{2+} as removal of the Ca^{2+} lead to reduced cell number. D) The average number of cells attached to the surfaces and the standard error of the mean for the functionalized and activated SPB are visualized in the plot.

Stability of SPB under cell culture conditions

To test if the bilayers were stable over a longer time period, cells were seeded on an E-cad/Fc functionalized, fluorescently labeled SPB. Cells and fluorescent signals were imaged immediately after cell seeding and rinsing (fig 4.11 A) and 14 h later (fig 4.11 B). Cells could attach to the functionalized SPB and the fluorescent signal was not altered

after 14 h, indicating that the cells did not destroy the bilayers. Cell adhesion after 14 h also indicated, that the cells were unable to detach the E-cad/Fc from the system.

Cell survival on mobile SPB

Cell-adhesive ligands linked to a viscous SPB might not resist the nanonewton forces generated by the cell which might result in the limitation of cell spreading, an activity required for survival of anchorage-dependent cells [136]. To study if the SPBs functionalized with E-cad/Fc provoke cell death or can support cell adhesion and growth, a cell live/dead assay was performed. Cells were cultured for 24 h on an E-cad/Fc functionalized SPB in 2-D. Afterwards, the cells were stained with calcein AM and ethidium homodimer to determine if the cells were still viable (fig 4.11 C). Cell survival was not diminished by the mobility of the ligand presentation, therefore we can assume that E-cad/Fc functionalized SPB can be used as a model system without reducing cell survival.
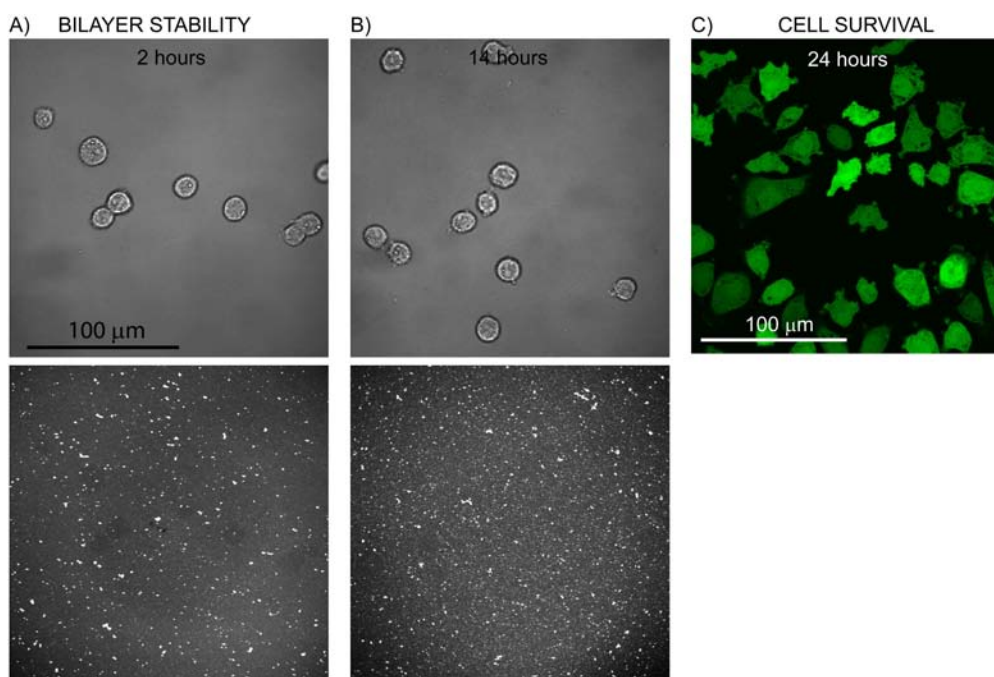
Figure 4.11: *Stability of E-cad/Fc functionalized SPB during cell culture and cell survival on a mobile E-cad/Fc functionalized SPB.* To investigate the stability of the E-cad/Fc functionalized SPB under cell culture condition, A) CLSM image of cells (top) and fluorescent signal of a 5% bDOPE/DOPC functionalized with E-cad/Fc (bottom) were imaged 2 h and B) 14 h after cell seeding. C) Live/dead staining was performed for CHO cells cultured on an E-cad/Fc functionalized SPB for 24 h. The calcein AM (green) cells are the living cells.
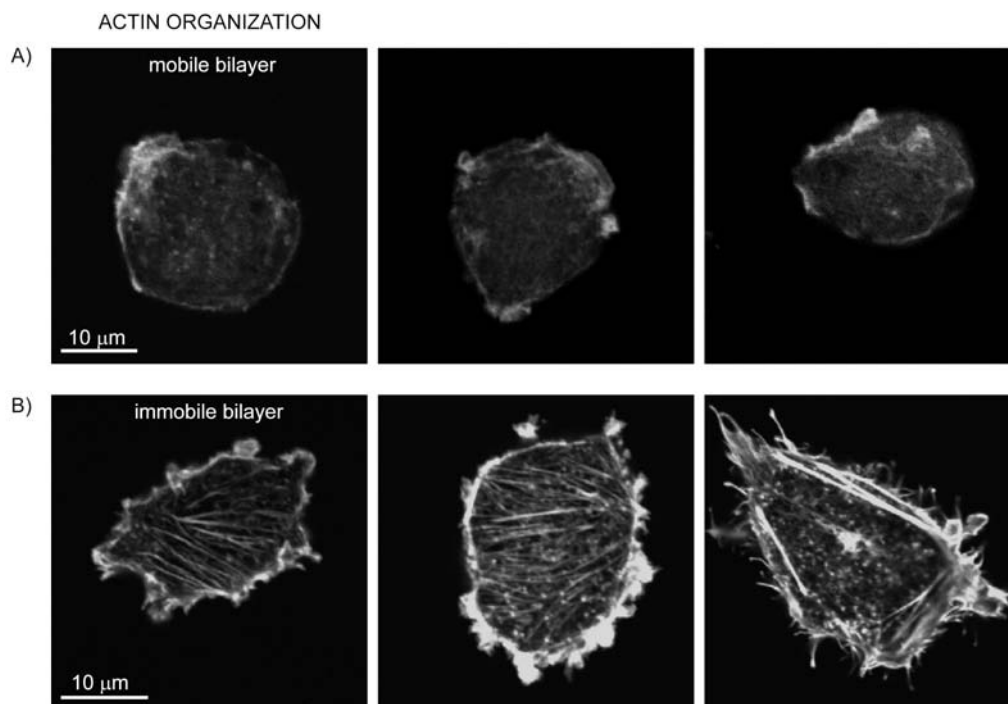
Figure 4.12: *Difference in actin formation depending on the mobility of the E-cad/Fc coating in 2-D.* A) A CHO cell (cell culture for 24 h) on a mobile 5% bDOPE/MPPC/E-cad SPB showed diffuse actin staining, while a B) CHO cell on an immobile bDOPE/MPPC/E-cad SPB showed similar actin formation to cells cultured in a Petri dish.

Cadherin mobility alters actin filament formation

Changes in mobility alters the cytoskeletal organization of a cell and therein its general behavior (as discussed in detail in chapter 7). Many cell responses are linked to the organization of the actin skeleton, such as proliferation [258] and differentiation [139]. Therefore, the difference in actin bundling was chosen as a demonstrative example of how the substrate mobility influences cell behavior. To visualize how the cellular response was altered by this environmental parameter, actin bundling was imaged on 2-D mobile and immobile E-cad/Fc functionalized SPB. Cells were fixed and actin stress fibers on mobile and immobile systems were stained with Phalloidin 488. It is clearly visible that cells on a mobile system (fig 4.12 A) built up different actin stress fibers than cells on an immobile substrate (fig 4.12 B). On the immobile substrate the cells showed distinct stress fibers similar to cells cultured on a Petri dish. The actin within cells cultured on the mobile system did not form stress fibers and was more diffuse. The different actin formation might be caused by ability to apply forces to the substrate. On an immobile substrate, the cell can anchor on the substrate and build up contractile forces which result

in a strengthening of the cytoskeleton. On a mobile system the ligand movement might hinder the generation of contractile forces and therefore stress fiber formation.

This example therefore demonstrated the different cell responses that the mobility of cell ligands provoked, and highlights the importance of a platform which can be used to study the influence of mobility and ligand clustering on cell behavior.

Presentation of mobile cadherins in 3-D

To show that the microwell platform is also suitable to study the dependence of ligand mobility on cell behavior in 3-D, cells were cultured on a microwell structure coated with mobile E-cad/Fc functionalized 5% bDOPE/DOPC SPB. DIC and fluorescent images showed that cells can specifically adhere inside microwells (fig 4.13 A). The actin staining was performed to visualize the cell inside the microwell structure (fig 4.13 B, C). In microwells coated with E-cad/Fc functionalized SPB, cells were located inside the microwells and their shape was restricted to the microwell dimensions. Initial results showed a similar trend in actin formation as observed on the 2-D substrates. The cells inside microwells were interacting with a mobile E-cad/Fc coating and the actin skeleton showed a more diffuse staining without any pronounced stress fibers.

Therefore, the platform may enable the investigation of the connection between mobility and dimensionality in a novel way thereby allowing us to gain further insight into how a cell senses dimensionality and how a cell responds to its neighboring cells inside a tissue.
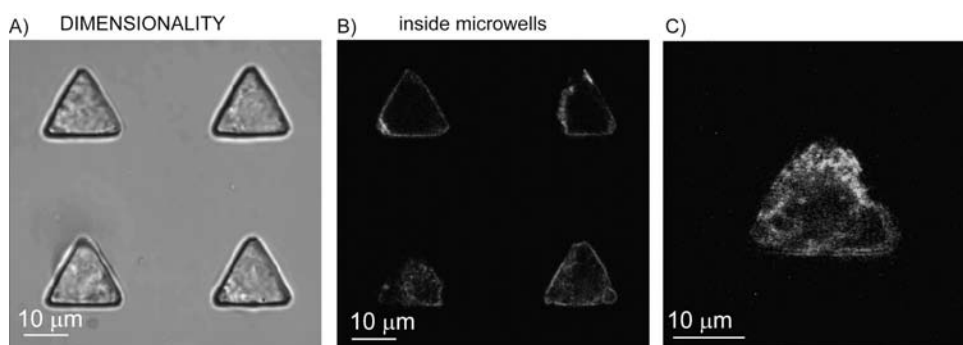

Figure 4.13: *CHO cell inside 3-D microwell coated with an E-cad/Fc functionalized SPB.* A) CHO cells were able to adhere inside a microwell for 24 h that was coated with a mobile bDOPE/DOPC/E-cad SPB. B) To visualize the CHO cell, actin staining was performed. C) The zoomed in image shows the actin skeleton of a single cell inside a bDOPE/DOPC/E-cad SPB microwell.

4.4 Conclusions and outlook

Monitoring of biotinylated vesicle surface interaction with QCM-D demonstrated the ability to build an SPB on oxidized PDMS and to further functionalize the SPB with E-cad/Fc via a biotin-SA linkage. Studies with FRAP demonstrated the mobility of both lipids and SA on PDMS. Furthermore, using a lipid with a T_M of 35 °C allowed for the presentation of a mobile and immobile SPB at physiologically relevant temperature range as analyzed by QCM-D and FRAP. Preliminary cell studies demonstrated that cell survival on a mobile E-cad/Fc functionalized SPB was not reduced and that cells can adhere specifically to E-cad/Fc functionalized SPB. The difference in actin staining between cells cultured on the mobile versus immobile platforms was a demonstrative example of how ligand mobility influences cell responses.

Next this mobile system was incorporated into the microwell structure that provides a 3-D environment. It was shown that the lipids diffused from the wall to the bottom, and *vice versa*, demonstrating the retained mobility of the SPB in a 3-D environment. Furthermore, the coating of microwells with E-cad/Fc functionalized SPB and the combination with cell culture resulted in an array of single cells in microwells. Hence, they specifically interacted with the E-cad/Fc and did not adhere to the passivated plateau. To summarize, this platform is expected to offer the possibility of studying events which are influenced by dimensionality and mobility of ligands. Ideally, it might be used to address a variety of biological questions, such as cadherin clustering or cell polarization. Furthermore, the investigation of cadherin binding strength and dynamics might provide further insight into homeostasis and therefore the deregulation of homeostasis which occurs during cancer formation.

Heterogeneous microwells presenting different biochemical cues on the walls and bottom

5.1 Background

Cell polarization and stem cell division

Cells *in vivo* often experience an asymmetric environment. These asymmetric stimuli result in cell polarization and are reflected in cell shape, protein distribution, and specific cell function [259]. This phenomena is observed in many cell types. Epithelial cells, for example, exhibit a characteristic apical-basolateral polarity (fig 5.1) that is critical for their function and dependent on a number of external stimuli, such as cell-substratum and cell-cell contacts [260]. This polarization of the cell plays an essential role in many cellular responses, such as vectorial transport of molecules, cell division, activation of immunoresponse, and cell differentiation [261].

The asymmetric stimulation of the microenvironment, resulting in cell polarization, also has a strong influence on stem cell differentiation. A process that is particularly fascinating is the extensive proliferation potential of stem cells and their ability to give rise to one or more differentiated cell types. A stem cell must accomplish a dual task of self-renewal and the generation of differentiated cells. A stem cell can divide symmetrically either into two daughter stem cells or two differentiated cells. Conversely asymmetric division results in one stem cell and one differentiated cell. The balance between stem cells and differentiated cells is important for the control over the cell population. This balance is necessary for the repair of tissue after injury or disease [262]. Studies have
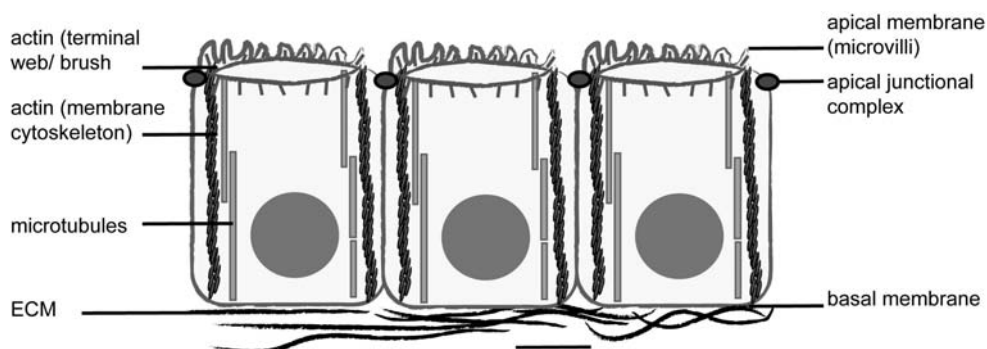
Figure 5.1: *Schematic of polarized epithelial cells.* Schematic representation of polarized epithelial cells and the organization of the actin and microtubule cytoskeleton within these cells is illustrated (adapted from [258].

shown that stem cell division and function is controlled by external cues from the microenvironment, the so called stem cell niche, and intrinsic genetic programs within the cell. Cell-cell interactions through adherens junctions, utilizing cadherins and catenins, and cell-matrix interactions with the ECM and basal lamina have been identified as important for determining maintenance, activation and differentiation of the neural stem cells [263, 264].

Heterogeneous display of proteins

To be a step closer to mimicking the cell in its natural environment, we aimed at developing a microwell variant where walls and bottom present different biochemical cues. The chemical contrast inside these microwells and the different surface coatings might be utilized to create adhesive contrast between basal lamina proteins and proteins present in cell-cell adhesion to mimic the 'asymmetric', heterogeneous display of proteins present in the physiological cell microenvironment (fig 5.2).

Microwells with a different wall or bottom coating have been previously described in literature. For example, microwells with PEG side walls and glass bottom were used for a cytometry platform for characterization and sorting of individual leukocytes [108]. Another approach presents microwells with agarose walls and glass bottom and showed that cadherin simultaneously stimulates and inhibits cell proliferation by altering cytoskeletal structure and tension. Microwells in PEG-hydrogels with modified bottoms allowing for the adsorption of Fc chimera-proteins were used for the investigation of the perturbation of single hematopoietic stem cell fates [265]. All these modifications presented to the cell a different bottom and wall coating where the wall is made of a non-cell-adhesive material. These microwells serve mainly for the isolation of a single cell and thereby
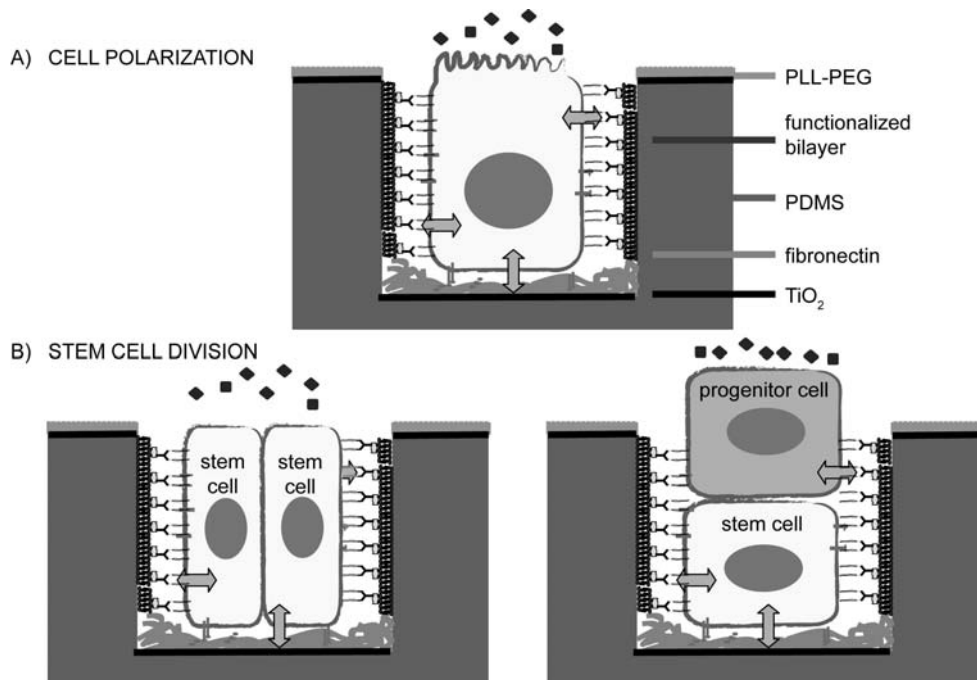
Figure 5.2: *Schematic of the envisioned biological relevance of microwells with wall-bottom variation.* The culture of cells inside heterogeneous coated microwells, with cadherin on the side walls and Fn on the bottom, is envisioned to present to the cell a more *in vivo*-like environment and A) might provoke cell polarization on a single cell level or B) steer the division of stem cells that can result in one stem cell and one differentiated cell or the maintenance of two stem cells.

facilitated observation of cell responses. The microwells with non-interactive walls are a possible continuation of the study with homogeneous Fn-coated wells (see chapters 6 and 7) to investigate if the differences seen in 3-D versus 2-D are also evident if there is a 3-D environment but non-interactive walls.

In contrast, we tried to present to the cell a well containing a different wall versus bottom coating, in the size of a single cell. Furthermore, the coatings of both the bottom and wall present cell-adhesive ligands and the cell can adhere in 3-D. This platform and its variation in wall-bottom coating might be an interesting tool to mimic the stem cell niche to elucidate the environmental cues which determine the mode of stem cell division or to study how polarization can be induced in single cells through interaction with engineered surfaces.

5.1.1   Approaches to achieve a different wall and bottom coating

To obtain a well with a different coating on the wall and on the bottom, we took advantage of the chemical contrast between SiO_2 and TiO_2 (fig 5.3). The functionalization of the TiO_2/SiO_2 patterned microwells was achieved using two different strategies resulting in an immobile PLL-*g*-PEG/Fn (wall/bottom) coating (fig 5.3 D) and a mobile bilayer/Fn coating (fig 5.3 E). In this study, we present the two approaches attempted to achieve a heterogeneous display of cell adhesive ligands, but no cell studies were performed.

The first approach exploits the specific binding of phosphates to TiO_2, but not to SiO_2. The chemical contrast results in a phosphate-SAM/PLL-*g*-PEG contrast, via SMAP (principle is explained in section 1.2.2) [126]. Ideally, this allows for a well functionalized with Fn on the bottom and PLL-*g*-PEG on the walls and plateau. The PLL-*g*-PEG might be further functionalized using PLL-*g*-PEG-biotin.

The second strategy was based on work by Rossetti *et al.* which demonstrated that vesicles adsorb differently on SiO_2 and TiO_2 [266]. Vesicles are particulary exciting as they can be used to form a mobile bilayer on the surface leading to biologically inspired patterns and cell membrane mimics (see section 1.1.3 and chapter 4). Researchers have shown that vesicles containing only phosphatidylcholines adsorb intact on TiO_2 [266–268]. Combined AFM and QCM-D studies revealed that vesicles adsorb onto the surface until very densely packed layers are formed, without formation of supported bilayers and can thus be removed by rinsing [268]. This is in contrast with the situation on SiO_2, where vesicle rupture and SPB formation is observed once a critical surface concentration is reached [23, 24, 267]. This could be exploited to selectively coat the side walls with an SPB, the bottom with Fn, and the plateau with PLL-*g*-PEG.

5.2   Experimental part

5.2.1   Ti coating and plateau passivation

For both approaches, the microwells were replicated into PDMS as described in 3.4. After replication, the samples were coated with Ti in a line-of-sight process, meaning the Ti is deposited on the surfaces orthogonal to the incoming material (fig 5.3 A), ideally, resulting in a Ti coating on the plateau and on the bottom of the wells, but without coating the walls (fig 5.3 B). The Ti deposition was perfomed by Kris Pataky, EPF Lausanne. First,
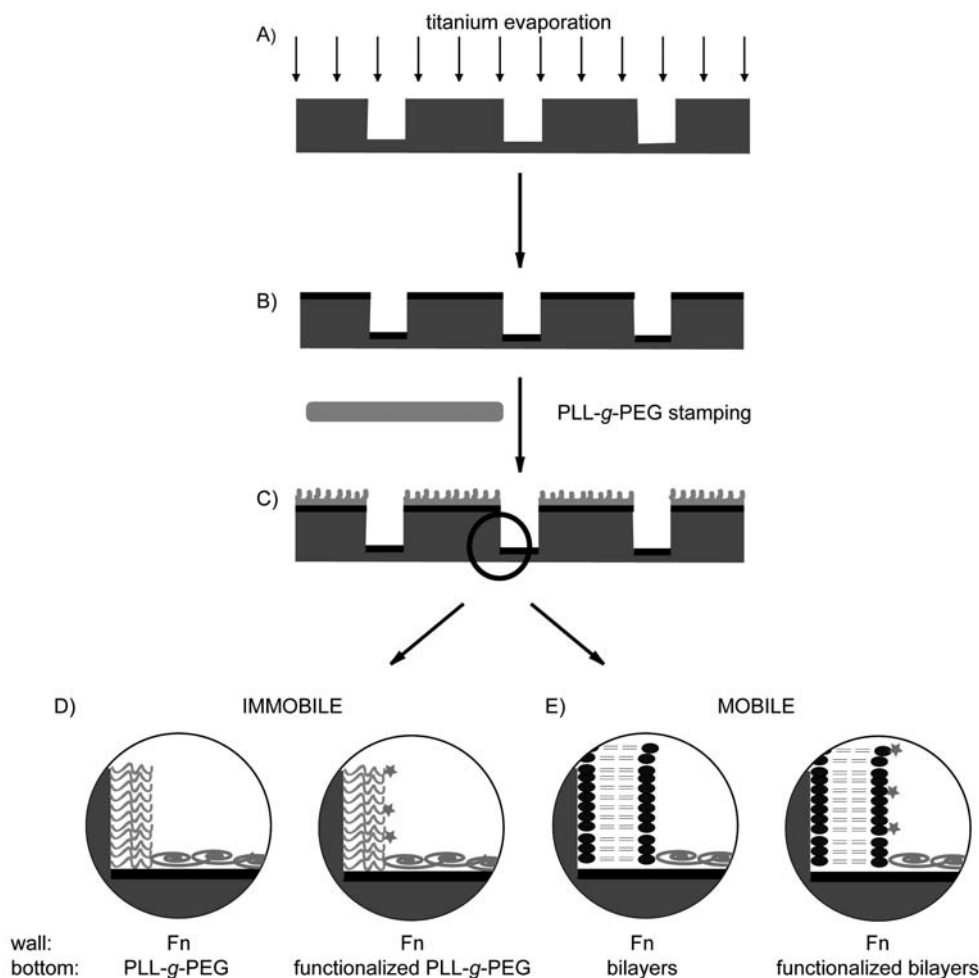
Figure 5.3: *Schematic of fabrication of chemical contrast and coating of wells.* A) Ti was deposited onto the PDMS microwell platform using a line-of-sight evaporation process, B) covering the plateau and the bottom of the wells with Ti. C) After air plasma treatment PLL-*g*-PEG was stamped with an inverted microcontact printing technique onto the plateau rendering it protein-resistant. D) PLL-*g*-PEG on the walls and Fn on the bottom present an immobile wall-bottom contrast coating. To render the PLL-*g*-PEG interactive for cells, functionalized PLL-*g*-PEG (*e.g.* RGD) might be used. E) For a mobile contrast, the walls of the wells were covered with an SPB and the bottom with Fn. To render the SPB interactive for cells, functionalized SPB (*e.g.* biotinylated lipids as presented in chapter 4) might be used.

the samples were oxygen plasma treated with a Tepla 300 (by PVA TePla) for 30 sec. Afterwards, Ti (99.99% purity) was evaporated using an evaporator Optics LAB 600 H (Leybold, Germany) (Ti layer thickness: 5 nm, evaporation rate: 4 Angstrom/sec, vacuum: 5.0×10^{-6} mbar).

The samples were air plasma treated for 30 sec (PDC-32G from Harrick Scientific Corporation, 0.1 mbar) and the PDMS oxidized into SiO_2 and Ti into TiO_2. Subsequently
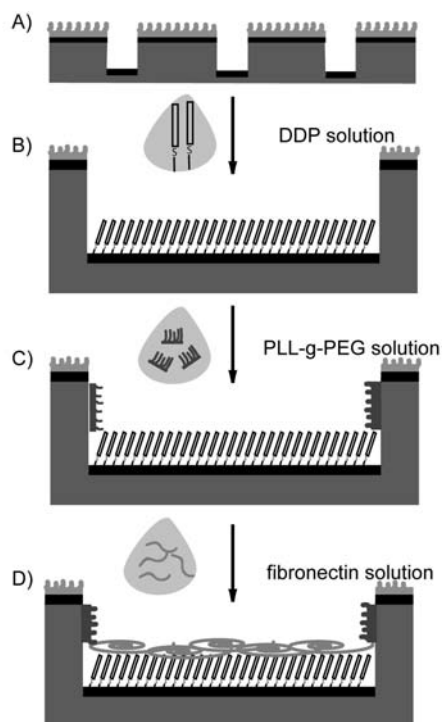
Figure 5.4: *Schematic of a PLL-g-PEG/Fn contrast inside the microwell.* This schematic visualizes the different steps in the coating process, unfortunately the results did not confirm the selectivity of the approach (see text). A) After passivation with PLL-*g*-PEG, B) the sample was exposed to a DDPO$_4$ solution that should specifically adsorb on the Ti surface of the bottom of the well. C) The exposure to PLL-*g*-PEG should result in a coating of the wall. D) Afterwards, Fn adsorption should be limited to the hydrophobic SAM resulting in a Fn-coated bottom.

the plateau of the TiO$_2$/SiO$_2$ patterned microwells was passivated with PLL-*g*-PEG by inverted microcontact printing using a PAAm stamp (fig 5.3 C) exactly as described for non-Ti-coated PDMS microwells (see section 3.5.1). Due to the negative charge on the TiO$_2$ surface, PLL-*g*-PEG was also able to adhere electrostatically to TiO$_2$ surfaces, similar to SiO$_2$.

5.2.2 PLL-*g*-PEG and fibronectin

For a PLL-*g*-PEG/Fn contrast, TiO$_2$ was specifically functionalized with alkane phosphate SAM through exposure to a solution containing the water soluble ammonium salt of dodecylphosphoric acid (DDPO$_4$H$_4$), in the following just called DDPO$_4$, for 24 h at room temperature (15 mg/100 ml in H$_2$O) (fig 5.4 B). After rinsing with PBS, the sample was incubated with PLL-*g*-PEG-rhodamine (PLL-*g*-PEG-rhod) (0.5 mg/ml in PBS, 1 h) and rinsed with PBS (fig 5.4 C). Finally, the bottom of the well was coated with Fn 488

by physisorption (25 μg/ml in PBS, 1 h) onto the hydrophobic alkane SAM regions and thoroughly rinsed before confocal imaging.

5.2.3   Bilayers and fibronectin

To achieve a microwell functionalized with SPB-coated walls and a Fn-coated bottom, the sample was modified in the following way (fig 5.5 A). DOPC vesicles (see section 3.1.7) have been demonstrated to selectively adsorb onto the SiO_2 regions of TiO_2/SiO_2 patterned microwells to form SPBs. Therefore, DOPC was mixed with 1% NBD-PC to visualize the vesicles with a 488 nm laser. After vesicle extrusion, the microwell surface was exposed to a vesicle solution containing 100 nm-sized DOPC/NBD-PC vesicles (0.5 mg/ml in HEPES) for 10 min (fig 5.5 B). After rinsing with PBS, Fn 633 (20 μg/ml in PBS) was incubated on the microwells for 1 h and afterwards thoroughly rinsed (fig 5.5 C). The samples were kept in solution at all times and imaged directly after surface modification was completed.

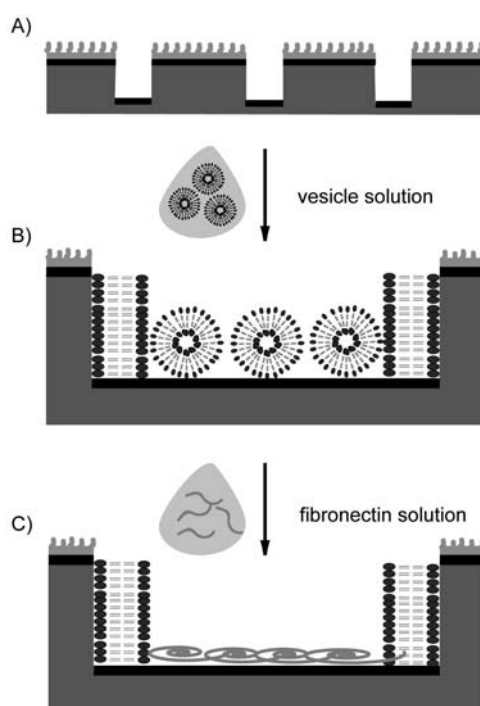**Figure 5.5:** *Bilayer/Fn contrast.* A) After passivation of the plateau with PLL-*g*-PEG by inverted microcontact printing, B) the microwell platform was exposed to a solution of DOPC vesicles that adsorbed and ruptured specifically on the oxidized PDMS wall surface of the wells. C) The exposure to Fn resulted in coating of the bottom of the microwell by displacement of the adorbed vesicles.

5.2.4 QCM-D measurements

The QCM-D experiments were performed by Dr. Mirren Charnley, ETH Zurich. The QCM-D crystals were treated the same as the microwell sample and the concentration of the solutions was as described above. Crystals were either TiO_2-coated or spin-coated PDMS.

5.3 Results and discussion

5.3.1 Characterization of the Ti coating

The surface modifications with fluorescent molecules as described below are only indirect proofs that the Ti was only adsorbed onto the plateau and on the bottom of the microwell, but not on the side walls. A more direct proof was needed to investigate whether Ti was absent from the side walls.

SEM imaging was performed on the Ti coated samples (fig 5.6 A). There was some wrinkling of the PDMS observed where the Ti was deposited. On the side walls of the microwells no wrinkling was observed which might be an indication that no Ti was deposited on the side walls (fig 5.6 B). Imaging of a larger feature of the microwell chip showed the wrinkling structure on the plateau and on the bottom of the well. The edge of the microwell (indicated by the arrow) marked the border between wrinkles and a flat PDMS surface.

To obtain more precise information about the chemical composition of the side walls and bottom of the microwells, Energy Dispersive X-ray (EDX) analysis was performed. Unfortunately, the analysis with EDX was not successful. Certain limitations made it impossible to measure a reliable spectra by EDX. Firstly, the layer of Ti was too thin and therefore the Ti signal was below the detection limit of the EDX, which needs the equivalent of roughly 3 mol% present on the surface to measure a reliable spectra. Secondly, due to the 3-D geometry of the sample the photons were scattered in different directions and EDX imaging of the sample was not possible. Other, more sensitive surface techniques are needed to determine the absence of Ti from the side walls, such as *e.g.* X-ray photoelectron spectroscopy (XPS). But the 3-D structure of the microwell structure might also be a limiting factor for other surface techniques.
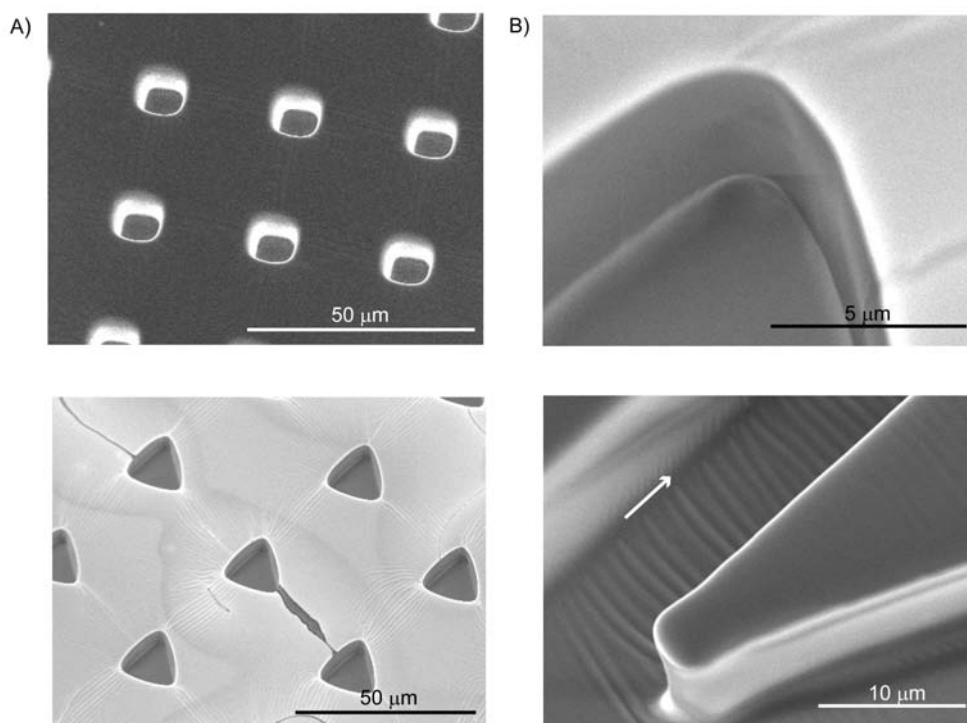
Figure 5.6: *SEM images of the microwell platform coated with Ti.* A) Overview images of microwells after a line-of-sight evaporation process of Ti. B) The larger images show clearly the wrinkling of the PDMS on the plateau and the bottom of the microwell, and the flat PDMS side walls. The edge (arrow) is the border between wrinkled and flat substrate.

5.3.2 PLL-*g*-PEG and fibronectin

This approach investigated the possibility of applying the SMAP technique to 3-D micro-wells, aiming towards a PLL-*g*-PEG coating on the side walls and Fn on the bottom of the microwell. Fig 5.7 A shows that, after adsorbing the alkane-phosphate SAMs to the bottom of the wells, the PLL-*g*-PEG-rhod only adsorbed onto the walls of the microwell as expected. The intensity plot showed a stronger fluorescent signal on the side walls, compared to the bottom and the plateau of the microwell. The intensity of fluorescence on the bottom and plateau was of a similarly low level and bleaching experiments shown in fig 5.7 B confirmed that there was no fluorescent signal on the plateau and the bottom of the microwell.

As shown in the representative fig 5.7 B it was observed that Fn was not restricted to the bottom of the wells. Bleaching experiments confirmed the presence of the fluorescent signal on the plateau of the structure. Because the fluorescence of the plateau and the bottom were of a similar intensity, we assumed that there was roughly the same amount
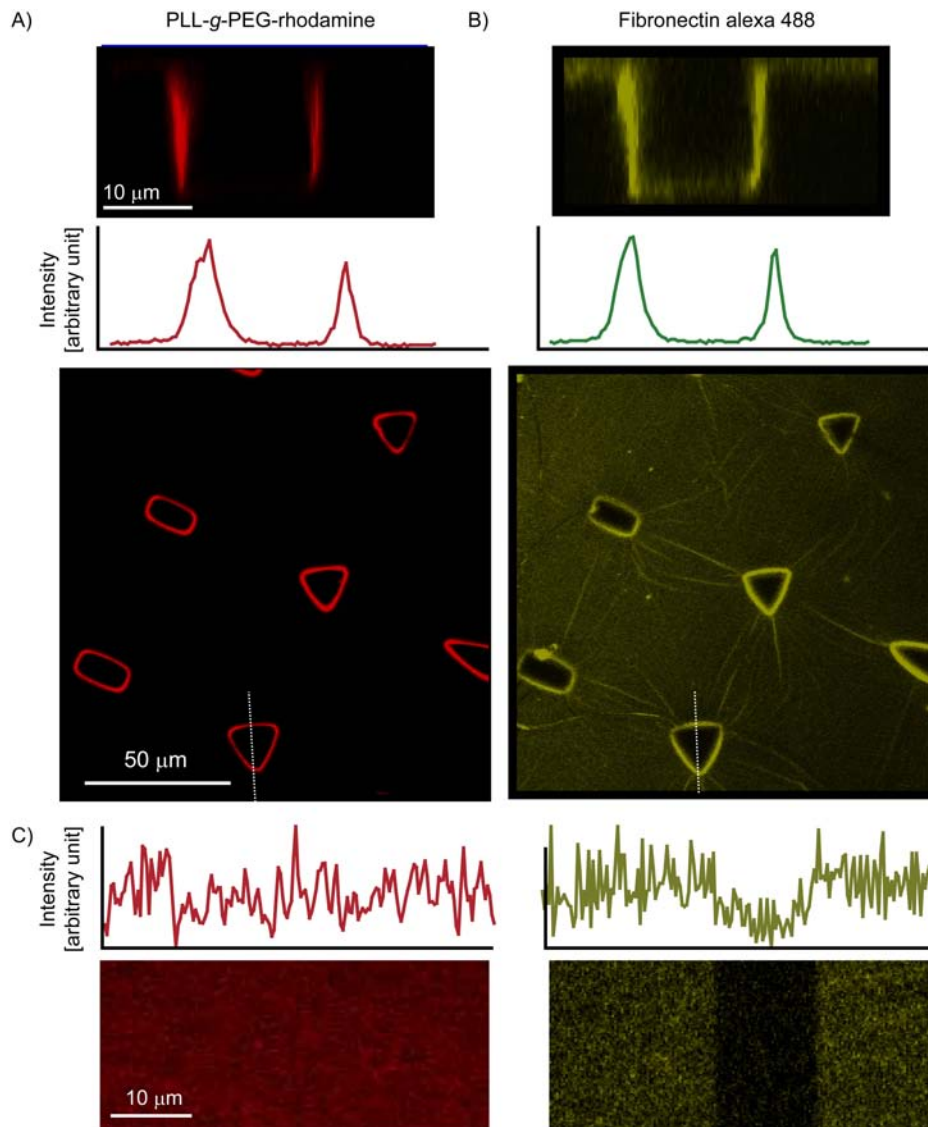
Figure 5.7: *CLSM images of defected PLL-g-PEG/Fn contrast.* A) shows a CLSM image and the side view of the PLL-*g*-PEG-rhod coating on the side walls, where the intensity plot showed that there is more PLL-*g*-PEG-rhod on the side walls of the well. On the plateau and bottom of the well the same intensity level was detected. Because of the bleaching experiments discussed below, it could be concluded that there was no detectable PLL-*g*-PEG-rhod adsorbing onto the plateau and bottom. B) represents the Fn 488 that in theory should specifically adsorb on the bottom of the well, but the Fn signal was visible all over the sample, indicating non-specific adsorption had occurred. The intensity plot showed that there was the same fluorescent intensity on the bottom of the wells and the plateau. C) The fluorescent intensity of PLL-*g*-PEG rhodamine and Fn 488 was plotted on an area on the plateau where a bleaching was performed. Left: The PLL-*g*-PEG rhodamine could not be bleached and therefore it can be concluded that there was no PLL-*g*-PEG rhodamine on the plateau. Right: Fn 488 on the plateau could be bleached as visible in the confocal image and the intensity plot. Therefore it can be concluded that Fn was present on the plateau.

Figure 5.8: *QCM-D measurements to determine the crosstalk between PLL-g-PEG, Fn and DDPO$_4$ simulating the experimental condition occurring on the plateau.* The black curve represents the experimental condition occurring on the plateau of the microwell. First, PLL-*g*-PEG was adsorbed onto a TiO$_2$ crystal and then the surface was exposed to a DDPO$_4$ solution. The DDPO$_4$ removed some of the PLL-*g*-PEG and afterwards, Fn adsorbed onto the PLL-*g*-PEG. The following exposure to SA did not result in any further mass uptake. The control (grey curve) shows the same procedure without exposure to the DDPO$_4$ solution and confirmed the protein-resistant properties of PLL-*g*-PEG.

of adsorbed Fn on the plateau and on the bottom. Because of the lower resolution in x-axis and the the cross signal from one confocal slice into the other, the fluorescent signal on the plateau (or well) can not be set in relation to the signal intensity on the side walls. However, it can be stated that there was Fn adsorption on the side wall, the plateau and the bottom. In summary, the Fn was distributed all over the microwell platform making it impossible to obtain a heterogenous wall-bottom coating.

The different experimental conditions on the plateau, the walls and the bottom of the microwell were also mimicked in QCM-D studies to examine the cross talk between the different molecules. To study the situation on the plateau (fig 5.8), a TiO$_2$ coated QCM-D crystal was initially exposed to a PLL-*g*-PEG solution, because it was not possible to passivate the crystal by inverted microcontact printing of PLL-*g*-PEG. To mimic the situation on the plateau, the PLL-*g*-PEG layer formed on the TiO$_2$ crystal was exposed to DDPO$_4$. QCM-D results showed that the exposure to a DDPO$_4$ solution resulted in a positive followed by a negative frequency change. This indicated that some of the PLL-*g*-PEG was removed and replaced by DDPO$_4$. It is probable that this was a result of the DDPO$_4$ TiO$_2$ interaction being stronger than the TiO$_2$ PLL-*g*-PEG interaction. The

following exposure of the surface to Fn showed a mass uptake, indicating that the PLL-*g*-PEG lost its resistance to protein adsorption or that the Fn was adsorbing to the DDPO$_4$ on the surface. This QCM-D curve correlated with the findings of the CLSM images where Fn was adsorbing on the plateau of the microwell substrate. For the control measurement, the PLL-*g*-PEG was subsequently exposed to a FN and SA solution and showed no mass uptake, as expected.

To study the experimental condition on the walls, especially the protein resistance of PLL-*g*-PEG-biotin, an oxidized PDMS surface with a PLL-*g*-PEG-biotin layer was exposed to a Fn solution and monitored by QCM-D (fig 5.9). No mass uptake was detected, indicating that PLL-*g*-PEG-biotin was resistant to Fn adsorption. The following exposure to SA showed a mass increase ($\Delta f = -37$Hz) similar to the control experiment ($\Delta f = -36$Hz) where the PLL-*g*-PEG-biotin layer was directly exposed to SA without any Fn exposure step. This data was not confirmed by the CLSM images where Fn adsorption was detected on the side walls of the microwell. A possible explanation might be that there were some impurities on the side wall that allowed for DDPO$_4$ adsorption and therefore compromised the resistance of PLL-*g*-PEG-biotin against protein adsorption. The analysis of Ti impurities on the side walls was unfortunately not possible, as discussed in section 5.3.1.

Figure 5.9: *QCM-D measurements to determine the crosstalk between PLL-g-PEG-biotin, Fn and SA simulating the experimental condition occurring on the walls.* The black curve represents the experimental condition occurring on the wall of the microwell. First, PLL-*g*-PEG-biotin was adsorbed onto TiO$_2$ and afterwards the surface was exposed to a Fn solution. There was no mass uptake of Fn on the PLL-*g*-PEG-biotin and the following exposure of the surface to SA resulted in a mass uptake as expected. The control (grey curve) shows the same procedure without exposure to Fn.
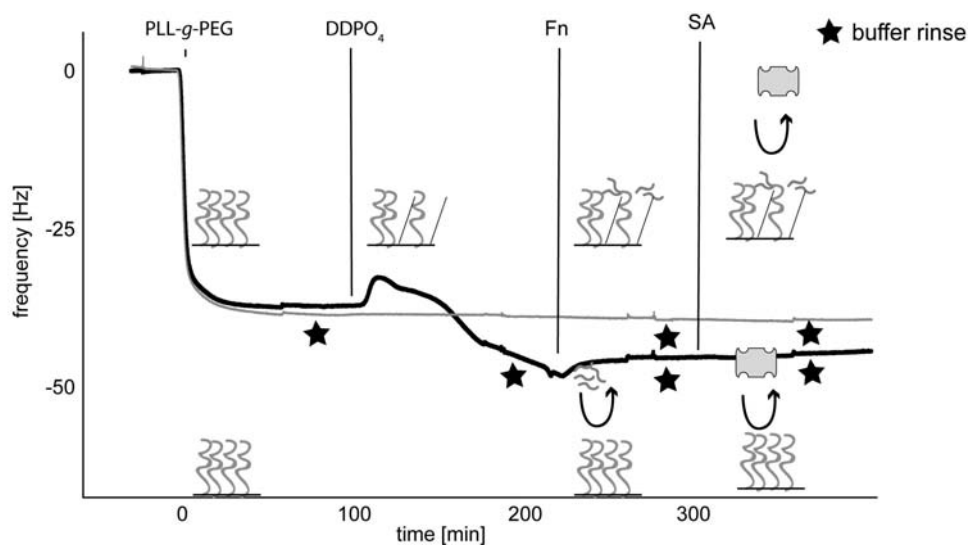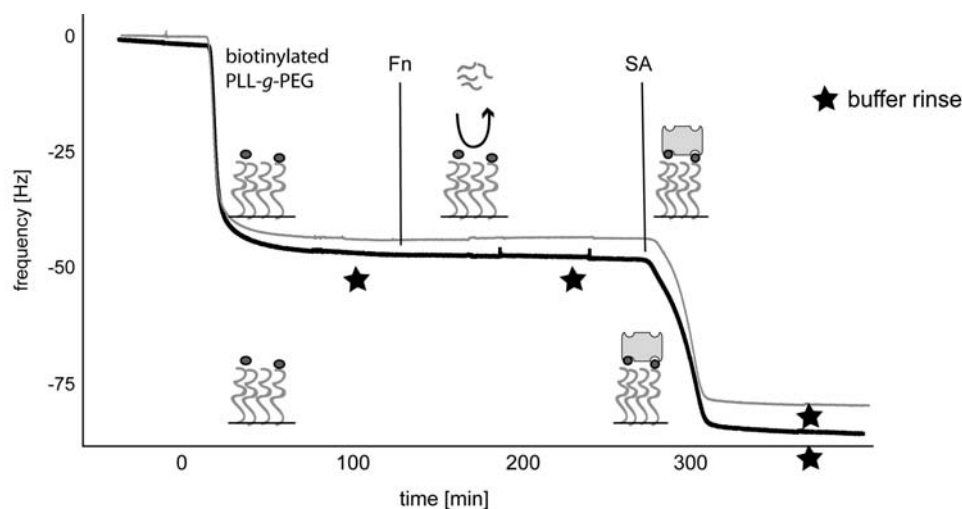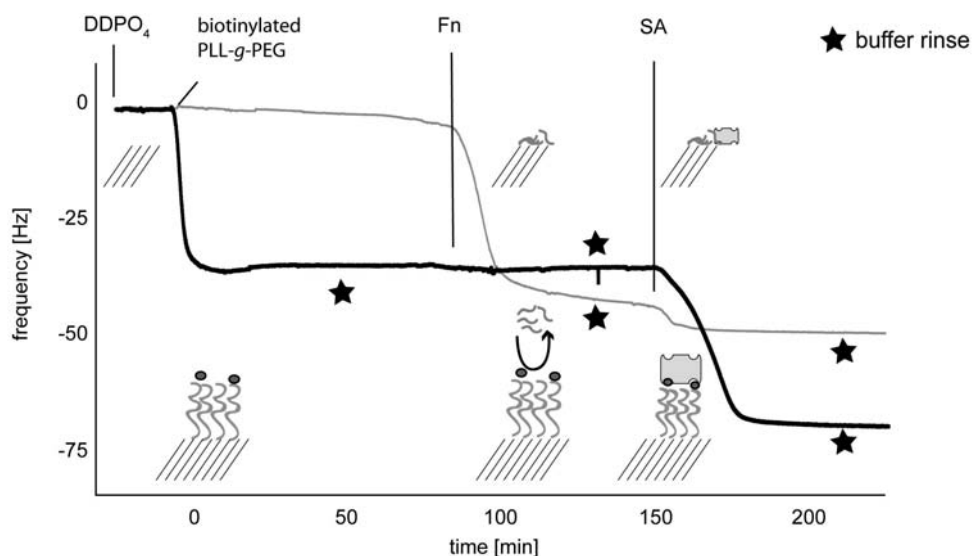
Figure 5.10: *QCM-D measurements to determine the crosstalk between PLL-g-PEG, Fn and DDPO₄ simulating the experimental condition occurring on the bottom.* The black curve represents the experimental condition occurring on the bottom of the microwell. First, a $DDPO_4$ coated surface was exposed to PLL-*g*-PEG-biotin and resulted in a mass increase, indicating PLL-*g*-PEG adsorption on the $DDPO_4$ layer. The following exposure to Fn showed no uptake of Fn and the final exposure to SA showed a decrease in frequency, indicating mass uptake. The control (grey curve) shows the same procedure without exposure to PLL-*g*-PEG and showed the mass uptake after the $DDPO_4$ coated surface was exposed subsequently to Fn and SA.

The imitation of the experimental conditions on the bottom of the microwells started with a $DDPO_4$ coated QCM-D crystal (fig 5.10). The following exposure to PLL-*g*-PEG-biotin led to an adsorption of PLL-*g*-PEG-biotin on the $DDPO_4$ layer and after Fn adsorption no change in frequency was detected. The control experiment showed a strong decrease in frequency if Fn was directly adsorbed onto the $DDPO_4$ layer.

The zero frequency shift observed in QCM-D may be caused because the PLL-*g*-PEG-biotin rendered the $DDPO_4$ surface protein resistant or some PLL-*g*-PEG-biotin was replaced by the same amount of Fn so that the total mass did not change and was, therefore, not detectable. Michel *et al.* also reported PLL-*g*-PEG adsorption on the dodecyl phosphate SAM probably due to hydrophobic-hydrophobic interactions. However, exposure to serum led to a replacement of the PLL-*g*-PEG by serum [126]. The CLSM images agreed with the hypothesis that Fn replaced some of the PLL-*g*-PEG-biotin, however, there was only a weak fluorescent signal on the bottom of the microwell detectable. A likely explanation for this result is that the PLL-*g*-PEG-biotin that adsorbed onto the $DDPO_4$ was not completely replaced by Fn, but reduced the potential of Fn to adsorb onto the $DDPO_4$ layer. It is possible that serum replaces the PLL-*g*-PEG more efficiently

because it is a mixture of various proteins. A surface analytical technique, *e.g.* XPS or secondary ion mass spectroscopy, would help to determine the amount of replaced or adsorbed PLL-*g*-PEG-biotin and Fn.

Due to these observations, this approach of heterogeneous wall functionalization was not further followed.

5.3.3   Bilayers and fibronectin

This approach exploited the selective formation of SPB from DOPC vesicles on SiO_2, but not on TiO_2. Fig 5.12 A shows the bottom of a microwell after addition of DOPC vesicles. It was clearly visible that there were vesicles adsorbing on the bottom of the microwell. After exposure to the Fn solution, the bottom of the wells were fully covered with Fn and the vesicles were removed. This suggests that the interaction of Fn with the TiO_2 surface was stronger than the vesicle surface interaction with TiO_2. Therefore the vesicles that were present on the bottom of the microwell must have been removed by Fn. The red spots in fig 5.12 B might be some remaining vesicles on the surface or rather more likely the signal of the bilayer coating from the wall that was visible because of a gradual transition between the Fn coating to the SPB or a wall/bottom border that is not fully straight.

The lack of Fn adsorption to the side walls indicated that the bilayer successfully prevented non-specific protein adsorption. The side view demonstrates the selectivity of the coating process; the passivated plateau showed neither DOPC/NBD-PC nor Fn signal, the walls were covered with DOPC/NBD-PC and the Fn signal was only present on the bottom of the microwell (fig 5.12 B). The fluorescent intensity profile of a selectively coated microwell showed a strong signal of the Fn on the bottom of the microwell (fig 5.12 A) and a strong DOPC/NBD-PC signal on the side walls (fig 5.12 B). A reconstruction, done with the imaris software, visualized the microwell with the two different coatings in 3-D (fig 5.12 C).
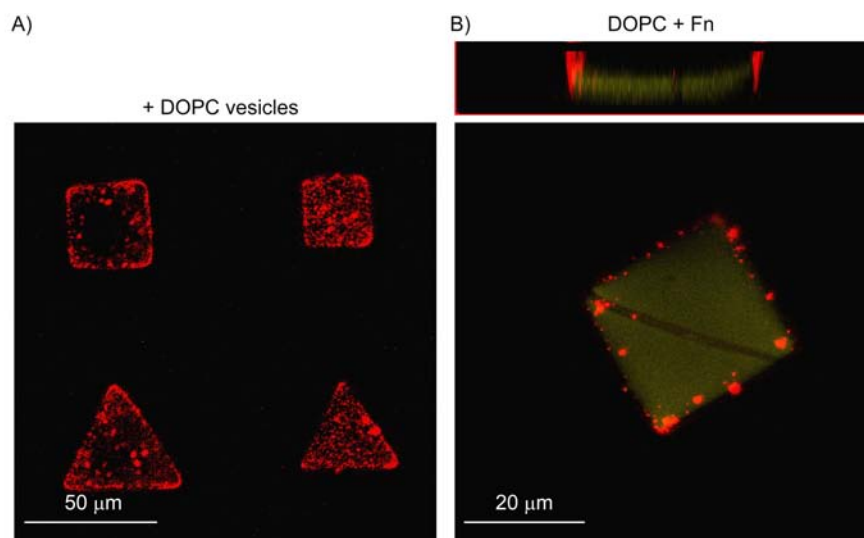
Figure 5.11: *Confocal images of bilayer/Fn contrast.* A) The confocal microscope slice focused on the bottom of the microwell. First, the surface was exposed to a DOPC/NBD-PC vesicle solution and the bottom of the well showed the presence of adsorbed vesicles. B) The subsequent Fn 633 addition and rinsing removed most vesicles on the bottom of the microwell and Fn adsorbed onto the bottom. The red spots on the side walls are most likely due to signals from the red-fluorescent bilayer on the walls "shining into" the confocal fluorescence image of Fn (green) due to non-straight wall/bottom border.

Therefore, we achieved a wall-bottom biochemical contrast in this case whereby DOPC vesicles were selectively immobilized onto the SiO_2 regions of TiO_2/SiO_2 patterned microwells to form an SPB while the Fn was only able to cover the bottom of the microwell. To present to cells an interactive coating, we have to present a biotinylated SPB which can be further functionalized with cell adhesive proteins. The crosstalk between the biotinylated SPB and Fn has to be investigated and is discussed in the next section. The mobility of the SPB on the side wall could not be investigated due to technical issues it is not possible to bleach a defined area on a side wall and image the fluorescence recovery. Therefore, we refer to the mobility study in section 4.3.1, where the mobility of an SPB inside a microwell confirmed a mobile SPB coating.

Crosstalk between biotinylated lipids and Fn

This methodology of selectively adsorbing SPB on the walls and Fn on the bottom can be further exploited to coat the sides of the microwell with biotinylated SPB which could be further functionalized with cadherins etc. Ideally, this would allow cells to not only adhere to the Fn on the bottom but also to interact with the mobile coating on the side walls of the microwells. The crosstalk between the biotinylated SPB and Fn was therefore
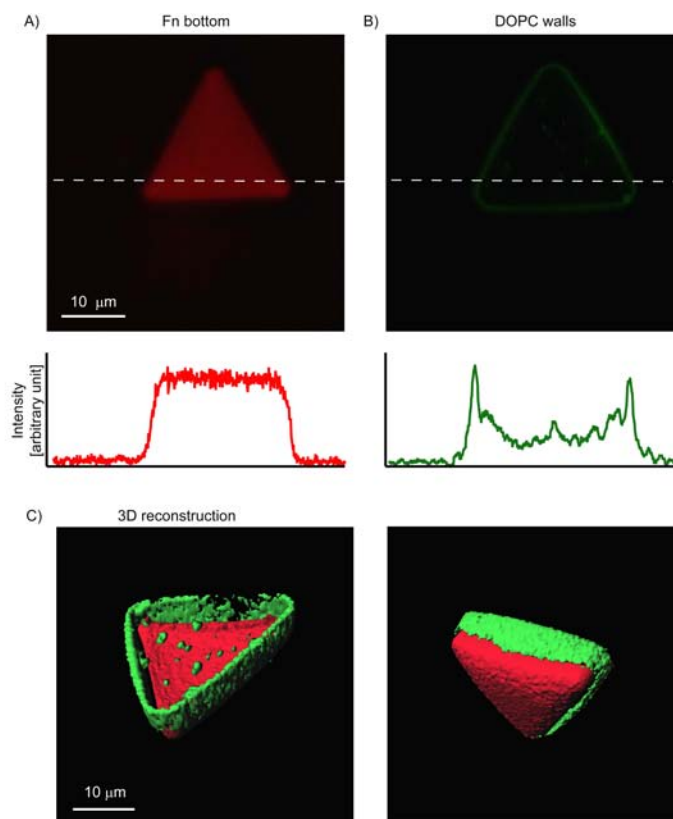
Figure 5.12: *Confocal images of bilayer/Fn contrast and 3-D reconstruction.* A) Z-projection of confocal image of the Fn 633 signal (red) which adsorbed onto the bottom of the microwell and for which the intensity plot is shown. B) Z-projection of confocal image of the DOPC/NBC-PC (green) signal showed fluorescent signal on the side walls and the intensity plot confirmed the higher fluorescent intensity on the side walls compared to the bottom. C) An imaris reconstruction of the microwell with DOPC/NBD-PC coated side walls and Fn 633 coated bottom is shown.

investigated to determine if this heterogeneous display remained intact when biotinylated vesicles were used.

To determine the crosstalk between the different materials, QCM-D measurements were performed. The investigation of the crosstalk between the SPB formed from biotinylated lipids and Fn showed the resistance of the biotinylated SPB against Fn adsorption. Furthermore, the biotinylated SPB retained the ability to specifically bind to SA. The investigation of the crosstalk on the Fn-coated bottom of the microwell showed that after SA injection, some of the Fn was removed and/or replaced by SA. Unfortunately it is not possible to determine with QCM-D how much of the Fn mass is replaced by SA and how much SA was able to adsorb to the surface.
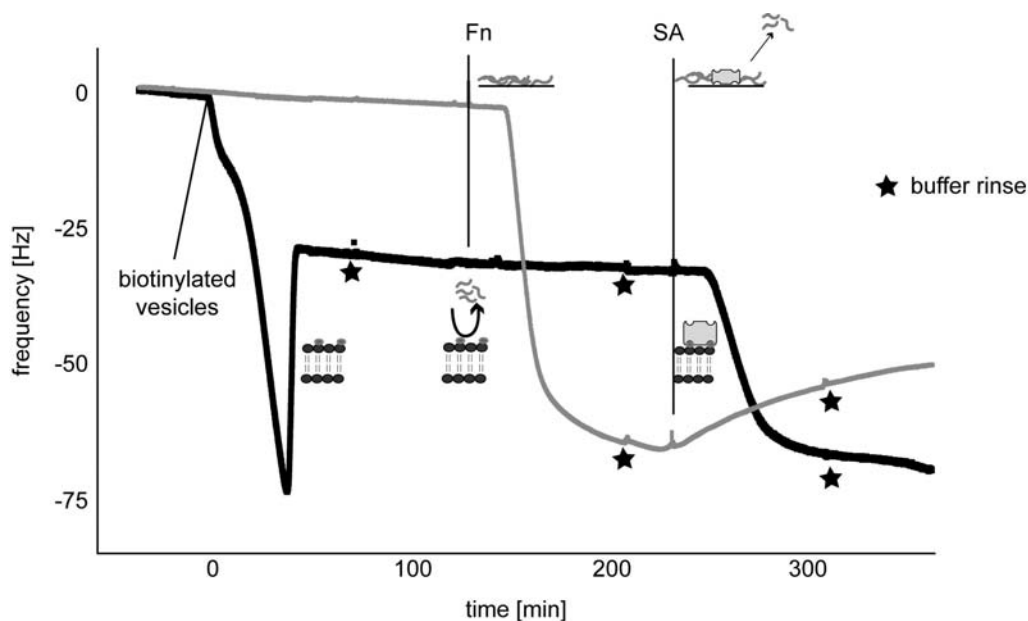
Figure 5.13: *QCM-D measurements to determine the potential crosstalk between DOPC and Fn.* The black curve shows the situation of the SPB occurring on the side wall of the microwell. Biotinylated vesicles built an SPB on the surface and the injection of Fn did not result in a frequency change, therefore no Fn adsorption was detectable. The following SA injection showed a frequency decrease, indicating mass uptake of SA. The grey curve represents the situation of the bottom of the microwell. After SA injection, the adsorbed Fn is removed and/or replaced by SA.

Other techniques are needed to determine if and how much SA adsorbed on the surface. If we want to investigate the sample in liquid, microscopy with differently labeled Fn and SA may be possible. However, microscopy is not suited to quantitatively determine the adsorbed mass of SA. To determine the amount of adsorbed SA techniques, such as XPS or secondary ion mass spectrometry, might be helpful. However, this techniques need to be performed in vacuum which means the sample has to be dried.

5.4   Conclusion and outlook

Two strategies to coat the side walls and the bottom of the microwells with different biochemical functionalities were explored in this chapter. Both take advantage of the chemical contrast of SiO_2 and TiO_2.

The approach used to coat the walls of the well with PLL-*g*-PEG and the bottom with Fn, following adsorption of $DDPO_4$, was not successful. However some adjustments could be made in future studies. To work with a wall-bottom variation involving $DDPO_4$

it may be necessary to only coat the bottom of the well with TiO_2 and not the plateau, using an aligned mask. In this way, the stamped PLL-g-PEG on the plateau might not be compromised by the $DDPO_4$ and maintain its protein resistance because $DDPO_4$ does not interact with SiO_2. Therefore the PLL-g-PEG should not be replaced during the $DDPO_4$ exposure. The stable passivation of the plateau might allow for further functionalization of the microwell. But the PLL-g-PEG-biotin may still adsorb non-specifically to the $DDPO_4$ layer as shown in the QCM-D data.

We demonstrated with the second approach that the chemical contrast was successfully transferred into a biochemical contrast, with Fn restricted to the bottom of the well, bilayer on the sides, and PLL-g-PEG on the plateau. The mobility of the SPB inside microwells is an important prerequisite for a mobile system. As already mentioned, it can be assumed that the SPB inside microwells presents a mobile platform (for characterization and discussion about mobile bilayers inside microwells see section 4.3.1). However, if there are some Ti impurities present on the SPB side walls, the mobility of the SPB might be (slightly) reduced compared to an SPB inside a microwell made purely of PDMS. This will need to be investigated in future studies.

Alternative methods to functionalize the side walls differently from the bottom of the microwell might also be explored. To obtain a mobile coating on the side walls and on the bottom, vesicles containing 20% – 50% DOPS might be used. In the absence of calcium, they build a bilayer on SiO_2 but are repelled on TiO_2. After rinsing, more vesicles can be added in the presence of calcium which facilitates bilayer formation on TiO_2. To obtain a biochemical contrast, biotinylated vesicles could be used to coat the SiO_2, and vesicles containing NTA subsequently added to coat TiO_2 or *vice versa* as described by Rossetti *et al*. [266]. The further functionalization of the coatings via biotin-SA or via proteins exposing sequential histidines [269] would allow for functionalization of the microwell with two different proteins. However, as for the other approaches, the crosstalk between the two strategies would have to be investigated first as mobility of the bilayers might result in a mixture of the two components.

Another way to heterogeneously coat the microwells would involve an alternative chemical contrast. Gold and TiO_2, or gold and SiO_2 contrasts, allow for specific interactions with certain molecules, which have also been described in the literature [47, 270, 271]. To produce the chemical contrast, the first metal (*e.g.* Au) is evaporated on a tilted microwell sample. The plateau shadows the bottom of the microwell and only the wall can be coated with the first metal. The second step involves a line-of-sight

evaporation and covers the bottom of the microwell with the second metal (*e.g.* TiO_2). Thiolated proteins or amino sequences like arginine-glycine-aspartic acid (RGD), which are known to interact with cells, adsorb specifically onto gold, while phosphorylated proteins interact specifically with TiO_2. This would result in, for example, thiolated RGD on the bottom, and biotinylated SAMs on the side wall, thus allowing for further cadherin functionalization.

Summing up, our results demonstrate that there are ways to coat the walls of the microwell differently from the floor. The approach with the bilayers on the side wall and the Fn on the bottom showed positive first results. This technique might offer the potential to study how external stimuli influence cell polarization or stem cell division/ differentiation. Control over the niche and particularly the knowledge of how the niche influences stem cells might help in the longer term to develop therapeutic approaches to human degenerative diseases.

Viability of cells in microwells and validation of
characterization procedures by microscopy

6.1   Introduction

The previous chapters demonstrated that the microwell structure can be replicated into
both hard and soft PDMS (fig 6.1 A). Furthermore, cell adhesion was confined to inside
the microwells, after surface passivation on the plateaus and modification of the wells with
adhesive ligands, and typically about 45% of the wells were filled in the case of HUVECs
(fig 6.1 B). Before addressing specific biological questions using the microwell platform,
certain biological parameters needed to be investigated. The following section describes
cell survival in microwells and determines the suitable microwell size/volume to control
cell shape in 3-D. Furthermore, it was investigated if there was diffusion limitation of
molecules, such as staining agents, at the bottom of the microwells. Additionally, actin
staining was performed to show the compatibility of the technique with high-resolution
microscopy.

6.1.1   Apoptosis and cell survival

Cells can grow and divide, or enter the programmed cell death (apoptosis). Apoptosis
involves a series of biochemical events leading from cell shrinking and blebbing, changes
in the cell membrane, and loss of attachment from the substrate, to nuclear fragmentation,
chromatin condensation, and finally DNA fragmentation [272]. It triggers phagocytosis
without causing inflammation. Apoptosis can be induced if the cell is beyond repair,
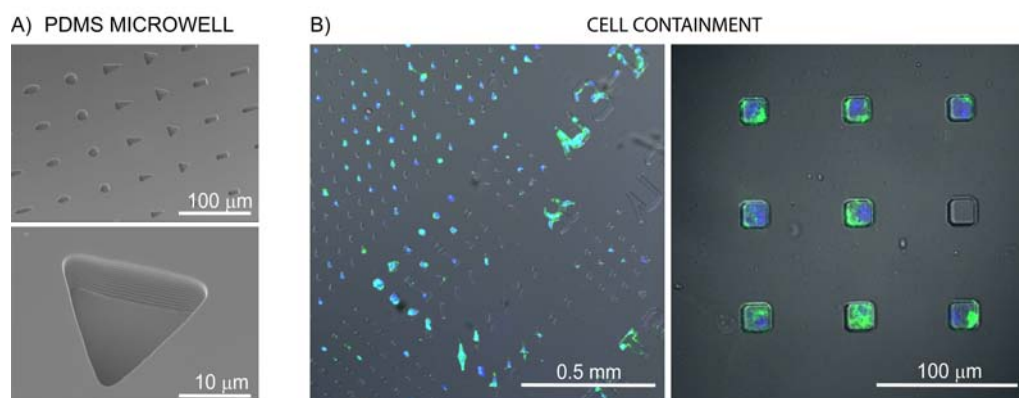
Figure 6.1: *Microwells replicated into PDMS and with cell culture.* A) Scanning electron microscopy images of PDMS replicas of the microfabricated wells of various shapes in hard (1 MPa) PDMS are shown. B) Overlays of DIC and fluorescent confocal images acquired with 10x air or 60x oil objectives are shown of HUVECs in microwells stained with Alexa 488-phalloidin (actin, green) and ethidium homodimer (nuclei, blue) after 24 h in culture. About 45% of the wells were filled with cells.

infected with a virus or exposed to external stress, such as starvation. Furthermore, apoptosis is crucial for regulating the stability and development of a tissue and maintaining homeostasis, the balance between cell division and cell death. In contrast to apoptosis, cells exposed to a major injury or low oxygen conditions die a necrotic cell death. During necrosis, the cell swells, becomes leaky and finally ruptures leading to cellular and nuclear lysis. The cellular contents are released in an uncontrolled manner into the surrounding tissue and damage the surrounding cells causing a strong inflammatory response in the corresponding tissue [272]. Therefore there are different pathways leading to cell death, but in this thesis the main focus is on living cells versus dying cells in general.

Apoptosis is involved in many processes, like morphogenesis, as not only the proliferation of cells, but also apoptosis is critical to define the shape of a tissue, such as mouse paws [273] or branching capillary networks [274], like blood vessels. Inhibition of the formation of new capillaries has been shown to block cell growth, *e.g.* solid tumor growth. Extracellular stimuli, such as soluble secreted proteins, proteins bound to the surface of cells, or components of the ECM, have shown to influence cell size and population size. Different adhesion receptors appeared able to influence the rate of cell survival. Basement membrane ECM, but not Fn or collagen, was shown to suppress apoptosis [136, 275]. The density of the ECM ligands also influences cell survival, whereby increasing the density of ECM adsorbed on the surface decreases apoptosis rates [276].

Furthermore, the shape of a cell itself depends on the tissue structure and can have a major impact on cell growth, cell division and cell survival. Cell density has an influence on the shape of a cell and early studies have shown that high cell density may induce apoptosis [277]. Artificial cell confinement on patterned 2-D surfaces can also steer cell fate and induce apoptosis, maintain cells in a quiescent state, or permit progression through the cell cycle [136, 145, 278]. Chen *et al.* have presented how the local geometry might represent a fundamental mechanism which is responsible for cell survival and death and was discussed in chapter 1.2.3 (fig 1.13).

The goal of this section was to investigate if cells survive inside microwells and furthermore, if there is a correlation between spreading area, dimensionality and cell survival in comparison with cells cultured on 2-D patterned surfaces.

6.2 Experimental Section

6.2.1 Substrates

The microwells were replicated and chemically modified as described in section 3.4. In this study 10 μm deep microwells (circles, squares, triangles, rectangles) coated with Fn were used (section 3.5.1). The microwell size varied between a projected area of 100 μm^2 (a 10×10 μm^2 square as an example), to 1200 μm^2 (*e.g.* a 34×34 μm^2 square or a circle with a diameter of 39 μm). Patterned 2-D Fn samples were prepared by the MAPL technique (section 3.3.2).

6.2.2 Cell culture

Fn-coated microwells were seeded with 5×10^4 HUVECs/cm^2. After seeding, HUVECs were allowed to adhere within the microwells for 30 min, subsequently the unbound cells on the non-adhesive background were removed by gentle rinsing by pipette. Cells were then cultured for 24 h (except for the long term viability assay, see below) in either low (2%) or high (10%) FCS prior to cell staining and imaging.

The 2-D patterns were produced by MAPL on a glass slide (see section 3.3.2) and HUVECs were seeded with a density of 10^4 cells/cm^2 and cultured for 24 h.

6.2.3   Visualization of actin, nuclei and fibronectin

For actin stress fiber and cell nucleus imaging, cells were stained with the standard protocol described in 3.6.2. For testing the efficacy of immunohistochemistry (IHC) within microwells, 2-D and 3-D samples were coated with Fn labeled with either Alexa 488 or Alexa 633 prior to cell seeding. After 24 h cell culture, samples were fixed and blocked as described in 3.6.2. Microwells were next incubated with a sheep anti-human Fn polyclonal antibody (1:200 in PBS; Serotec AHP08) for 1 h, rinsed thoroughly with PBS, and finally incubated with rhodamine conjugated donkey anti-sheep IgG secondary antibody for 1 h. Samples were rinsed thoroughly with PBS prior to imaging.

6.2.4   Cell viability

Microwell samples containing HUVECs were tested for cell survival according to the standard protocol in chapter 3.6.2. The cells were cultured for 24 h, 2 days, 3 days, or 7 days in the microwells before staining and imaging. For the long term cell survival studies, the average cell survival rate and standard deviation of the mean of cells in different shaped wells (circle, square, rectangle, triangle) and well sizes (spreading area between 100 and 1200 μm^2) were calculated. To study the influence of the spreading area on 2-D, the survival data determined on square-shaped patterns with 20 and 25 μm side length were combined to one data set because both showed similarly increased apoptosis. The square shaped islands with 30 μm side length were considered as one separate group. In 3-D, 10 μm deep wells with different shapes were imaged and divided into three size groups. The small wells corresponded to a spreading area between 100 and 200 μm^2, the medium sized ones between 220 and 330 μm^2 and the large ones to a spreading area between 400 and 1200 μm^2. For the negative control, HUVECs were rinsed with methanol before the viability staining. Data for each cell viability value was acquired from at least 3 separate experiments from which average and standard deviation of the mean was calculated.

6.3 Results and discussion

6.3.1 Cell survival and apoptosis

First, the potential toxicity of PDMS for cells was investigated on flat, Fn-coated PDMS surfaces. $93 \pm 3\%$ of HUVECs in 10% serum on glass at 75% confluence were viable, and viability was not inhibited when cells were cultured in low serum on stiff PDMS (1 MPa), where $94 \pm 3\%$ of the cells were viable, or on soft PDMS (12 kPa), where $96 \pm 2\%$ of the cells survived. The negative control of methanol treated cells showed no cell survival (fig 6.2). Thus, both the stiff and soft PDMS was not toxic for cells, in agreement with previously published data [207].
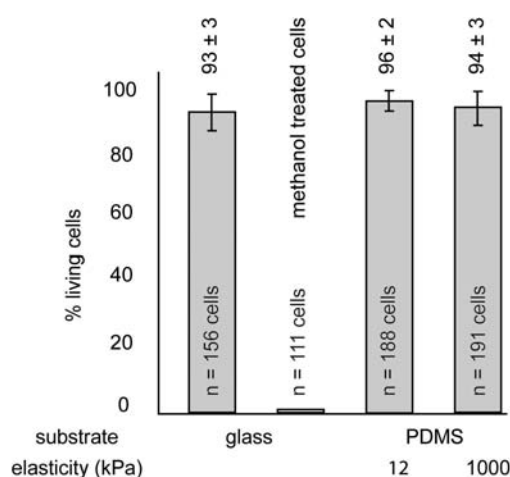
Figure 6.2: *Influence of PDMS on HUVEC survival.* HUVECs on flat, soft (12 kPa) and hard (1 MPa) Fn-coated PDMS showed a similar survival rate in comparison to cells cultured on Fn-coated glass surfaces after 24 h culture. The negative control of methanol treated cells showed no cell survival. Therefore, PDMS itself had no toxic influence on cells. The average and standard deviation of the mean is plotted. The differences between cells cultured on Fn-coated glass, on soft and hard PDMS were not significant.

Long term survival of cells inside microwells
Secondly, it was investigated whether long term culture (7 days) inside the microwells was possible. Positive staining for calcein and exclusion of ethidium homodimer-1 from cell nuclei was used to determine if cell confinement in 3-D microwells initiated cell death. Fig 6.3 A shows cells cultured inside 10 μm deep, square-shaped microwells. The green cells are stained with calcein which is indicative of cell survival, while the red cell (arrow) is stained with ethidium homodimer-1, an indication of dead cells. Since cells on a flat 2-D substrate grew over the whole sample after 7 days, only the cell survival rates of

Figure 6.3: *Cell survival inside microwells over 7 days culture time.* Cell viability was verified for HUVECs, whose viability was judged by staining for calcein AM (viable cells, green) and ethidium homodimer (apoptotic cells, red). HUVECS were cultured in 10 μm deep wells (circle, square, triangular, rectangular, spindle) with a projected area between 100 and 1200 μm^2. A) HUVECs cultured for one day within the microwell platform were imaged. B) The survival rate of HUVECs inside microwells was investigated up to 7 days. There was a drop in viability after 3 days, but remained constant until day 7 with most of the cells alive. Average, standard deviation of the mean and t-test are plotted.

cells inside microwells were compared. Therefore, cells were cultured inside microwells of different shapes (squares, circles, rectangles, triangle) and different spreading areas (100 − 1200 μm^2) for 24 h and 93 ± 2% of the cells survived. There was a slight, but non-significant drop in cell survival at day 3 with only 77 ± 7% of the cells still viable (p = 0.21). After day 7, the cell survival did not drop further and was observed to be 81 ± 4% (fig 6.3 B). It was visible that cell survival was slightly, but not significantly, diminished inside microwells compared between day 1 and 7 (p = 0.06). But the survival rate after a week of 81 ± 4% indicated that a high proportion of the cells were viable and that the platform can be used for long term studies of cells in 3-D microwells. This is an important feature which enables studies on long term cell behavior, such as differentiation of stem cells, within the microwells.

Influence of well size on apoptosis in comparison to cells on 2-D pattern

The investigation of the dependence of cell survival on well size was a crucial part of this study. It provided further insights into the effect of cell shape and dimensionality on cell survival. Cell confinement on small 2-D patterns led to apoptosis as described in the literature [136]. Chen *et al*. demonstrated that ∼50% of human and bovine capillary endothelial cells showed apoptotic behavior when cultured on circles with 20 μm diameter

(312 μm^2 spreading area). On patterns with a spreading area of 500 μm^2 $\sim$95% of the cells survived.

Our findings confirmed this trend. $64 \pm 15\%$ of HUVECs on small 2-D Fn patterns (square-shaped Fn islands with 20 or 25 μm side length, 400 or 625 μm spreading area) showed ethidium homodimer-1 staining, indicating dying cells. Culturing cells on larger Fn islands (square-shaped Fn islands with 30 μm side length, 900 μm^2 spreading area) resulted in a cell survival rate of $95 \pm 3\%$ which was in good agreement with cells cultured on flat, homogeneously coated Fn substrates ($93 \pm 3\%$ survival) (fig 6.4). The slight difference in cell spreading area between Chen's study and ours is probably caused by the use of different cell types.

In 3-D, cell confinement in medium sized microwells with a projected 2-D surface area between 240 and 330 μm^2 resulted in a level of cell survival ($95 \pm 3\%$) which was not significantly different from the viability observed after culture in larger microwells (400 – 1200 μm^2 spreading area) or control experiments on flat surfaces. However, microwells with a well bottom surface area between 100 and 200 μm^2 resulted in an apparent decrease in cell survival to $90 \pm 2\%$. Cell survival was slightly, but not significantly diminished (p = 0.34), and therefore the majority of the cells survived inside small microwells.

Considering that a cell can adhere in 3-D, *e.g.* a square shaped well presents five adhesion areas inside a microwell, the total surface area has also been taken into account. The very small microwells with a spreading area of 100 μm^2 correspond, *e.g.* to squares with 10 μm^2 side length and a total surface area of 500 μm^2 (100 μm^2 bottom area + 4 $\times$ 100 μm^2 side wall area). $90 \pm 2\%$ of cells cultured within these small wells (100 – 200 μm^2 spreading ares) were viable compared to cells on 2-D patterns where only $36 \pm 17\%$ survived on patterns with a spreading area of 400 or 625 μm^2. Therefore limitations in spreading area did not significantly induce cell death in a 3-D environment, which was in contrast to cells on a 2-D pattern. The increase in dimensionality enabled the cell to overcome cell death induced by spreading limitations. Other mechanism might be activated in 3-D which prevent programmed cell death. Therefore, the microwell platform allowed for long term cell studies and cells survived for up to 7 days in both small and large microwells.

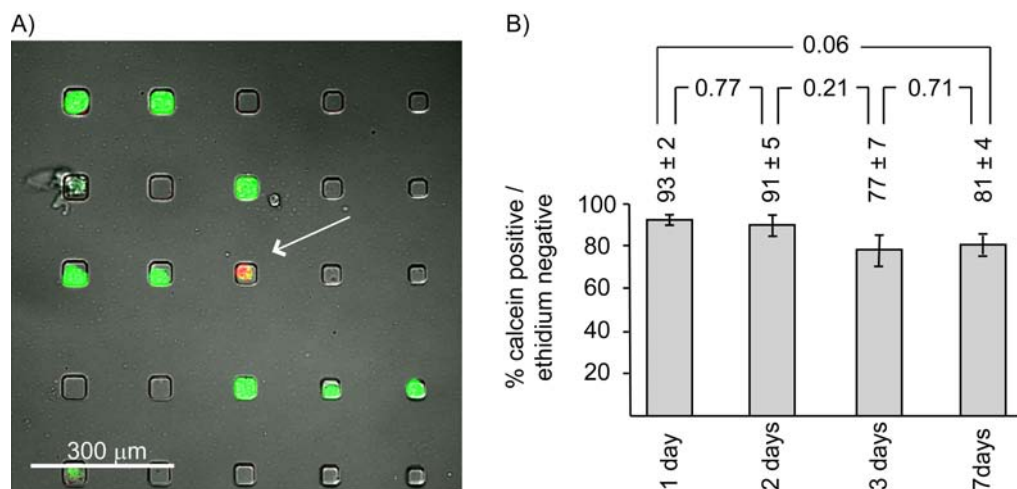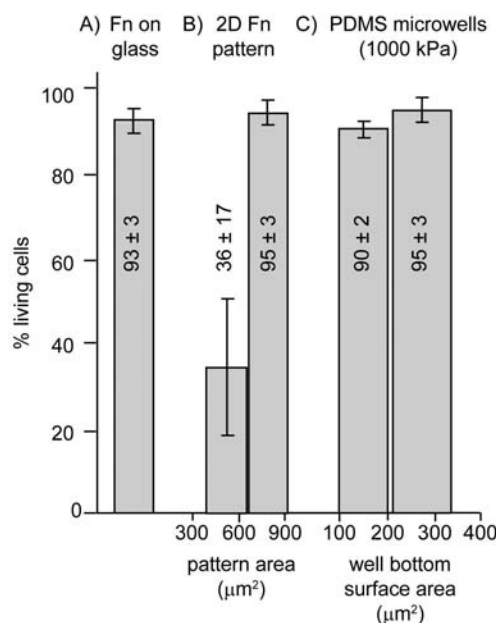**Figure 6.4:** *Cell survival inside small microwells.* Cell viability was verified for HUVECs, whose viability was judged by staining for calcein AM (viable cells) and ethidium homodimer (apoptotic cells). The percentage of calcein positive/ethidium negative cells after 24 hours in culture (10% FCS media) are shown for cells on A) flat Fn-coated glass, B) single cells on 2-D Fn patterns, on both small (400 or 625 μm^2) and larger (900 μm^2) pattern size, and C) single cells in hard microwells with a projected surface area of between 100 and 200μm^2 and between 240 and 330 μm^2 and a well depth of 10 μm. Average and standard deviation of the mean are plotted.

6.3.2   Well size

The concept of the microwell technique relies on a cell-adhesive surface inside 3-D microstructures with fixed volume and shape which matches that of a single cell. Cell shape is only completely controlled by the microwell when cell and microwell volumes are similar. This fit was only rarely achieved using a surface with only one type of microwell because cells vary in size. However, the use of a library of wells of different shapes and sizes on the same culture platform allowed for the selection of cells which were fully constrained in 3-D, but not protruding from the top of the microwell and thereby losing the control over cell shape. The range of microwell volumes adequate for 3-D shape control of HUVECs was determined by analyzing confocal z-stacks images of calcein positive cells to determine the right well size.

If the wells were too small for the cells, the cell fitted perfectly in the bottom area of the microwell, but protruded from the top, losing its defined shape (fig 6.5 A). If the microwells were too large, the cell filled the bottom of the microwell, but not the entire
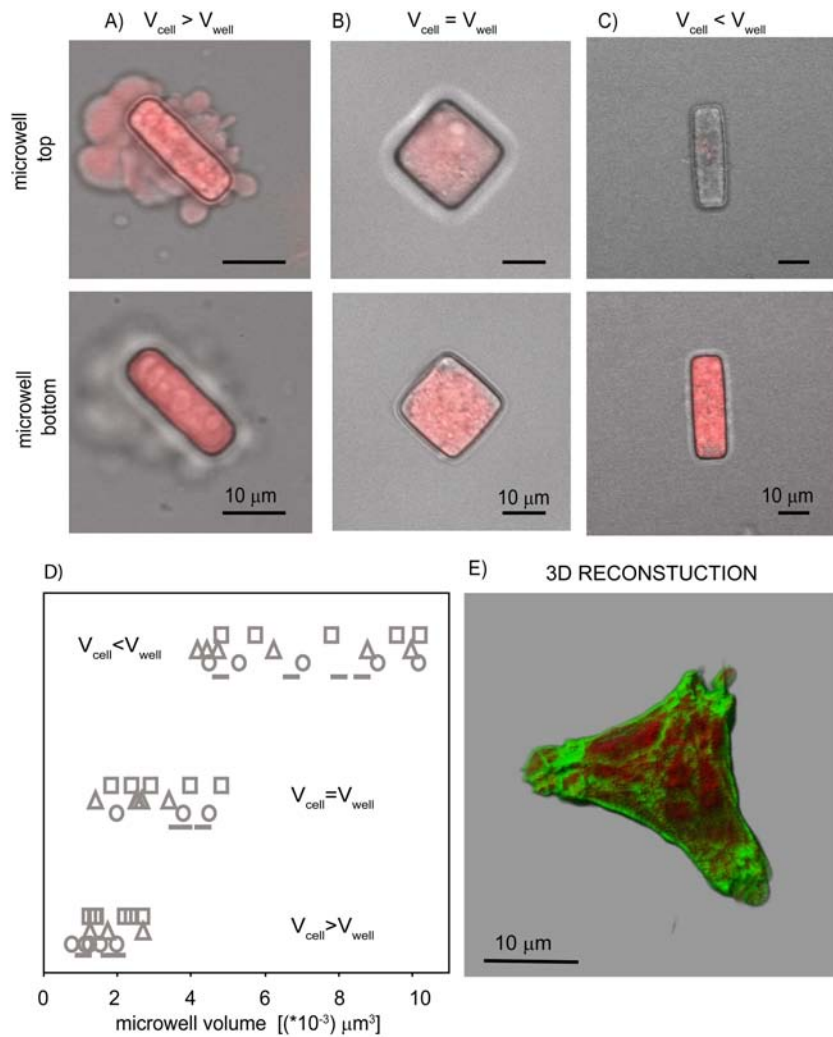
Figure 6.5: *Control of cell shape depends on well size.* A library of microwells which covered a wide range of projected surface areas with 10 μm depth were used to demonstrate that the fidelity of cell shape control within microwells depended upon the ratio of cell volume to well volume. Images are shown of A) an endothelial cell in a smaller well, B) a cell in a well of approximately equal volume, C) and a cell in a larger well. Confocal slices were taken at the upper and lower planes of microwells which were 10 μm deep. Images shown are confocal overlays of calcein AM-labeled living cells (red) on the DIC transmitted images (grayscale). D) The range of well volumes were quantified and divided into three groups (well volume is smaller, equal or larger than cells). Quantification was based on confocal z-stacks taken with 3 μm increments, and each triangular (triangles), circular (circles), square (squares), or rectangular data point (dashed line) represents at least 2 cell measurements in that size category. E) Cell inside a triangular microwell is shown, after visualization of actin (green, phalloidin) and nucleus (red, ethidium homodimer), on which a 3-D reconstruction was performed.

microwell. The cell spread as in a 2-D environment and the additional dimensionality aspect of cell patterning was lost (fig 6.5 C). If the microwell and cell volume were equal, the cell filled the microwell perfectly and took the shape of the well (fig 6.5 B). An analysis of 115 cells in 10 μm deep wells revealed that for a primary HUVEC culture, well volumes of 2×10^3 to 4.5×10^3 μm^3 were sufficient to control 3-D cell shape. This corresponds to a 10 μm deep well with a circular shape with a diameter of $15 - 24$ μm or a square with a side length of $14 - 21$ μm (fig 6.5 D). Cell shape did not appear to affect the ability of HUVECs to completely fill the microwells. For instance, cells were as efficient at filling spindle-shaped wells with sharp corners as they were at filling circles or squares.

It was difficult to determine whether one or two cells were filling a well with calcein staining. Nuclear staining with ethidium homodimer-1, in combination with actin staining using phalloidin confirmed that microwells within this volume range were generally filled with only one cell (> 90%). Fig 6.5 E shows a 3-D reconstruction of a HUVEC in a triangular microwell. It was clearly visible that the microwell shape was nicely transferred to the cell. This study showed that the variation in cell size, and therefore microwell size, is an important parameter which needs to be considered when performing cell patterning in 3-D.

6.3.3   Visualizing cells inside microwells

High-resolution microscopy

To test whether the microwell approach is compatible with high-resolution microscopy, intracellular features were imaged. Phalloidin and ethidium homodimer staining of actin and nuclei, was performed and imaged with a 60x oil objective. In this section, stress fiber and nucleus staining were used as a proof of principle study to show the microwell structure was compatible with high-resolution microscopy. Actin organization inside microwells is discussed in detail in chapter 7. In contrast to very large microwells where cells formed a monolayer as in traditional 2-D cultures (Fig 6.6 A), the actin cytoskeleton of cells whose 3-D shapes were fully confined by microwells were remarkably 3-D. Prominent actin stress fibers were often aligned along the long axis of the microwell (Fig 6.6 B-D). In addition, nuclear shape could easily be resolved inside microwells and had a shape resembling the shape of the microwell (Fig 6.6 C). These images show that the microwell technique was successfully combined with high-resolution microscopy. Due to
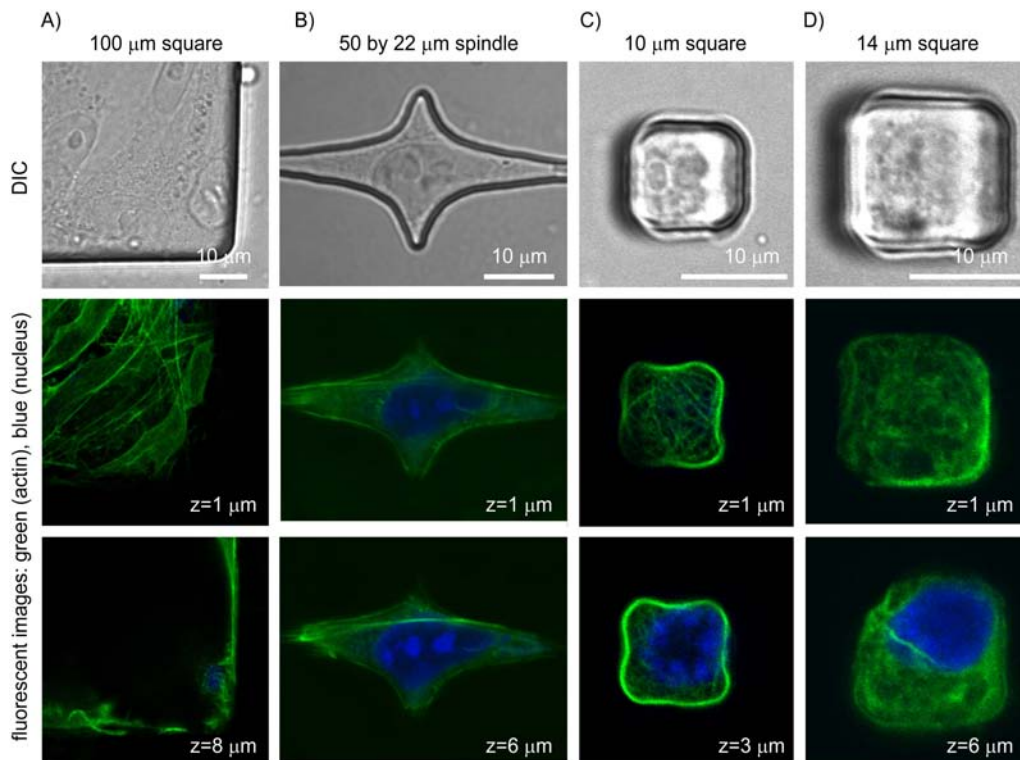
Figure 6.6: *Imaging of intracellular features of a cell inside a 10 μm deep microwell.* DIC and fluorescent confocal images are shown of cell nuclei (ethidium homodimer; blue) and actin cytoskeletal networks (Alexa 488- phalloidin; green). A) HUVECs cultured for 24 h are shown in a large microwell, B) a spindle-shaped microwell which was slightly bigger than the confined cell, and C) 10 μm and D) 14 μm square microwells which adequately controlled the 3-D shape of cells. Confocal slices are shown at different height positions in the microwells where z = 0 indicates the microwell bottom.

the incorporation of the microwell platform into a standard Petri dish, high-resolution live imaging was possible. This demonstrates one of the advantages of the microwell structure over less controlled 3-D systems, like matrices, which have a certain thickness which makes live high-resolution microscopy difficult [194].

Staining control

Although microwells were fabricated into thin films to permit high-resolution microscopy of cellular features, we needed to rule out the possibility that the microwell culture platform might limit the ability to visualize intracellular proteins with IHC due to diffusive issues. Therefore, we tested the efficacy of IHC staining of Fn which was bound to the bottom surface of microwells containing a HUVEC compared with Fn bound to a glass surface underneath an adherent HUVEC. Fn was previously labeled with Alexa 488 or Alexa 633 and adsorbed inside microwells or on a glass surface (fig 6.7 A). After 24 h in

cell culture, Fn was additionally IHC stained and visualized with a rhodamine-conjugated secondary antibody (fig 6.7 B). Fig 6.7 A-C are representative images of Fn labeled or stained on glass or inside microwells. The correlation coefficients between images of adsorbed Fn, which was previously labeled with Alexa 488 or Alexa 633, and IHC-stained Fn were calculated (fig 6.7 D). Diffusion limited IHC staining in microwells would lead to a lower correlation coefficient between images of microwell bottoms relative to correlation coefficients of images on glass surfaces. However, fig 6.7 demonstrates that Fn on the bottom surface of microwells (correlation coefficient 0.92 ± 0.1) containing cells was stained and imaged using IHC as effectively as Fn underneath cells on 2-D glass (correlation coefficient 0.88 ± 0.12). The correlation coefficients (fig 6.7 D) were comparable both on the glass surface as well as inside the microwells. In addition, similar results were found when Alexa 488- or Alexa 633-labeled Fn results were compared to the rhodamine labeled secondary antibody results, thus excluding a contribution from fluorescent bleed. In conclusion, the microwell platform permits IHC staining inside wells and is an appropriate tool to image intracellular features with high-resolution microscopy in 3-D.
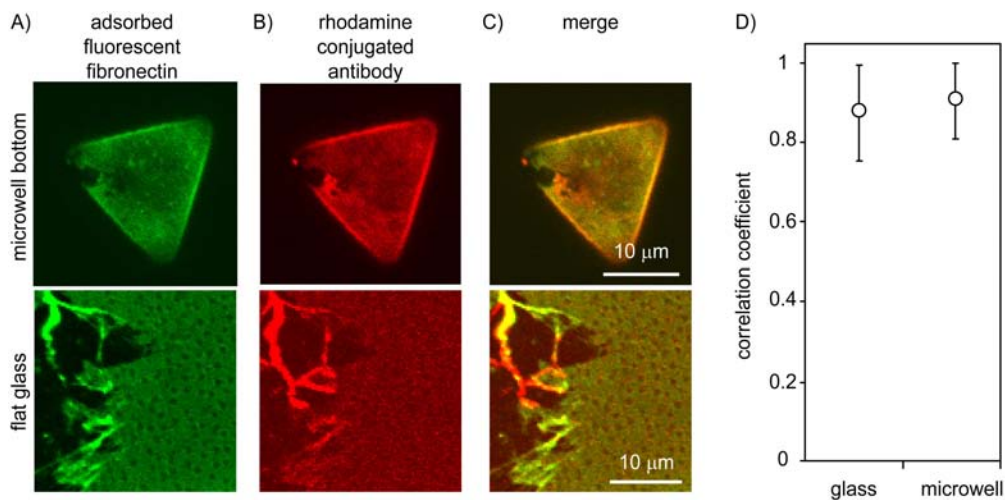
Figure 6.7: *Staining control on bottom of microwell versus a flat surface.* Confocal images focusing on the Fn-coated surface are shown of A) adsorbed fluorescent Fn and B) IHC-stained Fn using a rhodamine labeled secondary antibody. C) Merged images are shown for a 20 μm edge triangular microwell filled with a single HUVEC and Fn underneath a small portion of a well spread HUVEC on flat glass. Correlation coefficients were calculated D) to quantify the efficacy of IHC underneath cells in microwells relative to cells adherent to flat glass substrates to determine whether increased diffusive barriers are present using microwell samples. All fields of view were 28 by 28 μm, confocal settings, such as laser transmissivity and photomultiplier tube voltage, were kept constant, and raw data images were used for correlation coefficient calculations.

6.4 Conclusion

This chapter demonstrates that our microwell thin PDMS film substrates are compatible with conventional culturing assays and high-resolution, inverted stage fluorescence microscopy (CLSM) used in cell biology. Cells were shown to survive up to 7 days inside the microwells. The most striking fact was that cells survived culture inside small microwells and dimensionality enabled the cell to overcome cell death caused by limited spreading area, as it was observed on 2-D patterns [136]. Furthermore, flat hard and soft PDMS showed no toxic effect on cells and was therefore a suitable material to produce microwells of different stiffnesses (see chapter 7). The results presented in this chapter demonstrated that the microwell structure is a suitable tool for investigating the influence of, *e.g.* dimensionality and elasticity on cell behavior, while controlling the 3-D shape of the cell.

Rigidity- and shape-dependent cytoskeleton assembly and
metabolism difference in 2-D and 3-D

7.1   Background

In this chapter, we sought to determine whether cells are responsive to a 3-D arrange-
ment of adhesive contacts and whether cell sensitivity to shape and rigidity, as well as
metabolic activity, are altered relative to 2-D controls. Therefore, we compare the cyto-
skeletal characteristics of single cells adhered either on microfabricated adhesive islands
(2-D) or in microwells (3-D) of controlled size, shape and rigidity. Studies of cytoskeletal
organization were performed because it is extremely sensitive to environmental proper-
ties and has a profound influence on cell behavior (see section 1.1.1 and 1.2.3). The
cell's ability to migrate, apply contractile force to their surrounding and divide requires
an intact actin cytoskeleton. The actin cytoskeleton is a force-bearing network that links
intracellular force generation to extracellular matrix attachments. Most cells probe their
microenvironment as they anchor through focal adhesions, pull on their environment, and
respond through cytoskeletal organization to the resistance that the cell senses. In return,
the cell responds to the environment by adjusting adhesion [185] and its cytoskeleton
[174]. Soft and rigid 2-D substrates lead to either the absence or presence of a filamen-
tous actin network [175], and cell shape confinement can also switch actin cytoskeleton
assembly off. Importantly, the ability to build an actin cytoskeleton and the ability to gen-
erate contractile forces are a requisite step in the response of cells to their environment.
For example, cell shape dictates the organized structure of the cytoskeleton, which then
controls the orientation of the axis of cell division [137]. Inhibition of actin cytoskeleton

assembly or intracellular proteins that mediate or control cell contractility, such as non-muscle myosin II, blocks human mesenchymal stem cells from differentiating in response to these physical cues [181]. To determine whether shape- and rigidity-dependent assembly of an actin cytoskeleton is orthogonal or dependent upon the dimensionality of cell contact with its surroundings, the actin cytoskeleton was visualized using high-resolution confocal microscopy on 2-D patterned surfaces and 3-D microwell platforms. We show that actin cytoskeleton assembly, metabolic activity and Fn rearrangement are dependent upon 3-D matrix adhesions, substrate rigidity, and cell shape.

7.2 Experimental Section

7.2.1 Substrates

2-D micropatterned glass substrates for the study of actin organization and Fn rearrangement where produced by the MAPL technique (section 3.3.2). For the production of the microwell arrays and the flat PDMS substrates, soft and hard PDMS was used (section 3.4). Its stiffness can be controlled by varying the cross-linking density as discussed in section 3.2.2.

7.2.2 Actin

HFF cells, myosin IIA knockout, and myosion IIB knockdown cells were seeded on the sample and cultured for 24 h prior to fixation and actin staining. Details about cell lines and actin staining are described in chapter 3.6.

7.2.3 Fibronectin rearrangement

To assess the rearrangement of Fn within microwells and on 2-D surfaces, samples were coated with Fn labeled with Alexa 488 (Molecular Probes, Switzerland) prior to cell seeding. After 90 minutes, samples were fixed and blocked as described in section 3.6.2. To quantify the surface area where Fn rearrangement occurred, a Matlab analysis was performed (fig 7.1). Briefly, the fluorescent signal of Fn labeled with Alexa 488, which was adsorbed on the surface, was measured without cells. Hence the background intensity

distribution of the homogeneous coated Fn was obtained. The highest and lowest intensity values were further used as upper and lower intensity threshold values. The intensity of the Fn area below a cell was measured with these threshold values, determining the percentage of surface below (removal of Fn) and above (accumulation of Fn) the threshold. The sum of this two values resulted in the total percentage of the area where Fn rearrangement occurred.
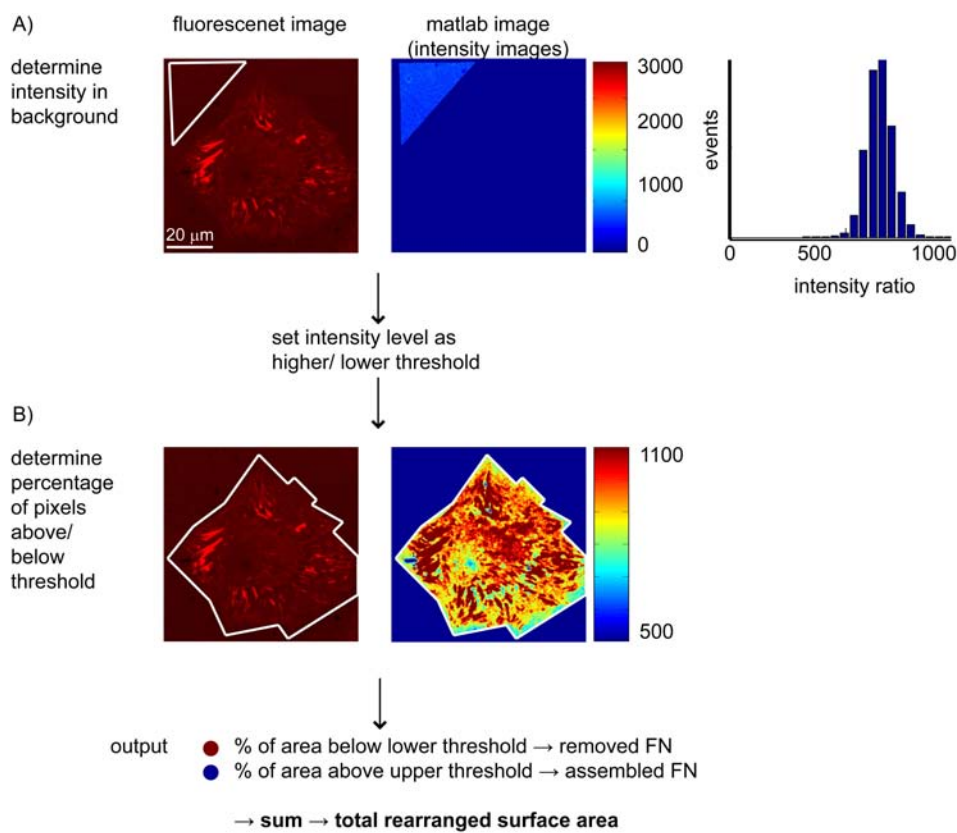
Figure 7.1: *Analysis of Fn rearrangement.* The principle of Matlab analysis of the Fn rearrangement. First, the intensity of a Fn-coated surface without cell is measured (A). The histogram gives the upper and lower intensity values of the coated area. These values are set as higher and lower threshold and the intensity of a Fn-coated surface with a cell is measured (B). The area below the lower threshold is colored blue, indicating removed Fn, the area above the upper threshold is red, indicating assembled Fn. The sum of these two values corresponds to the total rearranged surface area

7.2.4   Mitochondrial membrane potential

To determine the mitochondrial membrane potential and therefore the metabolic activity of cells cultured on 2-D surfaces or in microwells, HFF cells were stained with tetramethylrhodamine ethyl ester (TMRE, section 3.6.2). First, it was investigated whether differences in fluorescent intensity could be related to different metabolic activities. Therefore, the cells were kept for 30 min at either 30°C or 37°C in 10% serum media and 5% CO_2 and imaged. The imaging of cells cultured on 2-D patterns and inside microwells was always performed at 37°C. To analyze the images, Matlab was used and the average fluorescent intensity of a cell determined. The background was subtracted and the pixels with an intensity under 150 were filtered out to determine the average pixel intensity. This ensured zero intensity pixels were filtered out, as their presence would lower the average of fluorescent signal drastically.

7.3   Results and discussion

7.3.1   Actin

Going 3-D alters actin cytoskeleton assembly in response to cell shape

To address whether a 3-D arrangement of cell adhesion to extracellular matrix molecules can influence cytoskeletal organization, we investigated the spatial arrangement of actin in fibroblast cells cultured in microwells in comparison with cells on a 2-D patterned surface of the same projected area. We chose to use fibroblast cells since they normally reside in a 3-D matrix *in vivo*, but are often studied on 2-D platforms *in vitro* (for example [170]). The microwells were coated with Fn and shaped in different forms with well volumes close to the average volume of a single cell. First, the spatial arrangement of the actin network was investigated. Therefore images were taken as high-resolution confocal z-stacks and the actin filament formation on every slice was observed. The different confocal slices represent different positions within the cell and the intensity of the fluorescent signal of the actin and the nucleus was quantified and plotted versus well depth. On 2-D patterns, actin was most abundant at the interface between the cell and the substrate (fig 7.2 A). The 3-D reconstruction showed a flat cell with no prominent 3-D actin
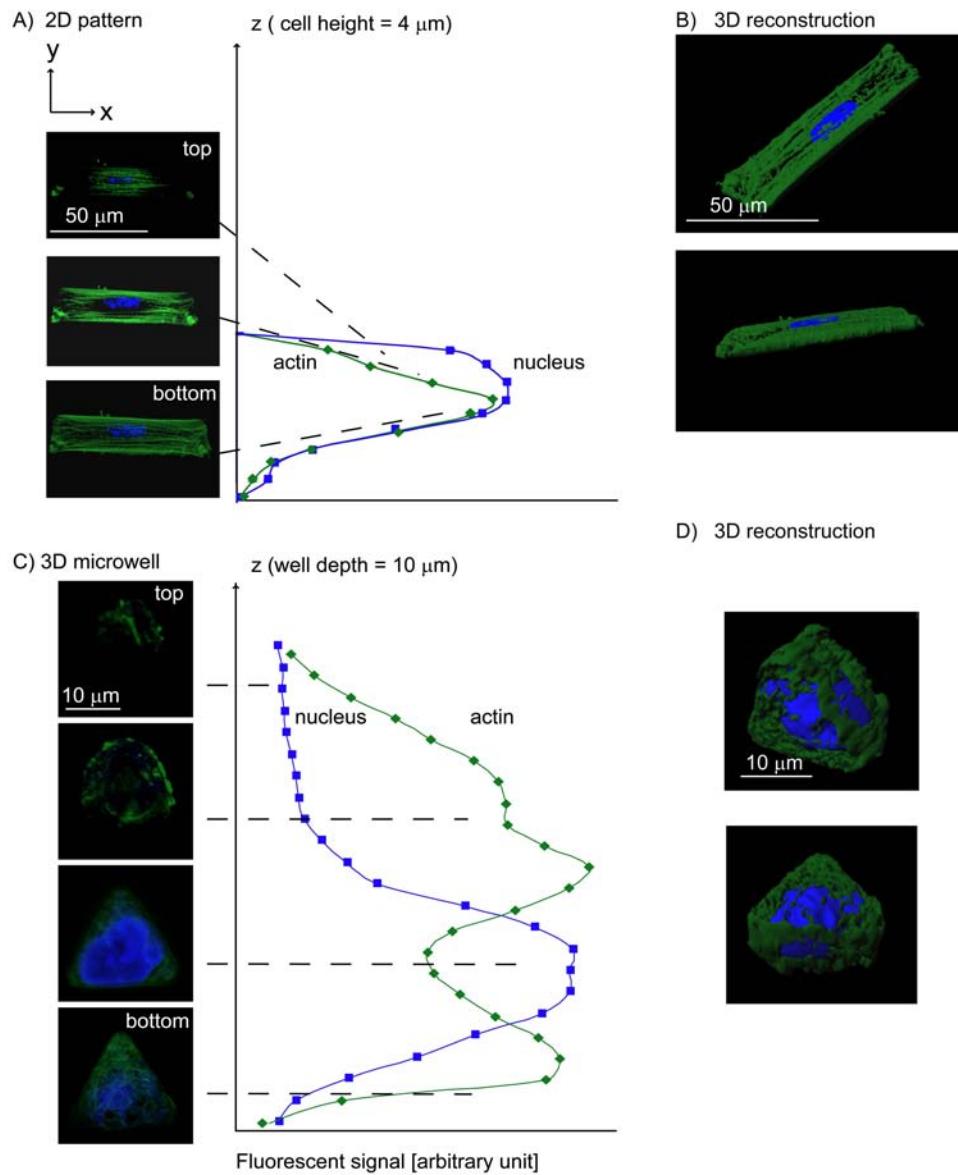
Figure 7.2: *3-D organization of actin skeleton inside microwells versus 2-D surfaces.* To visualize the altered actin organization on 2-D versus 3-D microwells, the fluorescent signal of actin (Phalloidin 488) and nucleus (ethidium homodimer) was quantified on a 2-D pattern and inside a 3-D microwell. A) The actin on a 2-D pattern was most abundant on the interface between the cell and the substrate. B) The reconstruction of a cell on a 2-D pattern shows a flat cell with stress fibers along the long axis but little 3-D arrangement of actin. C) The quantification of actin inside a 3-D microwells shows an actin accumulation at the interface between the cell and the bottom of the well and furthermore, on top of the microwell, covering the nucleus. The middle area of the microwell is mostly filled with the nucleus. D) The 3-D reconstruction shows the 3-D rearrangement of the actin that is like a scaffold all around the nucleus.

network surrounding the nucleus (fig 7.2 B). The prominent features were the stress fibers along the long axis of the pattern, mainly on the contact area of the cell with the substrate. Above the cell nucleus, there were clearly less stress fibers visible.

In 3-D, the actin skeleton was most clearly visible in the bottom image plane. Upper planes showed peripheral bands of strong actin intensity while the middle was filled with the nucleus. Above the nucleus there was again actin filament assembly observable, although it was less clear than below the nucleus. The plotting of the fluorescent signals of actin and the nucleus confirmed that the actin filament assembly was prominently on the bottom of the microwell and above the nucleus, where the actin spanned all over the cell (fig 7.2 C). Reduced actin formation was observed in the middle of the cell where the nucleus was located. Nuclear position varied from cell to cell but was often slightly shifted towards the bottom of the cell. The 3-D rearrangement of the actin cytoskeleton fibers was also clearly visible in the 3-D reconstruction (fig 7.2 D).

In 3-D microwells, fibroblasts were cultivated within wells with similar degree of spreading and cell shape as on 2-D patterns to clarify whether this actin filament assembly was altered in microwells relative to cells on 2-D patterns. Actin filament assembly was most clear visible on the bottom plane of the microwell. Due to technical limitations in quantifying actin filament assembly inside microwells, we show consistently images of the bottom plane of the well. Furthermore, a library of different single cells inside microwells is provided in fig 7.8 in order to show the variation of actin filament assembly and to demonstrate the reproducible cell response to the 3-D environment.

On 2-D patterns, inhibition of cell spreading led to an inhibition of actin cytoskeleton assembly, particularly the linear actin structures that resemble stress fibers (fig 7.3 A). On bigger patterns (surface area > 1000 μm^2), the cell could build an actin network with stress fibers along the long axis of the pattern. Decreasing the pattern size resulted in loss of actin fiber formation on 800 μm^2 and smaller patterns. Furthermore, cell viability on small 2-D patterns was decreased, with only 36% of the cells being viable, similar to previous reports. On larger 2-D patterns and in 3-D microwells the cell survival was similar to cells on a homogeneous coated surface (section 6.3.1) [136].

Fibroblast cells constrained within small microwells (100 μm^2 projected area, 10 μm deep / 500 μm^2 total, i.e., wall and bottom, surface areas) that were cast in PDMS with a stiffness of 1 MPa assembled an actin filament network, independent of well shape (fig 7.3 C). As described above, the cytoskeleton exhibited a 3-D arrangement in microwells and was not only limited to the cell-substrate interface in contrast to cells on 2-D
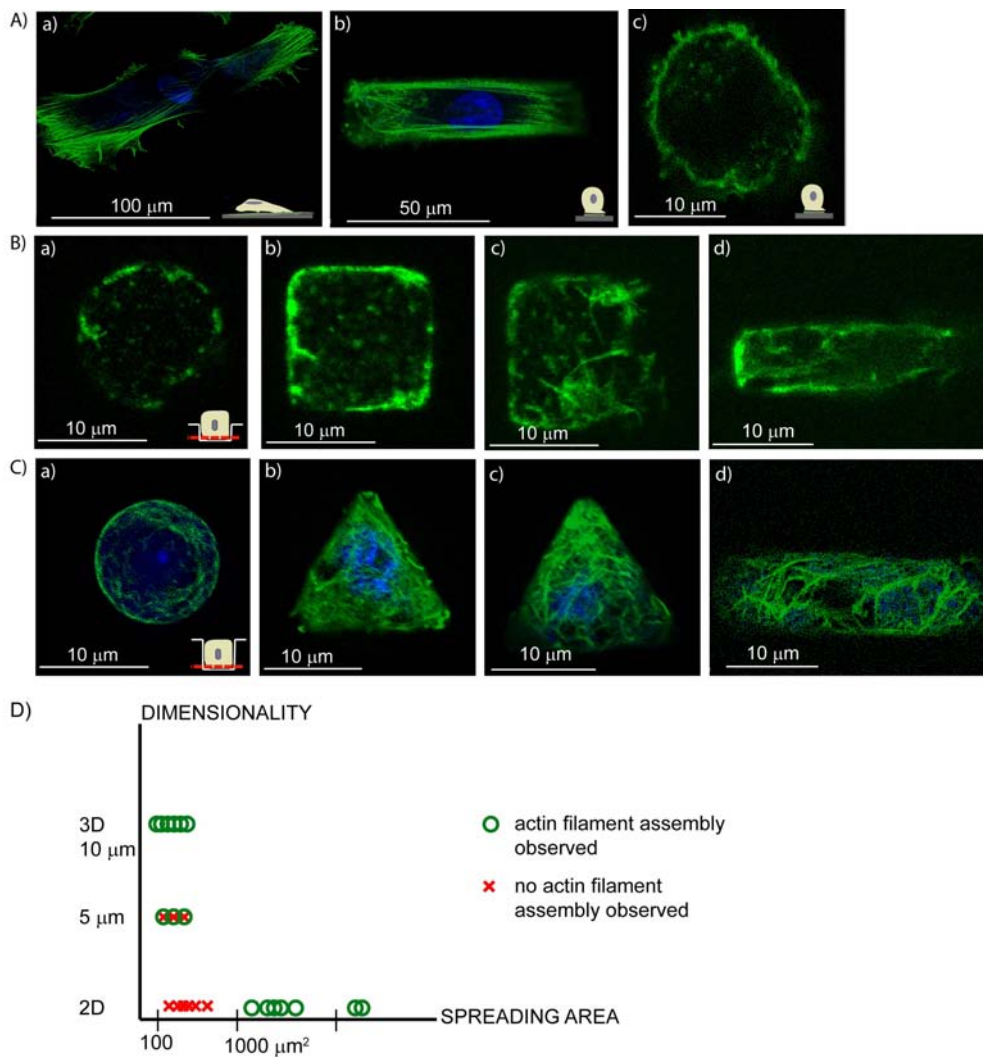
Figure 7.3: *Reduction of actin filament assembly due to small spreading area is overcome by going into 3-D.* To test whether a 3-D arrangement of cell matrix contact altered actin cytoskeleton assembly, actin filament assembly was visualized using phalloidin Alexa 488 staining and the nucleus with ethidium homodimer on A) flat surfaces, B) in 5 μm deep microwells, and C) in 10 μm deep microwells. A) Cells on both a 2-D surface which was a) homogeneously coated with fibronectin (no spreading limitation); b) and on a relatively large pattern (20 by 80 μm rectangle) formed stress fibers which were clearly visible in all imaged cells. However, c) cells on small patterns (12 μm circle) showed little to no actin fiber formation. B) Cells inside 5 μm deep microwells showed a, b) heterogeneous patterns of actin filament assembly where approximately half looked similar to cells on small 2-D pattern, whereas c, d) half showed actin filament assembly. C) In contrast, fibroblast cells inside 10 μm deep microwells of all shapes and 2-D projected areas assembled an actin filament network. D) The schematic of spreading area versus dimensionality shows that a cell can only build up an actin network if the cell has a certain spreading area. This critical range of spreading area is shifted towards smaller areas if the cell is able to interact with a 3-D matrix.

surfaces. Furthermore, inside the microwells the cells did not show a decreased viability due to limited spreading area, as was observed on 2-D (section 6.3.1) [136]. To investigate if there is a critical well depth below which the cell cannot sense 3-D contacts, and the cell is effectively experiencing a 2-D environment, actin staining with phalloidin was additionally studied in 5 μm deep wells (fig 7.3 B, 7.9). At this intermediate depth, some cells were still able to assemble actin filaments similar to the 10 μm deep wells, whereas others showed no actin network, similar to a small 2-D pattern. These data suggest that the decision to assemble an actin cytoskeleton is an all or none response, with some cells not responding to dimensionality at this intermediate well height (fig 7.3 D).

Going 3-D alters actin cytoskeleton assembly in response to substrate stiffnes

Environmental properties on cell responses are intimately linked. Substrate stiffness itself affects cell spreading and hence cell shape, therefore the relative impact of these factors remains an outstanding question. Therefore, cells were cultured on flat substrates and inside microwells that were cast in either hard (1 MPa) or soft PDMS (20 kPa). This independent coupling of dimensionality and stiffness sought to determine whether rigidity sensation is dependent upon dimensionality. On flat 2-D substrates, cells showed no difference in actin formation regarding the two stiffnesses (fig 7.4 A, C) and showed strong actin fiber formation. The substrate stiffness below which fibroblasts were incapable of making an actin cytoskeleton was clearly lower than 20 kPa. In 3-D microwells, the cells were able to build up an actin network in contact with a hard substrate as described in the previous paragraph (fig 7.4 B). Remarkably, if a cell was exposed to a 3-D arrangement of cell contacts and softer substrate stiffness, cytoskeleton assembly was diminished (fig 7.4 D, 7.10). Although the same microscopy settings were used for both hard and soft microwells, no actin filament assembly was detectable in soft microwells. The regime of stiffness sensation seemed to be shifted toward harder substrates in a 3-D environment compared to 2-D. This result showed that the 3-D environment within soft microwells drastically alters actin cytoskeleton assembly. A cell experienced the same stiffness on soft 2-D substrates and inside soft 3-D microwells, but 3-D stimulation of actin filament assembly required a threshold substrate stiffness which was dramatically higher than that required for actin filament assembly for cells on 2-D culture surfaces. Mechanosensing properties and actin filament assembly were not only dependent on substrate stiffness, but they were dependent upon both stiffness and dimensionality indicating a synergic relationship between the two parameters stiffness and dimensionality (fig 7.4 E).
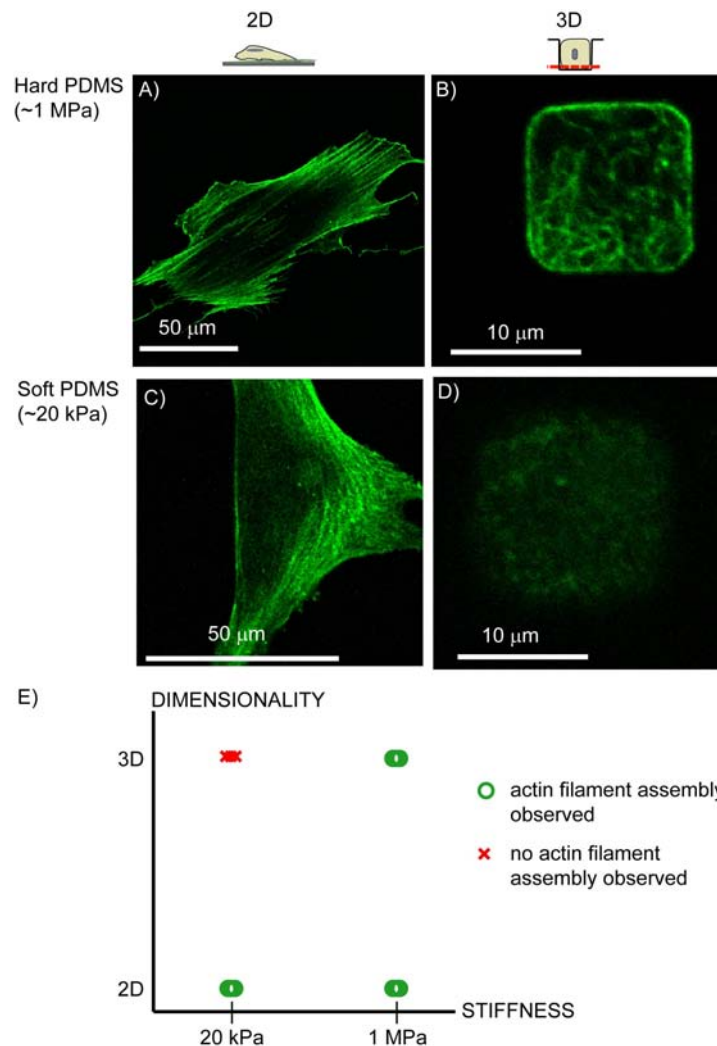
Figure 7.4: *Dimensionality alters the rigidity below which assembly of the actin cytoskeleton is diminished.* In order to test whether substrate stiffness impacted the stimulation of actin filament assembly in a 3-D environment, fibroblast cells were cultured on 2-D surfaces or in microwells that were A, B) 1 MPa or B, D) 20 kPa and actin visualized with phalloidin Alexa 488. A) On hard substrates, cells formed actin stress fibers on homogeneously coated 2-D surfaces as well as B) inside 3-D microwells. C) On soft substrates, actin stress fibers were observed on homogeneous coated 2-D substrates. D) In contrast actin filament assembly was inhibited inside soft 3-D microwells. E) The schematic of stiffness versus dimensionality shows that a cell can only build up an actin network if the substrate has a certain stiffness. This critical range of stiffness is shifted towards higher stiffnesses if the cell is able to interact with a 3-D matrix.

Myosin

Cell-generated force is a necessary prerequisite for Fn matrix production and the hindrance of Fn matrix rearrangement indicated reduced cell contractility. This was in contrast with the ability of a cell to build up an actin skeleton. Myosin II is known to play an important role in cell migration and the generation of traction forces (see 1.1.1). Blocking

of myosin has been shown to prevent actin formation and therefore, the actin formation of mouse embryonic fibroblast cells with silenced in myosin IIA by SiRNA or knockout myosin IIB were cultured in microwells and assayed for actin bundling.

On 2-D, the Myosin IIA wild type showed clear stress fiber formation, similar to the results obtained by Cai *et al*. with this cell type [279]. Myosin IIA knockdown cells showed similar actin organization as the wild type; this was unexpected as previously less actin staining was observed for the Myosin knockdown cells [279]. In 3-D, the actin of the Myosin IIA wild type looked similar to the actin observed in wild type cells on 2-D. Likewise, similar actin formation could be observed for the Myosin IIA knockdown cells in 3-D and on 2-D. Furthermore, the Myosin IIAknockdown cells and the wild type arranged similar actin structures inside 3-D microwells (fig 7.5 A, B, fig 7.11).

On 2-D, the Myosin IIB wild type showed distinct lamellipodia formation. Meshel *et al*. showed some lamellipodia formation, but they were less pronounced than in this instance [280]. In contrast, the Myosin IIB knockout cells showed a rounded morphology with actin fibers predominately oriented towards the center of the cell. In 3-D, the actin of the Myosin IIB wild type looked similar to the actin observed within cells cultured on 2-D, but the morphology changed since lamellipodia was no longer detectable. The actin organization for the Myosin IIB knockout cells looked similar in both 2-D and 3-D cases. Furthermore, the Myosin IIB knockout cells and the wild type organized similar actin structure inside 3-D microwells (fig 7.5 C, D, fig 7.12).

Previous studies suggested that myosin IIA is mainly involved in cell adhesion, cell shape [281] and motility on 2-D surfaces [279]. Conversely myosin IIB is important for the guidance of cell movement by coordinating protrusive activities and stabilizing cell polarity [282] and for lamellipodia formation and motility in a 3-D environment [280]. By deletion of nonmuscle myosin heavy chain II, motile processes and cell migration are not blocked, but the ability to generate large forces is greatly decreased [283]. When considering the involvement of contractile forces to actin filament assembly, we have to regard that it has been shown that myosin IIA contributes ~60% of traction forces and its IIB isoform ~30% [279]. Furthermore, previous work has shown that myosin IIB knockout cells can contract 3-D collagen gels three times less than the wild type [280], indicating a diminished but not extinct ability to build up contractile forces inside a cell. Therefore, the ability to generate traction forces is not completely blocked. Since not all the myosins isoforms were blocked simultaneously, we can not make any conclusion about the involvement of cell contractility in this type of actin fibril assembly.
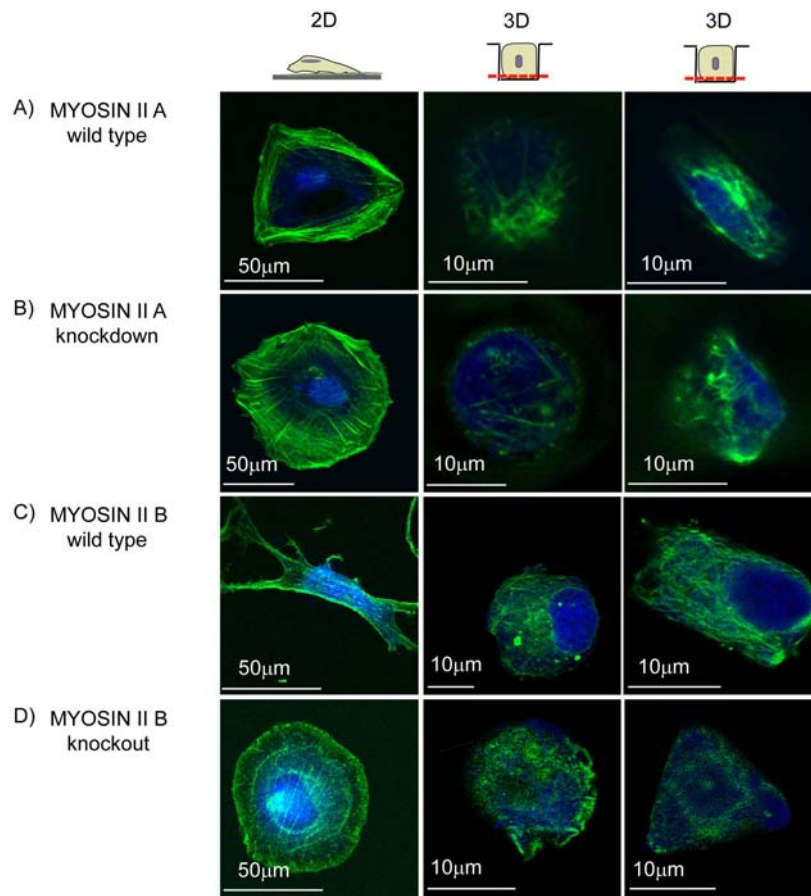
Figure 7.5: *Actin bundling in silenced myosin IIA and myosin IIB knockout cells.* Actin was visualized using phalloidin Alexa 488 staining and the nucleus with ethidium homodimer. A) The wild type and B) silenced myosin IIA cells on a 2-D (left) and inside 10 μm deep microwells showed the same characteristics of actin bundling. C) Additionally, the wild type and D) myosin IIB knockout cells showed no significant difference in actin formation both on 2-D surfaces (left) and inside 3-D microwells.

Overall the cells were able to build up an actin network, but the actin cytoskeleton was heterogeneous from cell to cell. Therefore it was difficult to draw any conclusions from the actin formation in the cells. Furthermore, it is difficult to study other effects of myosin, *e.g.* lamellipodia formation and migration, in this platform. If cells are trapped inside 3-D microwells and restricted in their spreading area, we also eliminated their ability to migrate. Therefore it is not possible to draw any conclusion about the migratory behavior in 3-D and the migratory behavior was not studied on 2-D surfaces. Furthermore, lamellipodia formation and ruffling of the membrane [284] was difficult to observe because a cell with a restricted shape cannot form elongated lamellipodia as these would have to penetrate the PDMS walls.

7.3.2 Fibronectin rearrangement

Fn is a major ECM component for many cell types that is regularly remodeled by cells such as fibroblasts that populate tissue stroma [285]. This process, like the production of a Fn matrix (fibrillogenesis), is required for both development and wound healing and is strongly influenced by the microenvironment of cells [286]. Cell shape, or spreading area, and dimensionality enhance or decrease the amount of rearranged matrix. Since extracellular Fn matrix fiber formation requires cell contractility [287, 288], we next asked whether fibroblast cells in microwells rearranged surface adsorbed Fn into fibers in situations where actin filament assembly was observed.

Homogenous versus patterned 2-D surfaces

2-D Fn patterns with protein islands and cell resistant background were produced by the MAPL technique [124]. The size of the patterns varied between 100 and 1600 μm^2. Quantitative analysis of the rearranged surface area on 2-D pattern showed that cell spreading inhibition progressively limited Fn rearrangement with decreasing pattern size ((fig 7.6 A-D, G). The percentage of Fn rearrangement increased with increasing pattern size from $0.6 \pm 0.5\%$ rearranged surface area on < 500 μm^2 patterns to $4.1 \pm 1.8\%$ on larger, > 1500 μm^2 patterns, but did not reach the level of rearrangement observed on a homogenously coated surface of $19.2 \pm 5.6\%$.

Furthermore, Fn rearrangement on 2-D patterns showed a dependence on the pattern shape. On squares, Fn rearrangement occurred predominantly on the edges, in contrast to circles, where the Fn was rearranged regularly on the periphery of the pattern. The dependence of pattern size and shape dependence corresponds with findings about focal adhesions on a cell adhesive pattern. The amount focal adhesions increased in direct proportion to cell spreading and they localized along the periphery of the small islands that experienced highest tensional stress [289]. The more focal adhesions, the more the cell can interact with its environment and the higher is potential to rearrange the Fn.

2-D versus 3-D substrates

Fn rearrangement was also investigated in the 3-D microwells. Within very small 3-D microwells (size range 100-200 μm^2 projected surface area / 500-765 μm^2 total surface area), Fn rearrangement into fibrils was inhibited (fig 7.6 E), similar to the 2-D case with the same spreading area. In bigger microwells (size range 1100-1600 μm^2 projected sur-
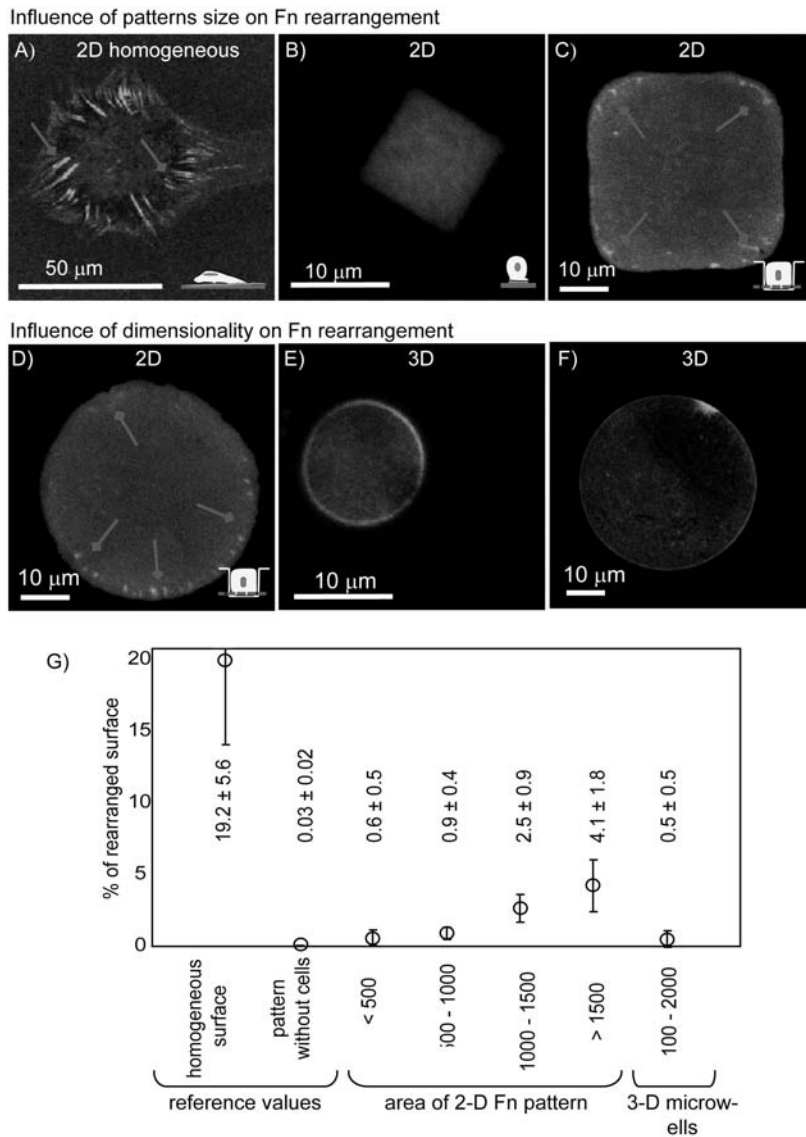
Figure 7.6: *The dependence of Fn rearrangement on spreading area and dimensionality.* The influence of spreading area and dimensionality on Fn rearrangement (Fn, fluorescently labeled with Alexa 488) was investigated on 2-D and 3-D platforms. A) Cells on homogeneously coated surfaces rearranged the Fn matrix to a large extent. The bright green areas indicate an accumulation of Fn, while the darker areas indicate removed Fn. B) Cells with limited spreading area on small Fn pattern were not able to rearrange the Fn matrix. C) With increasing spreading area, cells rearranged more and more the Fn matrix. Square shaped pattern (2500 μm^2) and D) circular pattern (1900 μm^2) show how the cell rearranges the Fn starting from corners. Cells inside 3-D microwells were rarely able to rearrange the Fn on the bottom of the well. E) Culture of cells in small microwells (113 μm^2 projected area) hindered the Fn rearrangement similar to small 2-D pattern, F) but even cell culture in bigger microwells (1900 μm^2 projected area) did not allow for Fn rearrangement. G) Matlab calculations allowed for quantification of the percentage of rearranged surface area by the cell. Details about the analysis are shown in fig 7.1.

face area / 2426-3200 μm^2 total surface area), no Fn rearrangement occurred (fig 7.6 F), which was in contrast to the 2-D patterns of the same size, where the cell was able to re-arrange Fn in its environment. Cells which adequately filled microwells rarely rearranged Fn from the microwell surfaces, but in rare cases where Fn rearrangement occurred it generally proceeded from one corner inwards.

7.3.3   Cell metabolism is dependent on spreading area

The metabolism of a cell is dependent on mitochondrial activity. To investigate the dependence of the metabolism of cells on spreading area and dimensionality, the mitochondrial membrane potential was determined by staining the cells with TMRE (fig 7.7 A-E). The quantification of the fluorescent signals allowed the fluorescent intensity, as determined by mitochondrial membrane potential, to be correlated to metabolic activity of a cell (fig 7.7 F). As a control, mitochondrial membrane potential was imaged and quantified in cells at 37°C and 30°C. The more intense signal for cells at 37°C, in comparison to cells at 30°C, indicated the greater metabolic activity of cells at 37°C, as expected ($p < 0.001$). This indicated that this method can be used to quantify the fluorescent signal and thereby determine the metabolic activity within cells.

Next, we sought to determine whether environmental properties that were shown to influence actin cytoskeleton assembly affected the metabolic activity of cells. Inhibition of cell spreading decreased the metabolic activity of cells. On 2-D patterns and inside 3-D microwells, the metabolic activity was elevated for cells with a spreading area greater than 500 μm^2, when compared to smaller patterns. The difference between the metabolic activity on small and big 2-D patterns ($p < 0.01$) and 3-D microwells ($p < 0.001$) was statistically significant. Dimensionality itself also influenced the metabolic activity. There was a small, but statistically significant increase in activity from the small 2-D patterns to the small 3-D microwells ($p < 0.05$). The difference in metabolic activity between cells on big (> 500 μm^2) 2-D patterns and within big 3-D microwells was even more pronounced ($p < 0.001$). In general, we conclude that the metabolic activity of a cell was affected by the dimensionality of a cell and was increased in a 3-D environment.
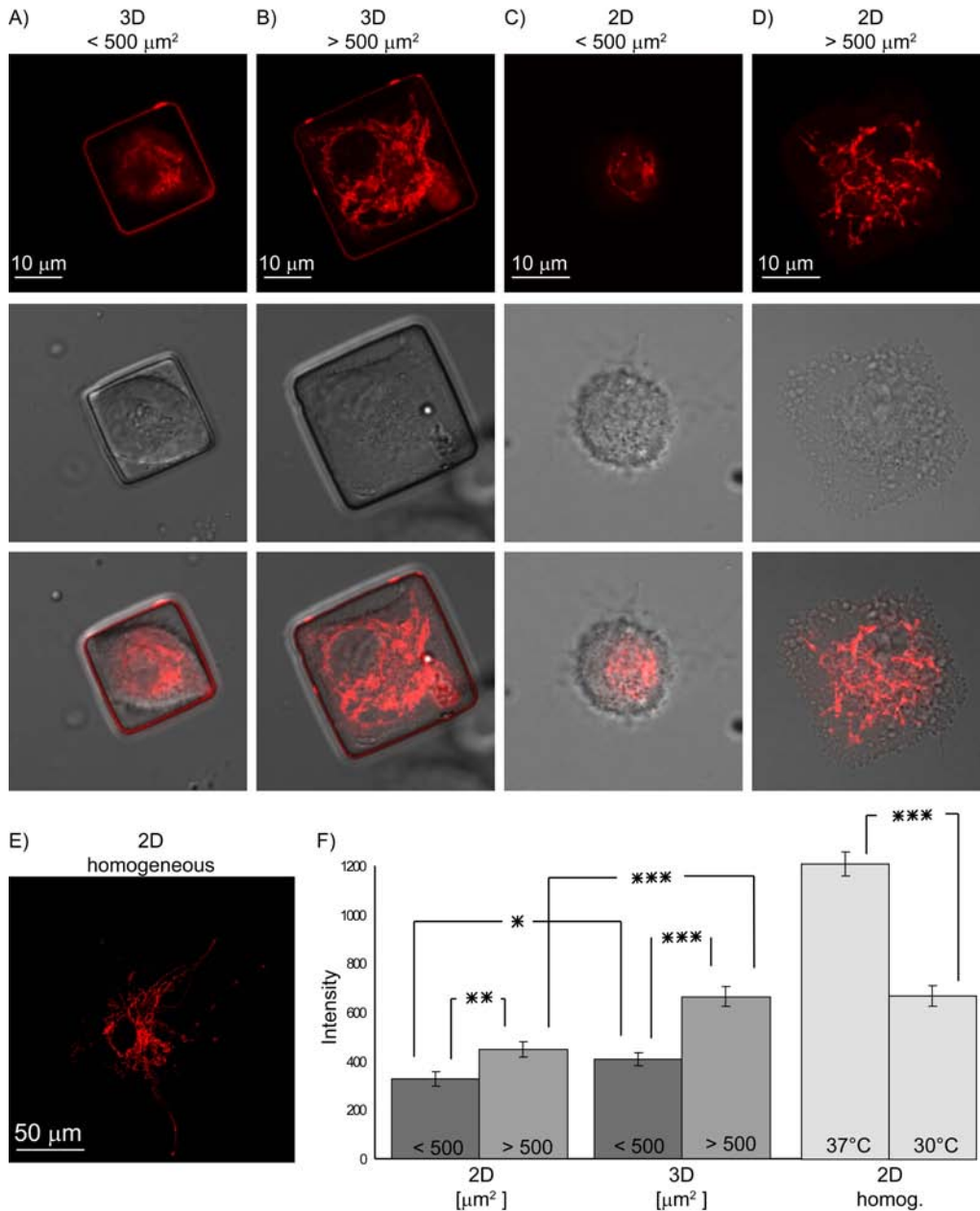
Figure 7.7: *The dependence of cell metabolism on dimensionality and spreading area.* To investigate the influence of spreading area and dimensionality on cell metabolism, cells were cultured A) inside small 3-D microwells (spreading area < 500 μm^2), B) big microwells (> 500 μm^2) and C) on small and D) big 2-D patterns and stained for mitochondrial membrane potential (TMRE). E) As a reference, cells were cultured on homogeneously coated surfaces at 30°C and 37°C. F) The quantification of the fluorescent signals shows the difference in metabolic activity depending on dimensionality and spreading area. Average fluorescent intensity and the standard error of the mean are plotted (* < 0.05, ** < 0.01, *** < 0.001).

7.4   Conclusion and outlook

Most cells *in vivo* have a 3-D arrangement of contacts with their surroundings. In this study, we sought to determine whether a 3-D arrangement of cell contacts with extracellular matrix can direct actin cytoskeleton assembly using a novel single cell culture system that permits independent control of cell shape, substrate rigidity, and dimensionality of contacts. Actin cytoskeleton assembly was studied due to its pervasive demonstration as an important coupling mechanism between external stimuli, such as cell shape or substrate rigidity, with downstream cellular responses, such as differentiation [170, 175]. The actin skeleton was visualized using fluorescently labeled phalloidin. It has been reported that phalloidin is unable to bind to monomeric G-actin, and hence fluorescence is only seen where active filaments are present [214]. The visualization of actin filaments with high-resolution microscopy and the same parameter settings for the different conditions allow for a qualitative comparison between the different environmental stimuli and the cell's response in actin filament assembly. This study showed that matrix dimensionality, matrix rigidity, and cell shape are not orthogonal stimuli which regulate actin cytoskeleton assembly, but rather that fibroblast cells integrate all three stimuli. Thus, cell behavior appears to be intimately co-regulated by dimensionality, stiffness, and cell shape. These data hint at the complexity of cell sensory machinery and support recent observations that experiments using 2-D cell culture platforms may not accurately predict the behavior of cells in their native, 3-D context [92]

3-D overcame shape-dependent inhibition of cytoskeleton assembly
The extracellular matrix plays an essential role in regulating cell behavior. For example, the control of cell shape on 2-D patterned surfaces regulates cell cycle progression and the commitment of stem cells to different lineages through control of endogenous RhoA activity and cytoskeletal tension [139, 290]. It is also well established that cell shape on 2-D patterns regulates cytoskeletal structure [290] and thereby cell contractility [187], since the actin cytoskeleton is a force-bearing network that is necessary for application of cell contractile forces to the extracellular matrix. Since studies that analyzed cell functions in response to cell shapes or extents of cell spreading that were controlled with engineered cell culture environments have, to the best of our knowledge, been performed exclusively on 2-D patterns, we sought to determine whether 3-D adhesion regulates cell shape-dependent control of actin cytoskeleton assembly.

In this study, we demonstrated that dimensionality fundamentally regulates cell shape-dependent control of actin filament assembly and organization. The actin cytoskeleton, visualized using phalloidin staining, varies tremendously between cells on 2-D compared to a 3-D patterned surface, even though the images of 2-D and 3-D were taken with identical microscopy settings. If a cell is limited in its spreading area on a 2-D platform, it is hindered to assemble an actin filament network, as has been described elsewhere [290]. However if the same projected area is presented in a 3-D environment, the cell assembles an actin network that was also distinct from the actin cytoskeleton assembled by well-spread cells in 2-D. Actin filaments appear as an entangled network with little or no straight stress fibers visible. Even if the total adhesive surface of the floor and walls was taken into account (500 μm^2 total surface area for the small microwells), these cells would still not assemble visible actin structures on a 2-D surface of the same projected area, which corresponds to a square pattern of 22 μm side length. The formation of an actin network demonstrates that the cell may be capable of generating contractile forces [187, 291]. However, the Fn rearrangement study suggested that cell contractile forces were not applied, at least in a vector parallel to the walls or floor of the microwell, since matrix rearrangement of Fn that was adsorbed to the PDMS walls of the microwell was rarely seen. Even though the walls were not considered in this study due to the difficulty of quantifying fibronectin fluorescence in vertical planes via confocal microscopy, it appears qualitatively that the Fn on the walls was also not rearranged. Thus, these data may suggest that cell behavior on 2-D patterned surfaces with limited cell spreading may not be recapitulated in 3-D environments which limit cell spreading. However, cell contractility-dependent control of shape-dependent stem cell differentiation and cell proliferation necessitates future studies to determine if cells in 3-D microenvironments with limited cell spreading are contractile.

3-D alters rigidity dependent control of actin cytoskeleton assembly

The stiffness of the extracellular matrix also fundamentally impacts on cell behavior in both 2-D and 3-D. Substrate stiffness has been shown to regulate actin cytoskeleton assembly in both 3-D gels and on 2-D substrates [175, 292], but no study has studied cell shape, dimensionality, and substrate stiffness independently. Therefore, the microwell platform was used with different stiffnesses of PDMS in order to determine if stiffness fundamentally altered the 3-D dependent assembly of actin structures in confined cells. In order to inhibit actin cytoskeleton assembly in 2-D, cells must be cultured on very soft substrates, such as polyacrylamide gels, that reach stiffness values (approx. 6 Pa) that

are less than those that can be achieved with PDMS [175]. It has been shown that actin stress fiber formation and cell spreading are absent for many cell types on soft substrates, although this behavior is cell type specific [169, 293]. However, for the 3-D case, the stiffness below which cells do not assemble actin structures that are stained with phalloidin is much higher, and hence PDMS was a sufficient substrate material for this study. The soft PDMS (20 kPa), which is still relatively stiff by fibroblast standards, did allow for actin filament assembly on flat, 2-D surfaces but not in 3-D. Since the numerous studies on the sensitivity of cells to substrate rigidity also demonstrated that this mechanism was mediated via cell contractility, an altered actin organization, or inhibition of actin filament assembly, may also influence the cell behavior in response to extracellular matrix stiffness. The metabolism of cells in 3-D microwells was also increased compared to cells with the same substrate stiffness and extent of cell spreading on 2-D surfaces, suggesting that altered cytoskeleton assembly may hint at a broader responsiveness of cells to 3-D adhesion. Therefore, we conclude that 3-D adhesion fundamentally influences the cell's ability to probe other physical properties of the cell microenvironment such as stiffness.

In conclusion, the importance of understanding the intimate relationship between local microenvironmental properties and cell function has recently been illustrated with a number of key studies. For example, matrix stiffness has been proposed to regulate the malignant phenotype of cancer cells [166], the geometric arrangement of cell contacts was shown to alter the response of skin cells to cytotoxic agents [128], and the susceptibility of cells to non-viral gene delivery depends upon the stiffness of 2-D culture substrates [294]. A thorough understanding of the cell sensory toolbox might allow the development of engineered tissues or the maintenance of cell phenotypes, such as hepatocytes, that are important in drug toxicity screening. The data presented here confirm previous studies that 3-D contact is part of this toolbox, but specifically this data indicates that these stimuli are integrated by the cell and do not function independently. The different microenvironmental properties, such as rigidity, cell shape, and geometric arrangement of cell contact, are not orthogonal to one another. These parameters should be varied independently if we are to fully map the cell sensory toolbox, and we speculate that cell responsiveness to other stimuli, for example soluble signaling molecules or gradients in physical properties such as concentration or stiffness, may also be altered in 3-D versus 2-D environments. Future studies should consider that 2-D *in vitro* models may not accurately predict 3-D cell behavior.

7.5 Appendix: Libraries of cells inside microwells

This section provides libraries of different single cells inside microwells because quantification of actin filaments inside microwells was not possible. We show consistently images of the bottom plane of the well.
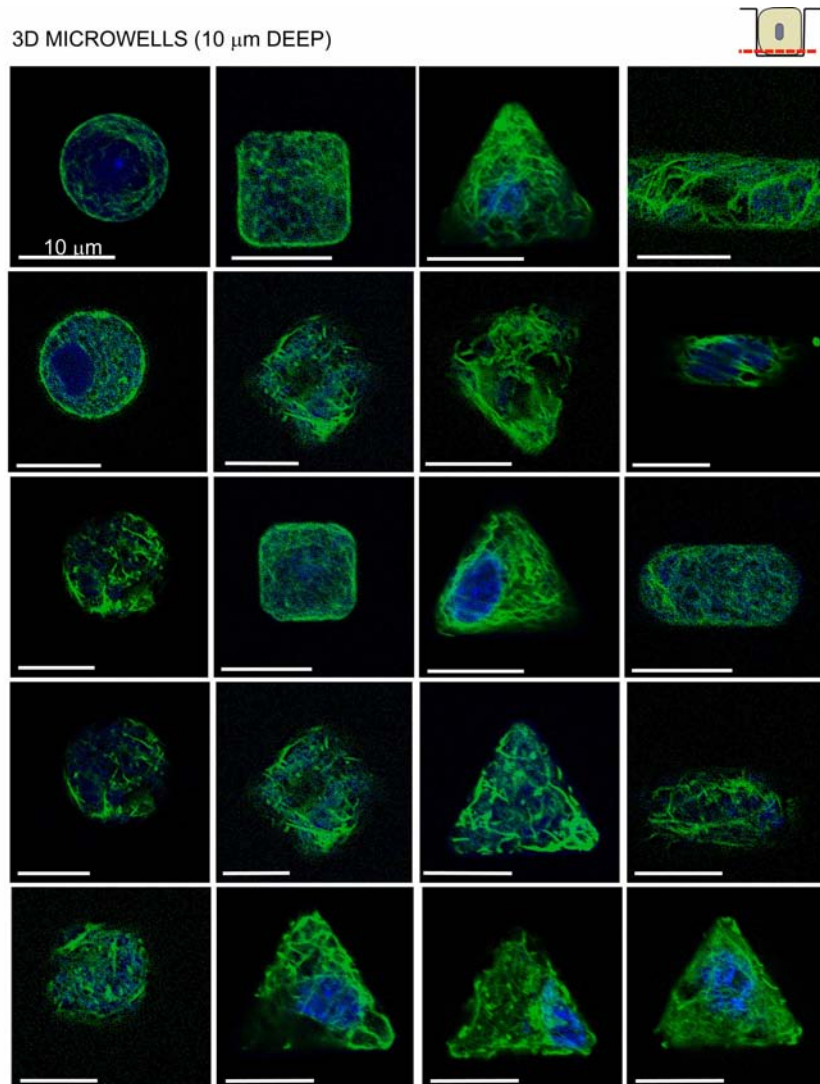
Figure 7.8: *Library of different microwell shapes and actin formation in 10 μm deep, hard wells.* Actin filament assembly was visualized using phalloidin Alexa 488, the nucleus with ethidium-homodimer. It shows the reproducibility of the actin formation inside small, 10 μm deep microwells. This figure provides a library of different cells inside microwells (circles, squares, triangles, rectangles).
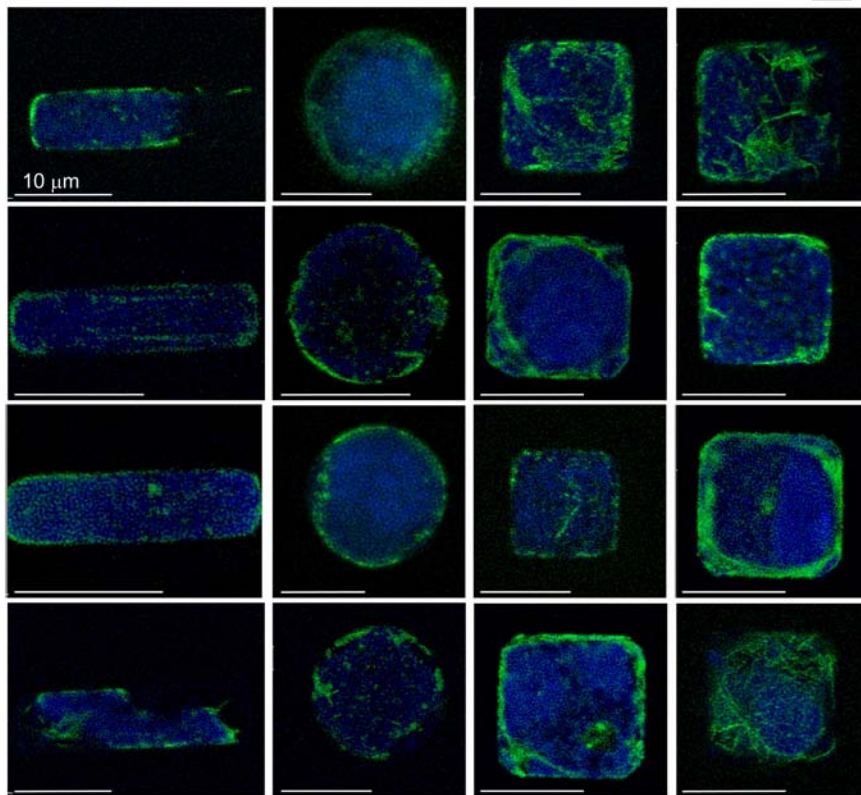
Figure 7.9: *Library of actin skeleton of cells inside shallow microwells (5 μm).* Actin filament assembly was visualized using phalloidin Alexa 488, the nucleus with ethidium-homodimer. It shows the actin formation inside small, 5 μm deep microwells. This figure provides a library of different cells inside microwells (rectangles, circles, squares).
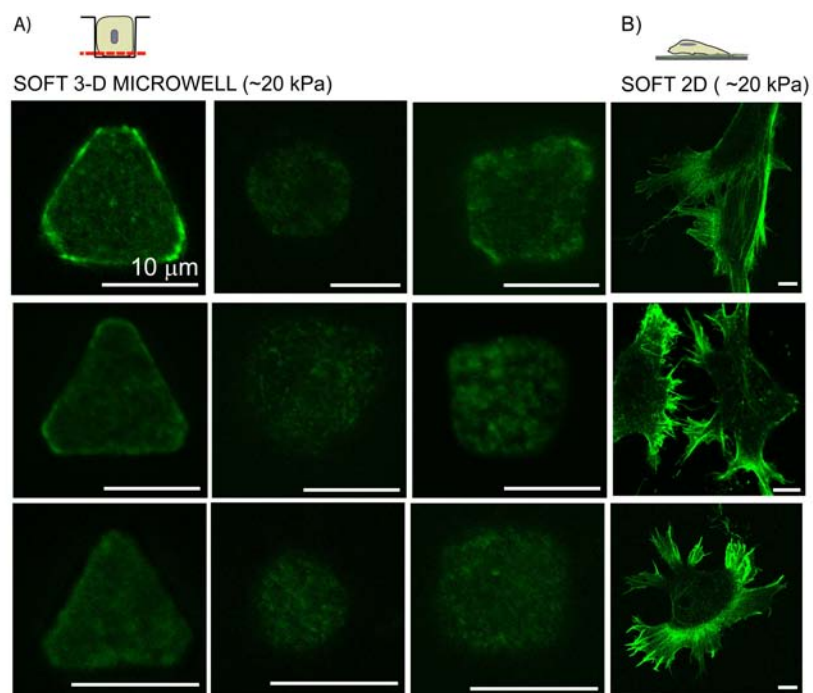
Figure 7.10: *Library of actin skeleton of cells inside 10 µm deep, soft microwells (20 kPa).* Actin filament assembly was visualized using phalloidin Alexa 488. It shows the reproducibility of the A) hindrance of actin filament assembly inside soft, 10 µm deep (20 kPa) microwells. This figure provides a library of different cells inside microwells (circles, squares, triangles). B) Cells on a flat 2-D substrate of the same stiffness show clear actin filament formation.
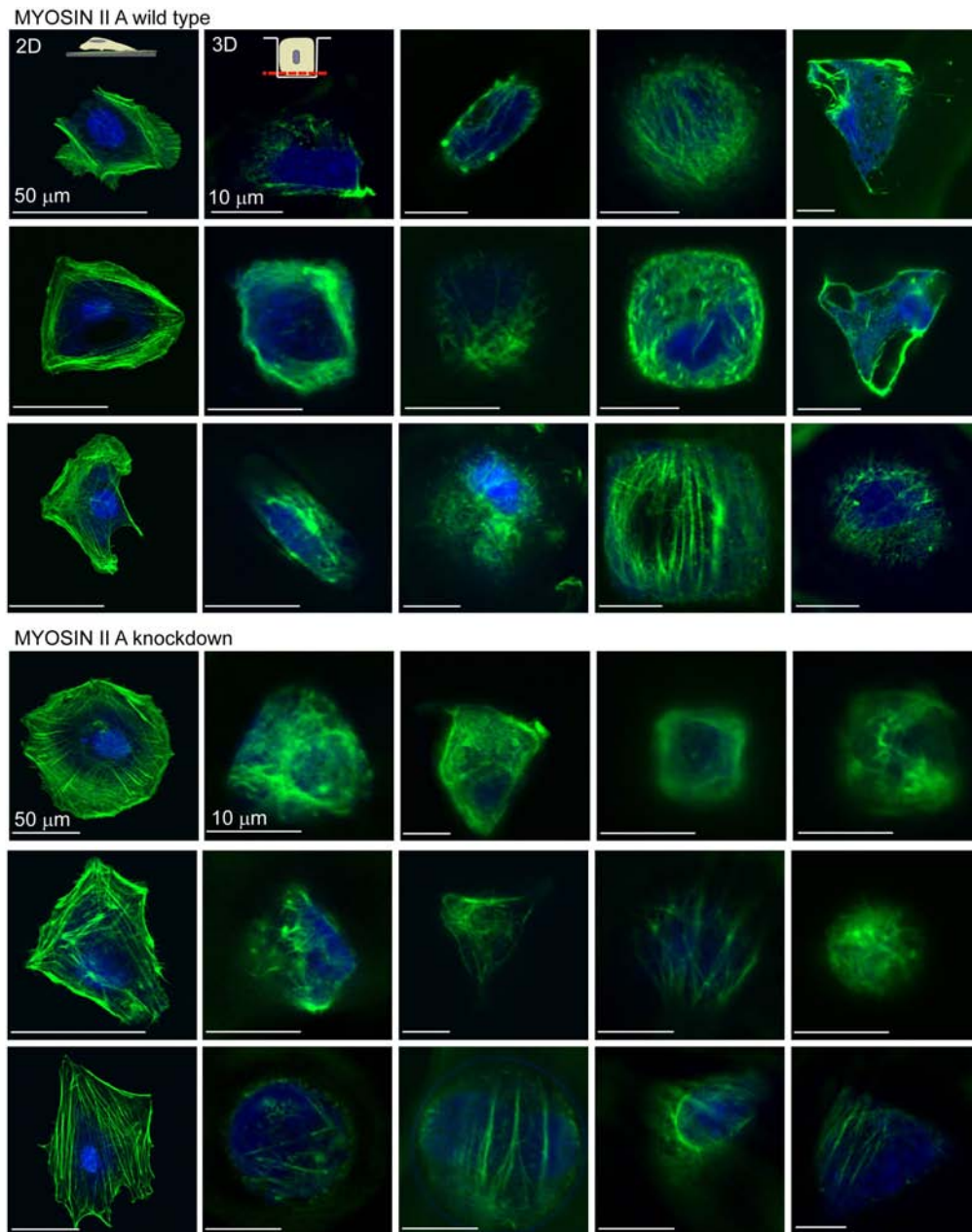
Figure 7.11: *Library of actin skeleton of myosin IIA knockdown cells and wild types on 2-D control surfaces and inside 10 μm deep microwells.* Actin bundling was visualized using phalloidin Alexa 488, the nucleus with ethidium-homodimer. Myosin IIA knockdown cells show the reproducibility of the actin formation inside small, 10 μm deep microwells, this figure provides a library of different cells inside microwells (circles, squares, triangles, rectangles).
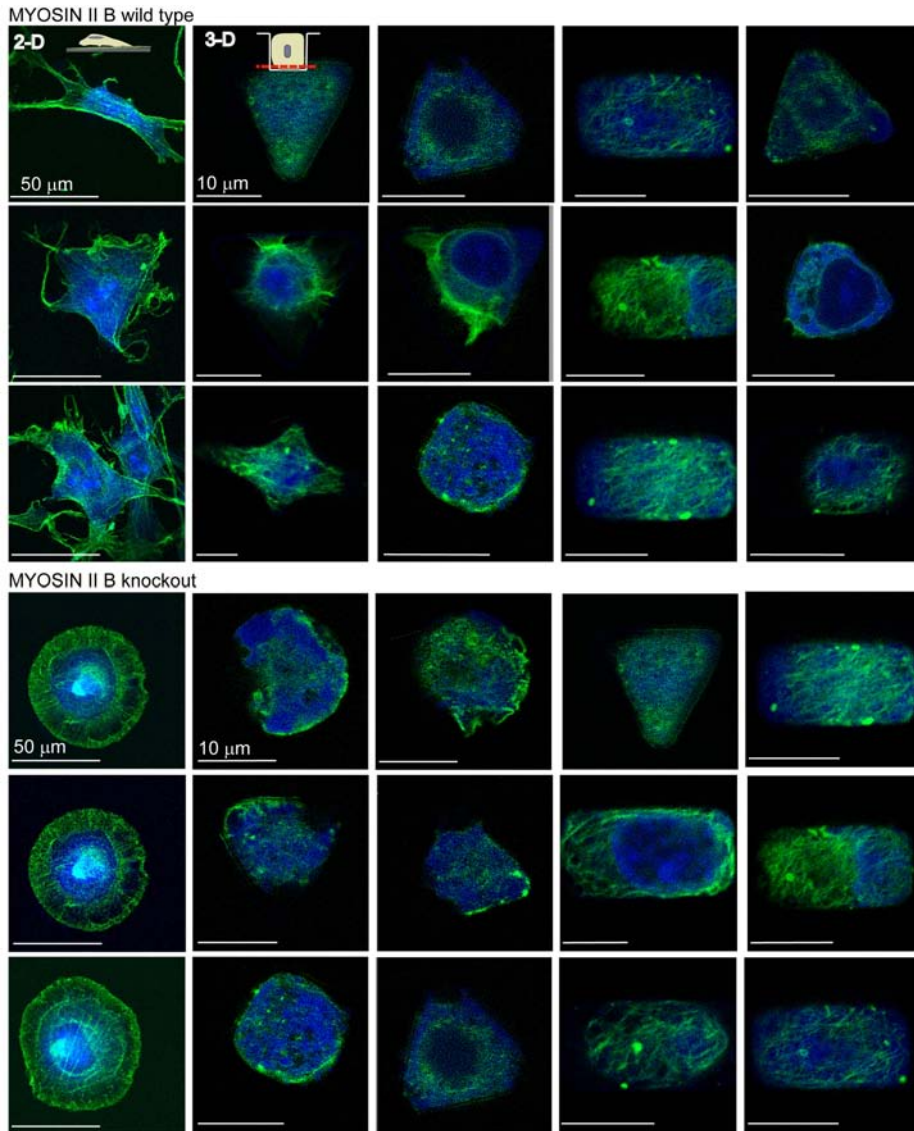
Figure 7.12: *Library of actin skeleton of myosin IIB knockout cells and the wild type on 2-D control surfaces and inside 10 μm deep microwells.* Actin bundling was visualized using phalloidin Alexa 488, the nucleus with ethidium-homodimer. Myosin IIB knockout cells show the reproducibility of the actin formation inside small, 10 μm deep microwells, this figure provides a library of different cells on 2-D substrates and inside microwells (circles, squares, triangles, rectangles).

Conclusions and outlook

8.1   Conclusions

The overall goal of this thesis was to establish a novel culture substrate which allowed the investigation of different parameters of a cell's microenvironment, such as stiffness and spreading area, independently, in 3-D and on the level of single isolated cells. The platform has already been developed by M. Dusseiller, M. Smith, V. Vogel and M. Textor and was further developed in this thesis towards a more complex biochemical microenvironment. Furthermore, the interaction between different properties of the microenvironment on cell behavior was investigated to reveal insights into the question as to the effect of dimensionality on the cell's response to external stimuli.

8.1.1   Microwell platform fabrication and development

The method for culturing single cells inside a well controlled 3-D microenvironment was developed by Dusseiller *et al.* [200]. Briefly, the microwell structure was produced by standard photolithography and transferred into PDMS. The chemical modification of the surface provided a cell adhesive environment inside the microwell and a passivated plateau, which was resistant against protein adsorption and cell adhesion. Hence, cells only adhere inside the microwells.

In this thesis, the platform was further developed to provide different adhesive environments within the wells, namely a mobile coating via functionalized SPB in one case and a variation in the coating of the wall and bottom of the microwell in another.

Mobile and immobile E-cadherin coating inside microwells

One of the aims was to engineer a single cell microenvironment that should more closely mimic cell-cell contacts *in vivo*. Therefore microwells were coated with E-cad/Fc functionalized supported phospholipid bilayers (SPBs). Characterization of biotinylated SPBs with QCM-D demonstrated an SPB was successfully formed on oxidized PDMS, and it was possible to further functionalize the SPB with E-cad/Fc via a biotin-streptavidin (SA) linkage. Studies with FRAP demonstrated the retained mobility of both the lipids and SA on PDMS. Furthermore, through the usage of a lipid with a T_M of 35 °C the PDMS was functionalized with an SPB that could be switched between laterally mobile and immobile lipids within a physiologically relevant temperature range, as analyzed by QCM-D and FRAP. Preliminary cell studies demonstrated that cells can adhere specifically to E-cad/Fc functionalized SPBs and conversely unspecific binding is limited. The difference in actin staining of a cell on a mobile versus immobile platform is a demonstrative example of how ligand mobility influences cell behavior.

Furthermore, this mobile system was combined with the 3-D microwell structure. It was shown that the lipids diffused from the wall to the bottom and *vice versa*, presenting a mobile system in a 3-D environment. Furthermore, the coating of microwells with E-cad/Fc functionalized SPBs and the combination with cell culture resulted in an array of single cells within the microwells. Hence, they interacted with the E-cad/Fc and did not adhere to the passivated plateau.

Heterogeneous wall-bottom coating

To present a heterogeneous arrangement of cell adhesive environments, feasibility studies were performed to modify the microwell with contrasting wall versus bottom coatings. The line-of-sight vapor deposition of Ti led to a chemical contrast of Ti on the plateau and on the bottom of the well while the side walls still presented PDMS. After plasma treatment, this chemical contrast was oxidized to form a SiO_2 and TiO_2 contrast. After PLL-*g*-PEG passivation of the plateau, the substrate was exposed to a vesicle solution. The vesicles ruptured selectively on the SiO_2 surface to form an SPB. The additional exposure to Fn in combination with the protein-resistant characteristics of the SPB led to a selective Fn coating on the TiO_2-coated well bottom. Therefore the microwell was successfully functionalized with a contrasting SPB/Fn wall/bottom coating.

8.1.2 Dimensionality altered cell viability, actin fibril assembly and mechanosensation

It was demonstrated that the microwell platform consisting of thin PDMS film substrates was compatible with conventional culturing assays, staining and high-resolution microscopy-based characterization tools used in cell biology. Furthermore, cells were shown to survive up to 7 days inside the microwells. A particularly striking observation was that $90 \pm 2\%$ of cells survived culture inside small microwells (spreading area between 100 and 200 μm^2) demonstrating that dimensionality enabled the cell to overcome cell death caused by limited spreading area. This was in stark contrast to cells which were limited in spreading area on 2-D patterns where only $36 \pm 15\%$ of the cells survived on patterns with a spreading area of 400 or 625 μm^2.

In this work, dimensionality was also shown to fundamentally regulate cell shape-dependent control of actin filament assembly and organization. The actin cytoskeleton varied tremendously between cells on 2-D compared to a 3-D patterned surface. If a cell was limited in its spreading area on a 2-D platform, it's ability to assemble an actin filament network was hindered. However, if the same projected area was presented in a 3-D environment, the cells assembled an actin network that was distinct from the actin cytoskeleton assembled by well-spread cells in 2-D. Actin filaments appeared to form an entangled network with little or no straight stress fibers visible. Even if the total adhesive surface of the floor and walls was taken into account (500 μm^2 total surface area for the small microwells), the area was still less than the minimum spreading required in 2-D for the cell to form visible actin structures.

Furthermore, stiffness of the substrate altered the 3-D dependent assembly of actin structures in cells confined within the microwells. Therefore, the microwell structure was used with PDMS of two different stiffnesses (Young's modulus of 20 kPa and 1 MPa). The cells cultured on soft PDMS formed actin filaments on flat, 2-D surfaces but not in 3-D. Numerous studies investigating the sensitivity of cells to substrate rigidity have demonstrated that this mechanism is mediated by cell contractility. Therefore an altered actin organization, or inhibition of actin filament assembly, may also influence the cell behavior in response to extracellular matrix stiffness. The metabolism of cells in 3-D microwells was also increased compared to cells with the same substrate stiffness and same extent of cell spreading on 2-D surfaces, suggesting that altered cytoskeleton assembly may hint at a broader responsiveness of cells to 3-D adhesion. Therefore, we conclude that 3-D

adhesion fundamentally influences the cell's ability to probe other physical properties of the cell microenvironment, such as stiffness.

8.2   Outlook

Since every chapter ended with a short outlook for the individual projects discussed, this outlook centers on possible future applications of the microwell platform. One example, the aspect of cell division inside microwells, is discussed in the next section. For more detailed information an internal report is available.

One possible application for the microwell substrate is the study of stem cell differentiation, as differentiation has been shown to be influenced by external stimuli, such as substrate stiffness and spreading area. Additionally, the microwell structure might be used to investigate the influence of dimensionality on stem cell behavior (running project at EMPA St.Gallen by Markus Rottmar and Katharina Maniura). Cell survival in microwells for at least 7 days is essential to study stem cell differentiation, which has been achieved; however, longer culture time may be needed requiring further optimization, particular in regard to stable passivation of plateaus.

Based on the array of wells, and therefore cells, another possible direction for the microwell substrate would be its development into a high-throughput technique. This might be useful to test new drugs or possible toxic effects of chemicals on cells, as it has been reported that 3-D systems trigger a more *in vivo* like cell response when compared to 2-D model systems [92] (running project at ETHZ by Maria Håkanson and Marcus Textor).

Cell division inside microwells

An interesting aspect to investigate is whether cells inside microwells enter a quiescent state due to contact with the environment and small spreading area, as it is observed with confluent cells, or if cells are still able to divide. Preliminary studies were therefore performed to investigative the ability of the cells to divide in the microwell. Fig 8.1 shows cells in a circular and triangular well. Interestingly, the cells were still able to divide inside these microwells. It was clearly visible that the cell built up a mitotic spindle and divided afterwards (fig 8.1 A). Once the cell had divided there were two possible arrangements of the daughter cells, either both could remain within the confines of the microwell, or one
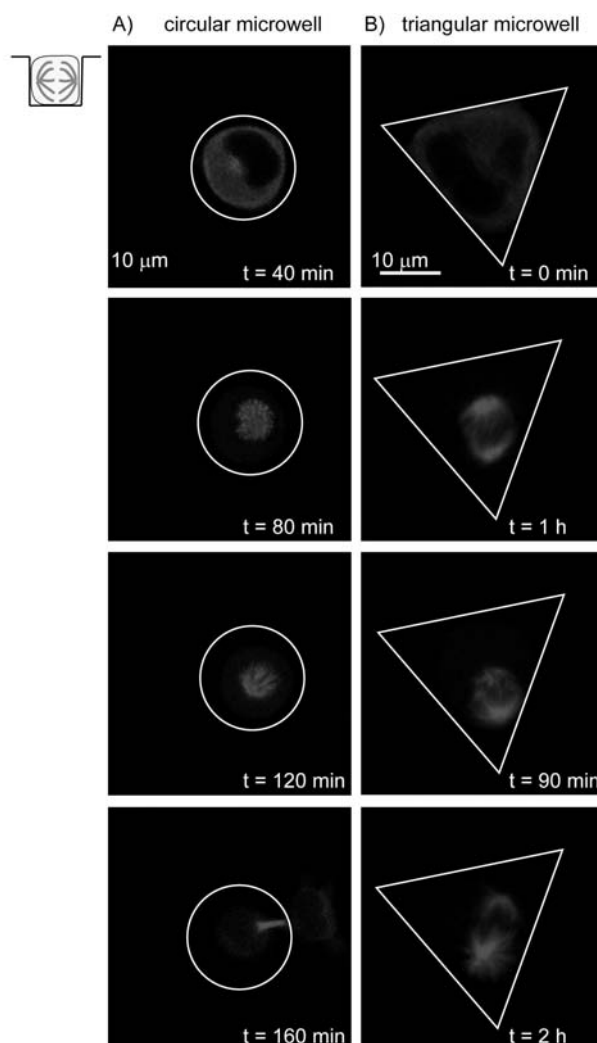
Figure 8.1: *Cell division inside a microwell.* HeLa cells (cherry labeled tubulin) were able to divide inside microwells. A) A cell inside a circular well with 22 μm diameter divided. B) Also in triangular wells with a side length of 30 μm the cell was still able to divide. The orientation of the spindle axis within the cells could be observed using real time fluorescent microscopy. However, in these images the formation of the daughter cells is not shown as the time lapse ended before cell division was complete.

could remain and the other migrate out of the microwell. In these initial experiments both outcomes were observed.

Once the ability of the cells to divide in the microwell was determined, we were interested to explore whether the well shape influenced the orientation of the cell division axis. Cells on 2-D patterns divided as previously described in the literature (fig 8.2 A) [137] with the mitotic spindle orienting parallel to the long axis of the pattern. Experiments in the 3-D microwells of the same shapes showed the same trend as cells on 2-D patterns
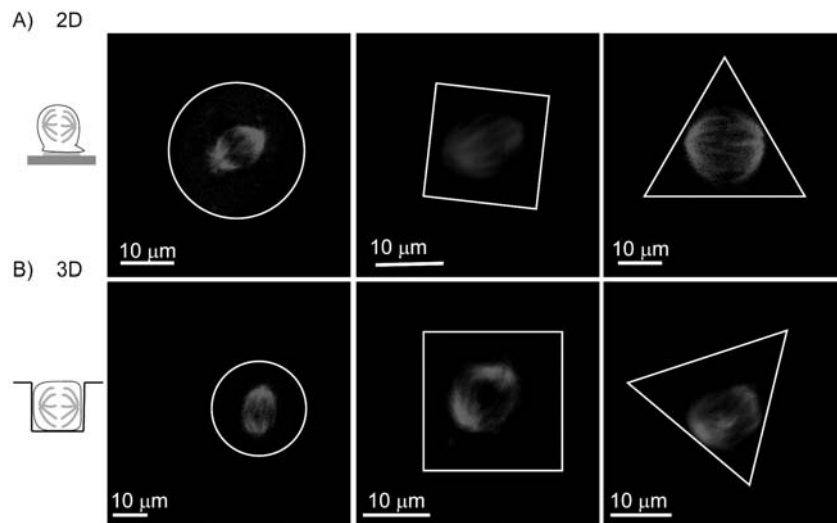
Figure 8.2: *Cell division axis is dependent on pattern shape.* HeLa cells divided depending on the shape of the pattern. A) The mitotic spindle orientation on 2-D pattern was similar to cells inside B) microwells with the same shape. Circular patterns had no favorite division axis due to symmetric reasons. In a square shaped well, the cell normally divided along the diagonal axis of the well. Cells cultured within triangular shaped wells favored the division along the longest axis from one corner to the side of the other side.

(fig 8.2 B). Inside circular wells, the mitotic spindle was observed and due to its symmetry there was no favorite axis of spindle orientation. When cells were cultured in square shaped wells we saw that the cell built up the mitotic spindle so that it was parallel to the diagonal axis, the longest axis of the pattern. In a triangular well, the mitotic spindle was often oriented along the axis from one corner to the middle of the other side.

These preliminary results indicate that the microwell culture substrate might be used to study the influence of geometry and dimensionality on the division of cells. Processes, such as wound healing and embryogenesis, are considered to be largely driven by the local influences on cell proliferation, which are determined by cell shape. Therefore, this platform might help to investigate how structuring processes within tissue are influenced by external cues and how they determine the future shape of the tissue.

Potential and limitations

It has been shown that the microwell structure is useful to investigate the interplay between different environmental properties, such as stiffness, (bio)chemical cues and dimensionality. However, it needs to be taken into consideration that such an engineered platform is never able to simulate closely the environment of a cell *in vivo*. For example, stiffness limitations of the PDMS can be bypassed by changing the microwell material

and working with, for example, a hydrogel platform. But to what extent the microwells structure can be reliably transferred into very soft material is arguable.

The bigger challenge is the exact mimic of the biochemical environment of a cell and it is likely that engineered systems are always constrained by the reduced and simplified presentations of biochemical ligands. For example, the cell-cell contact mimic via cadherin-functionalized SPB coupled only the extracellular part of the cadherin to the SPB, and was therefore isolated from the intercellular machinery present in neighboring cells of tissues. This might result in a triggering of different cell responses compared to a cell *in vivo* or no response as the down stream signalling can not be activated. Therefore, it is unlikely the platform will ever fully mimic the full complexity of a cell-cell contact.

Furthermore, the microwell platform cannot be modified by the cell itself and should not be confused with approaches presenting tissue engineering scaffolds to the cells. The cell inside the microwell is always isolated as a single cell and therefore direct stimuli from neighboring cells are completely absent which might trigger different cell responses when compared to cells in a tissue. Larger microwells with multiple cells inside the well might be needed to achieve more significant comparisons to cells *in vivo*. Nevertheless, the microwell substrate is a useful platform to study biophysical fundamentals because the individual microenvironmental parameters can be independently controlled and their impact on cell behavior studied, as well as their potential use as a microarray format for high-thoughput cell-based assays.

References

[1] Alberts, B., Johnson, A., Lewis, J., Raff, M., Roberts, K. and Walter, P. *Molecular Biology of the cell*. Garland Science, 4th edition edition, 2002.

[2] Chardin, P., Boquet, P., Madaule, P., Popoff, M. R., Rubin, E. J. and Gill, D. M. The Mammalian G-Protein Rhoc Is Adp-Ribosylated by Clostridium-Botulinum Exoenzyme C-3 and Affects Actin Microfilaments in Vero Cells. *EMBO J.*, **8**(4), 1087–1092, 1989.

[3] Giry, M., Popoff, M. R., Voneichelstreiber, C. and Boquet, P. Transient Expression of Rhoa, Rhob, and Rhoc Gtpases in Hela-Cells Potentiates Resistance to Clostridium-Difficile Toxin-a and Toxin-B but Not to Clostridium-Sordellii Lethal Toxin. *Infect. Immun.*, **63**(10), 4063–4071, 1995.

[4] Paterson, H. F., Self, A. J., Garrett, M. D., Just, I., Aktories, K. and Hall, A. Microinjection of Recombinant-P21rho Induces Rapid Changes in Cell Morphology. *J. Cell Biol.*, **111**(3), 1001–1007, 1990.

[5] Ishizaki, T., Maekawa, M., Fujisawa, K., Okawa, K., Iwamatsu, A., Fujita, A., Watanabe, N., Saito, Y., Kakizuka, A., Morii, N. and Narumiya, S. The small GTP-binding protein Rho binds to and activates a 160 kDa Ser/Thr protein kinase homologous to myotonic dystrophy kinase. *EMBO J.*, **15**(8), 1885–1893, 1996.

[6] Leung, T., Manser, E., Tan, L. and Lim, L. A Novel Serine/Threonine Kinase Binding the Ras-Related Rhoa Gtpase Which Translocates the Kinase to Peripheral Membranes. *J. Biol. Chem.*, **270**(49), 29051–29054, 1995.

[7] Katoh, K., Kano, Y., Amano, M., Onishi, H., Kaibuchi, K. and Fujiwara, K. Rho-kinase-mediated contraction of isolated stress fibers. *J. Cell Biol.*, **153**(3), 569–583, 2001.

[8] Bhadriraju, K., Yang, M., Alom Ruiz, S., Pirone, D., Tan, J. and Chen, C. S. Activation of ROCK by RhoA is regulated by cell adhesion, shape, and cytoskeletal tension. *Exp. Cell Res.*, **313**(16), 3616–3623, 2007.

[9] Pfeffer, W. *Physiology of plants*. 1881.

[10] Overton, E. Uber die osmotischen Eigenschaften der lebenden Pflanzen und Tierzelle. *Vjsch. Naturf. Ges. Zurich*, **.**, 159–201, 1895.

[11] Heimburg, T. Coupling of chain melting and bilayer structure: domains, rafts, elasticity and fusion. *Planar Lipid Bilayers (Blms) and Their Applications*, **7**, 269–293, 2003.

[12] Singer, S. J. and Nicolson, G. L. The Fluid Mosaic Model of the Structure of Cell Membranes. *Science*, **175**(4023), 720–731, 1972.

[13] Ritchie, K. and Spector, J. Single molecule studies of molecular diffusion in cellular membranes: Determining membrane structure. *Biopolymers*, **87**, 95–101, 2007.

[14] Gennis, R. B. *Biomembranes: Molecular Structure and Function*. Springer Verlag, 1989.

[15] Tanaka, M. and Sackmann, E. Supported membranes as biofunctional interfaces and smart biosensor platforms. *Physica Status Solidi a-Applications and Materials Science*, **203**(14), 3452–3462, 2006.

[16] Groves, J. T. and Dustin, M. L. Supported planar bilayers in studies on immune cell adhesion and communication. *J. Immunol. Methods*, **278**(1-2), 19–32, 2003.

[17] Thid, D., Holm, K., Eriksson, P. S., Ekeroth, J., Kasemo, B. and Gold, J. Supported phospholipid bilayers as a platform for neural progenitor cell culture. *Journal of Biomedical Materials Research Part A*, **84A**(4), 940–953, 2008.

[18] Svedhem, S., Dahlborg, D., Ekeroth, J., Kelly, J., Hook, F. and Gold, J. In Situ Peptide-Modified Supported Lipid Bilayers for Controlled Cell Attachment. *Langmuir*, **19**(17), 6730–6736, 2003.

[19] Perez, T. D., Nelson, W. J., Boxer, S. G. and Kam, L. E-Cadherin Tethered to Micropatterned Supported Lipid Bilayers as a Model for Cell Adhesion. *Langmuir*, **21**(25), 11963–11968, 2005.

[20] Irvine, D. J. and Doh, J. S. Synthetic surfaces as artificial antigen presenting cells in the study of T cell receptor triggering and immunological synapse formation. *Seminars in Immunology*, **19**(4), 245–254, 2007.

[21] Berat, R., Remy-Zolghadry, M., Gounou, C., Manigand, C., Tan, S., Salto, C., Arenas, E., Bordenave, L. and Brisson, A. R. Peptide-presenting two-dimensional protein matrix on supported lipid bilayers: An efficient platform for cell adhesion. *Biointerphases*, **2**(4), 165–172, 2007.

[22] Tamm, L. K. and McConnell, H. M. Supported phospholipid bilayers. *Biophys. J.*, **47**(1), 105–113, 1985.

[23] Keller, C. A. and Kasemo, B. Surface Specific Kinetics of Lipid Vesicle Adsorption Measured with a Quartz Crystal Microbalance. *Biophys. J.*, **75**(3), 1397–1402, 1998.

[24] Richter, R., Mukhopadhyay, A. and Brisson, A. Pathways of lipid vesicle deposition on solid surfaces: A combined QCM-D and AFM study. *Biophys. J.*, **85**(5), 3035–3047, 2003.

[25] Seantier, B., Breffa, C., Felix, O. and Decher, G. In Situ Investigations of the Formation of Mixed Supported Lipid Bilayers Close to the Phase Transition Temperature. *Nano Lett.*, **4**(1), 5–10, 2004.

[26] Reimhult, E., Hook, F. and Kasemo, B. Intact Vesicle Adsorption and Supported Biomembrane Formation from Vesicles in Solution; Influence of Surface Chemistry, Vesicle Size, Temperature, and Osmotic Pressure. *Langmuir*, **19**(5), 1681–1691, 2003.

[27] Keller, C. A., Glasmastar, K., Zhdanov, V. P. and Kasemo, B. Formation of Supported Membranes from Vesicles. *Phys. Rev. Lett.*, **84**(23), 5443, 2000.

[28] Ross, E. E., Bondurant, B., Spratt, T., Conboy, J. C., O'Brien, D. F. and Saavedra, S. S. Formation of self-assembled, air-stable lipid bilayer membranes on solid supports. *Langmuir*, **17**(8), 2305–2307, 2001.

[29] Albertorio, F., Diaz, A. J., Yang, T. L., Chapa, V. A., Kataoka, S., Castellana, E. T. and Cremer, P. S. Fluid and air-stable lipopolymer membranes for biosensor applications. *Langmuir*, **21**(16), 7476–7482, 2005.

[30] Deng, Y., Wang, Y., Holtz, B., Li, J., Traaseth, N., Veglia, G., Stottrup, B. J., Elde, R., Pei, D., Guo, A. and Zhu, X. Y. Fluidic and Air-Stable Supported Lipid Bilayer and Cell-Mimicking Microarrays. *J. Am. Chem. Soc.*, **130**(19), 6267–6271, 2008.

[31] Holden, M. A., Jung, S. Y., Yang, T., Castellana, E. T. and Cremer, P. S. Creating Fluid and Air-Stable Solid Supported Lipid Bilayers. *J. Am. Chem. Soc.*, **126**(21), 6512–6513, 2004.

[32] Benkoski, J. J. and Hook, F. Lateral Mobility of Tethered Vesicle;DNA Assemblies. *The Journal of Physical Chemistry B*, **109**(19), 9773–9779, 2005.

[33] Armstrong, V. T., Brzustowicz, M. R., Wassall, S. R., Jenski, L. J. and Stillwell, W. Rapid flip-flop in polyunsaturated (docosahexaenoate) phospholipid membranes. *Arch. Biochem. Biophys.*, **414**(1), 74–82, 2003.

[34] John, K., Schreiber, S., Kubelt, J., Herrmann, A. and Muller, P. Transbilayer Movement of Phospholipids at the Main Phase Transition of Lipid Membranes: Implications for Rapid Flip-Flop in Biological Membranes. **83**(6), 3315–3323, 2002.

[35] Devaux, P. F. Lipid transmembrane asymmetry and flip-flop in biological membranes and in lipid bilayers : Current Opinion in Structural Biology 1993, 3:489-494. *Current Opinion in Structural Biology*, **3**(4), 489–494, 1993.

[36] Glasmastar, K., Larsson, C., Hook, F. and Kasemo, B. Protein adsorption on supported phospholipid bilayers. *J. Colloid Interface Sci.*, **246**(1), 40–47, 2002.

[37] Andersson, A.-S., Glasmastar, K., Sutherland, D., Lidberg, U. and Kasemo, B. Cell adhesion on supported lipid bilayers. *J. Biomed. Mater. Res.*, **64A**(4), 622–629, 2003.

[38] Kam, L. and Boxer, S. G. Cell adhesion to protein-micropatterned-supported lipid bilayer membranes. *J. Biomed. Mater. Res.*, **55**(4), 487–495, 2001.

[39] Groves, J. T., Mahal, L. K. and Bertozzi, C. R. Control of cell adhesion and growth with micropatterned supported lipid membranes. *Langmuir*, **17**(17), 5129–5133, 2001.

[40] Chapman, D. Biomembranes and New Hemocompatible Materials. *Langmuir*, **9**(1), 39–45, 1993.

[41] Hovis, J. S. and Boxer, S. G. Patterning and composition arrays of supported lipid bilayers by microcontact printing. *Langmuir*, **17**(11), 3400–3405, 2001.

[42] Lenz, P., Ajo-Franklin, C. M. and Boxer, S. G. Patterned Supported Lipid Bilayers and Monolayers on Poly(dimethylsiloxane). *Langmuir*, **20**(25), 11092–11099, 2004.

[43] Margolis, L. B., Dyatlovitskaya, E. V. and Bergelson, L. D. Cell-Lipid Interactions - Cell Attachment to Lipid Substrates. *Exp. Cell Res.*, **111**(2), 454–457, 1978.

[44] Nam, J.-M., Nair, P. M., Neve, R. M., Gray, J. W. and Groves, J. T. A Fluid Membrane-Based Soluble Ligand-Display System for Live-Cell Assays. *ChemBioChem*, **7**(3), 436–440, 2006.

[45] Larsson, C., Rodahl, M. and Hook, F. Characterization of DNA Immobilization and Subsequent Hybridization on a 2D Arrangement of Streptavidin on a Biotin-Modified Lipid Bilayer Supported on SiO2. *Anal. Chem.*, **75**(19), 5080–5087, 2003.

[46] Larsson, C., Bramfeldt, H., Wingren, C., Borrebaeck, C. and Hook, F. Gravimetric antigen detection utilizing antibody-modified lipid bilayers. *Anal. Biochem.*, **345**(1), 72–80, 2005.

[47] Svedhem, S., Pfeiffer, I., Larsson, C., Wingren, C., Borrebaeck, C. and Hook, F. Patterns of DNA-Labeled and scFv-Antibody-Carrying Lipid Vesicles Directed by Material-Specific Immobilization of DNA and Supported Lipid Bilayer Formation on an Au/SiO2 Template. *ChemBioChem*, **4**(4), 339–343, 2003.

[48] Bogdanov jr, A. A., Klibanov, A. L. and Torchilin, V. P. Protein immobilization on the surface of liposomes via carbodiimide activation in the presence of N-hydroxysulfosuccinimide. *FEBS Lett.*, **231**(2), 381–384, 1988.

[49] Chan, P. Y., Lawrence, M. B., Dustin, M. L., Ferguson, L. M., Golan, D. E. and Springer, T. A. Influence of receptor lateral mobility on adhesion strengthening between membranes containing LFA-3 and CD2. *J. Cell Biol.*, **115**(1), 245–255, 1991.

[50] Takai, Y., Reed, M. L., Burakoff, S. J. and Herrmann, S. H. Direct Evidence for a Receptor Ligand Interaction between the T-Cell Surface-Antigen Cd2 and Lymphocyte-Function-Associated Antigen-3. *Proc. Natl. Acad. Sci. U. S. A.*, **84**(19), 6864–6868, 1987.

[51] Hafeman, D. G., Vontscharner, V. and McConnell, H. M. Specific Antibody-Dependent Interactions between Macrophages and Lipid Haptens in Planar Lipid Monolayers. *Proc. Natl. Acad. Sci. U. S. A.*, **78**(7), 4552–4556, 1981.

[52] Mossman, K. D., Campi, G., Groves, J. T. and Dustin, M. L. Altered TCR Signaling from Geometrically Repatterned Immunological Synapses. *Science*, **310**(5751), 1191–1193, 2005.

[53] Stroumpoulis, D., Zhang, H., Rubalcava, L., Gliem, J. and Tirrell, M. Cell Adhesion and Growth to Peptide-Patterned Supported Lipid Membranes. *Langmuir*, **23**(7), 3849–3856, 2007.

[54] Tozeren, A., Sung, K. L., Sung, L. A., Dustin, M. L., Chan, P. Y., Springer, T. A. and Chien, S. Micromanipulation of adhesion of a Jurkat cell to a planar bilayer membrane containing lymphocyte function-associated antigen 3 molecules. *J. Cell Biol.*, **116**(4), 997–1006, 1992.

[55] Thid, D., Bally, M., Holm, K., Chessari, S., Tosatti, S., Textor, M. and Gold, J. Issues of Ligand Accessibility and Mobility in Initial Cell Attachment. *Langmuir*, **23**(23), 11693–11704, 2007.

[56] Garcia, A. S., Dellatore, S. M., Messersmith, P. B. and Miller, W. M. Effects of Supported Lipid Monolayer Fluidity on the Adhesion of Hematopoietic Progenitor Cell Lines to Fibronectin-Derived Peptide Ligands for (alpha)5(beta)1 and (alpha)4(beta)1 Integrins. *Langmuir*, **0**(0).

[57] Ochsenhirt, S. E., Kokkoli, E., McCarthy, J. B. and Tirrell, M. Effect of RGD secondary structure and the synergy site PHSRN on cell adhesion, spreading and specific integrin engagement. *Biomaterials*, **27**(20), 3863–3874, 2006.

[58] Jensen, T. W., Hu, B. H., Delatore, S. M., Garcia, A. S., Messersmith, P. B. and Miller, W. M. Lipopeptides incorporated into supported phospholipid monolayers have high specific activity at low incorporation levels. *J. Am. Chem. Soc.*, **126**(46), 15223–15230, 2004.

[59] Pakalns, T., Haverstick, K. L., Fields, G. B., McCarthy, J. B., Mooradian, D. L. and Tirrell, M. Cellular recognition of synthetic peptide amphiphiles in self-assembled monolayer films. *Biomaterials*, **20**(23-24), 2265–2279, 1999.

[60] Biesalski, M. A., Knaebel, A., Tu, R. and Tirrell, M. Cell adhesion on a polymerized peptide-amphiphile monolayer. *Biomaterials*, **27**(8), 1259–1269, 2006.

[61] Zhu, D.-M., Dustin, M. L., Cairo, C. W. and Golan, D. E. Analysis of Two-Dimensional Dissociation Constant of Laterally Mobile Cell Adhesion Molecules. *Biophys. J.*, **92**(3), 1022–1034, 2007.

[62] Bottaro, D. P., Liebmann-Vinson, A. and Heidaran, M. A. Molecular Signaling in Bioengineered Tissue Microenvironments. *Ann. N. Y. Acad. Sci.*, **961**(REPARATIVE MEDICINE: GROWING TISSUES AND ORGANS), 143–153, 2002.

[63] Blattler, T., Huwiler, C., Ochsner, M., Stadler, B., Solak, H., Voros, J. and Grandin, H. M. Nanopatterns with Biological Functions. *J. Nanosci. Nanotechnol.*, **6**, 2237–2264, 2006.

[64] Whitesides, G. M. W., A. P. The Intersection of Biology and Materials Science. *MRS Bulletin*, **31**, 19–27, 2006.

[65] Tirrell, M., Kokkoli, E. and Biesalski, M. The role of surface science in bioengineered materials. *Surface Science*, **500**(1-3), 61–83, 2002.

[66] Stevens, M. M. and George, J. H. Exploring and engineering the cell surface interface. *Science*, **310**(5751), 1135–1138, 2005.

[67] Harrison, R., G. The reaction of embryonic cells to solid structures. *J. Exp. Zool.*, **17**(4), 521–544, 1914.

[68] Hynes, R. O. Integrins: Versatility, modulation, and signaling in cell adhesion. *Cell*, **69**(1), 11–25, 1992.

[69] Clark, E. A. and Brugge, J. S. Integrins and Signal Transduction Pathways: The Road Taken. *Science*, **268**(5208), 233–239, 1995.

[70] Craig, S. W. and Johnson, R. P. Assembly of focal adhesions: progress, paradigms, and portents. *Curr. Opin. Cell Biol.*, **8**(1), 74–85, 1996.

[71] Delon, I. and Brown, N. H. Integrins and the actin cytoskeleton. *Curr. Opin. Cell Biol.*, **19**(1), 43–50, 2007.

[72] Sastry, S. K. and Burridge, K. Focal Adhesions: A Nexus for Intracellular Signaling and Cytoskeletal Dynamics. *Exp. Cell Res.*, **261**(1), 25–36, 2000.

[73] Geiger, B. and Bershadsky, A. Assembly and mechanosensory function of focal contacts. *Curr. Opin. Cell Biol.*, **13**(5), 584–592, 2001.

[74] Cohen, M., Joester, D., Geiger, B. and Addadi, L. Spatial and Temporal Sequence of Events in Cell Adhesion: From Molecular Recognition to Focal Adhesion Assembly. *ChemBioChem*, **5**(10), 1393–1399, 2004.

[75] Boudreau, N. and Bissell, M. J. Extracellular matrix signaling: integration of form and function in normal and malignant cells. *Curr. Opin. Cell Biol.*, **10**(5), 640–646, 1998.

[76] Geiger, B. and Bershadsky, A. Exploring the Neighborhood: Adhesion-Coupled Cell Mechanosensors. *Cell*, **110**(2), 139–142, 2002.

[77] Bershadsky, A. D., Ballestrem, C., Carramusa, L., Zilberman, Y., Gilquin, B., Khochbin, S., Alexandrova, A. Y., Verkhovsky, A. B., Shemesh, T. and Kozlov, M. M. Assembly and mechanosensory function of focal adhesions: experiments and models. *Eur. J. Cell Biol.*, **85**(3-4), 165–173, 2006.

[78] Ingber, D. E. Mechanosensation through integrins: Cells act locally but think globally. *PNAS*, **100**(4), 1472–1474, 2003.

[79] Chen, C., Tan, J. and Tien, J. Mechanotransduction at cell-matrix and cell-cell contacts. *Annu. Rev. Biomed. Eng.*, **6**, 275–302, 2004.

[80] Li, W. J., Laurencin, C. T., Caterson, E. J., Tuan, R. S. and Ko, F. K. Electrospun nanofibrous structure: A novel scaffold for tissue engineering. *J. Biomed. Mater. Res.*, **60**(4), 613–621, 2002.

[81] Blackwood, K. A., McKean, R., Canton, I., Freeman, C. O., Franklin, K. L., Cole, D., Brook, I., Farthing, P., Rimmer, S., Haycock, J. W., Ryan, A. J. and MacNeil, S. Development of biodegradable electrospun scaffolds for dermal replacement. *Biomaterials*, **29**(21), 3091–3104, 2008.

[82] Zhang, S., Gelain, F. and Zhao, X. Designer self-assembling peptide nanofiber scaffolds for 3D tissue cell cultures. *Semin. Cancer Biol.*, **15**(5), 413–420, 2005.

[83] Tan, W. and Desai, T. A. Microscale multilayer cocultures for biomimetic blood vessels. *J. Biomed. Mater. Res.*, **72A**(2), 146–160, 2005.

[84] Rimmer, S., Johnson, C., Zhao, B., Collier, J., Gilmore, L., Sabnis, S., Wyman, P., Sammon, C., Fullwood, N. J. and MacNeil, S. Epithelialization of hydrogels achieved by amine functionalization and co-culture with stromal cells. *Biomaterials*, **28**(35), 5319–5331, 2007.

[85] Weaver, V. M., Petersen, O. W., Wang, F., Larabell, C. A., Briand, P., Damsky, C. and Bissell, M. J. Reversion of the Malignant Phenotype of Human Breast Cells in Three-Dimensional Culture and In Vivo by Integrin Blocking Antibodies. *J. Cell Biol.*, **137**(1), 231–245, 1997.

[86] Dunn, J. C., Yarmush, M. L., Koebe, H. G. and Tompkins, R. G. Hepatocyte function and extracellular matrix geometry: long-term culture in a sandwich configuration [published erratum appears in FASEB J 1989 May;3(7):1873]. *FASEB J.*, **3**(2), 174–177, 1989.

[87] Cukierman, E., Pankov, R., Stevens, D. R. and Yamada, K. M. Taking Cell-Matrix Adhesions to the Third Dimension. *Science*, **294**(5547), 1708–1712, 2001.

[88] Beningo, K. A., Dembo, M. and Wang, Y.-l. Responses of fibroblasts to anchorage of dorsal extracellular matrix receptors. *Proc. Natl. Acad. Sci.*, **101**(52), 18024–18029, 2004.

[89] Sutherland, R. M. Cell and Environment Interactions in Tumor Microregions - the Multicell Spheroid Model. *Science*, **240**(4849), 177–184, 1988.

[90] Kunz-Schughart, L. A., Freyer, J. P., Hofstaedter, F. and Ebner, R. The Use of 3-D Cultures for High-Throughput Screening: The Multicellular Spheroid Model. *J Biomol Screen*, **9**(4), 273–285, 2004.

[91] Underhill, G. H. and Bhatia, S. N. High-throughput analysis of signals regulating stem cell fate and function. *Current Opinion in Chemical Biology*, **11**(4), 357–366, 2007.

[92] Griffith, L. G. and Swartz, M. A. Capturing complex 3D tissue physiology in vitro. *Nat Rev Mol Cell Biol*, **7**(3), 211–224, 2006.

[93] Di Carlo, D. and Lee, L. P. Dynamic Single-Cell Analysis for Quantitative Biology. *Anal Chem*, **78**(23), 7918–7925, 2006.

[94] Chin, V. L., Taupin, P., Sanga, S., Scheel, J., Gage, F. H. and Bhatia, S. N. Microfabricated platform for studying stem cell fates. *Biotechnol. Bioeng.*, **88**(3), 399–415, 2004.

[95] Rettig, J. R. and Folch, A. Large-Scale Single-Cell Trapping And Imaging Using Microwell Arrays. *Anal. Chem.*, **77**(17), 5628–5634, 2005.

[96] Ostuni, E., Chen, C. S., Ingber, D. E. and Whitesides, G. M. Selective Deposition of Proteins and Cells in Arrays of Microwells. *Langmuir*, **17**(9), 2828–2834, 2001.

[97] Lovchik, R., von Arx, C., Viviani, A. and Delamarche, E. Cellular microarrays for use with capillary-driven microfluidics. *Anal. Bioanal.Chem.*, **390**(3), 801–808, 2008.

[98] Dusseiller, M. R., Schlaepfer, D., Koch, M., Kroschewski, R. and Textor, M. An inverted micro-contact printing method on topographically structured polystyrene chips for arrayed micro-3-D culturing of single cells. *Biomaterials*, **26**(29), 5917–5925, 2005.

[99] Wan, J. H. and Morley, A. A. Cell kinetics of the K-562 cell line in microculture. *Stem Cells*, **3**(2), 106–115, 1985.

[100] Richelson, E. Microwell Assay Method for Biochemical Study of Cultured Cells. *Anal. Biochem.*, **52**(2), 563–573, 1973.

[101] Maroudas, N. G. Agarose Microwell Assay for Cell-Mediated Cytotoxicity. *J. Immunol. Methods*, **10**(4), 389–392, 1976.

[102] Cannon Jr, D. M., Winograd, N. and Ewing, A. G. Quantitative chemical analysis of single cells. *Annu. Rev. Biophys. Biomol. Struct.*, **29**(1), 239–263, 2000.

[103] Sims, C. E. and Allbritton, N. L. Analysis of single mammalian cells on-chip. *Lab Chip*, **7**(4), 423–440, 2007.

[104] Deutsch, M., Deutsch, A., Shirihai, O., Hurevich, I., Afrimzon, E., Shafran, Y. and Zurgil, N. A novel miniature cell retainer for correlative high content analysis of individual untethered non adherent cells. *Lab Chip*, **6**(8), 995–1000, 2006.

[105] Choi, I., Yang, Y. I., Kim, Y. J., Kim, Y., Hahn, J. S., Choi, K. and Yi, J. Directed Positioning of Single Cells in Microwells Fabricated by Scanning Probe Lithography and Wet Etching Methods. *Langmuir*, **24**(6), 2597–2602, 2008.

[106] Nelson, C. M. and Chen, C. S. Cell-cell signaling by direct contact increases cell proliferation via a PI3K-dependent signal. *FEBS Lett.*, **514**(2-3), 238–242, 2002.

[107] Khademhosseini, A., Yeh, J., Jon, S., Eng, G., Suh, K. Y., Burdick, J. A. and Langer, R. Molded polyethylene glycol microstructures for capturing cells within microfluidic devices. *Lab Chip*, **4**, 425–430, 2004.

[108] Revzin, A., Sekine, K., Sin, A., Tompkins, R. G. and Toner, M. Development of a microfabricated cytometry platform for characterization and sorting of individual leukocytes. *Lab Chip*, **5**(1), 30–37, 2005.

[109] Cordey, M., Limacher, M., Kobel, S., Taylor, V. and Lutolf, M. P. Enhancing the Reliability and Throughput of Neurosphere Culture on Hydrogel Microwell Arrays. *Stem Cells*, **26**(10), 2586–2594, 2008.

[110] Mohr, J. C., de Pablo, J. J. and Palecek, S. P. 3-D microwell culture of human embryonic stem cells. *Biomaterials*, **27**(36), 6032–6042, 2006.

[111] Rosenthal, A., Macdonald, A. and Voldman, J. Cell patterning chip for controlling the stem cell microenvironment. *Biomaterials*, **28**(21), 3208–3216, 2007.

[112] Park, S., Bearinger, J. P., Lautenschlager, E. P., Castner, D. G. and Healy, K. E. Surface modification of poly(ethylene terephthalate) angioplasty balloons with a hydrophilic poly(acrylamide-co-ethylene glycol) interpenetrating polymer network coating. *J. Biomed. Mater. Res.*, **53**(5), 568–576, 2000.

[113] Vermette, P. and Meagher, L. Interactions of phospholipid- and poly(ethylene glycol)-modified surfaces with biological systems: relation to physico-chemical properties and mechanisms. *Colloids Surf., B*, **28**(2-3), 153–198, 2003.

[114] Kingshott, P. and Griesser, H. J. Surfaces that resist bioadhesion. *Curr. Opin. Solid. State. Mater. Sci.*, **4**(4), 403–412, 1999.

[115] Dalsin, J. L., Lin, L. J., Tosatti, S., Voros, J., Textor, M. and Messersmith, P. B. Protein resistance of titanium oxide surfaces modified by biologically inspired mPEG-DOPA. *Langmuir*, **21**(2), 640–646, 2005.

[116] Green, R. J., Frazier, R. A., Shakesheff, K. M., Davies, M. C., Roberts, C. J. and Tendler, S. J. B. Surface plasmon resonance analysis of dynamic biological interactions with biomaterials. *Biomaterials*, **21**(18), 1823–1835, 2000.

[117] Amiji, M. and Park, K. Prevention of Protein Adsorption and Platelet-Adhesion on Surfaces by Peo Ppo Peo Triblock Copolymers. *Biomaterials*, **13**(10), 682–692, 1992.

[118] Prime, K. L. and Whitesides, G. M. Self-Assembled Organic Monolayers: Model Systems for Studying Adsorption of Proteins at Surfaces. *Science*, **252**(5009), 1164–1167, 1991.

[119] Ostuni, E., Chapman, R. G., Holmlin, R. E., Takayama, S. and Whitesides, G. M. A survey of structure-property relationships of surfaces that resist the adsorption of protein. *Langmuir*, **17**(18), 5605–5620, 2001.

[120] Bearinger, J. P., Castner, D. G., Golledge, S. L., Rezania, A., Hubchak, S. and Healy, K. E. P(AAm-co-EG) interpenetrating polymer networks grafted to oxide surfaces: Surface characterization, protein adsorption, and cell detachment studies. *Langmuir*, **13**(19), 5175–5183, 1997.

[121] Kenausis, G. L., Voros, J., Elbert, D. L., Huang, N., Hofer, R., Ruiz-Taylor, L., Textor, M., Hubbell, J. A. and Spencer, N. D. Poly(l-lysine)-g-Poly(ethylene glycol) Layers on Metal Oxide Surfaces: Attachment Mechanism and Effects of Polymer Architecture on Resistance to Protein Adsorption. *J. Phys. Chem. B*, **104**(14), 3298–3309, 2000.

[122] Pasche, S., De Paul, S. M., Voros, J., Spencer, N. D. and Textor, M. Poly(L-lysine)-graft-poly(ethylene glycol) assembled monolayers on niobium oxide surfaces: A quantitative study of the influence of polymer interfacial architecture on resistance to protein adsorption by ToF-SIMS and in situ OWLS. *Langmuir*, **19**(22), 9216–9225, 2003.

[123] VandeVondele, S., Voros, J. and Hubbell, J. A. RGD-grafted poly-l-lysine-graft-(polyethylene glycol) copolymers block non-specific protein adsorption while promoting cell adhesion. *Biotechnol Bioeng*, **82**(7), 784–90, 2003.

[124] Falconnet, D., Koenig, A., Assi, F. and Textor, M. A Combined Photolithographic and Molecular-Assembly Approach to Produce Functional Micropatterns for Applications in the Biosciences. *Adv. Funct. Mater.*, **14**(8), 749–756, 2004.

[125] Falconnet, D., Pasqui, D., Park, S., Eckert, R., Schift, H., Gobrecht, J., Barbucci, R. and Textor, M. A Novel Approach to Produce Protein Nanopatterns by Combining Nanoimprint Lithography and Molecular Self-Assembly. *Nano Lett.*, **4**(10), 1909–1914, 2004.

[126] Michel, R., Lussi, J. W., Csucs, G., Reviakine, I., Danuser, G., Ketterer, B., Hubbell, J. A., Textor, M. and Spencer, N. D. Selective Molecular Assembly Patterning: A New Approach to Micro- and Nanochemical Patterning of Surfaces for Biological Applications. *Langmuir*, **18**(8), 3281–3287, 2002.

[127] Lussi, J. W., Falconnet, D., Hubbell, J. A., Textor, M. and Csucs, G. Pattern stability under cell culture conditions–A comparative study of patterning methods based on PLL-g-PEG background passivation. *Biomaterials*, **27**(12), 2534–2541, 2006.

[128] Sun, T., Jackson, S., Haycock, J. W. and MacNeil, S. Culture of skin cells in 3D rather than 2D improves their ability to survive exposure to cytotoxic agents. *J. Biotechnol.*, **122**(3), 372–381, 2006.

[129] Bhadriraju, K. and Chen, C. S. Engineering cellular microenvironments to improve cell-based drug testing. *Drug Discovery Today*, **7**(11), 612–620, 2002.

[130] Cui, Z. F., Xu, X., Trainor, N., Triffitt, J. T., Urban, J. P. G. and Tirlapur, U. K. Application of multiple parallel perfused microbioreactors and three-dimensional stem cell culture for toxicity testing. *Toxicol. in Vitro*, **21**(7), 1318–1324, 2007.

[131] Wittelsberger, S. C., Kleene, K. and Penman, S. Progressive loss of shape-responsive metabolic controls in cells with increasingly transformed phenotype. *Cell*, **24**(3), 859–866, 1981.

[132] MacPherson, I. and Montagnier, L. Agar suspension culture for the selective assay of cells transformed by polyoma virus. *Virology*, **23**(2), 291–294, 1964.

[133] Sanders, F. K. and Burford, B. O. AScites Tumours From BHK.21 Cells Transformed in Vitro by Polyoma Virus. *Nature*, **201**(4921), 786–789, 1964.

[134] Maroudas, N. G., O'Neill, C. H. and Stanton, M. F. Fibroblast anchorage in carcinogenesis by fibres. *The Lancet*, **301**(7807), 807–809, 1973.

[135] Folkman, J. and Moscona, A. Role of cell shape in growth control. *Nature*, **273**(5661), 345–349, 1978.

[136] Chen, C. S., Mrksich, M., Huang, S., Whitesides, G. M. and Ingber, D. E. Geometric control of cell life and death. *Science*, **276**(5317), 1425–1428, 1997.

[137] Thery, M., Racine, V., Pepin, A., Piel, M., Chen, Y., Sibarita, J.-B. and Bornens, M. The extracellular matrix guides the orientation of the cell division axis. *Nat Cell Biol*, **7**(10), 947–953, 2005.

[138] Thery, M. and Bornens, M. Cell shape and cell division. *Curr. Opin. Cell Biol.*, **18**(6), 648–657, 2006.

[139] McBeath, R., Pirone, D. M., Nelson, C. M., Bhadriraju, K. and Chen, C. S. Cell Shape, Cytoskeletal Tension, and RhoA Regulate Stem Cell Lineage Commitment. *Dev. Cell.*, **6**(4), 483–495, 2004.

[140] Ito, Y. Surface micropatterning to regulate cell functions. *Biomaterials*, **20**(23-24), 2333–2342, 1999.

[141] Geissler, M. and Xia, Y. N. Patterning: Principles and some new developments. *Adv. Mater.*, **16**(15), 1249–1269, 2004.

[142] Bernard, A., Delamarche, E., Schmid, H., Michel, B., Bosshard Hans, R. and Biebuyck, H. Printing patterns of proteins. *Langmuir*, **14**(9), 2225–2229, 1998.

[143] Mrksich, M., Dike, L. E., Tien, J., Ingber, D. E. and Whitesides, G. M. Using Microcontact Printing to Pattern the Attachment of Mammalian Cells to Self-Assembled Monolayers of Alkanethiolates on Transparent Films of Gold and Silver. *Exp. Cell Res.*, **235**(2), 305–313, 1997.

[144] Mrksich, M. and Whitesides, G. M. Using Self-Assembled Monolayers to Understand the Interactions of Man-made Surfaces with Proteins and Cells. *Annu. Rev. Biophys. Biomol. Struct.*, **25**(1), 55–78, 1996.

[145] Dike, L., Chen, C., Mrksich, M., Tien, J., Whitesides, G. and Ingber, D. Geometric control of switching between growth, apoptosis, and differentiation during angiogenesis using micropatterned substrates. *In Vitro Cell. Dev. Biol.*, **35**(8), 441–448, 1999.

[146] Kane, R. S., Takayama, S., Ostuni, E., Ingber, D. E. and Whitesides, G. M. Patterning proteins and cells using soft lithography. *Biomaterials*, **20**(23-24), 2363–2376, 1999.

[147] Park, T. H. and Shuler, M. L. Integration of cell culture and microfabrication technology. *Biotechnol. Prog.*, **19**(2), 243–253, 2003.

[148] Tan, W. and Desai, T. A. Layer-by-layer microfluidics for biomimetic three-dimensional structures. *Biomaterials*, **25**(7-8 SU -), 1355–1364, 2004.

[149] Folch, A., Jo, B. H., Hurtado, O., Beebe, D. J. and Toner, M. Microfabricated elastomeric stencils for micropatterning cell cultures. *J Biomed Mater Res*, **52**(2), 346–53, 2000.

[150] Whitesides, G. M., Ostuni, E., Takayama, S., Jiang, X. Y. and Ingber, D. E. Soft lithography in biology and biochemistry. *Annu. Rev. Biomed. Eng.*, **3**, 335–373, 2001.

[151] Gallant, N. D., Capadona, J. R., Frazier, A. B., Collard, D. M. and Garcia, A. J. Micropatterned surfaces to engineer focal adhesions for analysis of cell adhesion strengthening. *Langmuir*, **18**(14), 5579–5584, 2002.

[152] Bischofs, I. B. and Schwarz, U. S. Cell organization in soft media due to active mechanosensing. *Proc. Natl. Acad. Sci. U. S. A.*, **100**(16), 9274–9279, 2003.

[153] Raghavan, S. and Chen, C. S. Micropatterned environments in cell biology. *Adv. Mater.*, **16**(15), 1303–1313, 2004.

[154] Watt, F. M., Jordan, P. W. and O'Neill, C. H. Cell Shape Controls Terminal Differentiation of Human Epidermal Keratinocytes. *Proc. Natl. Acad. Sci.*, **85**(15), 5576–5580, 1988.

[155] Heiduschka, P., Romann, I., Ecken, H., Schoning, M., Schuhmann, W. and Thanos, S. Defined adhesion and growth of neurones on artificial structured substrates. *Electrochim. Acta*, **47**(1), 299–307, 2001.

[156] Bousse, L. Whole cell biosensors. *Sens. Actuator B-Chem.*, **34**(1-3), 270–275, 1996.

[157] Gilchrist, K. H., Barker, V. N., Fletcher, L. E., DeBusschere, B. D., Ghanouni, P., Giovangrandi, L. and Kovacs, G. T. A. General purpose, field-portable cell-based biosensor platform. *Biosens. Bioelectron.*, **16**(7-8), 557–564, 2001.

[158] Blattler, T. M., Pasche, S., Textor, M. and Griesser, H. J. High Salt Stability and Protein Resistance of Poly(L-lysine)-g-poly(ethylene glycol) Copolymers Covalently Immobilized via Aldehyde Plasma Polymer Interlayers on Inorganic and Polymeric Substrates. *Langmuir*, **22**(13), 5760–5769, 2006.

[159] Gates, B. D., Xu, Q. B., Stewart, M., Ryan, D., Willson, C. G. and Whitesides, G. M. New approaches to nanofabrication: Molding, printing, and other techniques. *Chem. Rev.*, **105**(4), 1171–1196, 2005.

[160] Xia, Y. N. and Whitesides, G. M. Soft lithography. *Annu. Rev. Mater. Sci.*, **28**, 153–184, 1998.

[161] Spatz, J. P., Mossmer, S., Hartmann, C., Moller, M., Herzog, T., Krieger, M., Boyen, H. G., Ziemann, P. and Kabius, B. Ordered deposition of inorganic clusters from micellar block copolymer films. *Langmuir*, **16**(2), 407–415, 2000.

[162] Arnold, M., Cavalcanti-Adam, E. A., Glass, R., Blummel, J., Eck, W., Kantlehner, M., Kessler, H. and Spatz, J. P. Activation of integrin function by nanopatterned adhesive interfaces. *Chemphyschem*, **5**(3), 383–388, 2004.

[163] Cavalcanti-Adam, E. A., Volberg, T., Micoulet, A., Kessler, H., Geiger, B. and Spatz, J. Cell Spreading and Focal Adhesion Dynamics are Regulated by Spacing of Integrin Ligands. *Biophys. J.*, **92**(8), 2964–2974, 2007.

[164] McKnight, A. L., Kugel, J. L., Rossman, P. J., Manduca, A., Hartmann, L. C. and Ehman, R. L. MR Elastography of Breast Cancer: Preliminary Results. *Am. J. Roentgenol.*, **178**(6), 1411–1417, 2002.

[165] Bercoff, J., Chaffai, S., Tanter, M., Sandrin, L., Catheline, S., Fink, M., Gennisson, J. L. and Meunier, M. In vivo breast tumor detection using transient elastography. *Ultrasound Med. Biol.*, **29**(10), 1387–1396, 2003.

[166] Paszek, M. J., Zahir, N., Johnson, K. R., Lakins, J. N., Rozenberg, G. I., Gefen, A., Reinhart-King, C. A., Margulies, S. S., Dembo, M. and Boettiger, D. Tensional homeostasis and the malignant phenotype. *Cancer Cell*, **8**(3), 241–254, 2005.

[167] Discher, D. E., Janmey, P. and Wang, Y. L. Tissue cells feel and respond to the stiffness of their substrate. *Science*, **310**(5751), 1139–1143, 2005.

[168] Wells, R. G. The role of matrix stiffness in regulating cell behavior. *Hepatology*, **47**(4), 1394–1400, 2008.

[169] Georges, P. C. and Janmey, P. A. Cell type-specific response to growth on soft materials. *J Appl Physiol*, **98**(4), 1547–1553, 2005.

[170] Pelham, R. J., J. and Wang, Y. Cell locomotion and focal adhesions are regulated by substrate flexibility. *Proc Natl Acad Sci U S A*, **94**(25), 13661–5, 1997.

[171] Bershadsky, A. D., Balaban, N. Q. and Geiger, B. Adhesion-dependent cell mechanosensitivity. *Annu. Rev. Cell Dev. Biol.*, **19**(1), 677–695, 2003.

[172] Goffin, J. M., Pittet, P., Csucs, G., Lussi, J. W., Meister, J.-J. and Hinz, B. Focal adhesion size controls tension-dependent recruitment of alpha-smooth muscle actin to stress fibers. *J. Cell Biol.*, **172**(2), 1–10, 2006.

[173] Nicolas, A. and Safran, S. A. Limitation of cell adhesion by the elasticity of the extracellular matrix. *Biophys. J.*, **91**(1), 61–73, 2006.

[174] Peyton, S., Ghajar, C., Khatiwala, C. and Putnam, A. The emergence of ECM mechanics and cytoskeletal tension as important regulators of cell function. *Cell Biochem. Biophys.*, **47**(2), 300–320, 2007.

[175] Yeung, T., Georges, P. C., Flanagan, L. A., Marg, B., Ortiz, M., Funaki, M., Zahir, N., Ming, W., Weaver, V. and Janmey, P. A. Effects of substrate stiffness on cell morphology, cytoskeletal structure, and adhesion. *Cell Motil. Cytoskeleton*, **60**(1), 24–34, 2005.

[176] Lo, C.-M., Wang, H.-B., Dembo, M. and Wang, Y.-l. Cell Movement Is Guided by the Rigidity of the Substrate. *Biophys. J.*, **79**(1), 144–152, 2000.

[177] Gray, D. S., Tien, J. and Chen, C. S. Repositioning of cells by mechanotaxis on surfaces with micropatterned Young's modulus. *J Biomed Mater Res A*, **66**(3), 605–14, 2003.

[178] Zaman, M. H., Trapani, L. M., Siemeski, A., MacKellar, D., Gong, H., Kamm, R. D., Wells, A., Lauffenburger, D. A. and Matsudaira, P. Migration of tumor cells in 3D matrices is governed by matrix stiffness along with cell-matrix adhesion and proteolysis. *PNAS*, **103**(29), 10889–10894, 2006.

[179] Saez, A., Ghibaudo, M., Buguin, A., Silberzan, P. and Ladoux, B. Rigidity-driven growth and migration of epithelial cells on microstructured anisotropic substrates. *PNAS*, **104**(20), 8281–8286, 2007.

[180] Georges, P. C., Miller, W. J., Meaney, D. F., Sawyer, E. S. and Janmey, P. A. Matrices with Compliance Comparable to that of Brain Tissue Select Neuronal over Glial Growth in Mixed Cortical Cultures. *Biophys. J.*, **90**(8), 3012–3018, 2006.

[181] Engler, A. J., Sen, S., Sweeney, H. L. and Discher, D. E. Matrix Elasticity Directs Stem Cell Lineage Specification. *Cell*, **126**(4), 677–689, 2006.

[182] Wang, H.-B., Dembo, M. and Wang, Y.-L. Substrate flexibility regulates growth and apoptosis of normal but not transformed cells. *Am J Physiol Cell Physiol*, **279**(5), C1345–1350, 2000.

[183] Ingber, D. E. Cellular mechanotransduction: putting all the pieces together again. *FASEB J.*, **20**(7), 811–827, 2006.

[184] Vogel, V. and Sheetz, M. Local force and geometry sensing regulate cell functions. *Nat Rev Mol Cell Biol*, **7**(4), 265–275, 2006.

[185] Choquet, D., Felsenfeld, D. P. and Sheetz, M. P. Extracellular matrix rigidity causes strengthening of integrin-cytoskeleton linkages. *Cell*, **88**(1), 39–48, 1997.

[186] Harris, A. K., Wild, P. and Stopak, D. Silicone rubber substrata: a new wrinkle in the study of cell locomotion. *Science*, **208**(4440), 177–179, 1980.

[187] Tan, J. L., Tien, J., Pirone, D. M., Gray, D. S., Bhadriraju, K. and Chen, C. S. Cells lying on a bed of microneedles: An approach to isolate mechanical force. *Proc. Natl. Acad. Sci. U. S. A.*, **100**(4), 1484–1489, 2003.

[188] Rehfeldt, F., Engler, A. J., Eckhardt, A., Ahmed, F. and Discher, D. E. Cell responses to the mechanochemical microenvironment–Implications for regenerative medicine and drug delivery. *Adv. Drug Deliv. Rev.*, **59**(13), 1329–1339, 2007.

[189] Zhang, S. Beyond the Petri dish. *Nat Biotech*, **22**(2), 151–152, 2004.

[190] Abbott, A. Biology's new dimension. *Nature*, **424**(6951), 870–872, 2003.

[191] Cukierman, E., Pankov, R. and Yamada, K. M. Cell interactions with three-dimensional matrices. *Curr. Opin. Cell Biol.*, **14**(5), 633–640, 2002.

[192] Birgersdotter, A., Sandberg, R. and Ernberg, I. Gene expression perturbation in vitro–A growing case for three-dimensional (3D) culture systems. *Semin. Cancer Biol.*, **15**(5), 405–412, 2005.

[193] Webb, D. J. and Horwitz, A. F. New dimensions in cell migration. *Nat. Cell Biol.*, **5**(8), 690–692, 2003.

[194] Even-Ram, S. and Yamada, K. M. Cell migration in 3D matrix. *Curr. Opin. Cell Biol.*, **17**(5), 524–532, 2005.

[195] Benya, P. D. and Shaffer, J. D. Dedifferentiated chondrocytes reexpress the differentiated collagen phenotype when cultured in agarose gels. *Cell*, **30**(1), 215–224, 1982.

[196] Geiger, B. Cell Biology: Encounters in Space. *Science*, **294**(5547), 1661–1663, 2001.

[197] Roskelley, C. D., Desprez, P. Y. and Bissell, M. J. Extracellular matrix-dependent tissue-specific gene expression in mammary epithelial cells requires both physical and biochemical signal transduction. *Proc. Natl. Acad. Sci. U. S. A.*, **91**(26), 12378–12382, 1994.

[198] Green, J. A. and Yamada, K. M. Three-dimensional microenvironments modulate fibroblast signaling responses. *Adv. Drug Deliv. Rev.*, **59**(13), 1293–1298, 2007.

[199] Grinnell, F. and Lamke, C. R. Reorganization of hydrated collagen lattices by human skin fibroblasts. *J Cell Sci*, **66**(1), 51–63, 1984.

[200] Dusseiller, M. *Micro- and Nanoengineering the 3-Dimensional Environment of Cells in Culture*. PhD thesis, ETH Zurich, 2005.

[201] Dusseiller, M., Smith, M. L., Vogel, V. and Textor, M. Microfabricated three-dimensional environments for single cell studies. *Biointerphases*, **1**(1), P1–P4, 2006.

[202] Engvall, E. and Ruoslahti, E. Binding of soluble form of fibroblast surface protein, fibronectin, to collagen. *International Journal of Cancer*, **20**(1), 1–5, 1977.

[203] Miekka, S. I., Ingham, K. C. and Menache, D. Rapid methods for isolation of human plasma fibronectin. *Thrombosis Research*, **27**(1), 1–14, 1982.

[204] Antia, M., Islas, L. D., Boness, D. A., Baneyx, G. and Vogel, V. Single molecule fluorescence studies of surface-adsorbed fibronectin. *Biomaterials*, **27**(5), 679–690, 2006.

[205] Zhu, B., Chappuis-Flament, S., Wong, E., Jensen, I. E., Gumbiner, B. M. and Leckband, D. Functional Analysis of the Structural Basis of Homophilic Cadherin Adhesion. *Biophys. J.*, **84**(6), 4033–4042, 2003.

[206] Folch, A., Ayon, A., Hurtado, O., Schmidt, M. A. and Toner, M. Molding of deep polydimethylsiloxane microstructures for microfluidics and biological applications. *J Biomech Eng*, **121**(1), 28–34, 1999.

[207] Lee, J. N., Jiang, X., Ryan, D. and Whitesides, G. M. Compatibility of Mammalian Cells on Surfaces of Poly(dimethylsiloxane). *Langmuir*, **20**(26), 11684–11691, 2004.

[208] Flack, W. W., Soong, D. S., Bell, A. T. and Hess, D. W. A mathematical model for spin coating of polymer resists. *J. Appl. Phys.*, **56**(4), 1199–1206, 1984.

[209] Lee, S. and Voros, J. An Aqueous-Based Surface Modification of Poly(dimethylsiloxane) with Poly(ethylene glycol) to Prevent Biofouling. *Langmuir*, **21**(25), 11957–11962, 2005.

[210] Brown, X. Q., Ookawa, K. and Wong, J. Y. Evaluation of polydimethylsiloxane scaffolds with physiologically-relevant elastic moduli: interplay of substrate mechanics and surface chemistry effects on vascular smooth muscle cell response. *Biomaterials*, **26**(16), 3123–9, 2005.

[211] Sorribas, H., Padeste, C. and Tiefenauer, L. Photolithographic generation of protein micropatterns for neuron culture applications. *Biomaterials*, **23**(3), 893–900, 2002.

[212] Cooper, J. A. Effects of cytochalasin and phalloidin on actin. *J. Cell Biol.*, **105**(4), 1473–1478, 1987.

[213] Wehland, J., Osborn, M. and Weber, K. Phalloidin-induced actin polymerization in the cytoplasm of cultured cells interferes with cell locomotion and growth. *Proc. Natl. Acad. Sci. U. S. A.*, **74**(12), 5613–5617, 1977.

[214] Barden, J. A., Miki, M., Hambly, B. D. and Remedios, C. Localization of the phalloidin and nucleotide-binding sites on actin. *Eur. J. Biochem.*, **162**(3), 583–588, 1987.

[215] Eroglu, A., Russo, M. J., Bieganski, R., Fowler, A., Cheley, S., Bayley, H. and Toner, M. Intracellular trehalose improves the survival of cryopreserved mammalian cells. *Nat Biotech*, **18**(2), 163–167, 2000.

[216] Rodahl, M., Hook, F., Krozer, A., Brzezinski, P. and Kasemo, B. Quartz-Crystal Microbalance Setup for Frequency and Q-Factor Measurements in Gaseous and Liquid Environments. *Rev. Sci. Instrum.*, **66**(7), 3924–3930, 1995.

[217] Konash, P. L. and Bastiaans, G. J. Piezoelectric-Crystals as Detectors in Liquid-Chromatography. *Anal. Chem.*, **52**(12), 1929–1931, 1980.

[218] Nomura, T. and Okuhara, M. Frequency-Shifts of Piezoelectric Quartz Crystals Immersed in Organic Liquids. *Anal. Chim. Acta*, **142**(OCT), 281–284, 1982.

[219] Sauerbrey, G. Verwendung von Schwingquarzen zur Waegung duenner Schichte und zur Mikrowaegung. *Z. Phys. A: Hadrons Nucl.*, **155**, 206–222, 1959.

[220] Berquand, A., Mazeran, P. E., Pantigny, J., Proux-Delrouyre, V., Laval, J. M. and Bourdillon, C. Two-Step Formation of Streptavidin-Supported Lipid Bilayers by PEG-Triggered Vesicle Fusion. Fluorescence and Atomic Force Microscopy Characterization. *Langmuir*, **19**(5), 1700–1707, 2003.

[221] Axelrod, D., Koppel, D. E., Schlessinger, J., Elson, E. and Webb, W. W. Mobility Measurement by Analysis of Fluorescence Photobleaching Recovery Kinetics. *Biophys. J.*, **16**(9), 1055–1069, 1976.

[222] Soumpasis, D. M. Theoretical-Analysis of Fluorescence Photobleaching Recovery Experiments. *Biophys. J.*, **41**(1), 95–97, 1983.

[223] Takeichi, M. Morphogenetic roles of classic cadherins. *Curr. Opin. Cell Biol.*, **7**(5), 619–627, 1995.

[224] Gumbiner, B. M. Cell Adhesion: The Molecular Basis of Tissue Architecture and Morphogenesis. *Cell*, **84**(3), 345–357, 1996.

[225] Gumbiner, B. M. Regulation of cadherin-mediated adhesion in morphogenesis. *Nature Reviews Molecular Cell Biology*, **6**(8), 622–634, 2005.

[226] Matsunaga, M., Hatta, K. and Takeichi, M. Role of N-Cadherin Cell-Adhesion Molecules in the Histogenesis of Neural Retina. *Neuron*, **1**(4), 289–295, 1988.

[227] Bronner-Fraser, M., Wolf, J. J. and Murray, B. A. Effects of antibodies against N-cadherin and N-CAM on the cranial neural crest and neural tube. *Dev. Biol.*, **153**(2), 291–301, 1992.

[228] Takeichi, M. Cadherin Cell-Adhesion Receptors as a Morphogenetic Regulator. *Science*, **251**(5000), 1451–1455, 1991.

[229] Cavallaro, U. and Christofori, G. Cell adhesion and signalling by cadherins and Ig-CAMs in cancer. *Nat Rev Cancer*, **4**(2), 118–132, 2004.

[230] Yap, A. S. The Morphogenetic Role of Cadherin Cell Adhesion Molecules in Human Cancer: A Thematic Review. *Cancer Invest.*, **16**(4), 252 – 261, 1998.

[231] Mbalaviele, G., Dunstan, C. R., Sasaki, A., Williams, P. J., Mundy, G. R. and Yoneda, T. E-Cadherin Expression in Human Breast Cancer Cells Suppresses the Development of Osteolytic Bone Metastases in an Experimental Metastasis Model. *Cancer Res.*, **56**(17), 4063–4070, 1996.

[232] Frixen, U. H., Behrens, J., Sachs, M., Eberle, G., Voss, B., Warda, A., Lochner, D. and Birchmeier, W. E-cadherin-mediated cell-cell adhesion prevents invasiveness of human carcinoma cells. *J. Cell Biol.*, **113**(1), 173–185, 1991.

[233] Pokutta, S. and Weis, W. I. Structure and Mechanism of Cadherins and Catenins in Cell-Cell Contacts. *Annu. Rev. Cell Dev. Biol.*, **23**(1), 2007.

[234] Yamada, S., Pokutta, S., Drees, F., Weis, W. I. and Nelson, W. J. Deconstructing the Cadherin-Catenin-Actin Complex. *Cell*, **123**(5), 889–901, 2005.

[235] Weis, W. I. and Nelson, W. J. Re-solving the Cadherin-Catenin-Actin Conundrum. *J. Biol. Chem.*, **281**(47), 35593–35597, 2006.

[236] Yap, A. S., Brieher, W. M., Pruschy, M. and Gumbiner, B. M. Lateral clustering of the adhesive ectodomain: a fundamental determinant of cadherin function. *Curr. Biol.*, **7**(5), 308–315, 1997.

[237] Angres, B., Barth, A. and Nelson, W. J. Mechanism for transition from initial to stable cell-cell adhesion: Kinetic analysis of E-cadherin-mediated adhesion using a quantitative adhesion assay. *J. Cell Biol.*, **134**(2), 549–557, 1996.

[238] Kovacs, E. M. and Yap, A. S. Cell-cell contact: Cooperating clusters of actin and cadherin. *Curr. Biol.*, **18**(15), R667–R669, 2008.

[239] Sako, Y., Nagafuchi, A., Tsukita, S., Takeichi, M. and Kusumi, A. Cytoplasmic Regulation of the Movement of E-Cadherin on the Free Cell Surface as Studied by Optical Tweezers and Single Particle Tracking: Corralling and Tethering by the Membrane Skeleton. *J. Cell Biol.*, **140**(5), 1227–1240, 1998.

[240] Mege, R.-M., Gavard, J. and Lambert, M. Regulation of cell-cell junctions by the cytoskeleton. *Curr. Opin. Cell Biol.*, **18**(5), 541–548, 2006.

[241] Brieher, W. M., Yap, A. S. and Gumbiner, B. M. Lateral dimerization is required for the homophilic binding activity of C-cadherin. *J. Cell Biol.*, **135**(2), 487–496, 1996.

[242] Lambert, M., Padilla, F. and Mege, R. M. Immobilized dimers of N-cadherin-Fc chimera mimic cadherin-mediated cell contact formation: contribution of both outside-in and inside-out signals. *J Cell Sci*, **113**(12), 2207–2219, 2000.

[243] Drees, F., Reilein, A. and Nelson, W. J. Cell-Adhesion Assays. In *Methods Mol. Biol.*, volume 294, pages 303–320. 2004.

[244] Ochsner, M., Dusseiller, M. R., Grandin, H. M., Luna-Morris, S., Textor, M., Vogel, V. and Smith, M. L. Micro-well arrays for 3D shape control and high resolution analysis of single cells. *Lab Chip*, **7**(8), 1074–1077, 2007.

[245] Shahal, T., Melzak, K. A., Lowe, C. R. and Gizeli, E. Poly(dimethylsiloxane)-coated sensor devices for the formation of supported lipid bilayers and the subsequent study of membrane interactions. *Langmuir*, **24**(19), 11268–11275, 2008.

[246] Reimhult, E., Hook, F. and Kasemo, B. Temperature dependence of formation of a supported phospholipid bilayer from vesicles on SiO2. *Phys Rev E Stat Nonlin Soft Matter Phys*, **66**(5 Pt 1), 051905, 2002.

[247] Hook, F., Ray, A., Norden, B. and Kasemo, B. Characterization of PNA and DNA Immobilization and Subsequent Hybridization with DNA Using Acoustic-Shear-Wave Attenuation Measurements. *Langmuir*, **17**(26), 8305–8312, 2001.

[248] Huang, N. P., Voros, J., De Paul, S. M., Textor, M. and Spencer, N. D. Biotin-derivatized poly(L-lysine)-g-poly(ethylene glycol): A novel polymeric interface for bioaffinity sensing. *Langmuir*, **18**(1), 220–230, 2002.

[249] Reimhult, E., Larsson, C., Kasemo, B. and Hook, F. Simultaneous Surface Plasmon Resonance and Quartz Crystal Microbalance with Dissipation Monitoring Measurements of Biomolecular Adsorption Events Involving Structural Transformations and Variations in Coupled Water. *Anal. Chem.*, **76**(24), 7211–7220, 2004.

[250] Phillips, K. S. and Cheng, Q. Microfluidic Immunoassay for Bacterial Toxins with Supported Phospholipid Bilayer Membranes on Poly(dimethylsiloxane). *Anal. Chem.*, **77**(1), 327–334, 2005.

[251] Calvert, T. L. and Leckband, D. Two-Dimensional Protein Crystallization at Solid-Liquid Interfaces. *Langmuir*, **13**(25), 6737–6745, 1997.

[252] Reviakine, I. and Brisson, A. Streptavidin 2D crystals on supported phospholipid bilayers: Toward constructing anchored phospholipid bilayers. *Langmuir*, **17**(26), 8293–8299, 2001.

[253] Rossetti, F. F., Textor, M. and Reviakine, I. Asymmetric distribution of phosphatidyl serine in supported phospholipid bilayers on titanium dioxide. *Langmuir*, **22**(8), 3467–3473, 2006.

[254] Muller, D. J., Fotiadis, D., Scheuring, S., Müller, S. A. and Engel, A. Electrostatically Balanced Subnanometer Imaging of Biological Specimens by Atomic Force Microscope. *Biophys. J.*, **76**(2), 1101–1111, 1999.

[255] Patel, A. R. and Frank, C. W. Quantitative Analysis of Tethered Vesicle Assemblies by Quartz Crystal Microbalance with Dissipation Monitoring: Binding Dynamics and Bound Water Content. *Langmuir*, **22**(18), 7587–7599, 2006.

[256] Groves, J. T., Ulman, N. and Boxer, S. G. Micropatterning Fluid Lipid Bilayers on Solid Supports. *Science*, **275**(5300), 651–653, 1997.

[257] Mornet, S., Lambert, O., Duguet, E. and Brisson, A. The Formation of Supported Lipid Bilayers on Silica Nanoparticles Revealed by Cryoelectron Microscopy. *Nano Lett.*, **5**(2), 281–285, 2005.

[258] Nelson, C. M. and Chen, C. S. VE-cadherin simultaneously stimulates and inhibits cell proliferation by altering cytoskeletal structure and tension. *J Cell Sci*, **116**(17), 3571–3581, 2003.

[259] Nelson, W. J. Adaptation of core mechanisms to generate cell polarity. *Nature*, **422**(6933), 766–774, 2003.

[260] Wang, A. Z., Ojakian, G. K. and Nelson, W. J. Steps in the morphogenesis of a polarized epithelium. I. Uncoupling the roles of cell-cell and cell-substratum contact in establishing plasma membrane polarity in multicellular epithelial (MDCK) cysts. *J Cell Sci*, **95**(1), 137–151, 1990.

[261] hBraga, V. M. M. and Yap, A. S. The challenges of abundance: epithelial junctions and small GTPase signalling. *Curr. Opin. Cell Biol.*, **17**(5), 466–474, 2005.

[262] Morrison, S. J. and Kimble, J. Asymmetric and symmetric stem-cell divisions in development and cancer. *Nature*, **441**(7097), 1068–1074, 2006.

[263] Li, L. and Xie, T. Stem Cell Niche: Structure and Function. *Annu. Rev. Cell Dev. Biol.*, **21**(1), 605–631, 2005.

[264] Spradling, A., Drummond-Barbosa, D. and Kai, T. Stem cells find their niche. *Nature*, **414**(6859), 98–104, 2001.

[265] Lutolf, M. P., Doyonnas, R., Havenstrite, K., Koleckar, K. and Blau, H. M. Perturbationofsinglehematopoieticstemcellfatesinartificialniches. *Integr. Biol.*, **1**(1), 59–69, 2009.

[266] Rossetti, F. F., Bally, M., Michel, R., Textor, M. and Reviakine, I. Interactions between titanium dioxide and phosphatidyl serine-containing liposomes: Formation and patterning of supported phospholipid bilayers on the surface of a medically relevant material. *Langmuir*, **21**(14), 6443–6450, 2005.

[267] Reimhult, E., Hook, F. and Kasemo, B. Vesicle adsorption on SiO2 and TiO2: Dependence on vesicle size. *J. Chem. Phys.*, **117**(16), 7401–7404, 2002.

[268] Reviakine, I., Rossetti, F. F., Morozov, A. N. and Textor, M. Investigating the properties of supported vesicular layers on titanium dioxide by quartz crystal microbalance with dissipation measurements. *J. Chem. Phys.*, **122**(20), 2005.

[269] Schmitt, L., Dietrich, C. and Tampe, R. Synthesis and Characterization of Chelator-Lipids for Reversible Immobilization of Engineered Proteins at Self-Assembled Lipid Interfaces. *J. Am. Chem. Soc.*, **116**(19), 8485–8491, 1994.

[270] Denis, F. A., Hanarp, P., Sutherland, D. S. and Dufrene, Y. F. Nanoscale Chemical Patterns Fabricated by Using Colloidal Lithography and Self-Assembled Monolayers. *Langmuir*, **20**(21), 9335–9339, 2004.

[271] Agheli, H., Malmstrom, J., Larsson, E. M., Textor, M. and Sutherland, D. S. Large Area Protein Nanopatterning for Biological Applications. *Nano Lett.*, **6**(6), 1165–1171, 2006.

[272] Saraste, A. and Pulkki, K. Morphologic and biochemical hallmarks of apoptosis. *Cardiovasc. Res.*, **45**(3), 528–537, 2000.

[273] Wood, W., Turmaine, M., Weber, R., Camp, V., Maki, R. A., McKercher, S. R. and Martin, P. Mesenchymal cells engulf and clear apoptotic footplate cells in macrophageless PU.1 null mouse embryos. *Development*, **127**(24), 5245–5252, 2000.

[274] Holmgren, L., O'Reilly, M. S. and Folkman, J. Dormancy of micrometastases: Balanced proliferation and apoptosis in the presence of angiogenesis suppression. *Nat. Med.*, **1**(2), 149–153, 1995.

[275] Boudreau, N., Sympson, C. J., Werb, Z. and Bissell, M. J. Suppression of ICE and Apoptosis in Mammary Epithelial Cells by Extracellular Matrix. *Science*, **267**(5199), 891–893, 1995.

[276] Re, F., Zanetti, A., Sironi, M., Polentarutti, N., Lanfrancone, L., Dejana, E. and Colotta, F. Inhibition of anchorage-dependent cell spreading triggers apoptosis in cultured human endothelial cells. *J. Cell Biol.*, **127**(2), 537–546, 1994.

[277] Bursch, W., Lauer, B., Timmermann-Trosiener, I., Barthel, G., Schuppler, J. and Schulte-Hermann, R. Controlled death (apoptosis) of normal and putative preneoplastic cells in rat liver following withdrawal of tumor promoters. *Carcinogenesis*, **5**(4), 453–458, 1984.

[278] Chen, C. S., Mrksich, M., Huang, S., Whitesides, G. M. and Ingber, D. E. Micropatterned surfaces for control of cell shape, position, and function. *Biotechnol. Prog.*, **14**(3), 356–363, 1998.

[279] Cai, Y., Biais, N., Giannone, G., Tanase, M., Jiang, G., Hofman, J. M., Wiggins, C. H., Silberzan, P., Buguin, A., Ladoux, B. and Sheetz, M. P. Nonmuscle Myosin IIA-Dependent Force Inhibits Cell Spreading and Drives F-Actin Flow. *Biophys. J.*, **91**(10), 3907–3920, 2006.

[280] Meshel, A. S., Wei, Q., Adelstein, R. S. and Sheetz, M. P. Basic mechanism of three-dimensional collagen fibre transport by fibroblasts. *Nat Cell Biol*, **7**(2), 157–164, 2005.

[281] Wei, Q. and Adelstein, R. S. Conditional Expression of a Truncated Fragment of Nonmuscle Myosin II-A Alters Cell Shape but Not Cytokinesis in HeLa Cells. *Mol. Biol. Cell*, **11**(10), 3617–3627, 2000.

[282] Lo, C.-M., Buxton, D. B., Chua, G. C. H., Dembo, M., Adelstein, R. S. and Wang, Y.-L. Nonmuscle Myosin IIB Is Involved in the Guidance of Fibroblast Migration. *Mol. Biol. Cell*, **15**(3), 982–989, 2004.

[283] Jay, P. Y., Pham, P. A., Wong, S. A. and Elson, E. L. A mechanical function of myosin II in cell motility. *J Cell Sci*, **108**(1), 387–393, 1995.

[284] Even-Ram, S., Doyle, A. D., Conti, M. A., Matsumoto, K., Adelstein, R. S. and Yamada, K. M. Myosin IIA regulates cell motility and actomyosin-microtubule crosstalk. *Nat Cell Biol*, **9**(3), 299–309, 2007.

[285] Avnur, Z. and Geiger, B. The removal of extracellular fibronectin from areas of cell-substrate contact. *Cell*, **25**(1), 121–132, 1981.

[286] Ffrench-Constant, C., Van de Water, L., Dvorak, H. F. and Hynes, R. O. Reappearance of an embryonic pattern of fibronectin splicing during wound healing in the adult rat. *J. Cell Biol.*, **109**(2), 903–914, 1989.

[287] Halliday, N. L. and Tomasek, J. J. Mechanical Properties of the Extracellular Matrix Influence Fibronectin Fibril Assembly in Vitro. *Exp. Cell Res.*, **217**(1), 109–117, 1995.

[288] Zhong, C., Chrzanowska-Wodnicka, M., Brown, J., Shaub, A., Belkin, A. M. and Burridge, K. Rho-mediated Contractility Exposes a Cryptic Site in Fibronectin and Induces Fibronectin Matrix Assembly. *J. Cell Biol.*, **141**(2), 539–551, 1998.

[289] Chen, C. S., Alonso, J. L., Ostuni, E., Whitesides, G. M. and Ingber, D. E. Cell shape provides global control of focal adhesion assembly. *Biochem. Biophys. Res. Commun.*, **307**(2), 355–361, 2003.

[290] Huang, S., Chen, C. S. and Ingber, D. E. Control of Cyclin D1, p27Kip1, and Cell Cycle Progression in Human Capillary Endothelial Cells by Cell Shape and Cytoskeletal Tension. *Mol. Biol. Cell*, **9**(11), 3179–3193, 1998.

[291] Balaban, N. Q., Schwarz, U. S., Riveline, D., Goichberg, P., Tzur, G., Sabanay, I., Mahalu, D., Safran, S., Bershadsky, A., Addadi, L. and Geiger, B. Force and focal adhesion assembly: a close relationship studied using elastic micropatterned substrates. *Nat Cell Biol*, **3**(5), 466–472, 2001.

[292] Fringer, J. and Grinnell, F. Fibroblast Quiescence in Floating or Released Collagen Matrices. CONTRIBUTION OF THE ERK SIGNALING PATHWAY AND ACTIN CYTOSKELETAL ORGANIZATION. *J. Biol. Chem.*, **276**(33), 31047–31052, 2001.

[293] Engler, A., Bacakova, L., Newman, C., Hategan, A., Griffin, M. and Discher, D. Substrate Compliance versus Ligand Density in Cell on Gel Responses. *Biophys. J.*, **86**(1), 617–628, 2004.

[294] Kong, H. J., Liu, J., Riddle, K., Matsumoto, T., Leach, K. and Mooney, D. J. Non-viral gene delivery regulated by stiffness of cell adhesion substrates. *Nat. Mater.*, **4**(6), 460–464, 2005.

MIRJAM OCHSNER

Date of Birth:	February 10, 1978
Nationality:	Swiss, Citizen of Einsiedeln (SZ)
Present Address:	Schützengraben 2
	CH-8840 Einsiedeln
	Switzerland
Phone:	+41 78 661 00 77
Email:	mirjam.ochsner@mat.ethz.ch

EDUCATION

2005 – 2009	Doctoral student at the Laboratory for Surface Science and Technology, Department of Materials, Swiss Federal Institute of Technology (ETH Zurich)
2001/02	Exchange year at EPF Lausanne, Switzerland
1999 – 2005	Studies of Material Sciences and Engineering at ETH Zurich. Graduation with the degree 'Dipl. Werkstoff-Ing. ETH' (BSc and MSc Material Engineering)
1994 – 1998	Matura Typus Bi at the 'Stiftsschule Einsiedeln', Switzerland

EXPERIENCE

2005	Assistant at Laboratory for Surface Science and Technology
2004/05	Diploma thesis on solar cells, Chalmers University of Technology, Göteborg, Sweden
2003	Internship at Clariant, Augsburg, Germany
2002/03	Internship at Edward Life Sciences, Irvine CA, USA
2002	Internship at Seoul National University (SNU), Seoul, South Korea
2001	Student Assistant at the Institute for Metal Research, ETH Zurich, Switzerland

STUDENT THESES SUPERVISION

MASTER AND DIPLOMA THESES

2007/08 **Cells in Wells – Bilayer functionalization to mimic the cell-cell contact**
Gregory Romano, September 2007 – February 2008

2006 **Patterned Substrates for AHP Cell Attachment, Growth and Differentiation**
Patrick Hänseler, August – December 2006 (co-supervision with Michelle Grandin)

BACHELOR AND SEMESTER THESES

2006 **Development of an Efficient Protocol for Microcontact and Inverted Microcontact Printing onto Polymer Substrates**
Anita Bardill, March – July 2007

2008 **Untersuchung der Teilung humaner Zellen in microwell-arrays**
Maria Stammwitz, August – September 2008

PUBLICATIONS

JOURNAL ARTICLES

2008   **Beyond the Lotus Effect: Roughness Influences on Wetting over a Wide Surface-Energy Range**

D.M. Spori, T. Drobek, S. Zürcher, **M.Ochsner**, C. Sprecher, A. Mühlebach and N.D. Spencer

Langmuir **2008**, 24 (10), p. 5411–5417

2007   **Micro-well arrays for 3D shape control and high resolution analysis of single cells**

M. Ochsner, M.R. Dusseiller, H.M.Grandin, S. Luna-Morris, M. Textor, V. Vogel, M.L. Smith

Lab on a Chip, **2007**, 7, 8, p. 1074–1077

From macro-to micro-single chamber solid oxide fuel cells

B.E. Buergler, **M. Ochsner**, S. Vuillemin, L.J.Gauckler

Journal of Power Sources **2007**, 171, 2, p.310–320

2006   **Nanopatterns with Biological Function**

M. Ochsner, C. Huwiler, T. Blättler, , B. Städler, H. Solak, J. Vörös and H.M. Grandin

Journal of Nanoscience and Nanotechnology **2006**, Vol. 6, p. 2237–2264

JOURNAL ARTICLES IN PREPARATION

Rigidity- and shape-dependent cytoskeleton assembly and metabolism of primary fibroblast cells differ in 2-D and 3-D

M. Ochsner, M. Textor, V. Vogel, M.L. Smith

Ligand mobility and dimensionality sensation in cell-cell contact

M. Ochsner, G. Romano, M. Håkanson, M.L. Smith, E. Reimhult, D. Leckband, V. Vogel, M. Textor

ORAL PRESENTATIONS

2008   **Materials Colloquium**, ETH Zurich, Switzerland
Three-dimensional Microwell Array for Single Cell Analysis
M. Ochsner, Michael Smith, Michelle Grandin, Marcus Textor, Viola Vogel

       World Biomaterials, WBM 2008, Amsterdam, The Netherlands
Microwell platform to study actin organization and fibronectin rearrangement in 3D
M. Ochsner,Michael Smith, Michelle Grandin, Marcus Textor, Viola Vogel

2007   **SBE's 3rd International Conference on Bioengineering and Nanotechnology**, Singapore
Three-Dimensional micro-well array for single cell analysis
M.Ochsner, Michael Smith, Michelle Grandin, Marcus Textor

2006   **AVS 53st International Symposium 2006**, San Francisco, CA, USA
Micro-Three-dimensional Structuring Platform for Cell Culturing
M. Ochsner, Marc Dusseiller, Michelle Grandin, Marcus Textor

POSTER PRESENTATIONS

2008   **Gordon Research Conference, Signal Transduction By Engineered Extracellular Matrices, 2008**, Lewiston, ME, USA
Actin organization and fibronectin rearrangement in a controlled 3D microenvironment
M.Ochsner, Michael Smith, Viola Vogel, Marcus Textor

       Single Cell Analysis Workshop, SCAW 2008, ETH Zurich, Zurich, Switzerland
Microwell platform to study actin organization and fibronectin rearrangement in 3D
M.Ochsner, Michael Smith, Viola Vogel, Marcus Textor

2007   **Biosurf VII, Functional Interfaces for Directing Biological Response, 2007**,
University of Zurich, Switzerland
Defining cell shape in 3D
M.Ochsner, Michael Smith, Michelle Grandin, Marcus Textor

       ESF-EMBO Research Conference, Biological Surfaces & Interfaces, 2007,
Sant Feliu de Guixols, Spain
Micro-well array for single cell analysis in three-dimensions
M.Ochsner, Michael Smith, Michelle Grandin, Marcus Textor

2006   **Gordon Research Conference, Biointerface Science, 2006**, Les Diablerets,
Switzerland
Three-dimensional Microstructured Surfaces for Cell Culturing
M. Ochsner, Marc Dusseiller, Michelle Grandin, Marcus Textor

       ICN+T 2006, Basel, Switzerland
Engineered Surfaces for Micro-3-D Cell Culturing
M. Ochsner, Marc Dusseiller, Michelle Grandin, Marcus Textor

2005   **Workshop Cells at Interfaces, 2005**, Firenze, Italy
Engineering of microenvironments for cell-matrix and cell-cell adhesion studies
M. Ochsner, Marc Dusseiller, Michelle Grandin, and Marcus Textor